

Phenotypic Characterisation of Intra-Tumoural Heterogeneity in High Grade Serous Ovarian Cancer: Development of 3D Culture Systems to Model Tumour Behaviour and Heterogeneity

A Thesis submitted in fulfilment of the requirements for the degree of Doctor of Philosophy

Katherine Nixon

Imperial College London, Department of Surgery and Cancer

Declaration of Originality

I declare that the work completed and presented in this thesis is my own. Acknowledgement is given to all sources used in the production of this thesis and to the assistance received in completion of the work.

Copyright Declaration

The copyright of this thesis rests with the author. Unless otherwise indicated, its contents are licensed under a Creative Commons Attribution-Non Commercial 4.0 International Licence (CC BY-NC). Under this licence, you may copy and redistribute the material in any medium or format. You may also create and distribute modified versions of the work. This is on the condition that: you credit the author and do not use it, or any derivative works, for a commercial purpose. When reusing or sharing this work, ensure you make the licence terms clear to others by naming the licence and linking to the licence text. Where a work has been adapted, you should indicate that the work has been changed and describe those changes. Please seek permission from the copyright holder for uses of this work that are not included in this licence or permitted under UK Copyright Law.

This thesis is dedicated to my amazing family, who always know exactly how to support and encourage me and help me achieve my dreams.

Abstract

High grade serous ovarian cancer (HGSOC) remains the leading cause of death from a gynaecological malignancy. Disparity in response to treatment is observed, with most patients showing sensitivity to platinum therapies initially, only to later relapse with acquired platinum resistance. HGSOC is characterised by vast genomic instability and intra-tumoural heterogeneity (ITH), contributing to the variation in patient response rates and making development of longer term effective therapeutic approaches challenging.

In this project, I aimed to characterise the extent of spatial and temporal ITH in HGSOC, profiling tumour samples from multiple disseminated metastatic sites to understand the link between heterogeneity, response to treatment and patient outcome (n=49 patients, mean number of tumour samples obtained per patient =9, range 4-15). This project identified variations in apoptotic responses to platinum treatment between different metastatic sites within patients in 2D cultures.

To investigate this observed phenotypic heterogeneity further and assess the impact of the local tumour microenvironment on primary and metastatic HGSOC tumour cells' treatment responses, 3D organotypic models representing the peritoneal surface were designed. Variation in response to treatment was observed in both 2D and 3D culture platforms with reduced response to treatment seen in 3D organotypic cultures, highlighting the importance of more complex culture systems. An optimal culture design to incorporate elements of the tumour microenvironment in HGSOC was investigated through mass spectrometry analysis of ECM protein composition and development of *ex vivo* tumour tissue slices. Analysis of ECM composition showed broad heterogeneity across the patient cohort and between different anatomical locations (n=4 patients, n=5 sample sites per patient).

Through the development of culture platforms which more closely represent the *in vivo* state, the heterogeneity displayed in HGSOC can be further examined, leading to advancements in discovery of potential diagnostic and prognostic biomarkers, testing of novel therapeutics and improvements in patient outcomes.

Acknowledgements

This project could not have been completed without help from a great number of people. Firstly, a huge thank you to my supervisors. Prof Christina Fotopoulou, thank you so much for giving me the opportunity and encouraging me to be a part of an amazing team and for being a support to me along the path of my research studies and career. Dr Paula Cunnea, thank you for all your support, all your guidance day to day and your huge motivation and encouragement during both the writing-up and actual physical marathons.

I was part of a wonderful team in the Department of Surgery and Cancer and many people helped this project come together. Cristina Albert Morera helped me with many practical aspects in the lab and was a huge part of the flow cytometry work as well as becoming a friend. Thank you to Ratri for all her work on the ITH project. Other members of the group Tommy and Natasha helped make each day enjoyable.

MRes students Yinghan Su and Kate Chaerin Lee assisted in the development and analysis of the 3D models, including the cell population staining and flow cytometry work. Additionally, Kate helped with the ECM composition analysis and Western blotting.

Dr Ed Curry, Dr Haonan Lu and Chun Hei Kwok have all given much appreciated guidance with bioinformatics and advice on analysis of the mass spectrometry data. Chun Hei additionally provided the Kaplan-Meier plots for the ITH data.

Thank you to Professor Mikael Bjornstedt and Dr Sougat Misra at the Karolinska Institute in Stockholm who helped with the techniques for *ex vivo* tissue slices.

The DCBiosciences team, Keiryn, Peter and Armel provided the mass spectrometry services for the ECM study and gave support for the data analysis.

Additional thanks to Nona and the ECMC team for help with banking of the samples.

Most importantly, a huge thank you to all the patients who kindly consented to allowing their tumour samples to be part of the research study.

Many other members of the fourth floor and whole IRDB team have helped both practically and, through various bake off activities, christmas parties and ‘primary room’ sharing time, have become good friends.

This project could not have happened and been completed without the love and support of my family. The time course of the project has seen a wedding and two new additions to our family. James, Georgia and Rose, you are the most important people in my life. James, you have supported me endlessly through the project and kept us all going despite your own ridiculously

tiring shift schedule. G and RoRo, you are beautiful sunshine cuddles when things seem tough, thank you for putting up with the adults doing so much ‘stinky work’.

A ginormous thank you must be given to my wonderful parents Stephen and Maria who, not only have supported and encouraged me to achieve my goals throughout my life but also provided countless hours of childcare in the last couple of years to enable this project to be completed, you are amazing and we will be eternally grateful.

To all my family and friends, thank you for being brilliant, I love and appreciate you all so much!

Table of Contents

Title page……..…1
Declaration of Originality...……..……..…2
Copyright Declaration……..3
Abstract ……....5
Acknowledgements……...6
Table of Contents……..8
List of figures……...11
List of tables……16
Abbreviations……...17

1 Introduction..... 21
1.1 Introduction to ovarian cancer..... 21
1.2 Epithelial ovarian cancer subtypes..... 23
1.2.1 Clear Cell Carcinoma..... 23
1.2.2 Endometrioid Carcinoma..... 24
1.2.3 Mucinous Ovarian Carcinoma..... 24
1.2.4 Low grade serous ovarian carcinoma..... 25
1.3 Staging of Ovarian Cancers..... 26
1.4 Introduction to High Grade Serous Ovarian Cancer..... 27
1.4.1 Presentation..... 27
1.4.2 Aetiology..... 28
1.4.3 Management..... 31
1.4.4 Heterogeneity in HGSOC..... 33
1.4.5 Emergence of platinum resistance..... 36
1.5 Tumour microenvironment..... 43
1.6 Review of 3D culture systems..... 53
1.6.1 Use of immortalised cell lines vs primary tumour cell cultures..... 56
1.6.2 Structural platforms for 3D cultures..... 57
1.6.3 Spheroids..... 58
1.6.4 Organoids..... 59
1.6.5 3D Organotypic Models..... 61
1.6.6 Tumour explant/slice cultures..... 62
1.6.7 Patient derived xenografts..... 63
1.7 Project Background:..... 64
1.8 Hypothesis..... 65
1.9 Aims..... 65

2 Materials and Methods..... 67
2.1 Patient cohorts and tissue collection procedures..... 67
2.2 Stromal cell extraction..... 69
2.3 Establishment of primary HGSOC tumour cell cultures..... 71
2.4 Confirmation of stromal cell populations..... 71
2.5 3D organotypic model assembly..... 73
2.6 3D organotypic models flow cytometry apoptosis assays..... 76
2.7 Apoptosis assays..... 77
2.8 IC_{50} assays..... 77
2.9 Ki67 proliferation index immunohistochemistry (IHC)..... 78
2.10 Extracellular matrix protein lysate extraction..... 79
2.11 Tumour explant slice culture preparation..... 80
2.12 Slice culture treatment and immunohistochemistry (IHC)..... 80

2.13 Haematoxylin and Eosin staining 81
2.14 External IHC protocols for slice culture blocks 82

3 Results: Characterisation of intra-tumoural heterogeneity in HGSOC 85
3.1 Introduction 85
3.2 Overview of patient characteristics 86
Patient cohort 86
3.2.1 Figure ..... **Error! Bookmark not defined.**
3.3 Phenotypic heterogeneity – apoptosis assays 89
3.3.1 Evaluation of cisplatin induced apoptosis in relapse HGSOC 96
3.4 Phenotypic variation across the intra-abdominal cavity 98
3.5 Phenotypic Heterogeneity – heterogeneity in IC_{50} concentrations of cisplatin in different tumour sites 100
3.6 Ki67 proliferation index 102
3.7 Discussion 105

4 Results: Development of 3D Organotypic HGSOC Models 107
4.1 Introduction 107
4.2 Isolation of stromal cells 108
4.2.1 Imaging of stromal cell populations 109
4.2.2 Confirmation of cell populations 110
4.3 Optimisation and construction of 3D organotypic models and assay read-out 111
4.3.1 Processing of 3D organotypic models – Histological read-out optimisation 112
4.3.2 Processing of 3D organotypic models - Flow cytometry optimisation 113
4.4 Flow cytometry analysis of 3D organotypic models 115
4.4.1 Apoptotic response of ovarian cancer immortalised cells lines to Cisplatin treatment in 3D organotypic models 115
4.4.2 Apoptotic response of primary HGSOC tumour cells to cisplatin treatment in 3D organotypic models 119
4.5 Comparison and correlations between 3D model and 2D ITH phenotypic data 125
4.6 Discussion 129

5 Results: Elucidation of tumour extracellular matrix composition in HGSOC 132
5.1 Introduction 132
5.2 Patient and sample data 134
5.2.1 Sample information 134
5.2.2 Patient demographics 135
5.3 Mass Spectrometry data analysis of ECM composition in HGSOC samples 136
5.3.1 ECM protein composition shows heterogeneity across the sample cohort 136
5.3.2 Protein-protein interactions and pathway enrichments analysis 138
5.3.3 Analysis of variation in ECM composition between different anatomical sites 140
5.3.4 Primary tumour ECM composition analysis 143
5.3.5 Intra-abdominal heterogeneity in ECM composition observed 144
5.4 Examination of ECM proteins of interest 149
5.4.1 Collagen I 151
5.4.2 Collagen IV 152
5.4.3 Collagen VI 153
5.5 Discussion 156

6 Results: Development of *ex vivo* tumour slice culture models 158
6.1 Introduction 158
6.2 HGSOC *Ex vivo* tissue slice study outline 159
6.3 Optimisation of vibratome techniques 160

6.4 Confirmation of tissue slice architecture 162
6.5 Immunohistochemistry read-outs for omental *ex vivo* tumour tissue slices..... 163
6.5.1 Assessment of slice tissue viability over different culture periods.....163
6.5.2 IHC assessment of response to cisplatin treatment 166
6.6 Discussion 168
7 Discussion and Future Perspectives..... 170
8 References..... 181
9 Appendix 200

List of Figures

Figure 1.1: Principle Histological subtypes of Ovarian Cancer. Breakdown of the histological subtypes of epithelial and non-epithelial ovarian cancer and the known associated mutations and pathway alterations [6].....21

Figure 1.2: Ovarian Cancer lifetime risk. Diagrammatic representation of lifetime risk of developing ovarian cancer in the general population, around 1.6% in comparison to those with BRCA mutations (BRCA2 around 20%, BRCA1 around 60%[8]…….....22

Figure 1.3: Type 1 and Type 2 serous ovarian cancers. Overview of the distinguishing characteristic features between Type 1 and Type 2 serous ovarian cancers[12]……..22

Figure 1.4: Dualistic pathway of HGSOC precursor lesions. Proposed dualistic pathway for HGSOC pathogenesis with precursor lesions possible from both the ovarian surface epithelium and STIC lesions in the fallopian tubes[58]…….29

Figure 1.5: Dissemination patterns of HGSOC. Diagrammatic representation of the dissemination patterns of ovarian cancer showing spread of nodular disease throughout the peritoneal lined abdominal cavity.[62]……..30

Figure 1.6: Mechanism of action of Cisplatin. Diagram demonstrating the covalent binding of the platinum atom of cisplatin to N7 of guanine leading to eventual cell death[111]……...37

Figure 1.7: Emergence of platinum resistance in HGSOC. Diagram representing different platinum sensitivity groupings in HGSOC and the potential pathways to resistant disease [139]……40

Figure 1.8: Interactions between ovarian cancer cells and the extra-cellular matrix. Diagram demonstrating the relationships between ovarian cancer cells and the main ECM components in the tumour microenvironment in both primary and metastatic settings. (A) Primary tumour cells recruiting and corrupting tumour associated macrophages, cancer associated fibroblasts, T-cells and endothelial cells. There is upregulation of key ECM components such as fibronectin, hyaluronan, tenascin, versican and MMPs. Collagen fibres undergo remodelling to become thick fibrils and lack organised orientation. (B) Tumour cells, either existing alone or in spheroids, detach from the epithelium and travel in the ascitic fluid around the abdominal cavity. Extracellular matrix components are found within the aggregated cells and the ascitic fluid. (C) At distant metastatic sites along the peritoneal lining, tumour cells attach to the mesothelial cell covered peritoneum and invade to form secondary metastatic sites. Image taken from [147]……43

Figure 1.9: Representation of peritoneal layering architecture. Diagrammatic representation of the peritoneal lining and stromal architecture consisting of a mesothelial lining on the basement membrane, with extracellular matrix beneath containing fibroblasts, blood vessels and structural components such as collagen fibres. Diagram adapted from image [150]……44

Figure 1.10: Diagram of healthy peritoneum. Diagrammatic representation of healthy peritoneum which covers the intra-abdominal organs including the omentum [166]……..45

Figure 1.11: [A]Schematic representation of the peritoneal site of ovarian cancer displaying its structure and components. [B] Schematic representation of adherent ovarian cancer cell cluster proliferating, invading, and destroying basement membrane ECM tissue architecture of the peritoneal site ……51

Figure 1.12: Comparison of 2D and 3D culture systems. Diagram comparing advantages and disadvantages of different culture techniques considering 2D monolayer designs and more complex 3D culture systems. Adapted from [227, 228]…….54

Figure 1.13: Example of 3D organotypic model. 3D organotypic model diagram depicting the construction of omental layers with tumour cells (A) and (B) the use of model in testing of therapeutics. Taken from [146]……61

Figure 2.1: The intra-operative mapping tool (IMO). The intra-operative ovarian cancer mapping tool was used to guide systematic collection of tumour samples……..68

Figure 2.2: Diagrammatic representation of 3D organotypic model workflow. HGSOC tumour cells were isolated from tumour samples collected using IMO mapping at the time of primary debulking surgery. Stromal mesothelial cells and fibroblasts were isolated from non-cancerous omentum and cultured until confluent. Tumour cells were stained with CFSE ahead of application to 3D organotypic models for identification during flow cytometry analysis. Layered 3D organotypic models were constructed containing rat tail 1 collagen ECM, stromal cells then tumour cells were applied ahead of 24 hour treatment with 25μM cisplatin. Apoptosis and necrosis readouts were completed using flow cytometry analysis……73

Figure 2.3: Diagrammatic representation of the constructed 3D organotypic model. Image shows the different layers of the model reflecting the peritoneal lining……75

Figure 2.4: Example of 24 well plate culture setup. Diagrammatic example of 24 well plate with 2 tumour site samples. Cells seeded in triplicate in 2D and on 3D organotypic models. Samples treated with 25μM cisplatin for 24 hours then analysed for apoptosis and necrosis using flow cytometry alongside untreated controls……75

Figure 3.1: Kaplan-Meier outcome plots. a/b) Patient outcomes by clinical presentation. Kaplan-Meier curve showing the association between disease status (limited/localised peritoneal carcinosis; diffuse/military small nodule carcinosis) and progression free survival (a; $p = 0.25$) and overall survival (b; $p = 0.22$) ($n = 46$). c/d). Patient outcomes by tumour-free status (presence of residual disease) following primary debulking surgery. Kaplan-Meier curve showing the significant association between tumour-free status (n=40) vs non-tumour free (n=6) and progression free survival (c; $p = 0.067$) and overall survival (d; $p = 0.032$)……88

Figure 3.2: Heterogeneity in apoptotic response to cisplatin. Scatter dot plot of apoptotic response to cisplatin across the ITH patient cohort, displayed grouped by relapse status, wide heterogeneity is observed. Tumour cell samples were plated in triplicate, drug treated with 25μM cisplatin for 24hours. Apoptotic response was analysed via caspase 3/7 response assay and data normalised to viability and calculated as fold induction. Each data point represents individual tumour site response to cisplatin in each patient. Average of 9 sample sites per patient (range 4-15). There is significant difference seen between each patient overall response by Kruskal-Wallis testing P<0.0001).....90

Figure 3.3: Apoptotic response to cisplatin by clinical platinum sensitivity. Tumour cell samples were plated in triplicate, drug treated with 25μM cisplatin for 24hours then apoptotic response analysed via caspase 3/7 assay. Data was normalised to viability and calculated as fold induction. A- Platinum resistant cohort. B- No relapse cohort. C- Platinum sensitive cohort. There is variation in both the degree of response between sample sites within individual patients and across the patients, this is observed in all patient groups. There is significant variation in the average response between patients in each relapse category. Kruskal-Wallis test shows significant variation between overall patient response in the platinum resistant group p<0.0001, platinum sensitive group p<0.0001 and no relapse group p=0.048…….91

Figure 3.4: Tumour site apoptotic response to cisplatin grouped by relapse status. Individual tumour apoptotic results were combined and compared based on patient platinum relapse status. Platinum resistant n=106 tumour cultures, platinum sensitive n=269 tumour cultures, no relapse n=19 tumour cultures. No significant difference in average response to cisplatin was seen between the platinum resistant and platinum sensitive group (p=0.241); the platinum resistant group and the no relapse group (p=0.0789); and the platinum sensitive and no relapse group (p=0.1770)…….92

Figure 3.5: Apoptotic response of omentum tumour cells to cisplatin within the ITH cohort. A – Omental sample apoptotic response to 24hour 25μM cisplatin treatment, each bar represents a single patient sample, cells seeded in triplicate. Significant difference in response was observed across the cohort, p<0.0001 Kruskal-Wallis test. B – Omentum apoptotic results grouped by patient platinum sensitivity on clinical follow up. Platinum resistant samples n=8, platinum sensitive samples n=25. No significant difference was seen in response to cisplatin treatment between the two groups, Mann-Whitney test p=0.46)…….93

Figure 3.6: Median absolute deviation of apoptotic response. Box and whiskers plot showing median absolute deviation (MAD) of sample-wise apoptosis induction fold change of primary cell cultures from ITH patient samples (n=44, range 4-15 samples per patient), grouped by relapse status. (Kruskal-Wallis test p=0.7)…….94

Figure 3.7: Apoptotic response to cisplatin in individual cases. Phenotypic data from the ITH project cases, demonstrating wide heterogeneity in relative apoptotic responses to cisplatin across different anatomical areas and patients. Tumour cells were seeded in triplicate, treated for 24 hours with 25μM cisplatin then apoptotic response examined via caspase 3/7 assay. Case T16-156 (A) had clinical platinum refractory disease, case T16-213 (B) experienced platinum sensitive relapse whilst case T17-280 (C) did not relapse during the follow up period. Statistically significant difference in response to cisplatin could be seen between the individual tumour sites in each patient. (Kruskal-Wallis test: case T16-156 p<0.0001; case T16-213 p=0.0017; case T17-280 p=0.0036…….95

Figure 3.8: IMO mapping in example case. IMO mapping of primary and relapse tumour deposits in case T14-137 showing disseminated pattern of spread across the abdominal cavity at both initial presentation and relapse (relapse case number T17-067)…….96

Figure 3.9 : Apoptotic response to cisplatin in example case with subsequent relapse samples. ITH case T14-137 apoptosis data from tumour cells at A - primary debulking B - and relapse surgery. Tumour cells plated in triplicate. Y axis showing apoptosis assessed by relative caspase 3/7 induction normalised to viability following 24hours 25μM cisplatin treatment. X axis showing sample site by anatomical location. The samples from primary debulking showed statistically significant variation in response to treatment (Kruskal-Wallis test p=0.0106) whereas at relapse there was less variation between samples observed with no significant difference between the relapse sample response rates (Kruskal-Wallis test p=0.07)……...97

Figure 3.10 : Apoptotic response to cisplatin by IMO mapping. Box and whiskers plot showing apoptotic response to cisplatin in different IMO mapped regions. Sample numbers varied by region (A1=12, B1= 63, C1=10, A2=19 B2=68, C2=11, A3=30, B3=21, C3=12, ascites=10. No significant difference in average response to cisplatin was found between different anatomical regions using Kruskal-Wallis analysis p=0.57……..98

Figure 3.11: Apoptotic response to cisplatin by abdominal region. Box and whiskers plot comparing overall apoptotic response to cisplatin between upper, middle, and lower regions of the abdomen and ascites samples. Sample numbers: Upper abdomen=63, middle abdomen=98, lower abdomen=85, ascites=10. No significant difference in average apoptosis levels was observed between the groups by Kruskal-Wallis analysis p=0.57……99

Figure 3.12: Cisplatin IC_{50} values in example case. IC_{50} results for individual tumour samples for case T17-073. Samples tested from multiple sites across the abdominal cavity. The resulting μM cisplatin IC_{50} values for each anatomical location are described above each graph……..100

Figure 3.13: Ki67 staining image examples. Example of staining categories for percentage Ki67 proliferative index. Large images at 4x magnification, inserts at 20x. I = High Ki67, ii = moderate Ki67, iii = low Ki67, iv = No tumour, v&vi = examples of uninterpretable images……...102

Figure 3.14: Percentage Ki67 proliferative index. Percentage Ki67 proliferative index scores across the patient cohort (n= 46) by relapse status. Blue = platinum resistant relapse, black= platinum sensitive relapse, red = no relapse at the time of analysis. (n=5 samples per patient)……...…103

Figure 3.15: Median absolute deviation of Ki67 proliferation index. Median absolute deviation (MAD) of percentage Ki67 proliferation index shows no correlation with relapse status across the patient cohort. No significant difference was observed between the means of different groups with Kruskal-Wallis testing……104

Figure 3.16: Kaplan-Meier curves for Ki67 proliferative index association. Clinical association of Ki67 proliferative index scoring. Kaplan-Meier curve showing the association between the mean Ki67 proliferative index across different disseminated deposits within a patient and progression free survival (PFS, p = 0.92) and overall survival (OS, p = 0.79). Ki67 proliferative index staining was stratified into 3 categories: low (<20%), moderate (21-60%) and high (>60%) across the cohort (n=46)……...…104

Figure 4.1: Processing of omentum for stromal cell extraction. Non-cancerous omentum sample is obtained from theatre (A) in PBS, brought to the lab for processing (B), which involved dissecting to 1-3mm pieces with scalpels (C)……....108

Figure 4.2: Bright light confocal images of stromal cell populations. Bright light confocal images at 10x magnification of stromal cells from case T18-110 at different time points. A- Mesothelial cells isolated and cultured, images taken at 5 days when the cells are achieving confluence and have a characteristic 'cobblestone' appearance. B- Mesothelial cells after 2 weeks' culture have lost their regular morphology and appear senescent. C- Fibroblasts imaged at 5 days demonstrating a slower rate of proliferation compared to the mesothelial cells from the same patient. D- Fibroblasts at 2 weeks, still confluent but showing early signs of loss of structural integrity with bloating of appearance…..109

Figure 4.3: Confirmation of stromal cell populations. Immunofluorescence staining of primary stromal cells. Imaged on Leica Confocal SP5 40x magnification. Case T18-158. Isolated stromal cells were fixed, stained with primary antibody and incubated at 4^{o}C overnight before secondary antibody goat anti-mouse Alexa fluor 488 was applied. A – Mesothelial cells stained with calretinin antibody, DAPI and merged images shown, B- Normal fibroblasts stained with anti-fibroblast surface protein antibody, DAPI and merged images shown. C- There was evidence of cancer cell presence on microscopic examination of the cultures which was confirmed by staining for cancer associated fibroblasts (CAFs) with α-smooth muscle actin, DAPI and merged image shown. Associated negative controls displayed…….110

Figure 4.4: Diagram of 3D organotypic model design. Diagrammatic representation of the constructed 3D organotypic model depicting the different layers of the peritoneal lined omentum……111

Figure 4.5: Brightfield images of 3D organotypic models. Brightfield image at 10x magnification of 3D organotypic model taken from above showing A- different cell populations present. B - mesothelial cells' typical 'cobblestone' clustering, fibroblasts and PE01 ovarian cancer cell line tumour cell labelled……..112

Figure 4.6: Scatter plot FACS analysis of PE01 cell line in 3D model. 3D models containing untreated CFSE stained PE01 cell line cultures were analysed using flow cytometry with concurrent 2D monolayer cultures. Plot A- shows all cells detected in 2D cultures, analysed for apoptosis (Annexin shown in the PE-A channel)) and necrosis (7AAD, shown in the PerCP-Cy5-5-A channel). B – 3D PE01 cultures initially showed high levels of apoptosis and necrosis. CFSE labelled cells detected in the FITC channel. C – a reduction in apoptotic activity in 3D model cell cultures was seen following adjustments to culture composition and processing……...116

Figure 4.7: Scatter plots of FACS analysis 3D cell line models. Example scatter plots from experiment with SKOV3 cells. A –untreated SKOV3 cells in 2D culture. B – SKOV3 cells in 2D culture treated for 24hours with 25μM cisplatin. C- untreated SKOV3 cells in 3D organotypic model. D – SKOV3 cells in 3D organotypic culture treated for 24hours with 25μM cisplatin. All samples show initial selection of tumour cells in analysis via CFSE selection in FITC channel, doublet cells were then removed and analysis for apoptosis (Comp-PE-A) and necrosis (Comp-PerCP-Cy5-5-A)……...117

Figure 4.8: Apoptotic response of HGSOC cell lines to cisplatin in 2D and 3D organotypic models. Cell lines in 2D and 3D organotypic models are treated with 25μM cisplatin. For cell line models, cells were seeded in triplicate prior to 24-hour treatment. The y-axis shows apoptosis levels normalised to viability then expressed as a fold change. Triplicate assays performed. A- Bar chart shows apoptosis normalised to viability for the PE01 and SKOV3 cell lines. Both cell lines show 'expected' sensitivity profile in 2D culture, with the PE0, PE01 line appearing more sensitive than SKOV3. Both cell lines show reduced sensitivity in 3D culture environment. B- Further experiments during optimisation with PE01, PE04 and Kuramochi cell lines again show reduced sensitivity to cisplatin in 3D cultures. Variation in response to treatment between cell lines is observed. Replicate numbers too small to assess statistical significance, trend towards reduced sensitivity in 3D models seen……..118

Figure 4.9: Scatter plots from FACS analysis of 3D organotypic models with primary tumour cells. Case T17-233. Showing apoptosis, (y axis, higher levels shown in quadrant 1 in this example), and necrosis (x axis, higher levels shown in quadrant 3 in this example) readouts from multiple tumour site 3D models. A= Primary, B= Omentum, E= Left Paracolic area, F= Splenic area. Untreated (-ve) and 25μM cisplatin treated (+ve) results shown……...……...….120

Figure 4.10: Apoptotic response to cisplatin 2D culture vs 3D organotypic models case T17-233. Bar chart showing Case T17-233 response to cisplatin treatment across multiple tumour sites in both 2D cultures and 3D organotypic models. N=1 per tumour site culture. Assay readouts for apoptosis and necrosis were normalised to viability then expressed as a fold change of untreated……..……..121

Figure 4.11: Apoptotic response to cisplatin 2D culture vs 3D organotypic models case T18-011. Bar chart from case T18-011 showing multi tumour site analysis of apoptotic response to cisplatin in both 2D and 3D cultures. N=1 per tumour site cultures. Apoptosis and necrosis assay readouts were normalised to viability then expressed as a fold change of untreated control……..……122

Figure 4.12: Apoptotic response to cisplatin 2D culture vs 3D organotypic models, including ascites sample. Bar chart from case T18-085 showing multi tumour site analysis of apoptotic response to cisplatin in both 2D and 3D cultures. N=1 per tumour site culture. Ascites cultures were included in the assay and demonstrate the tendency towards reduced response in ascites samples to cisplatin which can be affected by the culture substrate……123

Figure 4.13: Grouped analysis of all 2D and 3D samples; **response to cisplatin treatment.** Flow cytometry apoptosis readouts from 2D cultures and 3D organotypic models from different cases were combined to observe for statistical significance. n=16 per group. Overall reduced response to cisplatin was observed in the 3D organotypic models (Mann-Whitney test p=0.0288)……..……..124

Figure 4.14: Correlation of apoptotic response in 2D cultures and 3D organotypic models analysed using different assays case T17-233. Graph A shows the bar chart representing response to cisplatin treatment between samples from flow cytometry readouts of 3D models and parallel 2D cultures. Graph B shows bar chart of phenotypic results of apoptotic response to cisplatin using caspase 3/7 assay. Correlation plots representing comparison between the response to cisplatin treatment in 2D ITH phenotypic cultures, 2D cultures processed in parallel with models and in 3D organotypic models. 2D phenotypic data vs 2D model data shows positive correlation with significant r value 0.999 (p=0.001) (C), positive non-significant correlation seen between 2D culture and 3D models (D and E)…….126

Figure 4.15: Correlation between apoptotic response in 2D cultures and 3D organotypic models analysed using different assays case T18-011. Graphs A&B show readouts for apoptotic response to cisplatin analysed by different assays, A- flow cytometry analysis of 2D cultures and 3D organotypic models. B – Phenotypic caspase 3/7 assays undertaken for the ITH project. Plots C, D and E show correlation analysis between the different techniques, non-significant trend towards negative correlation between the different 2D culture analyses was observed (C, p = 0.06) No correlation with 3D results was seen (D p=0.68 & E p=0.62)……128

Figure 5.1: Heatmap showing the relative expression of ECM proteins across the patient cohort. Limited clustering is seen based on sample site or patient…….136

Figure 5.2: Heatmaps by case. Individual case heatmaps showing minimal correlation of protein composition between the different sample sites in all patients……..137

Figure 5.3: Protein-protein interaction map showing the connections between identified upregulated proteins across the sample cohort………139

Figure 5.4: Volcano plots. Volcano plots showing ECM proteins identified by MS analysis, plot A shows proteins found across the primary samples, plot B shows omentum, C shows diaphragm samples, D shows paracolic, E shows splenic samples. Significant variation in the proteins discovered in the different anatomical regions is observed as well as a difference in the quantity of proteins expressed between different tumour sites…….142

Figure 5.5: Venn Diagram of case crossover. Venn diagram depicting the crossover observed in ECM composition between different primary samples. Log2 ratios with a cut off of 1.3 were included in the analysis. Case T16-060 did not have any proteins sufficiently expressed above the 1.3 cut off. Only 1 common component was identified across the remaining 3 cases……..143

Figure 5.6: Crossover in ECM proteins by abdominal region. Venn diagram showing the cross over in ECM proteins observed between the upper, middle and lower abdominal regions. Vast variation is seen with only 2 proteins observed to be present in all areas with log2ratio cut-off of 1.3……..145

Figure 5.7: Analysis of ADH 1A, 1B, 1C expression. A - Scatter plot showing log2 ratios of Alcohol dehydrogenase 1A, 1B and 1C across the sample cohort showing variation in expression between different anatomical locations. Significant differences in mean values per sample were observed by Kruskal-Wallis test (p= 0.02). B – Box and whiskers plot of log2 ratios organised by intra-abdominal region showing significant down regulation in the lower abdominal region compared to both the middle (p=0.0379) and upper (p=0.0343) regions using Mann-Whitney test……...147

Figure 5.8: Analysis of MFAP4 expression. A: Scatter plot showing variation in MFAP 4 ECM protein expression by sample site, no significant difference in mean expression values was found between samples. B: Box and whiskers plot showing MFAP4 expression by abdominal region. No significant difference in mean expression values between abdominal areas was found……148

Figure 5.9: MatrisomeBD data identified collagens in ovarian cancer metastatic sites[303]. Spectrum of collagen proportions identified in HGSOC omental metastatic deposits, compiled for public reference on the MatrisomeBD database……..149

Figure 5.10: ECM Collagen composition analysis. Box and whiskers plot showing the identified collagens within the ECM MS analysis across the sample cohort……..……..150

Figure 5.11: Collagen I expression analysis. Scatter plots showing Collagen I abundance in sample cohort. A - shows variation observed between different anatomical locations, with significant difference observed between sample sites (Kruskal-Wallis test p=0.0069) B - shows variation within individual patient cases with no significant difference in overall expression levels seen……..151

Figure 5.12: Collagen IV expression analysis. A shows a scatter plot of collagen IV values by sample site. Significant variation in the means across the anatomical areas was observed (Kruskal-Wallis analysis p= 0.001). B shows box and whiskers plot of collagen IV variation by abdominal region, with the difference between the middle and lower abdominal areas approaching significance (Mann-Whitney test p=0.053)……152

Figure 5.13: Collagen VI expression analysis. Scatter plots showing Collagen VI distribution displayed by individual sample site (A), by case (B) and further analysis of values within case T17-205 (C) showing the over expression observed in the primary sample which was significantly higher than the other sample sites (Kruskal-Wallis p=0.0005)…….154

Figure 5.14: Fibronectin expression analysis. A- scatter dot plot showing fibronectin expression across different sample sites, no significant difference was observed between expression levels across the locations (one-way anova test p=0.1710). Omental samples appear to have higher expression than primary samples but this was not statistically significant (Mann-Whitney test p=0.114). B – expression levels grouped by anatomical region. Significant variation in expression of fibronectin was seen comparing all regions (Kruskal-Wallis test p=0.0216) and specifically comparing lower region and middle (Mann-Whitney test p=0.0221)……155

Figure 6.1: Ex vivo slice culture study flowchart. A shows collection of tumour tissues assessed by IMO mapping tool, followed by slicing by vibratome then B: culture in multi-well plates 6 well plate with membrane inserts for drug treatment ahead of C: Immunohistochemistry staining of FFPE slices……..159

Figure 6.2: Images of tumour slice sample preparation. Tumour samples were prepared for vibratome sectioning by dividing into approx. 1cm pieces (A) and glued to the cutting platform of the vibratome before being positioned on the vibratome main body (B). Slices were taken (C) at 350 μm and then placed in 6 well plates with transwell inserts (D, E)…….161

Figure 6.3: Brightfield images of H&E stained ex vivo tumour tissue slices. Images taken at 10x magnification. Image A shows omentum tissue slice from case T18-243, image B shows liver metastasis slice from case T19-023……162

Figure 6.2: IHC staining of tissue slices from liver metastatic deposit from case T19-023. Images taken via NDP.view 2 software, main image at 10x, insert at 40x.images at 10xmagnification, scale bar 250um. Images A-D show slice culture at day 1, images E-H show day 4. A and E are H&E staining, B and F show PAX8 tumour cell confirmation, C and G show limited Ki67 positivity in both samples. D and H show cleaved caspase 3 staining……..164

Figure 6.3: IHC staining of tissue slices from omental metastatic deposit from case T18-281 at day both day 0 and after 10 days in culture. Images taken via NDP.view 2 software. Main images at 10x magnification, scale bar 250um., insert at 40x. A and E shows H&E confirmation of tissue structure, B and F shows positive PAX8 staining confirming presence of tumour cells. C and G shows Ki67 positive staining indicating ongoing proliferation activity at both time points. D and H show apoptotic activity through staining for cleaved caspase 3……165

Figure 6.4: Omentum sample from Case T18-243, tumour slices were cultured for 24 hours then drug treated with 25μM Cisplatin for 24 hours with untreated control undergoing media change. I Main images take at 10x magnification, scale bar 250um, inserts at 40x. Images A-D show sections from the untreated slice sample, images E- H show sections from the treated slice sample. Images A and E show H&E staining, B and F show PAX8 confirming tumour cell presence, C and G show Ki67 staining demonstrating proliferative cells in the untreated sample. D and H show cleaved caspase 3, with higher positivity observed in image H……..…167

List of Tables

Table 1.1 Overview of staging protocol. FIGO 2014 staging of ovarian, fallopian tube and peritoneal carcinomas[43]……...……27

Table 2.1: List of anatomical sites examined and numbers of samples across the cohort with corresponding IMO locations……..69

Table 2.2: Primary and secondary antibodies used for confirmation of cell type, with dilutions and incubation conditions………72

Table 2.3: Table summarising H&E staining protocol ……..81

Table 2.4: Summary table of antibodies and reagents used in the IHC by Section of Pathology, Department of Metabolism, Digestion and Reproduction at Charing Cross Hospital………83

Table 3.1: ITH project patient demographics data……86

Table 3.2: Cisplatin IC50 values in different metastatic sites. IC50 values for samples in relapse case T17-067. Whilst heterogeneity was seen, the values were consistently high across the samples showing reduced sensitivity at relapse……101

Table 4.1: Example of sample sites examined in different cases and apoptotic responses to cisplatin. Figure listing different cases where 3D organotypic models were examined and the variation in sample quantities and locations per case. Apoptosis levels normalised to viability and expressed as a fold change of untreated control in 3D models listed showing variation within sample sites and patients……124

Table 5.1: Table showing the sample sites studied profiled from 5 anatomical sites from 4 different patients……..134

Table 5.2: ECM Patient demographics. Showing the patient demographics across the 4 cases based on age, stage and grade of disease, disease state where 0 = limited or localised peritoneal carcinosis and 1 = diffuse milliary small nodule carcinosis and progression free survival (PFS calculated from date of surgery)……...……135

Table 5.3: Top 10 most significantly enriched pathways in STRING database analysis………..138

Table 9.1 Summary table of all patient sample and clinical data: including tumour sample sites, IMO locations and corresponding abdominal region, status after first line treatment, stage and residual disease after primary debulking……200

Table 9.1 Additional apoptotic data from the ITH project (table 1/4) Additional apoptotic data from the ITH cases, apoptosis measured by induction of cleaved caspase 3/7. Apoptosis normalised to viability and expressed as a fold change of untreated control. Broad heterogeneity observed in response to cisplatin between metastatic sites and individual patients……..…211

Table 9.2 Additional IC_{50} data from ITH project (table 1/3): Additional data from the ITH project, cisplatin IC_{50} values for individual sample sites in different cases. Variation in IC_{50} values is seen across the sample cohort……215

Abbreviations

7-AAD	7-amino-actinomycin
ABCB1	TP binding cassette subfamily B member 1
ADH	Alcohol dehydrogenases
AKT	Akt (Protein kinase B, PKB)
ARID1A	AT- rich interaction domain 1A
ATCC	American Type Culture Collection
BCI	Bart's Cancer Institute
BRAF	Serine/Threonine protein kinase B-Raf
BRCA1/2	Breast Cancer gene 1/2
Ca125	Cancer antigen 125
CAF	Cancer associated fibroblast
CCC	Clear cell carcinoma
CCNE1	Cyclin E1
CFSE	Carboxyfluorescein succinimidyl ester
CNA	Copy number alteration
CNV	Copy number variation
CRUK	Cancer Research UK
CT	Computerised tomography
CTNNB1	Catenin beta-1
DAB	Diaminobenzidine
DAPI	4′,6-diamidino-2-phenylindole
DBD	DNA binding domain
DPX	Di-N-Butyl Phthalate in Xylene
DTT	Dithiothreitol
DW	Distilled water
ECM	Extracellular matrix
ECMC	Experimental Cancer Medicine Centre
EDTA	Ethylenediaminetetraacetic acid
EGFR	Epidermal growth factor receptor
EMT	epithelial-mesenchymal transition
EOC	Epithelial ovarian cancer
ER	Oestrogen receptor
ERBB2	Erb-B2 Receptor Tyrosine Kinase 2
ERK	Extracellular-signal regulated kinase
ESGO	European society of gynaecological oncology
ESMO	European society for medical oncology
EtOH	Ethanol
FACS	Fluorescence-activated cell sorting
FCS	Foetal calf serum
FFPE	Formalin fixed, paraffin embedded
FIGO	International Federation of Gynaecology and Obstetrics

FITC	Fluorescein isothiocyanate
FT	Fallopian tubes
GCT	Germ cell tumour
GF-AFC	glycylphenylalanyl-aminofluoroumarin
GFP	Green Fluorescent Protein
GTP	Guanosine triphosphate
GYN	Gynaecology
H&E	Haematoxylin and Eosin
HGSOC	High grade serous ovarian cancer
HIF	Hypoxia-Inducible Factor
HNFH1B	Hepatocyte nuclear factor 1-beta
HNSCC	Head and neck squamous cell carcinoma
HR	Homologous repair
HRD	Homologous repair deficiency
HRP	Horseradish peroxidase
IC50	Half maximal inhibitory concentration
ICHTB	Imperial College Healthcare Tissue Bank
IHC	Immunohistochemistry
IL8	Interleukin 8
IMO	Intraoperative mapping of ovarian cancer
IQR	Interquartile range
ITH	Intratumoural heterogeneity
Ki67	Antigen Ki67
Ki67 PI	Ki67 proliferative index
KRAS	Kirsten rat sarcoma viral oncogene homolog
LGSOC	Low grade serous ovarian cancer
MAD	Median absolute deviation
MAP	Mitogen activated protein
MAPK	Mitogen-activated protein kinases
MDR1	Multidrug resistance protein
MEDICC	Minimum event distance for intra-tumour copy number comparison
MEK	Mitogen-activated protein kinase
MFAP	Microfibril-associated glycoprotein
MMP	Matrix metalloproteinases
MOC	Mucinous ovarian carcinoma
MRI	Magnetic resonance imaging
MS	Mass Spectrometry
MTT	Mono-tetrazolium salt: 3-(4,5-dimethylthiazol-2-yl)-2,5-diphenyl-2H-tetrazolium bromide
NHS	National Health Service
NICE	National Institute for Clinical Excellence
NIHR	National Institute for Health Research
NK T cells	Natural killer T cells

NRAS	Neuroblastoma RAS viral oncogene homolog
OS	Overall survival
OSE	Ovarian surface epithelium
PARP	Poly–ADP ribose polymerase
PAX8	Paired box gene 8
PBS	Phosphate buffered saline
PCR	Polymerase chain reaction
PDO	Patient derived organoids
PDX	Patient derived xenograft
PE	Phycoerythrin
PFA	Paraformaldehyde
PFS	Progression free survival
PIK3CA	Phosphatidylinositol-4,5-bisphosphate 3-kinase catalytic substrate a
PTEN	Phosphatase and tensin homolog
RAD51	DNA repair protein RAD51 homolog
RAF	RAF proto-oncogene serine/threonine-protein kinase
RAS	Rat sarcoma virus
RECAP	Repair capacity test
RNF43	Ring finger protein 43
RPMI	Roswell Park Memorial Institute
RPPA	Reverse phase protein array
SBOT	Serous borderline tumour
SCC	Squamous cell carcinoma
SCNA	Somatic copy number alterations
SCST	Sex cord stromal tumour
SD	Standard deviation
SDS	Sodium dodecyl sulphate
STIC	Serous tubal intra-epithelial carcinoma
STRING	Search tool for the retrieval of interacting genes
TAM	Tumour associated macrophages
TBS	Tris-buffered saline
TCGA	The cancer genome atlas
TGFBI	Transforming growth factor beta induced protein ig-h3
TME	Tumour microenvironment
TMP	Tumour-matrix protein
TMT	Tandem mass tag
TP53	Tumour protein 53
TRUST	Trial of upfront surgical therapy
TUNEL	Terminal deoxynucleotidyl transferase dUTP nick end labeling
VEGF	Vascular endothelial growth factor
WGS	Whole genome sequencing
WT1	Wilms tumour 1

Chapter 1

Introduction

1 Introduction

1.1 Introduction to ovarian cancer

Ovarian cancer is the sixth most common cancer in women with around 7500 new cases diagnosed each year in the UK[1] and is the most lethal of the gynaecological malignancies. The term Ovarian cancer encompasses a heterogeneous group of malignancies that vary in aetiology, molecular biology, and numerous other characteristics[2, 3]. Epithelial Ovarian cancer (EOC) is the most common subtype, accounting for around 90% of the total cases diagnosed[4]. The remaining 10% is composed of malignant germ cell tumours (GCT) and sex cord stromal tumours (SCST), of which the most common type are granulosa cell tumours[5].

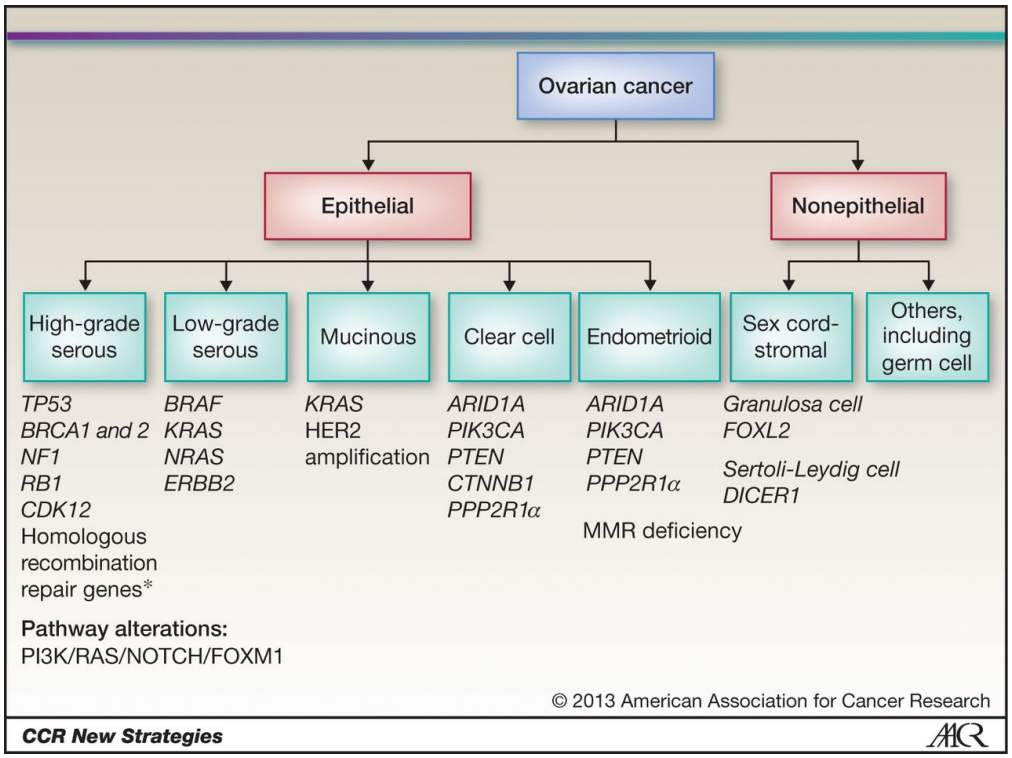


Figure 1.1: Principle Histological subtypes of Ovarian Cancer. *Breakdown of the histological subtypes of epithelial and non-epithelial ovarian cancer and the known associated mutations and pathway alterations [6]*

The lifetime risk of developing EOC is approximately 1.6% with the latest statistics estimating around 1 in 50 women being diagnosed in their lifetime[7].

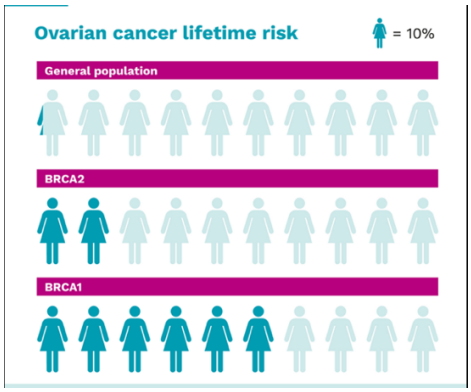


Figure 1.2: Ovarian Cancer lifetime risk. *Diagrammatic representation of lifetime risk of developing ovarian cancer in the general population, around 1.6% in comparison to those with BRCA mutations (BRCA2 around 20%, BRCA1 around 60%[8].*

EOC can be further sub-divided by histological subtype into – High and Low Grade Serous, Clear cell, Endometrioid and Mucinous. High Grade Serous Ovarian Cancer (HGSOC) accounts for around 70-80% of Epithelial ovarian cancers[9]. These histological subtypes were originally split into 2 different categories depending on their characteristics described by their grading. Type I cancers are characteristically more indolent in their behaviour with better understood precursor lesions from the ovary and more stable genomic profiles[10]. Type I cancers include low grade serous, low grade endometrioid, mucinous and clear cell carcinoma. Type II tend to be poorly differentiated, genetically unstable, highly aggressive high grade carcinomas and include high grade serous, high grade endometrioid and undifferentiated types[11].

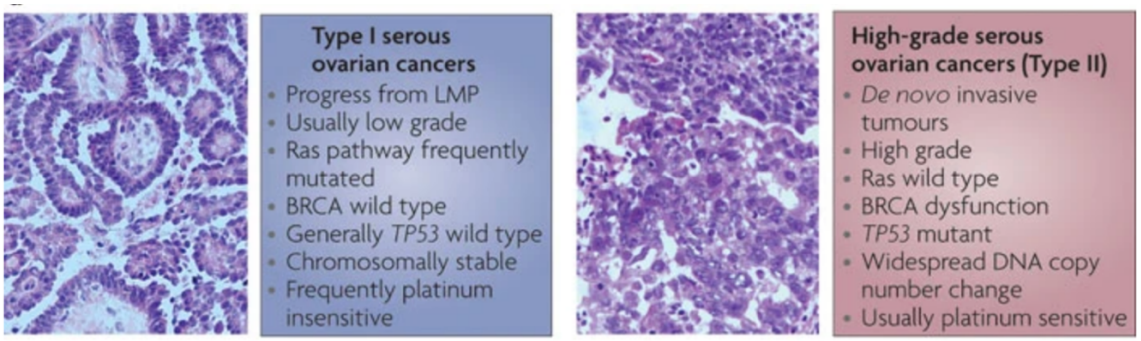


Figure 1.3: Type 1 and Type 2 serous ovarian cancers. *Overview of the distinguishing characteristic features between Type 1 and Type 2 serous ovarian cancers[12]*

This project focused on the study of High Grade Serous Ovarian Cancer (HGSOC) however a review of the other subtypes is given below.

1.2 Epithelial ovarian cancer subtypes

1.2.1 Clear Cell Carcinoma

Clear cell carcinoma (CCC) of the ovary is a distinct cancer subtype, occurring more predominantly in the younger population[13]. It is the second most common epithelial ovarian cancer, accounting for around 5-25% of cases, depending on geographical location[14]. There is variation in prevalence based on geography and ethnicity with more cases within populations in countries such as Japan, Korea and Taiwan[15]. It has clear links to the condition endometriosis and it is estimated around 50% of cases can be shown to be as a direct consequence of endometriosis[16].

Immunohistochemistry of clear cell carcinoma is typically positive for napsin A and hepatocyte nuclear factor 1-beta (HNF1β), and negative for Wilms tumour 1 (WT1) and estrogen receptor (ER). The most frequent gene alterations in clear cell carcinoma are in the AT-rich interaction domain 1A (*ARID1A*) and phosphatidylinositol-4,5-bisphosphate 3-kinase catalytic subunit α (*PIK3CA*) genes (both occurring in about 50% of cases)[17]. Unlike high-grade serous carcinoma, clear cell carcinomas usually negative for *p53* mutation and have a lower frequency of *BRCA1* and *BRCA2* mutations[18].

A higher proportion of patients with clear cell carcinoma are diagnosed at an early stage compared to other EOC subtypes with one study finding 62% of patients were stage 1 at diagnosis (54.6% stage IA, 28.2% IB and 17.3% IC)[19]. The prognosis of patients with clear cell carcinoma varies greatly depending on stage at diagnosis with an overall more favourable outcome than serous carcinomas if detected at stages I and II. The prognosis for diagnosis at stage III and IV is significantly poorer compared to that of patients with serous carcinomas [20].

Current guidance from the European Society for Medical Oncology-European Society of Gynaecological Oncology (ESMO-ESGO) consensus conference recommendations on ovarian cancer indicate that the benefit of adjuvant chemotherapy is uncertain for patients with stage IA, IB, and IC1 clear cell carcinoma, and no adjuvant chemotherapy is recommended for patients with stage IA, IB, and IC1 clear cell carcinoma who have had complete surgical staging[21]. Patients with later stage disease should receive adjuvant platinum-based chemotherapy as per standard protocols.

1.2.2 Endometrioid Carcinoma

Endometroid carcinoma accounts for around 10-15% of all EOC[22]. It also has an association with endometriosis and Lynch syndrome. There is often a synchronous diagnosis of endometrial cancer present with endometrioid cancer. The majority of cases are low grade and diagnosed at an early stage leading to a better prognosis. Low grade, FIGO grades 1-2, immunohistochemistry typically show a classical profile comprising WT1 negativity, wild-type tumour protein *p53* expression, and ER positivity[23]. High grade cases, FIGO grade 3 are much less common, with prevalence quoted around 5-19% of endometrioid ovarian cancer cases. Historically grade 3 cases have been difficult to distinguish between HGSOC using immunohistochemistry, with the use of WT1 staining becoming an important discriminating tool between the two. Cases previously diagnosed as endometrioid carcinoma have been reassigned to HGSOC following positive staining for WT1, the distinction between the two subtypes confirmed by transcriptomic data demonstrating nuclear WT1 expression in HGSOC cases as a distinguishing marker [24, 25]. The outcomes for high grade endometrioid cases are generally poor with one study finding 5 year overall survival of 38.6% [26]. Whole genome sequencing of endometrioid ovarian carcinomas has shown a distinct and heterogeneous genomic profile with significant mutations in *PTEN*, *CTNNB1, PIK3CA, KMT2D, KMT2B, PIK3R1, ARID1A* and *TP53*, demonstrating a similar profile to many uterine endometrioid carcinomas[27].

Current treatment protocols follow guidance based on stage as per FIGO staging and grade at diagnosis, with the mainstay of treatment being surgical cytoreduction +/- platinum based chemotherapy.

1.2.3 Mucinous Ovarian Carcinoma

Mucinous ovarian carcinoma (MOC) is a rare separate entity within the EOC diseases with current prevalence estimations of around 3% of EOC cases[28]. The distinction between true primary MOC tumours and mucinous carcinomas which have metastasised to the ovary (usually from the gastrointestinal tract, pancreas or gall bladder) has been notoriously difficult to distinguish as there is overlap in the expression and immunohistochemistry profiles[29, 30]. MOC is the most common subtype found amongst the under 40 EOC population, and the only risk factor found to be associated is smoking. Current theories of tumorigenesis recognise the

acquisition of cancer hallmarks driven by the stepwise collection of genetic events. Cheasley et al. investigated this progression pathway and proposed that mucinous benign cystadenomas and mucinous borderline ovarian tumours are presumed precursor lesions to MOC[31]. They found that the most frequent genetic event in MOC tumours was copy number loss or mutation in *CDKN2A* (76% of cases), followed by mutations in *KRAS* and *TP53* (both 64%). Amplification of *ERBB2* (26% of cases) and mutations in *RNF43, BRAF, PIK3CA* and *ARID1A* (8–12% of cases) were the next most frequent. They also found that primary MOC tumours were genetically distinct from high-grade serous ovarian, endometrial, gastric and colorectal tumours, including mucinous colorectal carcinomas and appendiceal cancers[31]. On investigating the link with benign precursor lesions, they found that MOC, including high grade MOC, share similar mutational profiles to benign and borderline precursors, for example mutations in *KRAS, BRAF* and/or *CDKN2A* were present in 95% borderline tumours, 95% grade 1 MOC, 88.6% grade 2 MOC and 83% grade 3 MOC[31].

Despite its individuality within EOC, the treatment protocols currently remain as per the umbrella guidance of surgery +/- systemic chemotherapy. Diagnosis is often fortunately at an early stage therefore surgery can be curative[32]. MOC tumours notoriously do not respond well to traditional platinum-based chemotherapy, median survival for stage III/IV is less than 15 months which is significantly less than serous and endometrioid subtypes. Due to the lack of observed HRD signatures or *BRCA* mutations within MOC tumours use of more targeted therapies such as PARP inhibitors is restricted. There is evidence that RAS/RAF inhibitors may be of benefit due to mutations in *BRAF/NRAS* and *KRAS* which have been found in over 70% of cases[32]. The PI3-kinase pathway may also be a potential target[33, 34].

1.2.4 Low grade serous ovarian carcinoma

Low grade serous ovarian carcinoma (LGSOC) accounts for around only 10-15% of all EOC[35]. There are several key clinical and molecular differences between low and high grade serous carcinoma. Patients diagnosed with LGSOC tend to fall into a lower age cohort and tend to have a better prognosis, despite a reduced response rate to traditional platinum/taxane based chemotherapy regimens. LGSOC has been hypothesized to arise from a serous cystadenoma or adenofibroma which progresses to serous borderline tumour (SBOT), to non-invasive micropapillary SBOT and then to invasive micropapillary serous borderline tumour in a slow stepwise fashion[36]. LGSOC tumours have been found to have varying rates of *BRAF* and

KRAS mutations in different studies[37]. They demonstrate alterations in MAP/ERK signalling but have a low prevalence of *p53* mutations[38]. *BRCA* mutations are rare in LGSOC [39].

Initial diagnosis follows a similar pathway with symptoms and investigations as per HGSOC. Serum cancer antigen 125 (CA125) should be measured and is usually above the cut-off 'normal' value, but its levels are lower than those measured in patients with HGSOC.

Primary debulking surgery is the cornerstone of management for higher stage disease, fertility sparing surgery can be considered for those in a younger age bracket and with stage IA-IC1 disease. If primary debulking surgery is performed, residual disease status has been shown to be an independent factor for prognosis[40].

LGSOC is a slow progressing disease and thus is less responsive to traditional platinum-based chemotherapy treatments. A proportion of LGSOC are found to be hormone receptor positive and this is an avenue being explored to expand treatment options. Additionally, MEK inhibitors are emerging as potential active agents and may well represent an effective therapeutic strategy in the future, possibly in combination therapies for example with BRAF inhibitors [41, 42].

1.3 Staging of Ovarian Cancers

Staging of EOC follows the International Federation of Gynaecological Oncology (FIGO) 2014 guidelines. Cancer staging is a core principle in understanding the severity of patients' clinical condition, predicting the outcome, and planning adequate treatment. Staging occurs at the initial presentation and is based on disease spread determined by findings on imaging undertaken e.g. computerised tomography of the abdomen, pelvis and chest; or through surgical staging with biopsies taken and sent for histological analysis. Surgical staging is more common in those presumed to have early stage disease on scan who may be having surgery aiming to treat disease whilst preserving fertility or to confirm early stage disease in those at time of presumed curative surgery. In some countries, laparoscopic surgery is performed as part of the staging journey to determine disease extent within the abdomen. This is not the routine practice within the UK. Currently for the purposes of staging, all ovarian cancers are grouped together within the FIGO criteria however treatment modalities may differ depending on the histological subtype. Once a stage has been assigned at diagnosis this is not altered irrespective of patterns of relapse.

I	Tumor confined to ovaries or fallopian tube(s)	T1
IA	Tumor limited to one ovary (capsule intact) or fallopian tube, No tumor on ovarian or fallopian tube surface No malignant cells in the ascites or peritoneal washings	T1a
IB	Tumor limited to both ovaries (capsules intact) or fallopian tubes No tumor on ovarian or fallopian tube surface No malignant cells in the ascites or peritoneal washings	T1b
IC	Tumor limited to one or both ovaries or fallopian tubes, with any of the following: IC1 Surgical spill intraoperatively IC2 Capsule ruptured before surgery or tumor on ovarian or fallopian tube surface IC3 Malignant cells present in the ascites or peritoneal washings	T1c
II	Tumor involves one or both ovaries or fallopian tubes with pelvic extension (below pelvic brim) or peritoneal cancer (Tp)	T2
IIA	Extension and/or implants on the uterus and/or fallopian tubes/and/or ovaries	T2a
IIB	Extension to other pelvic intraperitoneal tissues	T2b
III	Tumor involves one or both ovaries, or fallopian tubes, or primary peritoneal cancer, with cytologically or histologically confirmed spread to the peritoneum outside the pelvis and/or metastasis to the retroperitoneal lymph nodes	T3
IIIA	Metastasis to the retroperitoneal lymph nodes with or without microscopic peritoneal involvement beyond the pelvis	T1,T2,T3aN1
IIIA1	Positive retroperitoneal lymph nodes only (cytologically or histologically proven)	
IIIA1(i)	Metastasis ≤ 10 mm in greatest dimension (note this is tumor dimension and not lymph node dimension)	T3a/T3aN1
IIIA1(ii)	Metastasis > 10 mm in greatest dimension	
IIIA 2	Microscopic extrapelvic (above the pelvic brim) peritoneal involvement with or without positive retroperitoneal lymph nodes	T3a/T3aN1
IIIB	Macroscopic peritoneal metastases beyond the pelvic brim ≤ 2 cm in greatest dimension, with or without metastasis to the retroperitoneal lymph nodes	T3b/T3bN1
III C	Macroscopic peritoneal metastases beyond the pelvic brim > 2 cm in greatest dimension, with or without metastases to the retroperitoneal nodes (Note 1)	T3c/T3cN1
IV	Distant metastasis excluding peritoneal metastases Stage IV A: Pleural effusion with positive cytology Stage IV B: Metastases to extra-abdominal organs (including inguinal lymph nodes and lymph nodes outside of abdominal cavity) (Note 2) (Note 1: includes extension of tumor to capsule of liver and spleen without parenchymal involvement of either organ) (Note 2: Parenchymal metastases are Stage IV B)	Any T, Any N, M1 T3c/T3cN1)

Notes:
1. Includes extension of tumor to capsule of liver and spleen without parenchymal involvement of either organ.
2. Parenchymal metastases are Stage IV B.

Table 1.1 Overview of staging protocol. *FIGO 2014 staging of ovarian, fallopian tube and peritoneal carcinomas [43]*

1.4 Introduction to High Grade Serous Ovarian Cancer

1.4.1 Presentation

HGSOC is the most common subtype of EOC accounting for around 70-80% of cases. Despite continual advances in diagnostic techniques, it is still most commonly diagnosed at a late FIGO stage III-IV with broad dissemination of disease throughout the peritoneal cavity.

Mortality rates for HGSOC have remained rather static over the course of the last 40 years since the introduction of platinum-based chemotherapy agents[44]. This lack of improvement in mortality outcomes is despite advances in treatment options with advanced cytoreductive surgical techniques and introduction of novel targeted therapies. Whilst the introduction of PARP inhibitors has provided significant improvement in progression-free survival (PFS) statistics, overall survival (OS) is not being greatly affected [45]. The reasons for poor prognosis are multifactorial but include lack of screening tools, delayed presentation leading

to late stage at diagnosis, heterogeneity in tumour biology and the development of resistance to therapeutic agents.

One of the main challenges with HGSOC is the delayed diagnosis due to a very vague symptom profile at initial presentation. Patients may present with abdominal bloating, pain, weight change and bladder disturbance, all of which can be put down to other less sinister conditions and so do not always prompt timely investigation[46]. Once clinical suspicion has been raised, the diagnosis is made using imaging with ultrasound, CT and magnetic resonance (MR) scans. The tumour marker CA125 is used in conjunction with imaging to guide for likelihood of diagnoses, however it can be non-specific as a marker for HGSOC and in some cases, does not rise. The membrane bound protein CA125 was discovered in the 1980s when it was found on the surface of cells undergoing metaplastic change to Mullerian type epithelium[47]. It has proven to be elevated in parallel with gynaecological processes including HGSOC however can be increased due to other inflammatory causes and sometimes does not rise in HGSOC[48]. Confirmation of diagnosis can be made via imaging or surgical guided biopsy for histological analysis.

1.4.2 Aetiology

Factors found to increase the risk of developing HGSOC include age, with most diagnoses made after 40 years, a steep rise after 50, peaking in the 80s. Up to 20% of ovarian cancers have a hereditary component with the vast majority having *BRCA1* and *2* mutations; there is also an association with hereditary non-polyposis colorectal cancer [49]. Other risk factors include previous breast cancer, nulliparity, history of endometriosis, and also long-term use of hormone replacement therapy. Conversely, prolonged use of combined oral contraceptive medication, parity, and breastfeeding have been associated with risk reduction as well as history of tubal ligation and hysterectomy[50].

Different theories exist about the pathogenesis of HGSOC. Historically it was believed to arise from the epithelial surface of the ovary however there is now an increasing body of evidence that fallopian tube secretory epithelial cells may harbour the precursor lesion, and so in some cases where the disease is seen on the ovary this may already be a site of metastases[51, 52]. Supporters of the serous tubal intra epithelial carcinoma (STIC) precursor theory reference the finding of occult carcinomas in fallopian tubes during prophylactic bilateral

salpingoophorectomies for *BRCA* status [53, 54]. Studies have further reported genomic analysis of fallopian tube lesions suggesting STICs to be the precursor lesion for ovarian carcinoma with a possible indolent time of 7 years ahead of metastasis to the ovary prior to a rapid further dissemination[51]. Mutational analysis of HGSOC tumours with concurrent STIC lesions assessing *p53* immunostaining identified clonal relationships between the tumours and STIC lesions, indicating STICs to be the precursor lesion for the majority of samples analysed [55].

However, others debate that STICs are not found ubiquitously in HGSOC and that a dualistic pathway of tumourigenesis exists with different variables determining the likely precursor lesion[56]. It has been further supported that a dualistic pathway exists and determining the precursor lesion of origin may provide insight into patient response to treatment[57].

If one follows the fallopian tube-based theory of carcinogenesis, then HGSOC develops per definition in a state of diffusely disseminated disease. In most of these cases the tube itself can appear macroscopically normal which reduces the chances of the disease being detected at an early stage for example on imaging.

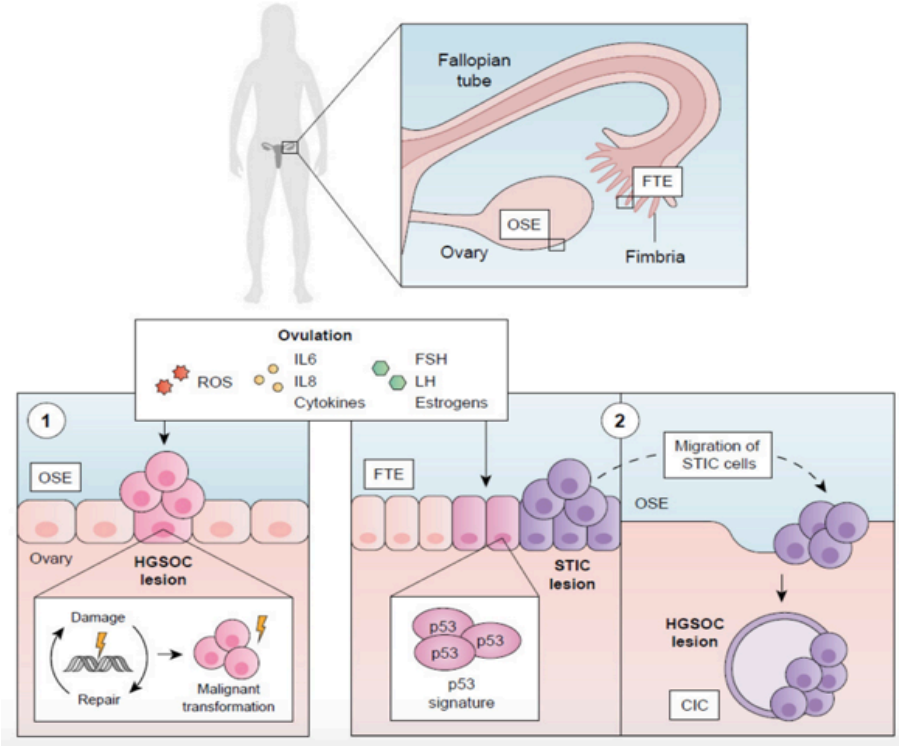


Figure 1.4: Dualistic pathway of HGSOC precursor lesions*. Proposed dualistic pathway for HGSOC pathogenesis with precursor lesions possible from both the ovarian surface epithelium and STIC lesions in the fallopian tubes[58].*

The consensus appears to be moving towards both options being likely, that precursor lesions may arise from either the ovarian surface epithelium or the fallopian tube. What also seems to be apparent is determining the origin could shed light on potential markers for diagnosis, response to treatment and prognosis [57].

Molecular and genetic data analysed from samples of patients taken from ovary, fallopian tube and in cases of primary peritoneal carcinoma infer a similar origin[59]. Therefore, these cancers are grouped together for determination of management strategies.

HGSOC tends to metastasise in a common pattern like a rash across the peritoneum in all quadrants of the abdominal cavity, in particular with gross infiltration of the adipocyte rich omentum[60]. Tumour cells shed from the ovaries and tubes into the peritoneal cavity then a diffuse spread of tumour cells across all intra-abdominal surfaces is facilitated by the circulation of physiologically occurring intra-peritoneal fluid. This rapid pattern of dissemination contributes to the subtle and deceptive nature of symptoms which are often ignored by patients when initially experienced[61]. In most cases where there is peritoneal dissemination, there will also be lymphogenic spread along the iliac and retroperitoneal route following the course of the ovarian vessels in chains along the aorta and vena cava to the level of the insertion of the renal vessels.

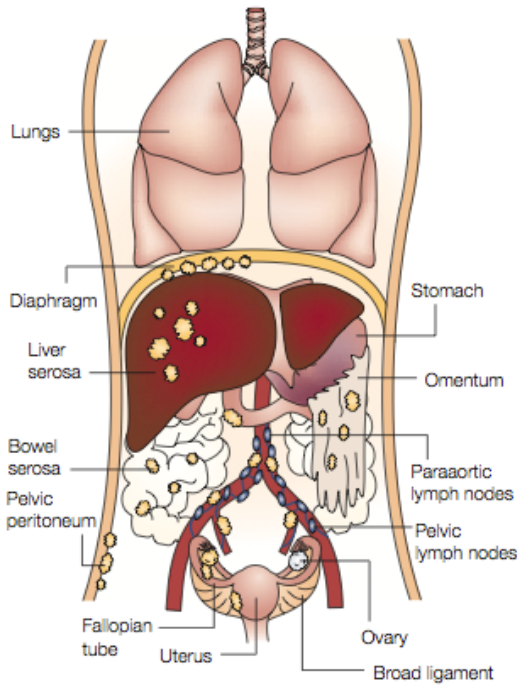


Figure 1.5: Dissemination patterns of HGSOC. *Diagrammatic representation of the dissemination patterns of ovarian cancer showing spread of nodular disease throughout the peritoneal lined abdominal cavity.[62]*

However, despite our understanding of the routes of metastatic spread we are still unable to associate patterns of tumour dissemination with clinical and surgical outcome, probability of relapse and platinum sensitivity[63].

1.4.3 Management

Over the last few decades, there has been significant clinical progression in the treatment of HGSOC, with advances in both surgery and therapeutic options. These include the development and addition of extensive cytoreductive techniques, refinement of surgical skills, dose-dense chemotherapy regimens, and introduction of novel targeted therapies. Nevertheless, the low cure rate of women with HGSOC has changed little since the revolutionary platinum-based treatment that was introduced over 30 years ago[64]. Management emphasis has moved from providing cure towards producing a chronic disease picture with the possibility of multiple treatment regimens[65].

Management and prognosis are determined by stage at presentation and histological grading following biopsy or debulking surgery.

Treatment of HGSOC is from a multidisciplinary approach with input from expert gynaecological oncologists, medical oncologists, pathologists, and radiologists. The mainstay of treatment is surgical cytoreduction (debulking surgery) combined with systemic agents.
Advanced age, FIGO stage IV disease and grossly visible residual disease post-surgery are associated with poor prognosis in HGSOC[66]. Complete macroscopic clearance of tumour during primary cytoreductive surgery is associated with more favourable survival outcomes[67]. Internationally, there is ongoing debate as to the best timing of surgery, whether this should be done at the outset of treatment (primary debulking), or following a course of neoadjuvant chemotherapy, with the argument that giving chemotherapy prior to surgery reduces tumour burden and therefore lessens the potential associated morbidity. However, the generally recommended course of treatment for those patients with good performance status and resectable disease is maximal effort primary cytoreductive surgery followed by adjuvant chemotherapy[68]. Neoadjuvant chemotherapy is used where the extent of the disease at the time of presentation is deemed to be not suitable for surgical resection or if the patient is not fit enough to undergo a primary debulking due to advanced age, low performance status, and comorbidities. Where some previous trials have suggested neoadjuvant chemotherapy prior to

interval debulking may show equal patient outcomes compared to primary debulking patients, there is the concern that the standard of surgical skills was not homogeneous at the participating centres which could lead to poorer outcomes if efforts towards total cytoreduction were not optimal. The TRUST (Trial of upfront surgical therapy - NCT02828618) trial is an international open, randomized, controlled multicentre trial investigating overall survival after primary debulking surgery versus neo-adjuvant chemotherapy and subsequent interval debulking surgery in patients with FIGO stage IIIB-IVB ovarian, tubal, and peritoneal carcinoma[69]. This has incorporated centres with standardised surgical techniques and quality therefore will be able to show comparable outcomes. Results are expected in 2024.

Following surgical management, the majority of patients will undergo systemic chemotherapy. Platinum based chemotherapy is the mainstay of systemic treatment, usually carboplatin +/- the addition of paclitaxel and up to 80% of patients will respond to first line treatment. 95% of patients will receive this combination as first line[70].

Carboplatin is a 'second-generation' platinum compound, with similar qualitative spectrum of activity to the previously highly utilised cisplatin. However, the toxicity profile of carboplatin is significantly better than cisplatin, with nephrotoxicity, neurotoxicity and ototoxicity occurring only infrequently with carboplatin. As with cisplatin, nausea and vomiting occur in many patients after carboplatin administration, however to a lesser degree. The dose-limiting toxicity of carboplatin is myelosuppression, with severe thrombocytopenia and less often leucopenia seen[71].

Additional systemic treatments in the form of the anti-angiogenic VEGF inhibitor Bevacizumab have been shown to significantly prolong progression free survival (PFS) and overall survival (OS) in those patients with residual disease post-surgery or with distant metastases[72, 73].

Multiple trials have investigated the use of PARP inhibitors as giving an additional benefit in those patients with *BRCA 1/2* mutations and in patients with homologous repair deficiency (HRD) positive tumours. Significant improvement in PFS in these select groups of patients has been shown and PARP inhibitors are now incorporated into treatment protocols in this setting[74]. The increasing recognition of the importance of testing for HRD status as well as

BRCA analysis of tumours is prompting the search for more reliable testing strategies[75]. After the success of multiple PARP inhibitor trials, current guidelines in the UK recommend first line PARP inhibitor use in patients with *BRCA* mutations or HRD positive tumours. Niraparib has also been licensed for maintenance therapy in patients without *BRCA* mutations in the UK[74, 76].

The barriers to improving outcomes in terms of PFS and OS lie with multiple issues which will be discussed further.

1.4.4 Heterogeneity in HGSOC

Tumour biology plays a huge part in the determination of response to treatment and patient outcome. Vast variation is seen in the behaviour of tumours, both between different patients and also between metastatic sites within the same patient in HGSOC. While these differences have been recognised, they are still not well understood.

Inter-tumoural heterogeneity refers to the different characteristics in tumour biology that exist between different patients with the same histological subtype[77]. This can arise due to genetic or environmental factors. For example analysis of TCGA data has shown a link between poor outcomes in HGSOC and expression of genes associated with obesity and lipid metabolism, specifically *CD36* and *TGFβ*[78]. Another study has suggested that obesity may be linked to increased peritoneal metastatic dissemination in HGSOC through activation of pro-inflammatory chemokines and recruitment of macrophages[79].

Intra-tumoural heterogeneity (ITH) refers to the variation displayed within and between tumours in one patient, occuring due to the existence of distinct subpopulations of cancer cells within tumour deposits. This heterogeneity can manifest as genetic, epigenetic, or phenotypic differences. In HGSOC, ITH has been observed at multiple levels, including subclonal genomic alterations, differential gene expression patterns, and diverse morphology and cellular behavior[80, 81]. Genetic profiling of patients' tumours including assessment of *BRCA 1/2* and HRD status is increasingly becoming recommended in the hope of developing patient targeted treatment protocols.

Genomic heterogeneity is reflected in the differences in DNA sequences and molecular profiles between tumour cells. HGSOC is characterised at the molecular level by ubiquitous *TP53*

mutations and a high frequency of homologous recombination DNA repair defects and copy number aberrations[82, 83]. As a transcription regulator p53 is directly involved in cellular homeostasis and genome regulation and plays an important role in tumour suppression[84]. Activation of p53 leads to different outcomes depending on the context of the cellular situation, including cell differentiation, cell cycle arrest and apoptosis[85]. Mutation of *TP53* can result in either loss-of-function or gain-of-function phenotypes. Loss-of-function mutations can lead to progression of cancer through the inability of the cell to induce either DNA repair or apoptotic cell death[86]. Gain-of-function mutations in *TP53* have been shown to increase tumour metastasis and promote resistance to chemotherapy[87, 88]. These widespread mutations result in disruption of key cellular processes, an unstable genetic character and heterogeneity. In HGSOC one study examined *TP53* sequencing data which showed mutation in *TP53* in 94% of cases, 62% were missense mutations with 82% of mutations being with the DNA binding domain (DBD)[89]. *TP53* mutations may result in loss of wild type function through loss of DNA-binding activity[90]. Analysis of TCGA data has suggested higher, practically universal mutations levels across HGSOC cases, 60.5% of which were missense mutations, 15.2% were frameshift mutations, 10.5% splice site, nonsense 10.7% and in-frame 3.22%[91].

TP53 mutations are found to have high correlation with copy number heterogeneity and chromosomal instability in tumours[92]. HGSOC displays high levels of copy number alterations (CNAs) leading to amplifications of oncogenes and tumour suppressor gene suppression. CNAs are a direct contributor to tumoural heterogeneity both between primary and metastatic sites and different patients[93]. Analysis of whole genome sequencing (WGS) of copy number data from tumour samples from 132 HGSOC patients identified 7 copy number signatures, further analysis showed variation in patient outcome dependent on copy number signature and a relationship between copy number signature and platinum resistance. Copy number signature 1 which showed oncogenic RAS signalling was predictive of platinum resistant relapse and poor outcome. Whereas copy number signature 3 which had *BRCA1/2* related HRD showed improved OS[94].

BRCA1 and *BRCA2* mutations are quoted to be found in 17-25% of HGSOC cases with 75% of these being germline mutations and 25% somatic [95]. Defects in homologous recombination repair (HRR) pathways occur in around a further 25% of patients distinct from *BRCA* mutations, but in part because of observed *BRCA1* methylation[91, 96]. *BRCA1* methylation quantitation has been found to be able to predict clinical response rates to the

PARP inhibitor Rucaparib[97]. Alternative HR defects involve mutations in HR pathway genes such as *RAD51C, RAD51D, PALB2*[98]. TCGA data analysis estimates around 50% of HGSOC tumours to display deficiency in homologous recombination[91]. The patients with *BRCA 1* and *2* mutations have been found to have better response rates to first and second line treatments with improvements in both PFS and OS[99][100].

One of the first studies to examine ITH was from the Shah group where they performed genomic profiling of HGSOC tumours from primary and metastatic sites in 6 patients and found vast heterogeneity with only 51.5% conservation of mutations present across all tumour samples within different patients[101]. They also found variation in the cellular frequencies within individual tumour deposits suggesting intra-tumoural clonal diversity. Mutations in expected genes e.g. *PIK3CA* were identified but found to not be consistent across all metastatic deposits from the same patient [101]. These discoveries highlight the potential difficulties in the search for targetable pathways with the lack of consistency seen between different patients and anatomical sites.

The Shah group further investigated heterogeneity in the immune profile of the tumour microenvironment (TME) in HGSOC. Analysis of WGS from 160 tumour samples from 42 chemotherapy naïve patients was performed. Tumour sample locations included the adnexa, omentum, peritoneum, bowel and ascites. Immune cell composition was observed to vary between anatomical locations within patients[102]. 10 major T and NK cell clusters and 41 minor clusters were identified and site specific cluster analysis was performed. Comparisons of the anatomical sites showed predominantly naïve/stem-like and memory T cell enrichment in the non-adnexal regions versus dysfunctional T cell enrichment in the adnexa in 19/31 patients. Higher in-site variation in T cell enrichment was seen in the adnexal samples compared to non-adnexal, suggesting co-existence of differentiated states within primary tumour locations. These findings reflect the immunoreactivity in early cancer development compared to the apparent immune escape in metastatic sites. Distinct inter-patient and intra-tumoural TME heterogeneity suggested that the mechanisms of immune response are not universal[102]. These results highlight the importance of development of personalised targeted therapies to address the issues tumoural and microenvironment heterogeneity present.

A further study analysing ITH through clonal variation in primary and metastatic samples found 70% more unique clones within tubo-ovarian samples compared to metastatic sites. Conversely, there were 14% less unique clones within ascites samples [103]. Many studies use

single site sampling for analysis, which, based on emerging data on metastatic site heterogeneity, are likely to not be representative of the whole tumour cohort.

Clinically, genomic heterogeneity in metastatic sites may have a direct impact on treatment selection for patients. As stated previously PARP inhibitors are now in widespread use for those patients with *BRCA* mutations or HRD positive tumours, although within the UK Niraparib is licensed as a maintenance treatment for patients without a *BRCA 1 or 2* mutation in Stage III-IV HGSOC[104]. Cunnea et. al observed that HRD status is not consistent across tumour samples collected from different tumour deposits within individual patients with 22% of patients showing mixed HR status i.e had tumours from different disseminated sites displaying HRD positive or negative tumours. Patients with all HR-proficient or variation in HR status (HR-mixed) in their tumour burden had a poorer PFS and OS than those with all HR deficient tumours [105]. The presence of variable HR tumours was also observed in a recent study, developing a new algorithm for estimating genomic instability scores (ovaHRDscar) for HR deficiency[106]. Furthermore, within our study, we also observed variability in *CCNE1* amplification in different disseminated tumour deposits. HGSOC cases with *CCNE1* amplification have been associated with platinum resistance and poor OS[107]. It has been suggested as a potentially actionable target[108].

Strategies for assessing biomarkers to stratify patients need to be examined and potentially revised to reduce the risk of patients being incorrectly stratified for treatment which, for example, could lead to them not being offered PARP inhibitor treatment. Expansion of biomarker testing to include profiling of multi-site tumour samples should be considered, in particular for those patients with genomic instability scores denoting HR status around the cut off for treatment stratification.

1.4.5 Emergence of platinum resistance

The main mechanism of action of both cisplatin and carboplatin is understood to involve their interaction with DNA and the formation of mono-adducts, mainly covalently interacting with N7 of guanine. This mono-adduct then evolves, through a second covalent binding, to a DNA crosslink. If these lesions are not repaired the consequence is a block of DNA synthesis and transcription. If sufficient DNA damage occurs the cell undergoes apoptotic cell death[109]. Around 80% of patients will have a good clinical response to platinum initially, however the majority will relapse during their disease time course with 10 year survival <30%[110].

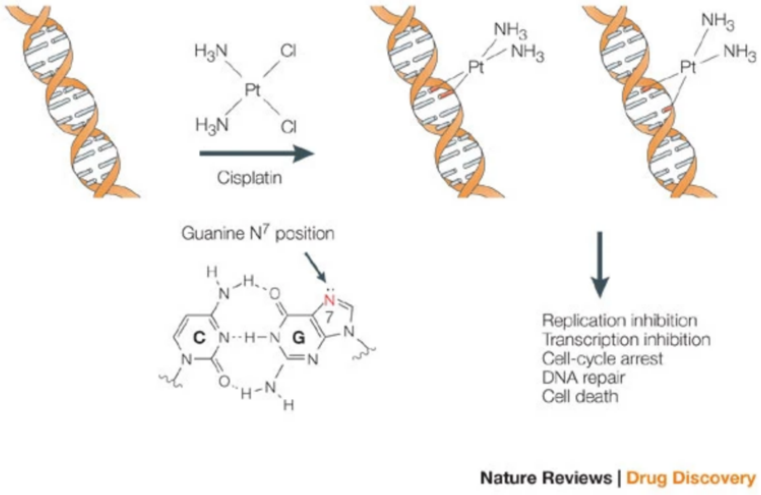


Figure 1.6: Mechanism of action of cisplatin. *Diagram demonstrating the covalent binding of the platinum atom of cisplatin to N7 of guanine leading to eventual cell death[111]*

The emergence of platinum resistance involves multiple potential mechanisms[112, 113]. Reduced intracellular accumulation of platinum due to increased efflux and/or decreased influx is a key mechanism of resistance[114]. Expression of the copper transporter proteins CTR1 and CTR2 have been suggested to correlate with platinum sensitivity in ovarian cancer cell lines[115, 116]. *ABCB1* encodes for the chemotherapy transporter Multidrug Resistance protein (MDR1). Functional experiments in ovarian cancer cell lines suggested that upregulation of MDR1, which promotes efflux of chemotherapy agents, resulted in reduced sensitivity to cisplatin, paclitaxel, docetaxel and doxorubicin and correlated with poor outcome[117]. Whole genome analysis of drug resistant HGSOC showed a transcriptional fusion between *ABCB1* and the upstream gene *SLC25A40* resulting in upregulation of *ABCB1* expression[118]. Q-RT-PCR analysis of post treatment HGSOC ascites samples suggested that the identified fusion only led to increased resistance to therapeutics which are MDR1 substrates such as paclitaxel, doxorubin and PARP inhibitors, not platinum compounds. Multiple treatment lines with MDR1 substrate therapeutics led to over expression of MDR1 and chemoresistance[119].

Alteration of cellular metabolic processes in response to differing tumour microenvironments can also influence platinum response [120]. Increased glucose metabolism within cancer cells has been shown to induce cisplatin resistance with Hexokinase 2 (HK2) overexpression shown to promote resistance via drug induced ERK-mediated autophagy[121].

Resistance to apoptosis is one of the main hallmarks of cancer with tumour cells developing a higher threshold to trigger apopotic pathways[122] often mediated through over expression of anti-apoptotic proteins such as Bcl-2[123]. These result from activation of pro-survival signalling pathways such as MAPK/ERK [124] and NF-κB activation following platinum treatment leading to defective apoptosis and increased resistance[125].

Platinum resistance is also affected by tumour cell DNA repair capacity given that the efficacy of platinum based compounds relies on the cell's ability to detect and repair DNA damage[126, 127]. *BRCA* status and HR function are highly important in determining platinum sensitivity in HGSOC, given that around 17-25% of patient tumours are found to have *BRCA 1* or *2* mutations and a further 25% have HR deficiency[128]. With alterations in these pathways causing both potential for increased resistance to platinum treatment but conversely, because of the pharmaceutical introduction of targeted therapeutics such as PARP inhibitors, are likely to have improved progression free survival outcomes[126].

Throughout tumourigenesis and metastatic spread genomic instability promotes acquisition of further DNA alterations, increasing tumour cell diversity and leading to the emergence of subpopulations of cells with differing molecular signatures through Darwinian selection[129, 130]. This evolutionary pathway can promote the emergence of resistant subclones through the development of advantageous genomic events in the selection process[131]. However conversely, high rates of chromosomal instability have paradoxically been shown to be advantageous in HGSOC due to a tendency towards platinum sensitivity[132].

Whole exome sequencing of primary and metastatic tumour samples from 6 HGSOC patients was performed by Masoodi et al. Evolutionary analysis evaluated somatic mutation and copy number variation (CNV) branching patterns between primary tumour and metastatic pairs. 51.8% of mutations and 28.6% of CNVs were shared between primary and metastatic pairs; 19.9% of mutations and 32.2% CNVs were unique to primary samples; 28.3% mutations and 35.2% CNVs were unique to metastatic deposits. Primary samples showed a significantly higher proportion of shared somatic mutations prior to dissemination whereas post dissemination significantly higher CNVs were seen. This lead to the suggestion that post dissemination there is higher chromosomal instability through CNVs, further genomic heterogeneity which therefore may contribute to treatment resistance[133].

Genomic analysis by Kotnik et al demonstrated no significant difference in mutational burden between matched primary and metastatic HGSOC patient samples however did discover long

term surviving patients had significantly higher somatic mutations (723) than the short-term survival group (591). This again suggests that less specific driver mutations and higher genetic instability leads to reduced treatment efficacy and worse patient outcome though conversely the number of CNVs was not significantly different between primary and metastatic sites[134]. Both of these studies involved only 6 patients with an average of 4 tumour sites studied per patient. They reached conflicting outcomes regarding CNV data illustrating the complexity of HGSOC and need for further larger studies involving more patients and sample site data.

ITH directly contributes to treatment resistance as the presence of subclonal populations with different sensitivity levels allows for the sensitive populations to respond at initial treatment whilst resistant clones later proliferate and lead to disease recurrence[112, 135]. The suggestion of 'cancer dormancy' whereby resistant clones remain indolent for significant time periods before causing recurrence with resistant disease is not well understood due to limited resources for examination[136]. It is suggested the underlying pathways involve mechanisms both limiting tumour growth and arresting tumour cell cycle[136]. Pro-growth signalling through Ras-MAPK pathway have been shown in some cancer types to be downregulated in dormant tumour cells, shown through reduced phospho-ERK whilst concurrent *p38* activation induces cell growth arrest[137]. In ovarian cancer spheroids AKT signalling has been found to be reduced leading to tumour cell quiescence[138].

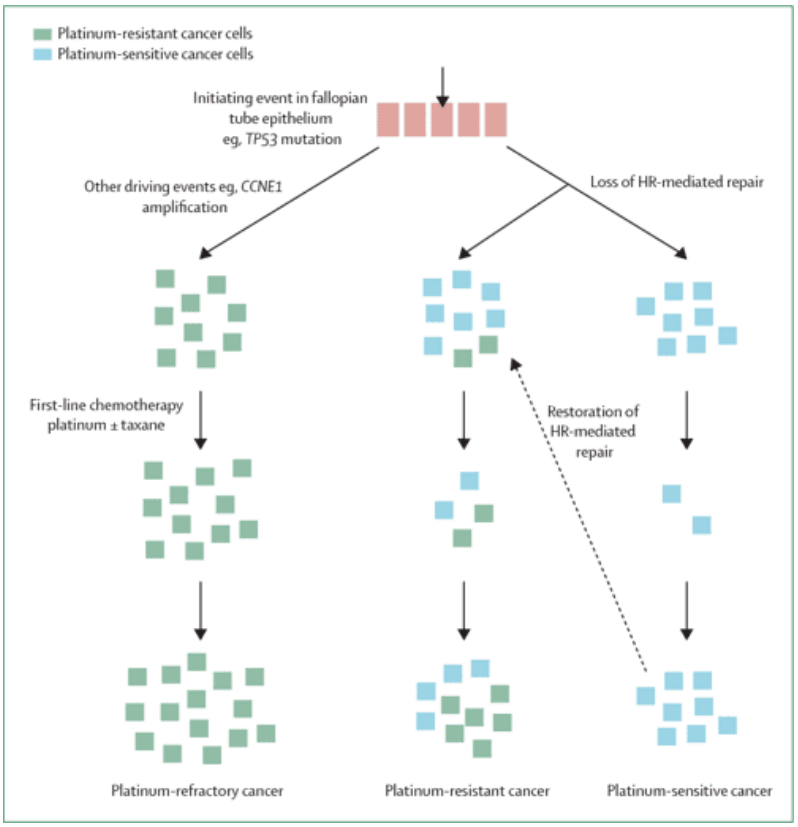


Figure 1.7: Emergence of platinum resistance in HGSOC. *Diagram representing different platinum sensitivity groupings in HGSOC and the potential pathways to resistant disease [139].*

Studies have investigated the hierarchy and generational patterns of clonal evolution. For example, the Brenton group developed the MEDICC algorithm (minimum event distance for intra-tumour copy number comparison) to look at patient-specific evolution in primary and metastatic samples obtained from patients with HGSOC. By reconstructing the tumour evolution in each patient, they observed vast levels of heterogeneity from patient to patient and between the metastatic site. It appeared that metastatic spread could occur both from the primary tumour to other sites and from metastases to metastases. They could also observe genomic differences between biopsies taken before neoadjuvant chemotherapy to those following treatment, suggesting that the treatment itself is provoking some genomic evolution. The degree of heterogeneity present in pre-treatment samples also appeared to contribute to potential relapse of disease with the suggestion that higher levels of heterogeneity as measured by a "clonal expansion index" give rise to early resistant clones which then prevail following treatment and cause recurrence[140]. Of note in this study however, the majority of patients had undergone neoadjuvant chemotherapy which may have influenced tumour genomes, also the numbers and locations of metastatic samples were limited to omentum, peritoneum and a

few ascites samples. Though common areas for metastatic spread, this may not depict the total heterogeneity from the broadly disseminated tumour burden observed in patients with advanced stage HGSOC.

The time between the end of chemotherapy and clinical relapse is used to determine platinum sensitivity. Longer than 6 months from the end of treatment to relapse is considered platinum sensitive disease, within 6 months of completion of chemotherapy timeframe is considered resistant. Progression during chemotherapy treatment is categorized as platinum refractory. This is a rather crude method of delineation which can only be determined after relapse has occurred and the opportunity to give a treatment which would be more useful from the outset in those with resistant disease has passed[141]. 20-30% of patients will have platinum resistant disease at presentation and of those with sensitive disease, 70-80% will develop therapy-resistant disease at some point[142]. Different groups have investigated the possibility of biomarkers with a prognostic capability for platinum sensitivity. For example, Uno et al. analysed tumour tissue from patients undergoing interval debulking surgery. Mass spectrometry analysis of tissue samples from tumours and their surrounding stroma showed 2 distinct patient groups. Group A had platinum detected in the stroma only and none in the tumour tissues whereas Group B had platinum in both the tumour tissue and stroma. They demonstrated that group A patients had an acquired platinum resistance. Post interval debulking surgery these patients went on to receive platinum therapy as per local protocols. Significantly more patients relapsed in a platinum resistant timeframe from group A (9/16 56.3%) compared to those in group B (0/11) who had platinum found in both stroma and tumour. The overall survival for those in group B was also significantly longer[143]. This suggested that in patients receiving neoadjuvant platinum based chemotherapy, platinum distribution at the time of interval debulking surgery could be a potential biomarker for true platinum resistance and therefore guide appropriate chemotherapy decisions post-operatively.

This highlights the diverse behaviour of HGSOC tumours and the need for more personalised treatment strategies. Although the majority of patients may respond to platinum in first line treatment, those that will not respond need a means of identification so they are not subjected to gruelling therapy processes which are unlikely to benefit them. There is also the additional problem of those who initially respond having the treatment provoke the emergence of resistant clones. Many of these previous studies however, despite offering valuable insight into the evolution of heterogeneity and platinum resistance, have often only used single site samples

from the primary tumours, and/or have had small patient numbers[118]. Only sampling limited areas of both primary and relapse tumour tissue does not depict the whole spectrum of heterogeneity within each patient. Although results have been reported with patterns in clonal evolution and potential genetic targets the variation seen in sequencing data between metastatic sites mean that not all tumours within a patient will be susceptible to the same targeted therapeutics[144]. Mixed HRD scores (both HRD positive and HRD negative scores) detected in different disseminated tumour sites sampled within approximately 22% of HGSOC patients (10/45), demonstrates the clinical necessity for further analysis with improved techniques for examination as patients could miss out on effective treatment options based on limited testing strategies[105]. Furthermore, variations in *CCNE1* copy number amplification/gain, known to be a biomarker of platinum resistance[118], were observed in different multi-site tumours from this HGSOC cohort. More disseminated tumours sampled at varying time points are required to gain better understanding of disease progression and therapeutic responses. Obtaining samples from multiple metastatic sites in a large cohort of patients is very difficult to achieve, due to the required access to the highly specialised cytoreductive surgeries with surgeons capable of delivering adequate samples. Utilising single site biopsies which can be gained from outpatient radiological procedures has therefore been favoured more commonly. The lack of ability to study tumours from multiple sites and use the analysis within drug development is potentially one of the factors giving rise to poor efficacy of new therapeutics at clinical testing stages.

It is evident that a wider understanding of the genomic and phenotypic characteristics of both primary and metastatic tumours in HGSOC is required in order to develop biomarkers to improve early detection of disease and prediction of treatment response. This needs to be assessed robustly with samples from large numbers of patients and multiple anatomical sites. However, given the variation in tumour profiles seen in metastatic sites, the inherent microenvironments of these different tumours need to be taken into consideration in any future analysis or development of predictive biomarkers.

1.5 Tumour microenvironment

The development of cancer is a process starting with mutations in genetic components vital for the regulation of 'normal' cell function, leading to over proliferation of cells and resulting in tumours evolving within the original tissue environment[145]. These interactions are crucial to the growth and proliferation of tumour tissue. In HGSOC, the tumour microenvironments are diverse due to the widespread dissemination pattern across the peritoneal lined abdominal cavity. The peritoneal lining through which the tumour cells invade consists of a mesothelial cell layer supported by the basement membrane on top of the extracellular matrix (ECM) containing fibroblasts, immune cells, blood vessels, lymphatics and adipocytes[146]. All these components constitute the tumour microenvironment (TME) which will vary in composition based on anatomical location.

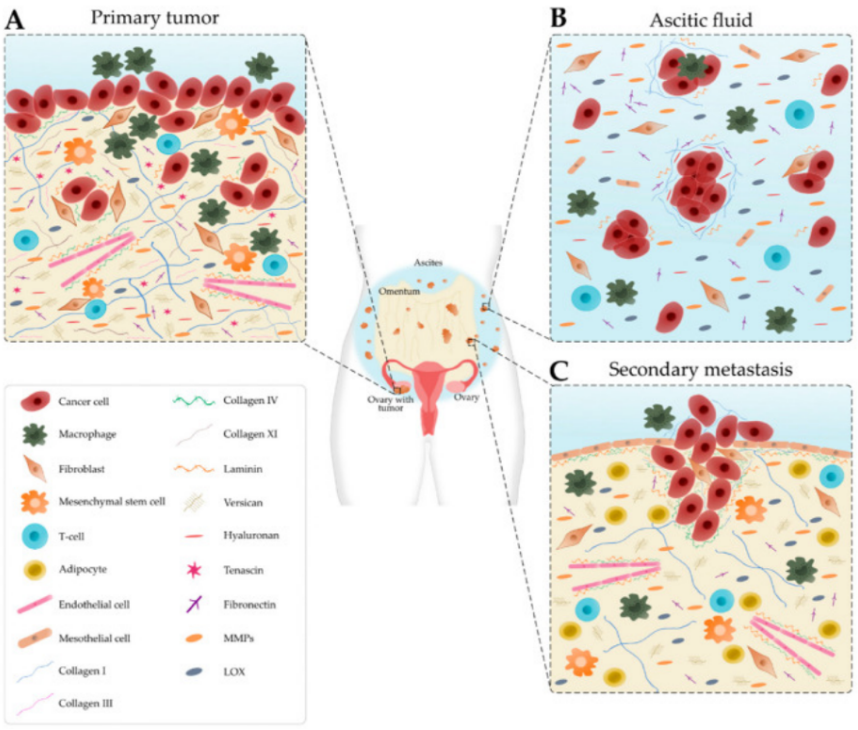


Figure 1.8: Interactions between ovarian cancer cells and the extra-cellular matrix*. Diagram demonstrating the relationships between ovarian cancer cells and the main ECM components in the tumour microenvironment in both primary and metastatic settings. (A) Primary tumour cells recruiting and corrupting tumour associated macrophages, cancer associated fibroblasts, T-cells and endothelial cells There is upregulation of key ECM components such as fibronectin, hyaluronan, tenascin, versican and MMPs. Collagen fibres undergo remodelling to become thick fibrils and lack organised orientation. (B) Tumour cells, either existing alone or in spheroids, detach from the epithelium and travel in the ascitic fluid around the abdominal cavity. Extracellular matrix components are found within the aggregated cells and the ascitic fluid. (C) At distant metastatic sites along the peritoneal lining, tumour cells attach to the mesothelial cell covered peritoneum and invade to form secondary metastatic sites. Image taken from [147].*

There is increasing evidence of the role microenvironments play in the progression of disease and response to treatment[148]. The important role the stroma plays in tumour functions must be better understood to aid discovery of potential therapeutic targets and to improve testing strategies in drug discovery [149]. Interaction between stromal cells and the ECM occurs in normal tissues via complex cell-cell and cell-ECM signalling pathways.

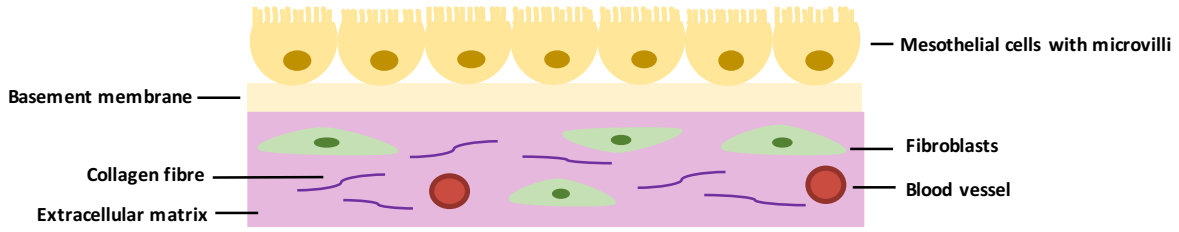


Figure 1.9: Representation of peritoneal layering architecture. *Diagrammatic representation of the peritoneal lining and stromal architecture consisting of a mesothelial lining on the basement membrane, with extracellular matrix beneath containing fibroblasts, blood vessels and structural components such as collagen fibres. Diagram adapted from image [150]*

The ECM is defined as the non-cellular constituent of tissues and organs. The matrix and matrix associated proteins have been collectively labelled the 'matrisome'[151]. It is essential for the regulation of tissue functions such as differentiation and homeostasis whilst also providing a physical supportive structure for the different cell populations present. Each tissue or organ evolves to have its own unique components dependent on desired function. However, all will have base constituents containing water, proteins and polysaccharides[152]. Cell adhesion to the ECM is supported by the binding of integrins to the ECM proteins[153]. It is now understood that in the early stages of tumour cell metastases, ECM components such as integrins, proteoglycans, glycosaminoglycans, glycoproteins and collagens trigger pathways leading to invasion, proliferation and dissemination[154-157].

Integrins, a group of transmembrane glycoproteins, are crucial for cell-ECM adhesion and are involved in cell cycle regulation. They are responsible for communication of the peri-cellular environmental signals through recruitment of protein mediators to integrin binding sites, forming adhesion complexes or the 'adhesome'[158]. Over 150 proteins have been found to interact at these integrin adhesion sites. These mediating proteins contain adaptor proteins, adhesion receptors, actin regulators and enzymes regulating adhesion signalling to the intracellular compartment[159]. Integrin mediated adhesion is also vital for cell cycle

progression through the G1/S checkpoint via regulation of cyclins, cyclin-dependent kinase inhibitors and genes involved in proliferation[160]. The interaction between integrins and growth factor receptors, either by indirect signalling crosstalk or physical association is essential for cell proliferation through regulation of the PI3K/AKT, MEK/ERK and small GTPase pathways. Loss of integrin mediated adhesion leads to cell separation from the ECM which triggers cell death via anoikis in healthy tissue[161].

Because of their vital cell-ECM interactions integrins play key roles in tumour cell migration and invasion. Neoplastic cells, unlike healthy cells are less reliant on cell-ECM adhesion for survival[162]. Examination of ECM and growth factor receptors in both non-malignant and malignant cells showed that malignant cells overexpressed integrins and epidermal growth factor receptor (EGFR). Addition of anti-β_1 integrin antibodies downregulated EGFR expression leading to reversed cellular disorganisation and reduced tumourigenicity in breast cancer cells[163].

Tumour cell interaction with the ECM is key to their ability to metastasise and invade other sites. They must be able to separate from the native tissue by breaking the adhesions to neighbouring cells and the basement membrane in order to travel to metastatic sites. Evidence has shown that tumour cells can alter their integrin signalling[164], with some integrins found to be linked to promoting tumour growth e.g. $\alpha v\beta_6$ and $\alpha v\beta_3$ integrin whilst $\alpha_2\beta_1$ and $\alpha_3\beta_1$ may suppress tumour progression[165].

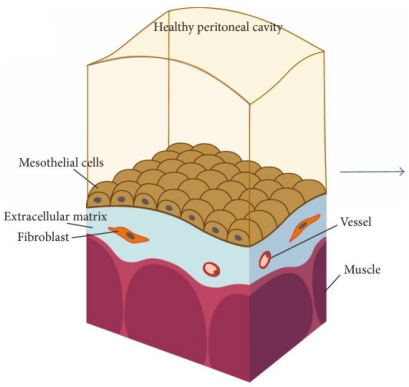


Figure 1.10: Diagram of healthy peritoneum. *Diagrammatic representation of healthy peritoneum which covers the intra-abdominal organs including the omentum [166].*

HGSOC metastasises in a different way compared to the haematogenous methods of many other solid cancers such as breast and colon. The seeding of tumour cell clusters from the ovary and distal fallopian tube enables a passive method of dissemination. After shedding into the

intra-abdominal peritoneal fluid, the single tumour cells or multicellular aggregates diffuse throughout the peritoneal cavity before adhering to the mesothelial cell lined peritoneum[167]. Investigating the processes of HGSOC invasion Iwanicki et. al used GFP expressing mesothelial cells to observe the interaction between HGSOC cell line tumour spheroids and the mesothelial cell layer. They observed that the tumour spheroids initially adhered across the surface of the mesothelial monolayer then subsequently invaded the layer through localised de-adhesion. Paxillin-GFP was used to observe for integrin mediated activity in mesothelial cell adhesion. Total internal reflection fluorescent microscopy examination demonstrated that the tumour spheroids affected the mesothelial cell adhesions and promoted matrix adhesion disassembly. These actions resulted in clearance of the mesothelial barrier to permit invasion of the tumour spheroids[168]. It has also been suggested that tumour cell induced apoptosis of mesothelial cells through the death ligand/receptor system Fas Ligand/Fas may be a mechanism for invasion[169].

Tumour cells are known to corrupt the microenvironment to promote invasion and growth. Whilst the mesothelial cell layer in HGSOC metastases act as an initial barrier to invasion, it has been shown that intra-peritoneal combined injection of mesothelial cells with ovarian cancer cells into immunocompromised mice increased peritoneal metastatic deposits compared to injection of cancer cells alone[170]. Kenny et. al showed that ovarian cancer cells stimulate mesothelial cells to secrete fibronectin, which was found to have increased expression in HGSOC omental deposits compared to primary samples. The higher fibronectin levels promoted by the tumour cells led to higher rates of adhesion, invasion and proliferation to the omental ECM through binding to cell surface integrins such as $\alpha_5\beta_1$ integrin. Moreover, co-culture of ovarian cancer cells with ECM in 3D models showed that promotion of fibronectin secretion led to increased matrix assembly[171].

Collagens make up around 30% of the ECM glycoproteins; non-collagenous proteins include fibronectin, laminin and tenascins[172]. 28 different collagens have been identified so far[173]. In the HGSOC TME, once through the mesothelial cell barrier tumour cells encounter collagen rich ECM and stromal cells such as fibroblasts, endothelial cells and immune cells. One study investigated the involvement of cadherins, a group of transmembrane proteins involved in cell-cell adhesion, on the invasion and disruption of collagen fibres by HGSOC cell lines. They observed that tumour cell invasion led to deformation of the collagen matrix and disruption of the normally organised fibre alignment. N-cadherin positive tumour cells and multicellular

aggregates showed increased motility and invasion into the collagen matrix compared to E-cadherin positive cells. They also observed that N-cadherin positive cells endogenously expressed matrix metalloproteinase-1 (MMP-1), a known catalyst for collagenolysis and matrix reorganisation[174, 175]. Another study examined the influence of hypoxia in the TME on mesothelial-tumour cell interactions in HGSOC. Solid tumours have hypoxic TME due to abnormal vasculature and high oxygen demands of proliferating tumour cells[176]. This hypoxic environment activates the hypoxia-inducible factor (HIF) pathway. HIF transcription factors HIF-1 and HIF-2 promote metastatic activity through activation of genes involved in immune evasion, invasion and alteration of TME niche[176]. HIF-1 and HIF-2 gene signatures have been found to be associated with reduced PFS and OS in ovarian cancer[177]. Natarajan et. al compared hypoxic gene signatures in matched primary and omental metastatic deposits from 9 chemotherapy naive HGSOC patients. They found 2431 genes which were differentially overexpressed in the metastatic sites compared to primary tumours. Functional gene enrichment analysis identified multiple genes involved in ECM organisation, ECM disassembly, collagen catabolic processes and collagen fibril organisation. IHC analysis of the omental deposits demonstrated positive staining for HIF-1 and HIF-2, confirming a hypoxic metastatic TME in omental metastatic sites. They found that mesotheial cells from omentum and isolated from ascites fluid expressed HIF-1 and HIF-2. Immunofluorescence examination of mesothelial cells revealed that in hypoxic situations collagen I secretion was enhanced compared to normoxic cultures[178].

The MMPs are a large group of endopeptidases with functions involving degradation of different protein components of the ECM. MMP-1 has been observed to be associated with Interleukin-8 (IL8) secretion and stimulation of angiogenesis in mouse models of ovarian cancer and through this pathway influencing metastasis and invasion[179]. MMP-2 has a role in the degradation of collagen IV, an important component of the basement membrane. Through this activity, it is understood that overexpression of MMP-2 leads to promotion of tumour cell invasion. Overexpression of MMP-2 has been shown to be associated with poor prognosis in ovarian cancer patients[180]. Additionally, MMP-7 and MMP-9 also have associations with poor outcomes in ovarian cancer due to their roles in ECM remodelling, tumour cell invasion and metastasis. MMP-9 is known to degrade ECM proteins through proteolytic cleavage, thus contributing to and regulating ECM remodelling[181], particularly, through its ability to degrade collagen IV and thus disrupt the basement membrane[181-185]. The importance of considering the TME for potential biomarkers of disease and possible

therapeutic targets has long been recognised. Constituents such as the MMP family have been extensively researched for potential game changing novel therapeutics including the MMP inhibitor Marimastat targeting metastatic spread[186]. However, early studies looking at MMP inhibitors were disappointing with little improvement in outcomes and severe side effects. 7 phase III trials have been commenced with Marimastat, which inhibits collagenase and angiogenesis, across different cancer types but failed to meet their primary end points with no benefit over standard treatments seen. The ovarian cancer trial design did not meet US or European standards[187, 188].

It is evident that the TME is hugely important to the establishment, growth and spread of cancer processes. Recently, protocols have been developed to decellularise the ECM and deplete intracellular proteins whilst enriching the ECM proteins for more in depth examination[189]. Mass spectrometry (MS) has been employed for comprehensive analysis and discovery of individual tissue and tumour microenvironmental niches[190]. These large volumes of data can be used to compare matrisomes between anatomical sites and also between different diseases. Over recent years MS techniques have been used for proteomic studies to produce sensitive, broad scale examination of biological processes[191]. 'Bottom up' proteomics allows the analysis of peptides obtained from digested proteins. Peptide samples are fractionated then undergo MS analysis. This utilises tandem mass tagging to label peptides which are then compared to theoretical tandem mass spectra obtained from protein databases. Identification of proteins present in a sample is achieved by applying the detected peptide sequences to recognised proteins[192]. Analysis of proteomic data is increasingly being recognised to be able to lead to the discovery of potential new diagnostic and prognostic biomarkers in cancer[193]. The use of established databases for examination of protein-protein interactions and pathway enrichment is providing insight into previously unrecognised potential targets[194, 195].

HGSOC has been suggested to demonstrate different subtypes dependent on the tumour 'stiffness' profile which has been observed to differ between patients based on levels of desmoplasia[196, 197]. Activation of stromal fibroblasts and reorganisation of ECM collagen fibres lead to a 'stiffer' tumour profile[189]. In healthy ovarian ECM, proteoglycans such as decorin and versican help to maintain architectural integrity and moderate interstitial pressure. In HGSOC, upregulation of versican, fibronectin, tenacin-c and tenacin-x and downregulation of decorin have been observed to be associated with poor outcome[198].

The Balkwill group performed an in-depth analysis of the TME to study matrix changes within HGSOC[199]. They studied 6 parameters of TME in omentum tumour samples from 36 HGSOC patients. They defined a disease score by the quantity of sample consumed by tumour cells and stroma and observed correlation between increased disease score and number of cancer associated fibroblasts (CAFs) and leucocytes present whilst adipocyte density diminished with higher disease score. The observed matrisome altered dependent on disease score with samples with low disease score showing higher proportions of collagen I, III and VI, fibrillin, α-2-macroprotein, lumican and heparin sulphate proteoglycan-2. High disease score samples showed increased fibrinogen, fibronectin, proteoglycans and secreted factors. A matrix index across the cohort was developed by measuring the ratio between positive and negative expression of regulated genes. This was found to significantly correlate with disease score and tissue stiffness and concluded that matrix index is indicative of a type of matrisome composition promoting tumour growth. Their data was corroborated in other data sets and in different cancers[199].

During initial tumourigenesis the ECM undergoes remodelling due to dysregulation of vital ECM processes causing abnormal cellular behaviour and growth, causing increased ECM deposition and angiogenesis[200]. The normal immune reaction is suppressed and immune cells in the microenvironment can become corrupted such as the case with tumour associated macrophages (TAMs). TAMs are understood to secrete TGFβI which has been found to be significantly upregulated in serous tubal intra-epithelial carcinoma (STIC) lesions and ovarian tissue in HGSOC cases and is believed to contribute to immunosuppression and progression of disease[201]. One study used MS analysis of TAMs secretome to investigate their potential pro-oncogenic mechanism in HGSOC. They found higher levels of TGFβ1, fibronectin and tenacin-c in ascites-derived TAM secretome, which have all been associated with tumour cell migration. TGFβ1 seemingly had a pro-adhesive effect on tumour cells *in vitro*. High concentrations of TGFβ1, fibronectin and tenascin-c were found to significantly correlate with reduced OS[202].

Stromal fibroblasts have long been established to be significantly involved in cancer processes. Fibroblasts are defined as non-vascular, non-inflammatory and non-epithelial cells within connective tissue[203]. In non-cancerous states fibroblasts are involved in production of connective tissue ECM components, they contribute to wound healing and tissue repair and

can promote angiogenesis[204, 205]. Fibroblasts are known to contribute to ECM structure through secretion of collagen I, III and V and fibronectin[206]. Their secretion of collagen IV and laminin helps construct the basement membrane and through secretion of MMPs they are highly involved in ECM deposition and homeostasis[207]. The development of cancer associated fibroblasts (CAFs) has been extensively studied in multiple cancer types, whilst the origins are not fully understood the variety of functions they provide to developing tumours have been closely examined[208]. The presence of CAFs in tumour microenvironments is observed to contribute to the more stiff and fibrotic subtype associated with poorer outcomes[209]. CAFs promote tumorigenesis via expression of pro-inflammatory gene signatures causing increases in neovascularisation and provoking corruption of the immune response[210]. One study found that initiation of tumour growth in dormant HGSOC cells was stimulated by stromal myofibroblast infiltration, stromal cells were involved with angiogenesis within the tumour through expression of angiopoietin-1 and angiopoietin-2[211]. CAFs can also act as a physical barrier to drug delivery to the tumour cells[212]. Wang et. al used a HGSOC mouse model to examine fibroblast involvement in response to cisplatin treatment. Tumour growth was increased in cisplatin treated mice co-injected with fibroblasts and ovarian cancer cells, compared to those with ovarian cancer cells alone. There was also reduced apoptosis observed via TUNEL analysis in the cisplatin treated mice in the presence of fibroblasts. The reduced sensitivity to cisplatin was suggested to be due to reduction in platinum induced DNA damage signalling in the presence of fibroblasts. Intracellular levels of cisplatin were also found to be reduced in the tumour cells when fibroblasts were co-cultured. On further examination, intracellular glutathione levels were elevated in ovarian cancer cells cultured with fibroblasts. Glutathione chelation can lead to cisplatin efflux from cells and so these results suggested fibroblast related platinum resistance is linked to high intracellular glutathione levels in ovarian cancer[213].

Zhang et. al demonstrated that higher proportions of CAFs are present in tumour samples from patients with advanced metastatic EOC than those at lower stages. 91 ovarian tissue samples (containing 10 borderline tumours, 11 benign tumours and 9 normal alongside malignant tumour samples) underwent IHC analysis for CAFs. Increased abundance of CAFs was associated with advanced stage disease[214]. Furthermore, when CAFs were added to cultures there was more invasion by tumour cells observed than when non-cancerous fibroblasts were used[214].

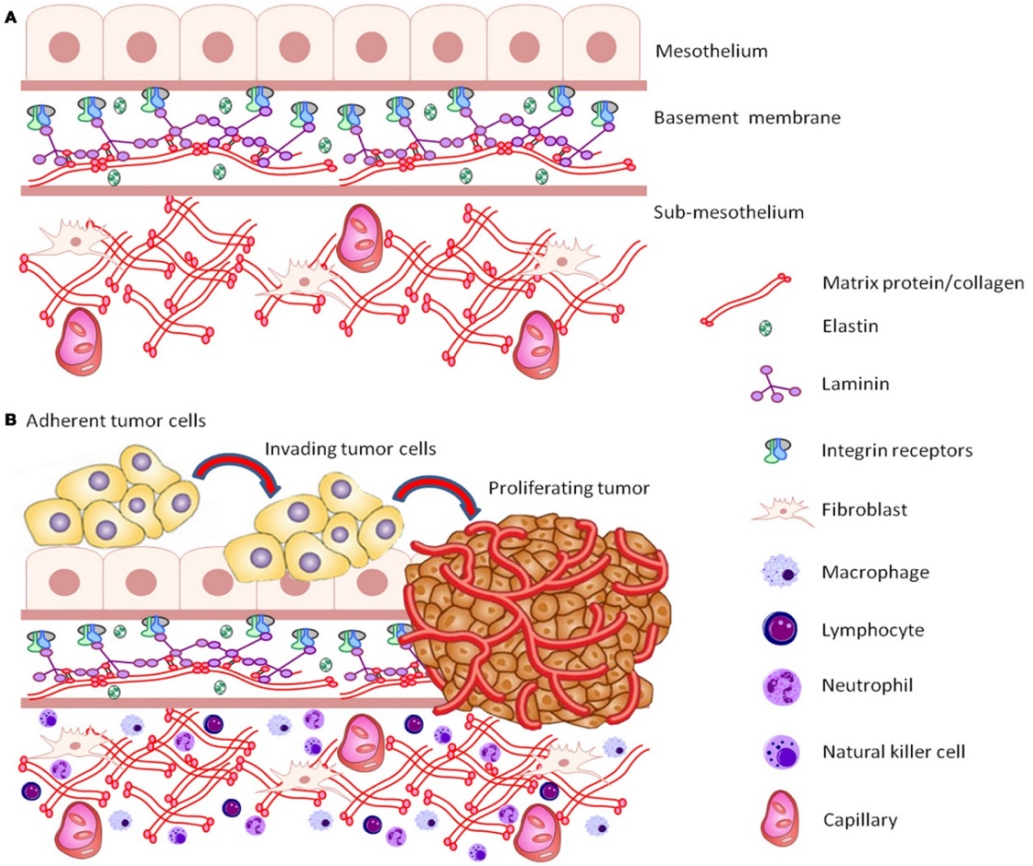


Figure 1.11: [A]Schematic representation of the peritoneal site of ovarian cancer displaying its structure and components. [B] Schematic representation of adherent ovarian cancer cell cluster proliferating, invading, and destroying basement membrane ECM tissue architecture of the peritoneal site.

The TME plays a vital role in response to drug treatments. One of the main barriers to effective evaluation of the efficacy of compounds in drug discovery is the platforms for cell culture used in both examination of disease development and therapeutic properties. In the pre-clinical trial stages of drug discovery most of the testing of therapeutics will occur in cell line models without incorporating components of the TME.

Studies utilizing analysis of the ECM protein compositions have discovered the importance of microenvironmental properties in determining the fate of cancer growth and progression and response to treatment. Majmudar et al examined the potential to predict tumour response to treatment in culture systems better reflecting the *in vivo* state[215] with the aim to determine the possibility of more personalized treatment options. They constructed *ex vivo* culture platforms using tissue slice/explant cultures. ECM protein components were determined for head and neck squamous cell carcinoma and colorectal carcinoma tumours. Tumours were decellularised to produce ECM protein lysates, which were analysed with MS and a 'cocktail' of the individual environmental tumour-matrix protein (TMP) compositions was created for

each individual tumour type. The slice culture platforms were coated with these different TMP mixtures and tumour slices cultured within. They were then treated with different therapeutics and response to treatment was analysed via an algorithm (CANscript) devised by the team. They found distinct TMPs in both types of cancer and between different subtypes by grade. Compared to uncoated controls, those tumour slices grown in their own TMP cocktail showed improved maintenance of tissue morphology and viability of cells. Comparisons between tumour slices grown with matched TMP versus those in unmatched showed greater proliferation in the matched samples. High grade tumours were better able to maintain proliferation in 'alien' TMP than low grade. They determined that context-dependent stromal-epithelial interaction is a critical requirement for tumour growth and survival. Using the matched cultures, Majumdar and colleagues analysed response to treatment *in vitro* and using their CANscript algorithm created a prediction of individual sample response to treatment for testing *in vivo*[215]. From this original study they have developed a company utilizing *ex vivo* tissue slices to enable prediction of individual patient response to treatment[216].
This study demonstrates the importance of microenvironment on tumour growth and response to treatment and highlights the requirement to consider the value of incorporating more complexity into drug discovery platforms in order to improve both efficiency in drug development and through this benefit patient outcomes.

Most of the examination of the TME in HGSOC has been performed either on primary tissue or on omentum metastatic deposits. The Lengyel group showed that fibronectin expression was increased in omental metastatic deposits compared to the primary tumour samples[171]. There has been minimal investigation into the TME of the other multiple metastatic sites involved in HGSOC. These differing TMEs are also likely to show differing ECM components which may contain potential biomarkers or targets.

1.6 Review of 3D culture systems

The culture of cells, whether immortalised cell lines or primary cultures, in 2D has been practiced since the 1900s [217]. The uses are vast and varied. The availability and relative affordability of immortalised cell lines make them attractive for culture systems where prolonged optimisation steps and replication of data mean cultures that are easy to establish and maintain *in vitro*, through multiple passages, are highly desirable. They are also simpler to manipulate to create the desired cell conditioning for analysis compared to primary cell cultures. The ability to mass produce, culture and maintain in viable culture means they can be utilised for high-throughput drug testing for example. The use of primary cells extracted from tissue samples can better represent the natural course of cell cycles when cultured *in vitro* compared to cell lines, though extraction and maintenance of viable cultures is more challenging[218]. Fundamentally however, the culture of both cell types using 2D techniques is flawed. Cells grown in a 2D environment lack many aspects of their natural state, with none of the physiology or anatomy of the *in vivo* setting[219]. The primary objectives for developing 3D cell culture systems vary widely, ranging from bioengineering advances to observing development of disease to drug discovery. In general, there is the common aim to deliver a system which more closely mimics the *in vivo* tissue microenvironment.

For drug delivery and efficacy 2D monolayer cultures have long been established *in vitro* as a safe way to test therapeutics prior to patient involved clinical trials[220]. However, delivering drugs to cells in this set up can lead to falsely encouraging outcomes, with less than 1% of all pre-clinical hits progressing to clinical trials. The only truly accurate method for testing efficacy of therapeutics is through patient centred trials, however, for obvious safety reasons there needs to be comprehensive screening prior to human exposure to avoid potentially harmful side effects.

In general, pre-clinical testing of potential pharmaceutical agents involves both extensive *in vitro* studies, with relevant immortalised cell lines, and validation in animal models to investigate efficacy and toxicity. Additionally, pharmacokinetic and pharmacological characteristics will be studied to investigate drug absorption, distribution, metabolism and excretion properties[221]. Over the last decade, research groups have demonstrated that the *in vivo* setting is more complex than 2D cultures can demonstrate and have stressed the

importance of inclusion of ECM components and a 3D structure to enable cells to more closely mimic their behaviour within humans[222, 223].

The culture design chosen for experimentation can also give rise to variety in gene expression exhibited by the cells in culture. One study found that RT-qPCR analysis of head and neck SCC (HNSCC) cell line spheroids showed upregulation of epithelial to mesenchymal transition (EMT) associated gene *CDH1* compared to concurrent 2D cultures. The 3D spheroid cultures also demonstrated reduced sensitivity to cisplatin compared to 2D cultures[224, 225].

One study used EOC cell lines to establish 3D spheroid cultures and analyse the morphological differences and protein expression between 2D and 3D cultures. They demonstrated histological differentiation consistent with their subtypes on IHC analysis of 3D spheroids, in comparison with no histological differentiation seen in their concurrent 2D cultures. Protein expression analysis showed upregulation of the adhesion marker E-cadherin in 3D culture compared to 2D. Lower proliferation rates were seen in the 3D cultures. 7 out of 11 of the cell lines used showed reduced sensitivity to cisplatin and paclitaxel in 3D compared to 2D[226].

3D cultures can be developed to reflect the complex *in vivo* setting and dynamics occurring between non-cancerous cells, extracellular matrix and tumour cells. Thus, the response of tumour cells to therapeutics can more accurately be established with cultures representing their natural state.

Increasing tumour complexity

2D monolayer 3D designs

	Primary Tumour cells	Immortalised cell lines	Organotypic models	Organoids	Ex vivo Tissue Slice	PDX
Ease of use	+/-	+	-	-	+/-	-
Maintenance of tumour morphology	-	-	-	-	+	+/-
Preservation of microenvironment/ heterogeneity	-	-	+/-	+/-	+	+/-
High throughput screens	+/-	+	+/-	+/-	-	-
Similarities with original tumour	-	-	+/-	+/-	+	+/-
Costs	+/-	+/-	+/-	+/-	+	-

Figure 1.12: Comparison of 2D and 3D culture systems. *Diagram comparing advantages and disadvantages of different culture techniques considering 2D monolayer designs and more complex 3D culture systems. Adapted from [227, 228]*

It is commonly accepted that 3D alternatives to 2D monolayer cultures are required. However there are some drawbacks that have prevented them becoming universally utilised thus far. Firstly, with a more complex set up comes increased cost, with often more expensive materials, (e.g. ECM scaffolds, fluidics devices) culture environmental requirements and potential for multiple cell types involved. There is also a question of the reproducibility of the models. The more complex a system design is, the higher the potential for subsequent experiments to lose validity. For example, in hydrogels there can be inconsistency in the placement of cells and unpredictability of organoid formation. This can give rise to differing results during revalidation[229]. The most commonly used commercially available matrix supporting 3D growth of cells, matrigel, also has recognized issues with consistency and reproducibility[230]. Given the potential for *in vivo* TME ECM composition variability it is difficult to get a truly representative design with standardised ECM scaffolds.

Variation in cell-signalling, protein expression and heterogeneity in culture systems can all lead to changes in drug metabolism from 2D to 3D settings with ovarian cancer spheroids showing increased expression of EMT markers and increased resistance to platinum compared to monolayer cultures[231].

During drug development if compounds show promise in the commonly used 2D monolayer *in vitro* setting, the next step is often to be incorporated into animal models e.g. immunodeficient mouse models. These provide a more complex tumour microenvironment which will help with studies into the drug delivery, efficacy and toxicity. A benefit of animal models over 3D model systems include observations of variable factors, such as age, on disease development and progression[232]. However, they also have disadvantages. Depending on the animal and type of model chosen, systems can be costly to set up, require intense upkeep and are low throughput for analysis. Furthermore, although the environment may have more complexity it will not fully mimic that of the human setting as the vasculature, immune system, anatomy, absorption and excretion of the compounds will all differ from those of humans. This can lead to inaccuracies in analysis of toxicity profiles and efficacy of therapeutics. There is also the ethical argument behind use of animals in drug testing which is constantly being scrutinized for better options to be sourced. Development of representative 3D culture systems will hopefully provide an alternative method for testing of compounds with less reliance on animal models prior to clinical trials. Though as mentioned above, animal models can have advantages over 3D designs in the study of evolving processes less able to be characterised *in vitro*.

As well as for discovery and testing of therapeutic agents, 3D cultures have also been developed to study the origin and progression of disease states. Kenny et. al have used 3D organotypic models of human omentum to extensively study the metastatic invasive process in HGSOC. They demonstrated that ovarian cancer cell line tumour cells were able to adhere to and invade through the mesothelial barrier significantly quicker than immortalised ovarian surface epithelial cells. Additionally, the presence of fibroblasts within the organotypic models promoted the invasion of tumour cells compared to culture containing mesothelial cells and ECM alone[233]. Such 3D systems represent a powerful tool for studying cancer biology, enabling us to model the dynamic evolution of neoplastic disease from the early stages to metastatic dissemination and the interactions with the microenvironment[234].

Tumour environments, as discussed, involve not only the tumour cells, but also complex ECM, stromal cells and immune cells. Cell signalling, adhesion, invasion and metastasis involve complex systems which cannot be replicated in a 2D format[235]. A number of different 3D culture systems have been developed and examined over the last few decades and will be discussed below.

1.6.1 Use of immortalised cell lines vs primary tumour cell cultures

As well as the environmental constituents within a culture system, the actual tumour cell representing the cancer needs to be considered. For high throughput drug assays, use of immortalised cell lines may be useful for initial stages. However it is now recognized that many of the established cell lines do not, in fact, represent the cancer type and characteristics they were believed to have originated from[236]. One of the main advantages for using immortalised cell lines is their ‘known’ phenotype which, for example in the case of ovarian cancer, can assist in establishing whether drugs may be useful in the treatment of ‘platinum sensitive’ or ‘platinum resistant’ disease. Furthermore, they are readily available and relatively cheap to maintain compared to access to primary tumour cells. They are also easily kept in culture for multiple passages for long periods of time without too much degeneration of their viability. However there has been concern about the cell type of origin with some of the established cell lines and their tendency towards genomic drift over time[237].

Primary cells are a more clinically relevant alternative to immortalised cell lines and can be either of tumour or stromal origin. These can be extracted and cultured in specialized media specific to their individual requirements. Studies using primary cells will gain data which more reliably reflects the situation within the tumour *in vivo*. However use of primary cells is more difficult and can be costly to derive and maintain. Researchers need access to tissue samples and the ability to process samples efficiently for maximum viability of cells. Primary cells are less easily transfected than cell lines and therefore analysis methods need adapting. They also may proliferate more slowly and will maintain viability for shorter time periods, limiting multiple concurrent experiments[238]. Whilst primary cells have been developed into immortalised new cell lines, the success rate is not high[239]. Access to patient samples can be difficult and usually involves obtaining tissue from single site biopsies or from ascites tumour spheroids. This limits the scope of data to single tissues/sample sites. In the context of HGSOC, the widespread nature of the dissemination pattern means testing of multiple sites is necessary to gain true understanding of the inherent tumour heterogeneity. Most studies using single site samples may gain vast information from different analyses in genomics, proteomics, immunologic profiling but multi-site examination is needed to fully appreciate the complexity of the disease.

1.6.2 Structural platforms for 3D cultures

With the development of different 3D cell techniques, it is recognized that different culture mediums are also required to support the cells and provide an architecture more representative of the *in vivo* state. The natural ECM is an elastic, diverse structure made from a variety of proteins and biopolymers. These elements have been incorporated into diverse hydrogels. The most common matrices that have been used are collagen, agarose gels, fibronectin, gelatin, laminin, and vitronectin[240]. Non-organic platforms are also available. A vast array of scaffold options have been developed for use depending on the cell or the purpose of study requirements. Establishing cells/spheroids/organoids within these scaffolds enables provision of some of the elements of the ECM which they would experience *in vivo*. As mentioned previously hydrogels and matrigels have the benefit of being able to be adapted to the culture requirements. However, concerns exist about inconsistencies for high throughput analysis, particularly about distribution of cells within the gel[235].

Type I collagen is a commonly used matrix component for culturing in 3D. Collagen plays a prominent role in maintaining the biologic and structural integrity of ECM. Therefore its use in a culture platform enhances the desired features of the native state *in vitro*[241]. Type I collagen is inexpensive, relatively easy to use and manipulate into the culture system required. Gels created from ECM components such as collagen or fibronectin contain bioactive ligands that engage receptors on cells. Polymers, such as polyethylene glycol, agarose, or alginate, are considered to be inert[242]. Recently, bioengineering approaches are presenting opportunities to develop novel patient specific cultures using 3D bioprinting methods to design ECM and patient individualized constructs in which to culture organoids[243]. 3D bioprinting techniques are also aiming to combat the potential inconsistencies in cell distribution seen in culture gels[235].

1.6.3 Spheroids

Tumour spheroids are one of the most versatile and utilised 3D models. Multicellular tumour spheroids, the aggregates formed from cancer cells, can be formed via a variety of methods. They can be self-assembling or forced to aggregate.

Spheroids are manufactured either in suspension or within non-adhesive scaffolds which provide an artificial matrix. Common substrates for spheroid scaffolds include agarose gels, collagen, matrigel and hyaluronic acid. The drawbacks of scaffold matrices for spheroid production are limitation in reproducibility of identical scaffolds across batches and analysis techniques for e.g. drug efficacy once the spheroids have embedded[244].

Methods for non-scaffold production include liquid overlay, hanging drop technique, rotary vessel/spinner flask or microtechniques with microfabricated chambers[245].

Once appropriate dimensions for spheroid growth have been achieved, spheroids should contain layers with cells of different phenotypic, functional and metabolic behaviours. Cell-cell interactions and cohesive behaviours are mediated through activation of adhesion receptors (e.g. E-Cadherins) and secretion of ECM proteins (e.g. collagen I and IV, fibronectin, laminin and lumican) and proteoglycans[246]. These interactions and the spheroid shape and density reproduce some of the characteristics of tumours in *in vivo* settings. The benefits of spheroid use are that they are relatively easy to produce and maintain and can be used to study many cancer types using established immortalised cell lines[247]. However, their lifespan is limited

due to perfusion difficulties and supply of nutrients to the centre of the spheroid through passive diffusion.

In HGSOC, disease spread is facilitated via tumour cells shedding from the ovary and fallopian tube into the peritoneal fluid and patients often develop large volumes of ascites containing tumour cells as both single cells and spheroids. These naturally occurring spheroids have been found to have upregulation of genes involved in chemoresistance[248]. Therefore, the study of ascitic spheroids in HGSOC is extremely relevant and has been used to examine both response to treatment and progression of disease through analysis of signalling pathways and cell-cell/cell-matrix interactions[249]. Velletri et. al developed HGSOC spheroids from dissociated cells from ascites. Ovarian cancer spheroids were generated over 8-12 days to tridimensional structures. Different properties of propagation of the spheroid structures were seen in different passages. Transcriptomic data of 3D spheroids compared to concurrent 2D cultures showed increased in EMT markers in 3D which increased between passages. The spheroids also retained expression profiles characteristic of the individual patients' tumours. Differential expression analysis revealed upregulation of pathways related to IL8 and integrin signalling in the spheroids, correlating with tumour growth and progression[250]. The Brenton group recently used ascites-derived HGSOC spheroids to correlate response to targeted therapies with somatic copy number alterations (SCNAs) and identify biomarkers for patient outcome linked to observed SCNAs[251].
In addition, to further optimise representative 3D cultures with spheroids, groups have assessed the incorporation of co-cultures with stromal cells in the design for their potential in drug screening. Tofani et. al showed that 3D co-cultures displayed upregulation of genes involved in tumourigenesis, angiogenesis and metastasis. [252].

1.6.4 Organoids

There is some debate as to the exact definition of an 'Organoid". The most commonly accepted description currently is 3D systems derived from stem cells consisting of organ-specific cell types that self-organise through cell sorting and spatially restricted lineage commitment[253]. However, it is also argued that it is not always necessary for stem cells to be used as the basis for development. Isolated tumour cells have also been used to produce the complex 3D systems incorporated with basement membrane and ECM components[254]. Organoid systems are self-organised and are usually developed from either pluripotent stem cells or adult stem cells

through the mimicking of organ regeneration *in vitro*[255]. In some cases, they have been shown to be histologically indistinguishable from human organs. Many organs and disease processes develop in different ways in e.g. mice compared to human. Therefore the development of organoids has enabled scientists to define the development of organ systems, anatomy and progression of disease more accurately than may previously have been theorised from animal models[256]. Organoid systems are versatile and have been used to study the development of many different organs and diseases.

Within ovarian cancer research patient-derived organoids have recently been used to study progression of disease and response to therapeutics. Organoids allow rapid assaying of phenotype–genotype correlations and drug sensitivity, while recapitulating patient response. Kopper et al established organoids derived from patient samples including both primary and metastatic sites. They also sampled non-cancerous fallopian tubes (FT) and ovarian surface epithelium (OSE) from patients undergoing prophylactic salpingoophorectomy. They had a good success rate in achieving organoid lines from both cancer (65% success rate) and non-cancer samples (85% success rate). Histological analysis of ovarian cancer organoids demonstrated their similarity to the carcinoma fields within the corresponding primary tumours and their distinction from non-malignant FT and OSE organoids [257]. They were also able to demonstrate the sustainability of organoids for long term use; whole genome sequencing (WGS) showed that when comparing the genomic landscape from early and late passage HGSOC organoids copy number variations (CNVs) were well maintained even after prolonged passaging. Intra-tumoural heterogeneity between primary and metastatic sites sampled could be observed in the primary samples and matched in the organoid lines derived from these sites. Additionally, both this study and others have shown the use of organoids in testing of therapeutics[258].
Nanki et al also derived ovarian cancer organoids from patient samples and could demonstrate similar CNVs between primary samples and organoids. They showed that tested drugs showed similar efficacies between primary and organoid samples and an expected response rate based on histological subtype[259].

Organoids provide an exciting prospect in the development and use of 3D culture systems. However, there are still limitations in what they can assess due to the lack of immune or stromal cells and vasculature. The possibility of perfusion systems to provide differing conditions to

mimic vascular supply is a potential future aide in representation of the *in vivo* microenvironment.

1.6.5 3D Organotypic Models

3D organotypic models are systems utilizing either single cell type, or co-cultures, designed to promote cellular differentiation, and to achieve *in vivo*–like 3D structure and organotypic functions[260].

The Lengyel group have extensively studied the dispersion patterns and invasion of ovarian cancer, developing a technique for 3D organotypic models using immortalised cancer cell lines and primary stromal cells to study these processes and the potential for high throughput therapeutic testing strategies.

Development of organotypic models requires understanding of the pathogenesis, dissemination pathways and structure of tumour microenvironments. As described earlier, in HGSOC, initial steps in metastasis involve transition from epithelial to mesenchymal type behaviour via alterations in cadherin and integrin expression[167]. The tumour clusters travel through the abdomen and attach to the mesothelial layer of the peritoneal lining which coats the surfaces and viscera within the abdomen including the adipose rich omentum.

The anatomical structure of the peritoneum lends itself to the concept of 3D organotypic models to create an *in vitro* mimic of the lining architecture. Kenny et al developed models constructed using a collagen base ECM layer containing non-cancerous fibroblasts, with a mesothelial lining layer on top of the fibroblast layer. Following preparation of the stromal cells in collagen, tumour cells were then added to the culture and progress monitored. Through this construction process the different steps in tumour growth, proliferation and invasion could be assessed.

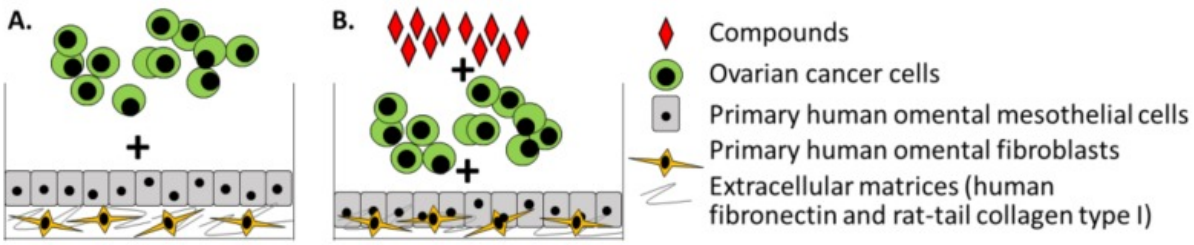


Figure* 1.*13: Example of 3D organotypic model. *3D organotypic model diagram depicting the construction of omental layers with tumour cells (A) and (B) the use of model in testing of therapeutics. Taken from [146].*

These models were initially used to assess the role of mesothelial cells in tumour invasion and metastasis, determining that they are actively involved in tumour cell colonisation and therefore promote invasion through the peritoneal lining. They were also further adapted to create high throughput drug testing platforms which is often a limiting factor in 3D culture systems[261]. Most of these experiments with organotypic models have used immortalised ovarian cancer cell lines due to their, as discussed, readily available nature and ease of use. To incorporate primary tumour cells into this 3D system would ideally give a more reliable, representative method of analysing HGSOC tumour cells.

1.6.6 Tumour explant/slice cultures

Tumour tissue slices or explants give perhaps one of the best opportunities to examine the tumour with its surrounding microenvironment. Tumour samples resected from patients are mechanically sliced, most commonly using a vibratome, which allows sectioning of tissues into >200 μm thick slices [262]. Slices are then cultured in platforms designed to best mimic the specific cancer type environment depending on perfusion requirements for nutrient delivery, pH and oxygenation delivery. Using these systems, a whole spectrum of solid tumour types can be studied[263]. Slice cultures have most commonly been used to study drug response *in vitro*. They have many positive aspects for 3D culture systems. However, they also have the drawbacks of being relatively short lived, with proliferation and viability maintained on average for around 5 days[264]. Direct access to patient tumours and ability to process the samples in a timely way is also required. Some of the culture platforms involve fluidic devices and costly equipment to maintain perfusion and viability. Reproducibility given the heterogeneity seen in cancer in general is tricky to reliably obtain[265]. Therefore, thorough representation of the disease *in vivo* is again limited in this model design, though it does provide more aspects of the microenvironment than many other 3D culture options. As discussed previously Majumder et al. have had great success in establishing reliable, patient specific tumour tissue slice cultures which preserve tumour characteristics and allow individualised prediction of response to treatment in certain cancers[215]. Gavert et al. have also employed tissue slice explants to discover novel biomarkers and test therapeutic opportunities in colorectal cancer[266]. Though not extensively investigated in HGSOC, *ex vivo* tumour slices have been used by the Van Gent group to analyse HRD status, initially in breast tumours and

more recently examined in HGSOC tumours, recognizing the importance of detection of HRD status beyond analysis for *BRCA* mutations[267][268].

Depending on the purpose for the tumour slices the culture design can be basic or more intricate. For example, different studies have found that using a membrane insert improves viability in the setup along with some rotational movement for optimising delivery of nutrients and oxygen[269]. For more complex study designs features such as fluidics devices for ongoing delivery and removal of nutrients and waste respectively are potential options being explored[270].

1.6.7 Patient derived xenografts

Patient derived xenografts (PDX) involve insertion of patient derived tumour cells or organoids into immunodeficient mouse models. PDXs provide elements of tumour microenvironment including vasculature and lymphatics to better represent the human setting[271]. They can then be used to study the development of tumour deposits, invasion and metastasis. Drug treatment response and toxicity can also be examined. They have been shown to grossly maintain tumour histopathology profiles and cellular composition[272]. Furthermore they appear to provide a good representative model for drug response compared to human trials in some cancers[273]. However, they are expensive models to establish, can have low success rate in generation and prove difficult to produce high throughput results[274]. Though many aspects of the tumour microenvironment may be present the anatomy and physiology of mice are not identical to humans and toxicity profiles are not fully reliable given the different metabolism pathways between mice and humans. There are also some recent findings suggesting the heterogeneity existing in tumours may give rise to lack of confidence in the maintenance of cancer profiles in PDX models[275]. However conversely, to investigate potential genetic drift, Cybula et. al showed that ovarian cancer PDX models could retain the molecular and histological characteristics of the original patient derived tumour, this was maintained over several passages and the mouse models also showed therapeutic response correlating with the patient of origin[276].

1.7 Project Background

Investigation into ITH in HGSOC to date has mainly focussed on understanding genomic and immune cell heterogeneity[101, 140, 277]. However, to improve patient outcomes, greater understanding is required, not only at a genomic level but also proteomic and functional levels to aide in the identification of diagnostic and prognostic markers.

Further to this, in order for conclusions to be drawn about tumour behaviour and responses to treatment, to properly model this tumour heterogeneity *in vitro* and to assist in the discovery and testing of novel therapeutics, improved, more clinically relevant, culture systems are required. These culture models should aim to reflect the diverse microenvironments of HGSOC tumours as close to the *in vivo* state as possible.

The ITH project was established in 2013 at the West London Centre for Gynaecology oncology based in Hammersmith Hospital, in collaboration with the Department of Surgery and Cancer, Imperial College London. To obtain further insight into the associations between spatial and temporal heterogeneity with metastatic dissemination, operative outcomes and response to platinum treatment, the ITH project evaluated tumour samples from HGSOC patients undergoing primary cytoreductive surgery. Patients were tracked over the course of their treatment and patterns of relapse, progression free intervals and overall survival were all examined. Multiple concurrent analyses including multi-omics profiling were carried out, the results of which are outside the scope of this thesis.

This thesis covers my work on the ITH patient cohort, including platinum response analysis and tumour proliferation status (Ki67) , with all results correlated to clinical treatment response and patient outcome. Further to these analyses, 3D model culture systems were developed to support the examination of variation in response to treatment in HGSOC.

1.8 Hypothesis

- The intra-tumoural heterogeneity observed in HGSOC patients contributes to variations in sensitivity to platinum treatment and patient outcome.

- The individual tumour microenvironments surrounding metastatic deposits in HGSOC can influence their response to platinum treatment.

- Incorporation of elements of the tumour microenvironment into 3D culture platforms can give more representative analysis of response to platinum treatment.

1.9 Aims

- To investigate the variation in *in vitro* response to platinum treatment through multi-site analysis of primary tumour samples from patients undergoing maximal effort primary cytoreductive surgery. Comparison of responses between individual patients and different anatomical sample sites.

- To develop 3D organotypic models reflecting the *in vivo* peritoneal microenvironment in which to culture primary tumour cells and analyse the impact of culture systems on response to platinum treatment.

- To evaluate *in vitro* and *ex vivo* 3D culture designs for use within HGSOC in studying tumour behaviour and variation in response to platinum therapy by incorporating analysis of the individualised tumour extra-cellular matrices.

Chapter 2

Materials and Methods

2 Materials and Methods

2.1 Patient cohorts and tissue collection procedures

The different experiments carried out within this project utilised primary cell cultures extracted from both cancerous and non-cancerous tissues. This involved collection of samples from two different cohorts of patients. For the construction of the 3D organotypic models it was necessary to have non-cancerous omental tissue for stromal cell extraction. Patients with macroscopically/radiologically 'normal' appearing omentum who were undergoing surgery where omentectomy or omental biopsy was to be performed were counselled and consented for sample collection prior to surgery.
For all experiments involving primary tumour cells, the ECM study and patient-derived explant slice cultures, the tumour tissue samples were collected from advanced stage HGSOC patients at the time of primary maximal effort debulking surgery and processed as described below.

The project was performed under the Hammersmith and Queen Charlotte's and Chelsea Research Ethics Committee approval, following full patient counselling and consent. The procedures involving human participants were done in accordance with the ethical standards of the institutional and/or national research committee and with the principles of the 1964 Declaration of Helsinki and its later amendments or comparable ethical standards. All approvals were in place for the use of human tumour and blood samples for this project. Human samples to be used in this research project were obtained from the Imperial College Healthcare Tissue Bank (ICHTB). ICHTB is supported by the National Institute for Health Research (NIHR) Biomedical Research Centre based at Imperial College Healthcare NHS Trust and Imperial College London. ICHTB is approved by Wales REC3 to release human material for research (22/WA/2836), and the samples for this project (R14142 plus amendments – ITH project, R15006 plus amendments – 3D organotypic models) were issued from sub-collection reference number GYN_HG_13_020.

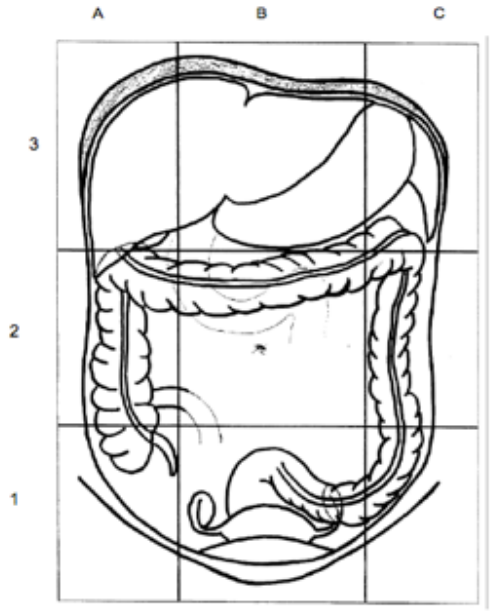
The ITH study was a collaborative project established within the West London Gynaecology Cancer Centre of Hammersmith Hospital, Imperial College NHS Trust. Patients were recruited between September 2013 and November 2018.

Eligibility for inclusion in this study involved patients undergoing primary maximal effort debulking surgery due to advanced stage III-IV HGSOC. Patients were required to be chemotherapy naïve and those with any secondary cancers or found to have non-HGSOC histology were excluded.

Tumour samples were collected in alignment with the recognised standardised intra-operative mapping tool (IMO) [278]. The IMO mapping tool showing labelled anatomical grid is shown in figure 2.1. Samples were obtained from primary and multiple metastatic sites with as much scope for comparable locations between patients as possible. Sites sampled across the patient cohort are displayed in table 2.1.

A full list of patients involved in the different parts of this project and clinical information are recorded in table 9.1 in the appendix.

Figure 2.1: The intra-operative mapping tool (IMO). *The intra-operative ovarian cancer mapping tool was used to guide systematic collection of tumour samples*



Tumour locations (primary and relapse)	*n=*	IMO location
Ovary (left & right)	50	B1
Omentum	49	B2
Diaphragm (left, central & right)	42	A3-C3
Mesentery	15	B2
Spleen	14	C3
Pelvic peritoneum	16	A1-C1
Paracolic (left & right)	11	A2, C2
Liver capsule	9	A3
Falciform ligament	9	B3
Large bowel	11	A2-C2
Bladder	5	B1
Recto-sigmoid	12	B1
Stomach	4	B3
Para aortic LN	4	B2
Small bowel	3	B2
Vagina	2	B1
Pancreatic area	2	B2
Morison's pouch	2	A3
Sub cutaneous abdominal nodule	2	B2
Uterus	1	B1
Porta Hepatis	1	A3
Pelvic LN	2	A1, C1
Psoas muscle	1	C1
Suprarenal LN/Coeliac trunk	2	B2
Gallbladder area	1	A3

Table 2.1: List of anatomical sites examined and numbers of samples across the cohort with corresponding IMO locations.

To isolate normal fibroblasts and mesothelial cells to construct 3D organotypic models, patients undergoing surgery with macroscopically normal-appearing omentum were consented for collection of biopsies of normal-appearing omentum to be obtained during their surgery.

2.2 Stromal cell extraction

Fibroblasts and mesothelial cells were extracted from macroscopically normal-appearing omentum tissue following protocols from the Lengyel group[261]. Omentum samples were collected during surgery directly into a sterile container containing cold phosphate buffered saline (PBS) and taken to the lab for processing. The omentum tissue was placed in a large petri dish with additional PBS. The surface of the omentum was scraped gently with a scalpel to obtain the first purification of mesothelial cells. The cells were dislodged into the PBS which was collected and centrifuged for 10 mins at 350xg. The cell pellet was resuspended in media

for primary cell work (termed complete primary media for this study) comprising RPMI 1640 media (Sigma-Aldrich, UK) with 20% (v/v) foetal calf serum (First Link, UK), 50 U/ml penicillin and 50 μg/ml streptomycin, 2 mM L-glutamine (Life Technologies, UK), 2 mM sodium pyruvate (Sigma-Aldrich) and 2.5 μg/ml insulin (Sigma-Aldrich). The resuspended cells were incubated as 'Purification 1'.

Additional PBS was added to the omentum tissue sample, and it was then dissected into 3mm sized pieces. Once dissected the tissue and PBS were transferred to a 50ml tube and stood upright to determine the volume of tissue present. The PBS under the tissue was removed by pipetting, collected and centrifuged for 10 mins at 300xg and the resulting cell pellet resuspended in complete primary media and added to Purification 1.

A solution of 50:50 PBS:1X Trypsin (Sigma-Aldrich), equal volume to that of the tissue, was added to the tubes containing the remaining tissue, and the tubes were placed on a shaking platform in an incubator at 37^{o}C and 5% CO_2 for 1 hour. The omental tissue was then removed from the solution and centrifuged for 10 mins at 350xg. Following this the mesothelial cells were resuspended and cultured in complete primary media as 'Purification 2'.

For the fibroblast extraction, the omental tissue was then immersed in an equal volume of a 1x collagenase type III/hyaluronidase solution (Worthington Biochemical). To make up 10ml of 10X solution: 150mg collagenase type III, 23.8mg hyaluronidase, 5ml PBS, 50 U/ml penicillin and 50 μg/ml streptomycin. 1X solution of required volume was obtained by diluting with PBS. The tissue and collagenase solution was placed on a shaking platform and incubated overnight at 37^{o}C and 5% CO_2. The following morning the tissue was removed, supernatant centrifuged for 10 minutes at 350xg, then pellet washed with media and centrifuged. The resulting pellet of fibroblasts was resuspended in complete primary media and incubated. These cells were cultured and observed over the next few days, media change was usually required around day 3-4 to remove erythrocytes and dead cells. The cells were able to be cultured in a healthy condition for up to 3 passages over 4 weeks with passaging and storing of cells possible, with viability preserved.

2.3 Establishment of primary HGSOC tumour cell cultures

At the time of primary maximal effort debulking surgery, tumour pieces from multiple disseminated sites within the patient were collected directly into sterile containers with RPMI 1640 media supplemented with 50 U/ml penicillin and 50μg/ml streptomycin. These were then immediately taken to the lab for processing. Following removal of a portion of tumour for snap and viable freezing (if sufficient tumour was available), the remaining tumour tissues were dissected into 1mm pieces and incubated with 2.4 U/ml dispase II (Roche, UK) for 1hr at 37^{o}C, 5% CO_2, the samples were gently shaken every 2 minutes. After 1 hour, complete primary media (composition as above) was added to the samples to stop the protease activity.
A 70 μM filter was used to pass the dissociated tumours using pressure from a 10ml syringe plunger and the resulting cell suspension was centrifuged at 450xg for 15 minutes. Red blood cell lysis buffer (Milteny Biotec, UK) was used to remove erythrocytes contaminating the sample. Once red cell lysis was completed, the tumour cells were incubated for 30 minutes in tissue culture flasks (size dependent on estimated cell number) to allow stromal cells to adhere to the plastic and thus to remove the stromal cells as a purification step from the final culture population. After 30 minutes the media containing the non-adhered tumour cells was transferred to new tissue culture flasks and incubated at 37^{o}C, 5% CO_2. The flasks were inspected and purity of cell cultures was estimated from observed cell morphology and confirmed using PAX8 immunofluorescence staining.

2.4 Confirmation of stromal cell populations

To confirm that the primary cell populations extracted for use in constructing the 3D organotypic models were indeed mesothelial cells and fibroblasts, we optimised a protocol for immunofluorescent staining and confocal microscopy. This staining protocol was applied to all cell cultures extracted from the macroscopically normal-appearing non-cancerous omental samples. The importance of checking each fibroblast and mesothelial cell culture was shown in one case where the macroscopically ‘non-cancerous’ appearing omentum showed tumour clusters on microscopy and stromal cells from this case were subsequently excluded from the study.

Extracted stromal cells were seeded into 6-well plates with sterilised coverslips and incubated at 37°C, 5% CO_2 for 48 hours, allowing the primary cells to adhere. Cells on the coverslips were then fixed with 4% paraformaldehyde (PFA) for 10 minutes then washed three times with PBS. The slides were then incubated with 200µl blocking buffer (TBS 1x + 0.5% Triton + 10% normal goat serum) for 1 hour at room temperature. The primary antibodies were diluted (1:200, TBS 1x + 0.1% triton + 10% normal goat serum) and applied for overnight incubation at 4°C (mesothelial cell: calretinin Mouse, 1:200 Abcam M7245; fibroblasts: anti-fibroblast Mouse 1:200 Abcam Ab11333; cancer-associated fibroblasts: α-smooth muscle actin Mouse, 1:200 Sigma A2547). The following day, after three washes with PBS, the coverslips were incubated with 200µl of the diluted secondary antibody (Alexa fluor 488, 1:2000) for 2 hours' incubation at 37°C.

Coverslips were then washed a further 3 times with PBS then coverslips were applied and mounted onto glass slides with prolong gold containing DAPI (Life technologies) then left to dry. The coverslips were sealed with nail varnish and cells imaged with SP5 confocal laser scanning microscope (Leica).

Primary Antibody	Origin	Catalogue number	Supplier	Dilution	Incubation time	Secondary antibody
Mesothelial cells Calretinin	Mouse	M7245	Abcam	1:200	Overnight 4℃	1:2000 Anti mouse IgG Alexa Fluor 488 goat
Fibroblasts Anti- Fibroblast	Mouse	Ab11333	Abcam	1:200	Overnight 4℃	1:2000 Anti mouse IgG Alexa Fluor 488 goat
Cancer associated fibroblasts (CAFs) α-smooth muscle actin	Mouse	A2547	Sigma	1:200	Overnight 4℃	1:2000 Anti mouse IgG Alexa Fluor 488 goat
Control	N/A	N/A	N/A	Blocking buffer	Overnight 4℃	1:2000 Anti mouse IgG Alexa Fluor 488 goat

Table 2.2: Primary and secondary antibodies used for confirmation of cell type, with dilutions and incubation conditions.

2.5 3D organotypic model assembly

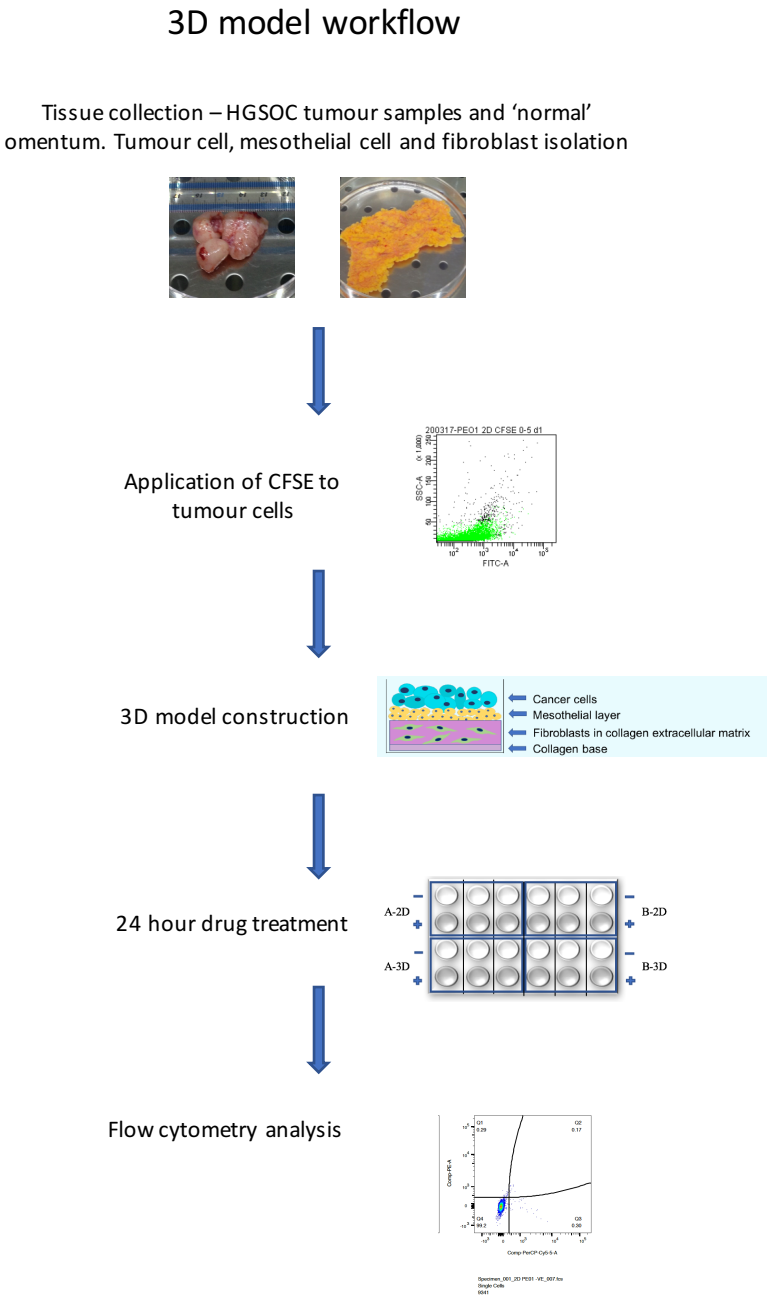


Figure 2.2: Diagrammatic representation of 3D organotypic model workflow. *HGSOC tumour cells were isolated from tumour samples collected using IMO mapping at the time of primary debulking surgery. Stromal mesothelial cells and fibroblasts were isolated from non-cancerous omentum and cultured until confluent. Tumour cells were stained with CFSE ahead of application to 3D organotypic models for identification during flow cytometry analysis. Layered 3D organotypic models were constructed containing rat tail 1 collagen ECM, stromal cells then tumour cells were applied ahead of 24hour treatment with 25uM cisplatin. Apoptosis and necrosis readouts were completed using flow cytometry analysis.*

To study the effect of the local tumour microenvironment, including stromal cells, on response to chemotherapy treatment, 3D organotypic models were designed, optimised and constructed based on omental stromal cells extracted from normal omental samples embedded within a collagen extracellular matrix (ECM). Organotypic models were originally constructed based on protocols from the Lengyel group, which were further optimised and adapted for the use of heterogeneous primary tumour cells.

3D organotypic models were constructed within 24 well culture plates within a transwell insert (Corning). A collagen-based extracellular matrix was assembled composed of 80% collagen I (Corning), 9% 10x minimal essential medium (Thermofisher), 1% foetal calf serum (First-link), 10% NaOH (0.34M).

On day 1, a base layer of 200µl ECM solution was applied to the transwell inserts, incubated at 37^{o}C, 5% CO_2 and allowed to solidify over 2 hours. Fibroblasts from culture were collected, counted and the required cell number centrifuged at 350xg for 10 minutes. Fibroblasts were re-suspended in ECM solution, 4000 fibroblasts per 500µl ECM per well, then the suspension was applied to each well, incubated at 37^{o}C, 5% CO_2 for 4 hours until the ECM solidified, and fibroblasts were observed to start spreading out within the matrix.

Mesothelial cells from culture were collected, counted, centrifuged and re-suspended in primary media. The ratio of fibroblasts to mesothelial cells required to form a representative omental organotypic model was optimised to 1:5 therefore in 24 well plates 20,000 mesothelial cells were seeded per well. In each well, 20,000 mesothelial cells were applied onto the top of the ECM/fibroblast layer in 500µl complete primary media. 500µl primary media was applied surrounding the transwell inserts. The models were then incubated overnight at 37^{o}C, 5% CO_2.

To enable flow cytometry analysis of the models following drug treatment, tumour cells were required to be stained with a fluorescent dye - CellTrace™ CFSE (Thermofisher) - prior to application on the models. This allowed them to be distinguished from the stromal cells during analysis. On day 1, prior to use, the primary HGSOC tumour cells were retrieved from the culture flasks, centrifuged and resuspended in 1ml PBS with 1µl CFSE (working concentration 5µM). The cell suspension was incubated at room temperature in the dark for 30 minutes then 5x volume of media added, centrifuged and resuspended in primary tissue culture media. CFSE-labelled tumour cells were then incubated at 37^{o}C, 5% CO_2 until ready to be applied to the models.

On day 2, the excess media was removed from the wells of 24well transwell inserts. The CFSE-labelled primary tumour cells were prepared and 50,000 cells per well were applied to the top of the models in 500µl of primary tissue culture media per well. 1ml of primary media was reapplied around the transwell inserts and they were incubated for 24 hours.

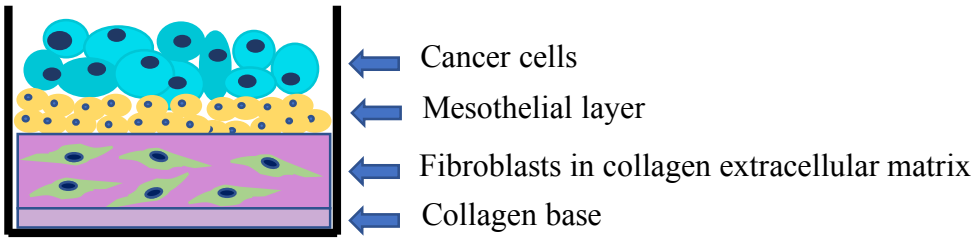


Figure 2.3: Diagrammatic representation of the constructed 3D organotypic model. *Image shows the different layers of the model reflecting the peritoneal lining*

.

To allow for comparison between 2D and 3D response to treatment primary tumour cells were also seeded into 24 well plates in the same numbers and incubated for 24 hours. Where possible depending on the number of tumour cells present, samples were seeded in duplicate or triplicate for both untreated and treated wells. Control wells contained CFSE-labelled untreated tumour cells and unlabelled untreated tumour cells.

The following day both 2D wells and 3D models were treated with 25µM cisplatin for 24 hours, to mirror the treatment protocol in the ITH apoptosis assays. Following drug treatment, flow cytometry analysis for apoptosis levels was performed.

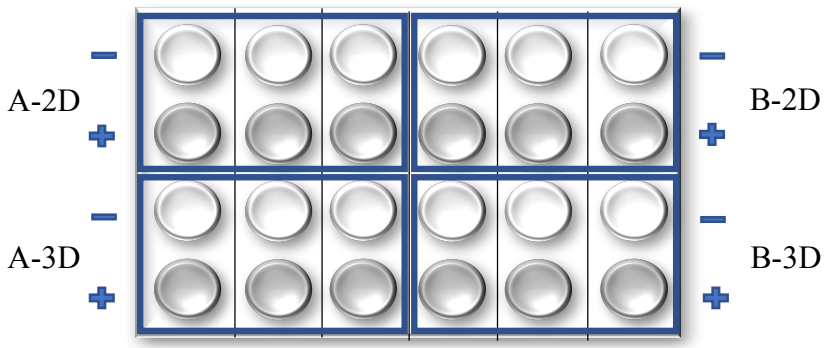


Figure 2.4: Example of 24 well plate culture setup. *Diagrammatic example of 24 well plate with 2 tumour site samples. Cells seeded in triplicate in 2D and on 3D organotypic models. Samples treated with 25µM cisplatin for 24 hours then analysed for apoptosis and necrosis using flow cytometry alongside untreated controls.*

2.6 3D organotypic models flow cytometry apoptosis assays

Following drug treatment with cisplatin 25μM for 24 hours, both 2D and 3D organotypic model samples were assessed for levels of apoptosis and necrosis. Protocols for cisplatin treatments in the ITH apoptosis assays had been optimised to 25μM dosing for 24hours ahead of caspase 3/7 analysis (section 2.7). To enable 2D and 3D comparison the same treatment protocol was used for the 3D culture analysis.
The initial protocol aimed to use immunohistochemistry to study response to treatment however during the optimisation process, several issues arose with the fixation process, therefore I sought an alternative readout for drug response and used flow cytometry analysis.

Any remaining media was removed from the models and retained to combine with the suspension from the models. Liberase solution at 0.3 units/μl (Sigma-Aldrich) was used to dissolve the collagen structure and release all cells into suspension. Models were incubated in liberase at 37^{o}C, 5% CO_2 for 1 hour. The suspension was then filtered to remove any remaining collagen. In parallel, during the model dissociation incubation period, the 2D treatments were trypsinised and the cells collected for analysis.
Cell pellets for each sample well (3D and 2D) were collected via centrifugation at 350xg for 10 minutes.

Apoptosis and necrosis levels were analysed using PE Annexin V apoptosis detection kit (BD Biosciences). Cells obtained from the 3D models and control 2D groups were gently resuspended in 100μl binding buffer as per the kit protocol and placed in labelled FACS tubes. 0.1μl of Annexin and 3μl 7AAD were added to the suspension. The tubes were gently vortexed then incubated for 15 minutes in the dark at room temperature. After 15 minutes, a further 400μl binding buffer was added to each tube then they were placed on ice to prevent degradation of the samples and transferred to the Flow cytometry facility for processing within 1 hour. The samples were run on a FACS Canto machine (BD Biosciences). Unlabelled primary tumour controls were processed initially to confirm forward and side scatter locations. Control samples for CFSE, Annexin and 7AAD were then run to confirm compensation protocols for the channels used. CFSE was detected in the FITC channel, tumour cells were gated and then any doublet cells excluded. Annexin was detected in the PE-A channel and

7AAD in the PerCP-Cy5-5-a. Following compensation for the multiple labels, the samples were run and readouts of apoptosis and necrosis obtained.

2.7 Apoptosis assays

For the ITH project, primary HGSOC tumour cells extracted from disseminated tumour sites were seeded into 96 well plates, each sample analysed in triplicate. They were then incubated for 48 hours to allow cells to adhere. Cisplatin at a concentration of 25μM was applied to the samples alongside media only controls and then incubated for 24 hours at 37^{o}C, 5% CO_2. This concentration was chosen based on IC_{50} data from testing of multiple reported cisplatin sensitive and resistant HGSOC cell lines by the ITH group prior to my starting the project. This concentration is more representative of a resistant cell line. Due to limited material from the primary cultures this dose was selected to treat with a consistent high concentration across all patient samples treated to ensure inducing an apoptotic response. The ApoTox-Glo Triplex Assay (Promega, US) was used to assess the apoptotic activity and cell viability within each well, measuring the active caspase-3/7 and normalising the caspase activity to the viability of each sample measured, following manufacture's protocol.

To first measure viability, GF-AFC reagent was added to the wells then incubated for minimum 30 minutes at 37^{o}C, 5% CO_2. The fluorescence signal was measured using LUMIstar OPTIMA (BMG LABTech) giving the proportion of viable cells remaining. Following this reading, as a measure of apoptosis, Caspase-Glo 3/7 reagent was applied to the wells then incubated for the same time as viability assay (minimum 30 minutes) at room temperature in the dark. The relative luminescence unit was measured using LUMIstar OPTIMA. Apoptosis levels were normalised to the relative cell viability and calculated as a fold change to the untreated cells.

2.8 IC_{50} assays

The multisite primary HGSOC tumour cells were seeded at 10,000 cells per well in a 96 well plate, in triplicate and incubated for 48 hours. Tumour cells were treated with two-fold serial dilutions from 100μM to 0μM Cisplatin for 72 hours and then half maximal inhibitory

concentration (IC50) values were measured using an MTT assay. After 72 hours MTT reagent (3-(4,5-dimethylthiazol-2-yl)-2,5-diphenyl tetrazolium bromide; Sigma-Aldrich) was added, resuspended in PBS at 3mg/ml. Stop solution (10% SDS, 0.01%HCl) was added after 3 hours then the plates were incubated for a further 24 hours. An Optimax tunable microplate reader was used to measure absorbance at 570nm, corrected for background, and normalised against the untreated wells.

2.9 Ki67 proliferation index immunohistochemistry (IHC)

For this study Ki67 staining was performed on frozen section samples from multiple anatomical locations from 46 patients. The staining was optimised and performed as a service by the BCI Pathology service at Barts Cancer Institute, Queen Mary University of London due to their expertise in working with frozen tissue sections and availability of automated staining with a Ventana platform. Scoring of Ki67 stained sections was performed by our collaborator Dr Stephen McQuaid (FRCPath), Queens University Belfast. H&E and Ki67 staining was used for determining Ki67 proliferative index (PI) by manual microscopic evaluation.

Frozen sections were taken adjacent to the tumour tissue used for molecular analyses. The sections were fixed in a 50:50 solution of acetone/methanol. Ki67 antibody Abcam ab16667 (clone SP6) was used with automated IHC performed on a Ventana platform with DAB as chromogen. Ki67 counts were performed on an average of 1000 tumour cells per slide at 20x magnification. Where fewer than 1000 tumour cells were present, the count was based on number of cells available. On assessment of staining, faint but specific nuclear expression was deemed positive. Two scorers were used for concordance of scoring. Moderate or borderline Ki67 scoring samples were subjected to a repeat “hot spot” count. Those samples judged as inadequate were omitted. Three scoring groups were established: Low (0-20% Ki67 PI), moderate (21-59% Ki67 PI) and high (>60% Ki67 PI). To examine the variation of Ki67 PI between tumour deposits and different patients the median absolute deviation (MAD) was determined.

2.10 Extracellular matrix protein lysate extraction

To study the diversity in the tumour microenvironment of disseminated HGSOC, with the aim to replicate the microenvironment dynamics in our 3D organotypic models, protein lysates were extracted from tumour samples taken from different anatomical locations in patients undergoing surgery for advanced HGSOC. Initial processing of tumour samples was performed as for the primary tumour cellular extraction to decellularise the tumour matrix (section 2.3), using dispase as described above, using a shorter incubation time in dispase (15 minutes). Following the incubation with dispase and filtration of the cells into suspension, the remaining tumour tissue was retained for protein extraction. The decellularised tumour ECM samples were sent for MS analysis.

Tumour tissues were placed in 50ml centrifuge tubes for homogenisation on ice. 1ml of a high salt buffer solution was added to each sample composed of 0.05M Tris pH 7.4, 3.4M NaCl, 4mM EDTA, 2mM N-ethylmaleimide, 25x protease inhibitor, 100x phosphatase inhibitor, 1mM DTT). The samples were homogenised in the tubes using a tissue homogeniser (Tissue Ruptor II, Qiagen). The homogenised mixture was centrifuged x3 times at 7000xg for 15 mins in 2ml eppendorf tubes. The supernatant was then discarded, and the pellet resuspended in 1ml of 2M urea buffer (0.15M NaCl, 0.05M Tris pH 7.4). Lysates were then incubated on a stirring platform in the cold room overnight. The following day, an aliquot (100µl) was removed for Western blot and stored at -20°C. The remaining suspension was centrifuged at 14,000g for 20 minutes. The supernatant was discarded and the pellets were stored at -80°C ahead of transfer to DC Biosciences facility, based in Dundee, Scotland, for MS analysis. At the facility, the laboratory team prepared them for MS analysis using internal DC Biosciences company protocols. Tandem mass tag (TMT) labelling was used for accurate quantification of the sample ECM protein composition, a method which allows for both reliable identification of the peptides and their relative abundance[279]. For data processing the protein compositions of each sample were normalised to a pool of total sample cohort proteins.

2.11 Tumour explant slice culture preparation

To investigate using better 3D models of cancer that incorporate a more representative tumour microenvironment, a vibratome was used to section whole tumour samples to obtain 200-600 μm tumour slices and culture techniques were optimised to maintain tumour slices in culture.

Tumour tissues were collected directly from primary maximal effort debulking surgeries as per usual collection protocol. Where tumour samples were >1cm with a dense appearance, slice cultures were taken. Tumours were kept in RPMI 1640 media supplemented with 50 U/ml penicillin and 50μg/ml streptomycin. The tumours were cut with a scalpel down to minimum 1cm cubed pieces. These were placed on a vibratome (Leica 1200S Vibratome) cutting platform and 350μm slices were taken across the whole sample. These were cultured in 6 well plates with standing cell culture inserts (Merk-Millipore) with 2ml complete primary media: RPMI 1640 media (Sigma-Aldrich, UK) with 20% (v/v) foetal calf serum (First Link, UK), 50 U/ml penicillin and 50 μg/ml streptomycin, 2 mM L-glutamine (Life Technologies, UK), 2 mM sodium pyruvate (Sigma-Aldrich) and 2.5 μg/ml insulin (Sigma-Aldrich).

2.12 Slice culture treatment and immunohistochemistry (IHC)

Tumour slices were incubated in primary media at 37^{o}C, 5% CO_2 for 24 hours then drug treated with cisplatin 25μM for 24 hours, with untreated controls receiving fresh primary media.
Media and cisplatin was subsequently removed from the tumour slices and they were fixed overnight in 10% formalin. Tissues were then placed in histology cassettes to maintain structural integrity. Next, they were rinsed with distilled water (DW) and stored in 70% ethanol (EtOH) until ready for embedding.
For dehydration, tissues were covered in 100% Ethanol (EtOH) for 1 hour, EtoH changed and repeated x3 times at room temperature. The final EtOH was removed and the tissues were left in Histoclear overnight. The following morning, samples were covered with paraffin wax and placed in an oven for 1 hour. Tissue slices were then embedded in paraffin wax and left to set, prior to sectioning. Formalin fixed paraffin embedded (FFPE) blocks were sectioned using a

microtome (Leica RM2235) at 5μm and mounted on Superfrost Plus glass slides. Sections were allowed to dry at 37^{o}C after sectioning.

2.13 Haematoxylin and Eosin staining

I carried out the initial staining with haematoxylin and eosin (H&E) to observe tissue structure and tumour content. Slides were heated in histology oven for 30 minutes prior to H&E staining, as per the protocol below.

Solution	Time
Histoclear	5 minutes
Histoclear	5 minutes
100% ETOH	2 minutes
100% ETOH	2 minutes
70% ETOH	1 minute
Distilled Water	Rinse
Haematoxylin	5 minutes
Running Water	5 minutes
Acid alcohol	Dip
Running Water	1 minute
Eosin	1 minute
70% ETOH	20 seconds
100% ETOH	30 seconds
100% ETOH	2 minutes
100% ETOH	2 minutes
Histoclear	2 minutes
Histoclear	2 minutes

Table 2.3: Table summarising H&E staining protocol

Slides were then gently dried then mounted in DPX with appropriately sized coverslips.

2.14 External IHC protocols for slice culture blocks

For consistent staining of the tumour tissue slices, using an automated staining platform (Ventana), external assistance with processing and immunohistochemistry was sought from the Section of Pathology, Department of Metabolism, Digestion and Reproduction, Imperial College at Charing Cross Hospital. Tumour tissue sections were immunostained for PAX8, Ki67 and Cleaved caspase 3 evaluation. Antibodies were selected based on literature reviews and optimised first in-house and subsequently by Hiromi Kudo, Section of Pathology, for use with FFPE tissue. Ki67 staining had been optimised by Hiromi Kudo previously and in use by the facility. The staining protocol has been supplied for the purposes of this project:

- FFPE tissue samples cut at 3μm using a microtome (Leica RM2235) and placed on superfrost plus coated glass slides.
- IHC detection of Cleaved Caspase3 (rabbit monoclonal anti-Human Cleaved Caspase3 protein, clone: 5A1E, Cell Signalling-marker of apoptosis), Ki67 (mouse monoclonal anti-Human ki67 protein, clone: K2, Leica-marker of proliferation), PAX8 (mouse monoclonal anti - Human PAX8 protein, clone: PAX8R1, Abcam-tumour marker) were diluted 1:100, ready to use, 1:50 and 1:100 respectively.
- Immunostaining was carried out using the automated Bond Leica RX (Leica Biosystems Newcastle, Ltd.) using on board heat-induced antigen retrieval with Bond Epitope Retrieval Solution 1 (citrate-based pH 6.0 for 20 min) for cleaved caspase3, Ki67 and Bond Epitope Retrieval Solution 2 (EDTA-based pH 9.0 solution for 20min) for PAX8.
- Endogenous peroxidase activity was blocked using 0.3% hydrogen peroxide for 5 min.
- The histological specimens were then incubated with the Primary Antibodies (cleaved caspase3 and PAX8 for 60 min; Ki67 for 15 min) at room temperature.
- Ahead of application of the Polymer reagent, the sections were incubated for 15 min (PAX8) and 8 min (Ki67) at room temperature with Rabbit anti-mouse IgG (Post Primary). No Post Primary was applied for cleaved caspase3 detection.
- Following this, the slides were incubated with Goat Anti-rabbit Poly-HRP-IgG (Polymer reagent) for 15 minutes at room temperature. The reactions were developed using a Bond polymer refine detection kit and followed by colour development with 3,3′-diaminobenzidine tetrahydrochloride as a chromogen for 10 min.

- The tissue sections were dehydrated in absolute alcohol, cleared in three changes of xylene, and then mounted with a mounting medium.

Primary Antibodies								Bond Leica RX		
Source	**Antibody**		**Clone**	**Cat No**	**Lot No.**	**Con.**	**Dilution and inc.**	**Ag Ret Reagent**	**IHC Protocol**	**Positive control**
Cell Signaling	cleaved Caspase3 (Asp175)CC3	RBmAB	5A1E	9664	22	40 µg/ml	1/100(1h)	H1(20 min)	60_NOPP_P15_D10E10	Human Tonsil(M12/20732 A2) (7621)
Abcam	PAX8	MmAB	PAX8R 1	ab53490	GR33484 68-5	0.1MG/ML	1/50 (1h)	H2(20min)	60_PP15_P15_D10E10	Human Ovary CC (7464)
Leica	ki67	MmAB	K2	PA0230	71084	n/a	RTU	H1(20 min)	Protocol F: 15_PP8_P8_D10	Human Tonsil(M12/20732 A2) (7621)

Table 2.4: Summary table of antibodies and reagents used in the IHC by Section of Pathology, Department of Metabolism, Digestion and Reproduction at Charing Cross Hospital.

Whole slide scans were taken on a NanoZoomer 2.0-HT (Hamamatsu, Shizuoka, Japan) scanner using NDP.scan 3.2.17 software. NDP.view 2 software was used for image viewing.

Chapter 3

Results: Characterisation of intra-tumoural heterogeneity in HGSOC

3 Results: Characterisation of intra-tumoural heterogeneity in HGSOC

3.1 Introduction

With the advent of platinum-based chemotherapy approximately 40 years ago, survival outcomes for ovarian cancer have greatly improved. However, there has been little advancement in cure rates since then and 10-year survival remains poor[280]. Recent improvements in surgical techniques and the inclusion of novel targeted systemic treatments such as PARP inhibitors are working towards better PFS, prolonging OS and creating more of a chronic illness disease pattern[281].

Personalised treatment strategies are needed to improve outcomes but this requires deeper understanding of the treatment response of individual tumours. It is known that approximately 25% of HGSOC cases may have a germline, somatic or epigenetic alteration in *BRCA1* and *BRCA2*. PARP inhibitors are now being used commonly as maintenance therapy showing improvements in PFS[282-285] for those patients with *BRCA* mutations and more recently are now administered to patients with positive HRD scores when analysed for HRD status.

Most studies assessing the genomic, proteomic and immunogenic landscapes of HGSOC have had small numbers of tumour samples or limited patient numbers, most often sampling the primary tumour or omentum and rarely outside of the abdomen[101, 286, 287]. Very little information is known about the tumour biology of distant metastatic sites. Also, some studies have focused on profiling primary tumour samples from patients following neoadjuvant chemotherapy[288]. In these cases, the previously given treatments may give rise to alterations in biological functions which are not observed in samples from chemo naïve patients[288].

The focus of this chapter is to characterise the phenotypic outcomes with regard to response to platinum treatment in the ITH patient cohort, to examine the potential variation present between disseminated tumour sites. Subsequent chapters will progress this further using different 3D culture systems. To note, data arising from the genomic and proteomic profiling of ITH project tumour samples was the basis of another PhD thesis in our group and is therefore outside the scope of this thesis.

3.2 Overview of patient characteristics

3.2.1 Patient cohort

Table 3.1: ITH project patient demographics data

Summary of patient clinical characteristics		**n =**	**%**
Number of patients		49	
Age at diagnosis	Mean	62	
	Range	32-91	
FIGO tumour stage	III	28	57.1
	IV	21	42.9
Residual disease	Tumour free (non-visible)	42	85.7
	Non-tumour free (any visible disease)	7	14.3
Surgical procedures	Bowel Resection	38	77.6
	Splenectomy	22	44.9
	Bulky LN resection	25	51
	Diaphragmatic and/or liver capsule resection	39	79.6
	Pleurectomy and/or paracardiac LN removal	11	22.5
Disease dissemination	Diffuse/miliary small nodule carcinosis	24	49
	Limited/localised peritoneal carcinosis	25	51
Clinical BRCA status	Wild-type	20	40.8
	BRCA1/2 mutant	9	18.4
	Not tested	20	40.8
First line chemotherapy	Completed first line chemotherapy	46	93.9
	Carboplatin	8	17.4
	Carboplatin & Paclitaxel	21	45.6
	Carboplatin & Paclitaxel & Bevacizumab	16	34.7
	Carboplatin & Paclitaxel & Avelumab	1	2.2
Relapse status following first line chemotherapy	Refractory/Resistant	11	22.5
	Sensitive	32	65.3
	No relapse	3	6.1
	Death not due to disease progression	3	6.1
Progression-free survival* (months)	median	17.5	
	IQR	11-23	
Overall survival* (months)	median	41.3	
	IQR	23.9-57.2	
Follow up* (months)	median	74.7	
	IQR	53.6-86.4	
Deceased during follow up*	Yes	31	67.4
	No	15	32.6
Samples collected at PDS	mean per patient	9	
	range	4-15	
Samples collected at relapse	mean per patient	3	
	range	1-7	

*excludes patients whose death was not due to disease progression

Between September 2013 and November 2018, 49 patients were recruited to the project. All patients underwent maximal effort primary cytoreductive surgery and tumour samples were collected from as many disseminated sites as possible. Patients were tracked along their treatment course and relapse samples obtained where possible at secondary debulking surgery or biopsy.

All 49 patients underwent primary debulking cytoreductive surgery with 42/49 (85.7%) achieving total macroscopic clearance. The median follow up time was 74.7 months (IQR 53.6-86.4). 46/49 (94%) received postoperative chemotherapy, most frequently a combination of carboplatin with paclitaxel +/- Bevacizumab (VEGF inhibitor). 43/49 (87.7%) experienced relapse in the follow up timeframe of whom 9 then underwent secondary debulking surgery and one patient had a biopsy collected at time of relapse.

Progression free survival was defined as time to relapse from date of surgery and patients were subsequently divided into either platinum sensitive disease, platinum resistant disease or no relapse. Platinum resistant disease was defined as relapse within 6 months from the end of platinum treatment. Platinum refractory disease involves progression during the chemotherapy treatment course. For the purposes of this study, those with platinum resistant disease and platinum refractory disease were combined.

Tumour samples were obtained from the primary tumour and as many metastatic sites as possible with a mean sample number of 9. The IMO mapping tool was used to categorise the tumour locations within the abdomen. In a few cases samples were obtained from outside the abdominal cavity e.g. paracardiac lymph nodes. The description of the disease spread was documented as either diffuse/miliary nodular carcinosis (49%) or discrete localised carcinosis (51%). There was no significant association observed between different patterns of carcinosis and progression-free ($p=0.25$) or overall survival. ($p=0.22$); Figure 3.1 a, b. As observed in previous studies, those patients where total macroscopic clearance was achieved had a significantly longer overall survival with a median OS of 45.5 months (IQR 22.6-59.2 months; $p=0.032$) compared to those with residual disease at 35.4 months (IQR 32.5-37.2), Figure 3.1 c, d.

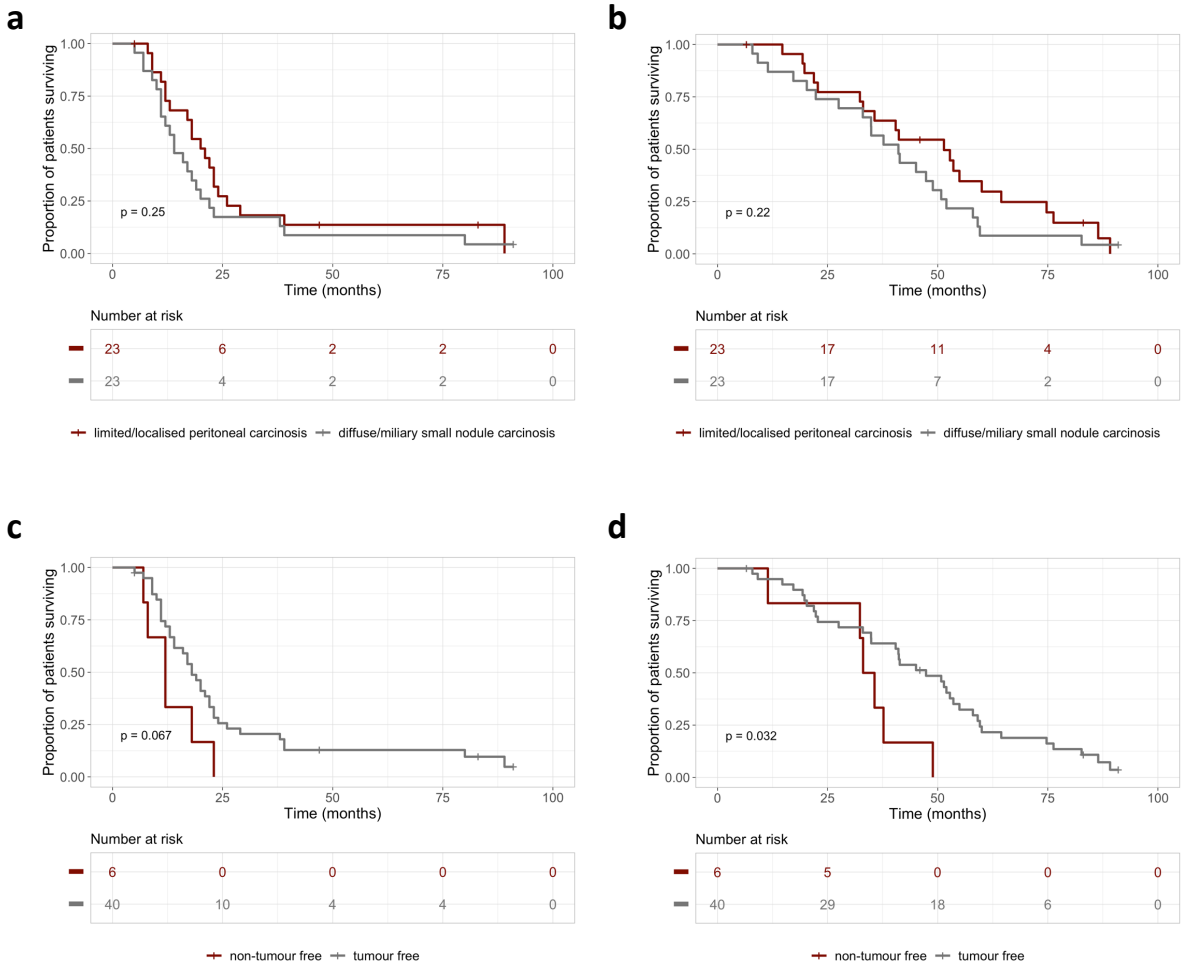


Figure 3.1: Kaplan-Meier outcome plots. a/b) *Patient outcomes by clinical presentation. Kaplan-Meier curve showing the association between disease status (limited/localised peritoneal carcinosis; diffuse/military small nodule carcinosis) and progression free survival (a; p = 0.25) and overall survival (b; p = 0.22) (n = 46). c/d) Patient outcomes by tumour-free status (presence of residual disease) following primary debulking surgery. Kaplan-Meier curve showing the significant association between tumour-free status (n=40) vs non-tumour free (n=6) and progression free survival (c; p = 0.067) and overall survival (d; p = 0.032).*

3.3 Phenotypic heterogeneity – apoptosis assays

Tumour samples were collected during surgery and immediately processed to extract primary tumour cells for culturing. The mean number of tumour samples obtained was 9 (range 4-15) per patient. During the course of this heterogeneity study over 400 primary tumour cell cultures were established. The extracted cells were placed in culture and then treated in triplicate with cisplatin 25μM for 24 hours. The following day apoptosis and viability levels across the sample populations were measured using the ApoTox-Glo Triplex Assay (Promega). Apoptosis data was normalised to viability and calculated as a fold change of untreated control samples. Relative apoptosis levels were then charted in Graphpad for comparison.

Across the patient cohort there was a range in apoptotic responses observed in response to cisplatin treatment. Some tumour sites showed high sensitivity to cisplatin treatment (high apoptosis levels) and others appeared much more resistant to treatment (low apoptosis levels). Heterogeneity in response to treatment was seen between individual tumour deposits within the same patients. There was also variation in the degree of heterogeneity observed within patients i.e. in the following graph figure 3.2, in case T14-012 the tumour deposits are all clustered together, whereas in T18-034 there was much more heterogeneity in the responses to cisplatin treatment.

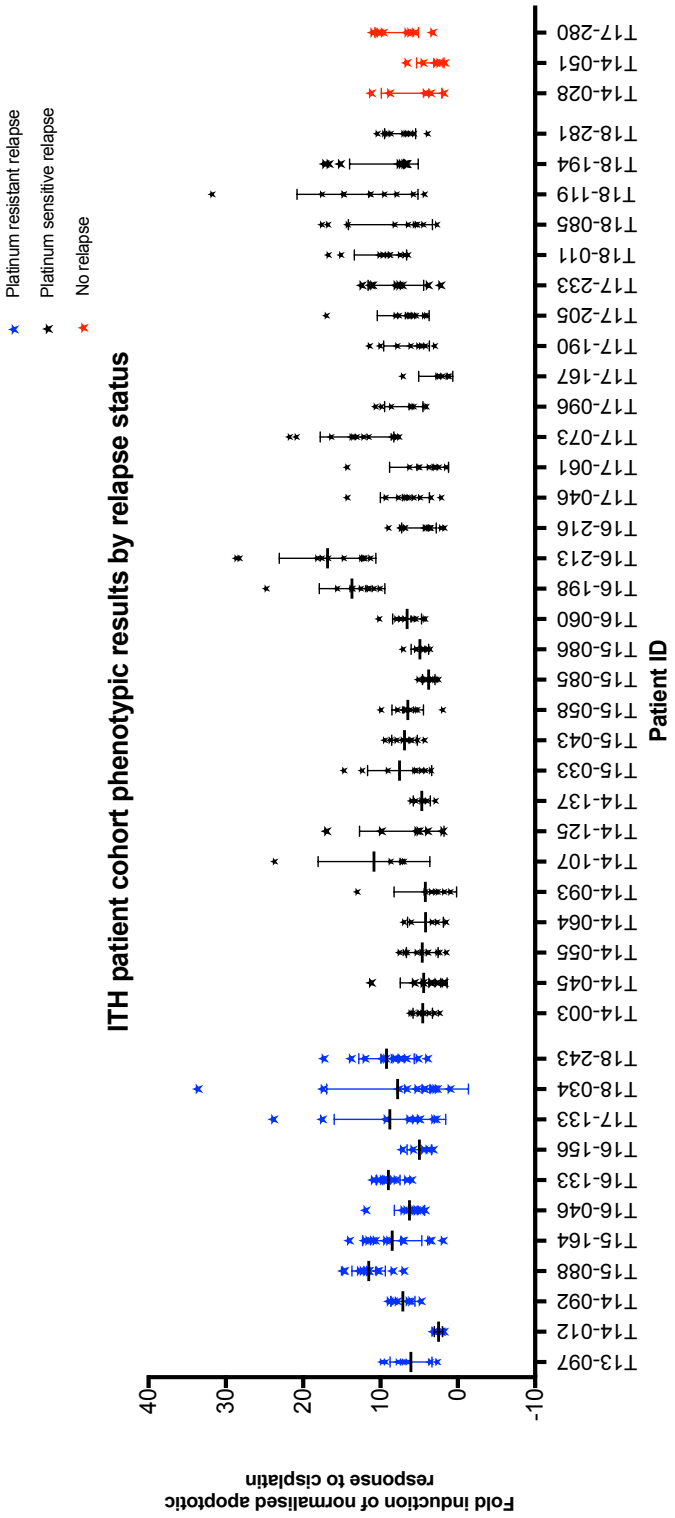


Figure 3.2: Heterogeneity in apoptotic response to cisplatin. *Scatter dot plot of apoptotic response to cisplatin across the ITH patient cohort, displayed grouped by relapse status, wide heterogeneity is observed. Tumour cell samples were plated in triplicate, drug treated with 25μM cisplatin for 24hours. Apoptotic response was analysed via caspase 3/7 response assay and data normalised to viability and calculated as fold induction. Each data point represents individual tumour site response to cisplatin in each patient. Average of 9 sample sites per patient (range 4-15). There is significant difference seen between each patient overall response by Kruskal-Wallis testing P<0.0001)*

When categorised by clinical response to platinum (resistant, sensitive, no relapse), the variation in response can be more easily observed across the different groups. In all groups, there is a wide range of platinum response between patients but also between tumour sites in individual patients (figure 3.3).

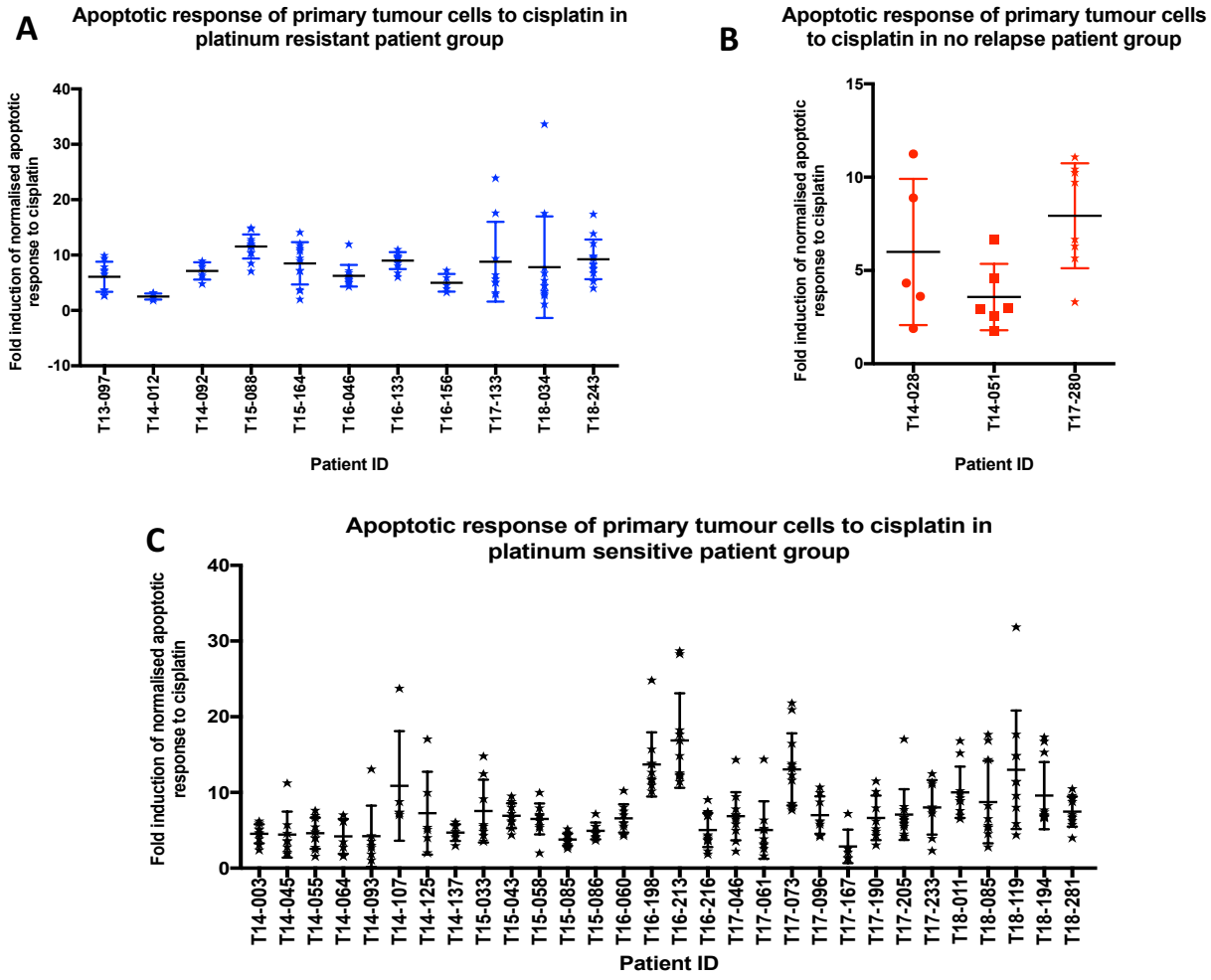


Figure 3.3: Apoptotic response to cisplatin by clinical platinum sensitivity*. Tumour cell samples were plated in triplicate, drug treated with 25μM cisplatin for 24hours then apoptotic response analysed via caspase 3/7 assay. Data was normalised to viability and calculated as fold induction. A- Platinum resistant cohort. B- No relapse cohort. C- Platinum sensitive cohort. There is variation in both the degree of response between sample sites within individual patients and across the patients, this is observed in all patient groups. There is significant variation in the average response between patients in each relapse category. Kruskal-Wallis test shows significant variation between overall patient response in the platinum resistant group $p<0.0001$, platinum sensitive group $p<0.0001$ and no relapse group $p=0.048$.*

There were 106 tumour samples giving apoptotic results in the platinum resistant patient group, 269 in the platinum sensitive group and 19 from the no relapse group. Combining the apoptotic response results by platinum status showed no significant variation in response to cisplatin treatment determined by relapse status, though the numbers in the no relapse group were much smaller (figure 3.4). When the no relapse and platinum sensitive group were combined, there remained no statistical difference between the groups.

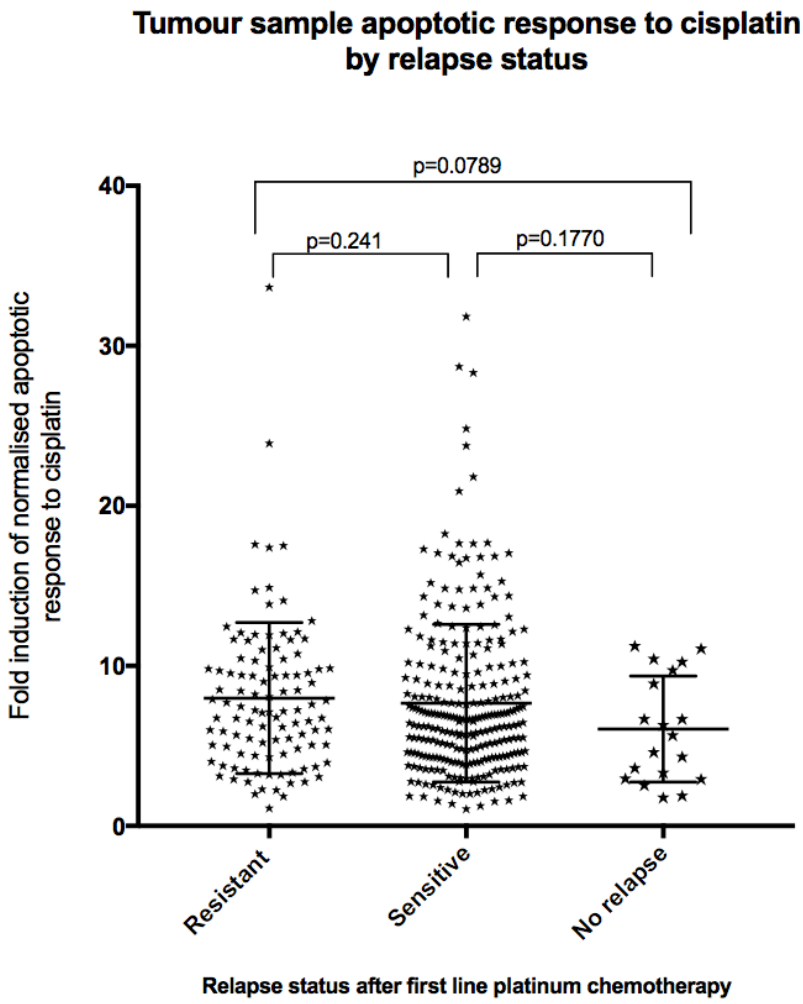


Figure 3.4: Tumour site apoptotic response to cisplatin grouped by relapse status*. Individual tumour apoptotic results were combined and compared based on patient platinum relapse status. Platinum resistant n= 106 tumour cultures, platinum sensitive n=269 tumour cultures, no relapse n=19 tumour cultures. No significant difference in average response to cisplatin was seen between the platinum resistant and platinum sensitive group (p=0.241); the platinum resistant group and the no relapse group (p=0.0789); and the platinum sensitive and no relapse group (p=0.1770).*

The omentum is often used as a site for biopsy to determine HGSOC diagnosis and for examination as part of research studies. On further analysis of the omentum samples' apoptotic response to cisplatin in the ITH patient cohort, the vast variation in sensitivity could be again observed with significant differences seen between individual patients' samples (figure 3.5, A). When the omentum sample responses were grouped by patient platinum sensitivity, no significant difference between the groups was seen, patients without relapse were grouped with the platinum sensitive patients. Variation in response could be seen within both groups (figure 3.5, B). This highlights the potential problems with single site sampling for analyses such as prediction of response to treatment. These results indicate it would not be possible to predict from one sample site whether a patient was going to have platinum sensitive disease or not.

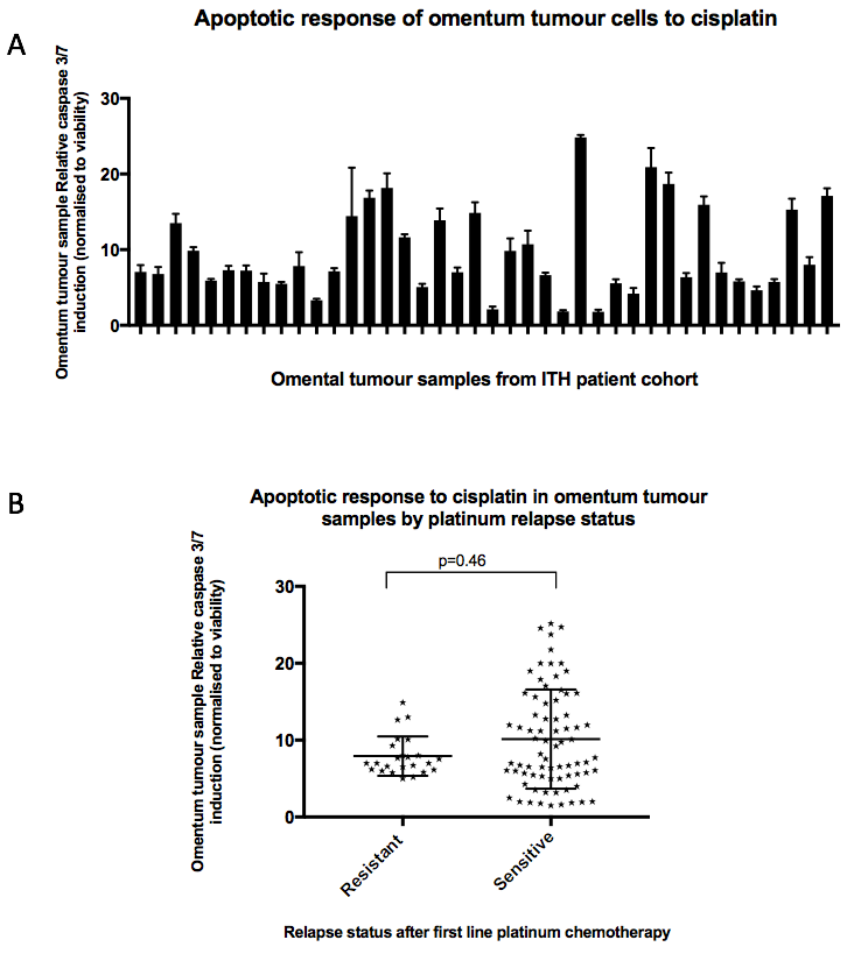


Figure 3.5: Apoptotic response of omentum tumour cells to cisplatin within the ITH cohort*. A – Omental sample apoptotic response to 24hour 25μM cisplatin treatment, each bar represents a single patient sample, cells seeded in triplicate. Significant difference in response was observed across the cohort, p<0.0001 Kruskal-Wallis test. B – Omentum apoptotic results grouped by patient platinum sensitivity on clinical follow up. Platinum resistant samples n=8, platinum sensitive samples n=25. No significant difference was seen in response to cisplatin treatment between the two groups, Mann-Whitney test p=0.46)*

In the omentum example above (figure 3.5), there appears to possibly be less variation in response in the platinum resistant group vs the platinum sensitive, standard deviation (SD) was 2.564 in the resistant group vs 6.457 in the sensitive group. To investigate whether the heterogeneity in tumour sample response within individual cases related to platinum sensitivity outcomes, median absolute deviation (MAD) examination of apoptotic response was analysed (figure 3.6). No significant pattern was observed in degree of heterogeneity in response to cisplatin treatment between patients based on overall platinum sensitivity determined during follow up.

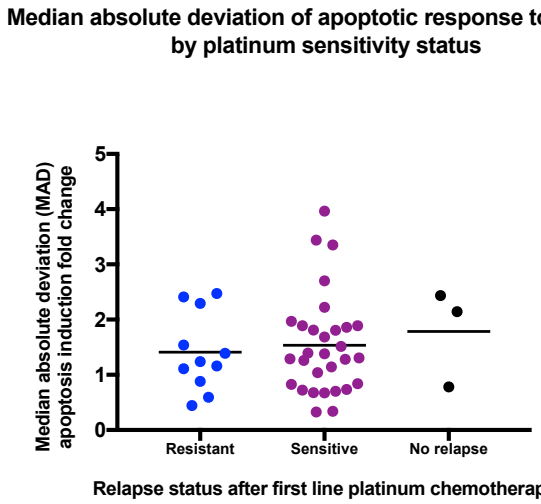


Figure* 3.6*: Median absolute deviation of apoptotic response. *Box and whiskers plot showing median absolute deviation (MAD) of sample-wise apoptosis induction fold change of primary cell cultures from ITH patient samples (n=44, range 4-15 samples per patient), grouped by relapse status. (Kruskal-Wallis test p=0.7).*

As seen above in the overall patient cohort (figure 3.2), wide phenotypic heterogeneity was observed between different sample sites within individual patients. The relative response rates of anatomical locations changed from patient to patient. For example, in case T16-156 (figure 3.7 A), the primary and omentum tumours have a higher response rate than many of the other sites, whereas in case T17-280 (figure 3.7 C) the omentum appears more resistant to cisplatin treatment. The cases below reflect differing clinical platinum statuses. Case T16-156 underwent successful debulking surgery to no macroscopic disease but unfortunately proved to have platinum refractory disease and relapsed within 5 months during chemotherapy treatment. Case T16-213 (figure 3.7 B) and T17-280 (figure 3.7, C) were also both optimally debulked to macroscopic tumour free status however patient T16-213 developed platinum sensitive relapse after 18 months and patient T17-280 has not relapsed. In each patient, statistically significant variation in response to cisplatin could be seen between sample sites.

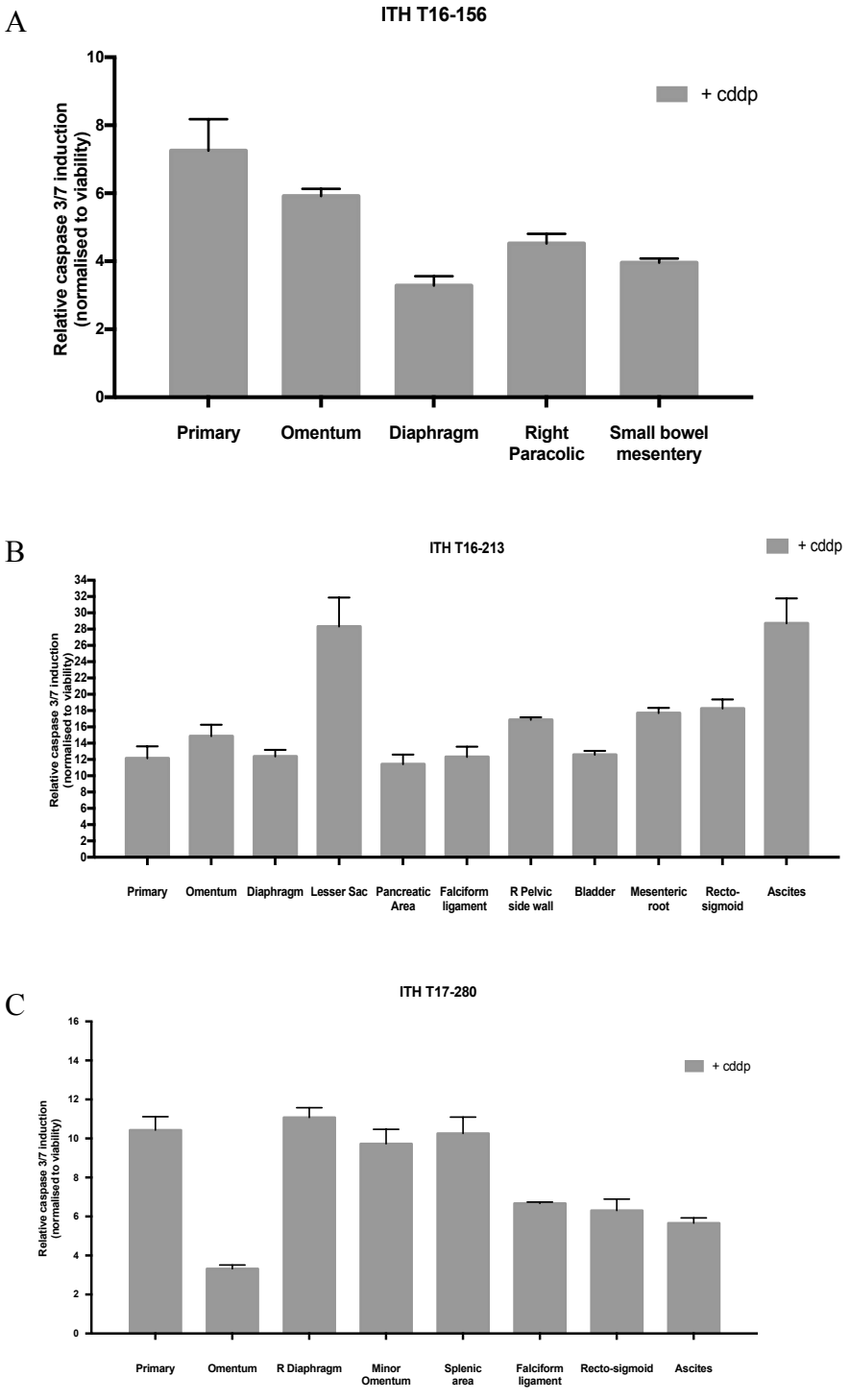
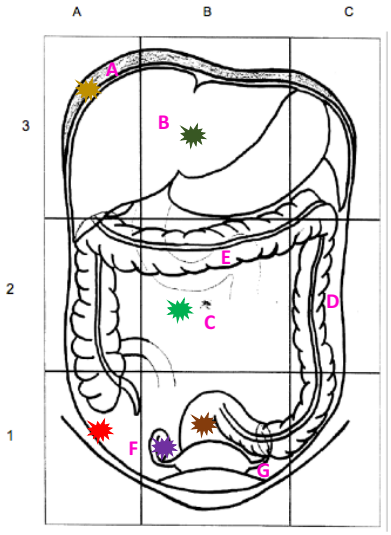


Figure* 3.7*: Apoptotic response to cisplatin in individual cases. *Phenotypic data from the ITH project cases, demonstrating wide heterogeneity in relative apoptotic responses to cisplatin across different anatomical areas and patients. Tumour cells were seeded in triplicate, treated for 24 hours with 25μM cisplatin then apoptotic response examined via caspase 3/7 assay. Case T16-156 (A) had clinical platinum refractory disease, case T16-213 (B) experienced platinum sensitive relapse whilst case T17-280 (C) did not relapse during the follow up time period. Statistically significant difference in response to cisplatin could be seen between the individual tumour sites in each patient. (Kruskal-Wallis test: case T16-156 p<0.0001; case T16-213 p=0.0017; case T17-280 p=0.0036*

3.3.1 Evaluation of cisplatin induced apoptosis in relapse HGSOC

Case T14-137 underwent primary debulking surgery with complete macroscopic tumour clearance. The IMO map below (figure 3.8) shows the anatomical locations of tumour deposits taken for analysis. Samples were obtained from throughout the abdominal cavity. This patient relapsed in a platinum sensitive timeframe after 15 months then went on to have secondary debulking surgery with samples obtained from the sites labelled in pink under the case number T17-067. The phenotypic data is shown below.



T14-137	Primary tumour
	Omentum
	Diaphragm
	R pelvic side wall
	Liver capsule
	Rectum
T17-067	A: Right Diaphragm
	B: Liver
	C: Mesentery
	D: Left Paracolic
	E: Large Bowel
	F: Psoas muscle
	G: Pelvis

Figure 3.8: IMO mapping in example case. *IMO mapping of primary and relapse tumour deposits in case T14-137 showing disseminated pattern of spread across the abdominal cavity at both initial presentation and relapse (relapse case number T17-067).*

For the primary surgery T14-137 (Figure 3.9 A), 6 sample sites were analysed. Phenotypic assays show heterogeneity between the response to cisplatin treatment in the primary tumour and different metastatic sites; the omentum was the most sensitive and the right pelvic side wall sample was the least. At relapse, further samples were obtained and analysed in the same way, shown in Figure 3.9 B. The relapse samples show greatly reduced response to cisplatin treatment and little variation in responses to platinum, with similar response rates observed across the different tumour cultures.

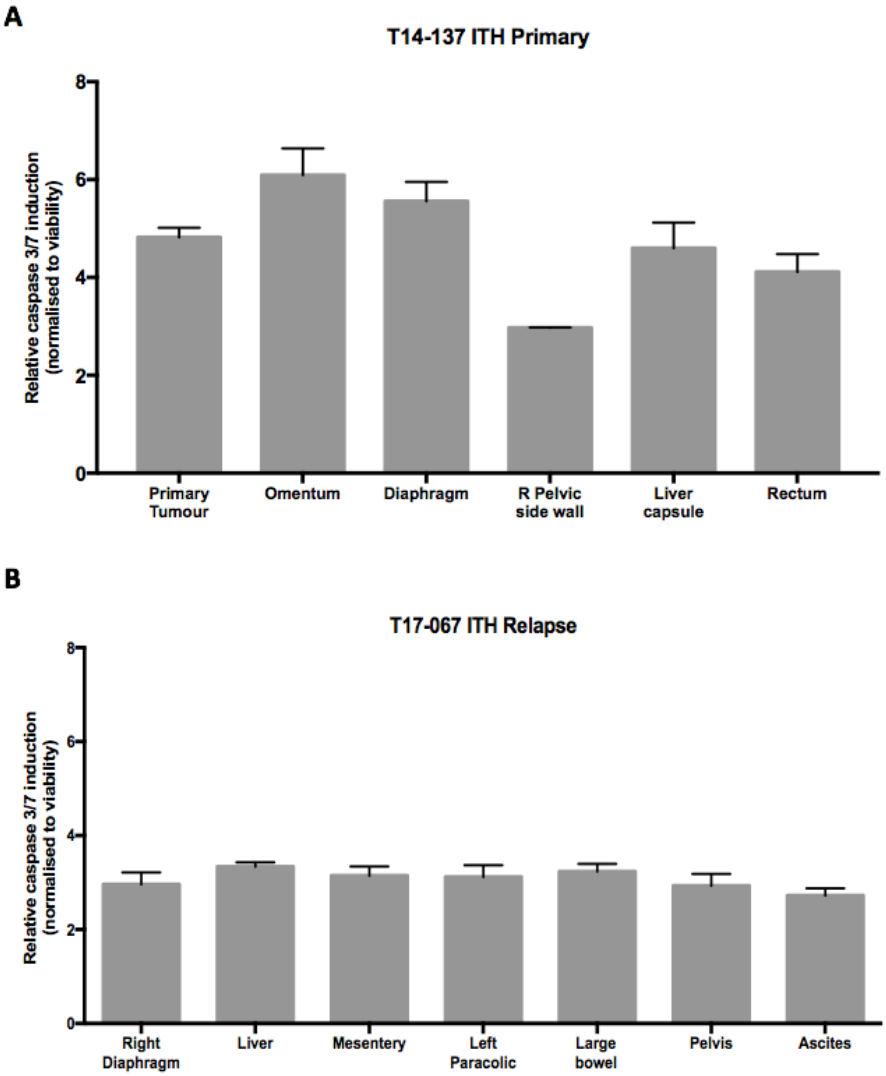


Figure 3.9: Apoptotic response to cisplatin in example case with subsequent relapse samples. *ITH case T14-137 apoptosis data from tumour cells at A - primary debulking B - and relapse surgery. Tumour cells plated in triplicate. Y axis showing apoptosis assessed by relative caspase 3/7 induction normalised to viability following 24hours 25μM cisplatin treatment. X axis showing sample site by anatomical location. The samples from primary debulking showed statistically significant variation in response to treatment (Kruskal-Wallis test p=0.0106) whereas at relapse there was less variation between samples observed with no significant difference between the relapse sample response rates (Kruskal-Wallis test p=0.07)*

3.4 Phenotypic variation across the intra-abdominal cavity

To examine the heterogeneity between sample site apoptotic response to cisplatin further, samples were grouped by anatomical locations into IMO mapped regions plus ascites separately. Variation can be seen within each region in response to treatment (figure 3.10). Some regions appear to display more heterogeneity than others, for example the min-max range shown in the B2 samples is much wider, whereas the spread for C3 is narrower. This is possibly due to the differing microenvironments expected in each area. In the B2 region, samples were collected from a variety of sites such as the omentum, small or large bowel, para-aortic lymph nodes and several others. Whereas in the C3 area, most samples were either from the diaphragmatic peritoneum or the spleen, however there was still heterogeneity observed.

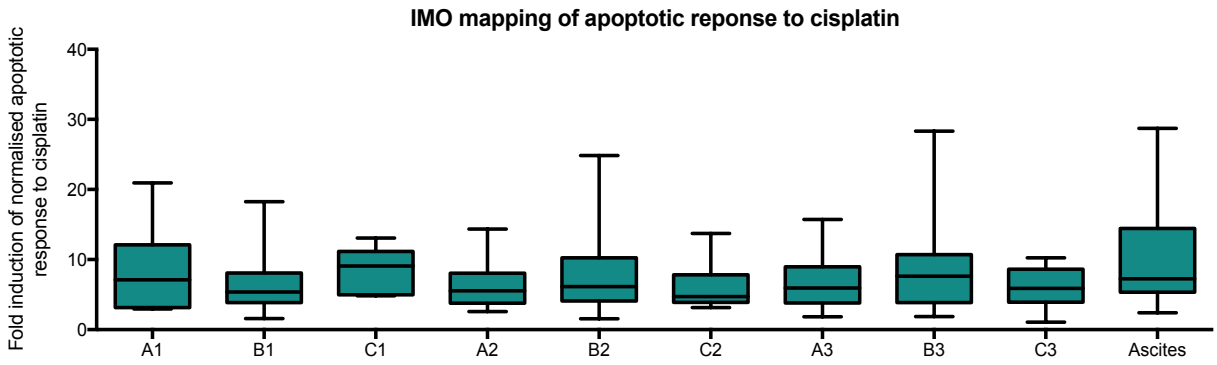


Figure 3.10: Apoptotic response to cisplatin by IMO mapping. *Box and whiskers plot showing apoptotic response to cisplatin in different IMO mapped regions. Sample numbers varied by region (A1=12, B1= 63, C1=10, A2=19 B2=68, C2=11, A3=30, B3=21, C3=12, ascites=10. No significant difference in average response to cisplatin was found between different anatomical regions using Kruskal-Wallis analysis p=0.57.*

On dividing samples into wider intra-abdominal regions 'upper', 'middle' and 'lower' there was no significant difference observed in response to cisplatin treatment between the different regions, or when compared to the ascites results. Again, heterogeneity within each area was observed (figure 3.11).

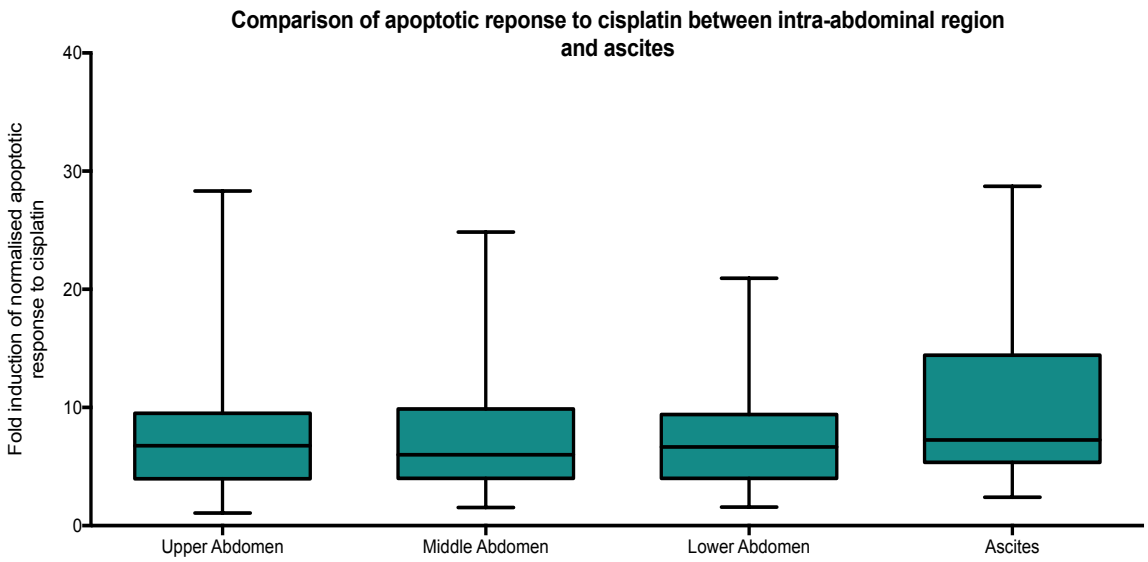


Figure 3.11: Apoptotic response to cisplatin by abdominal region. *Box and whiskers plot comparing overall apoptotic response to cisplatin between upper, middle, and lower regions of the abdomen and ascites samples. Sample numbers: Upper abdomen=63, middle abdomen=98, lower abdomen=85, ascites=10. No significant difference in average apoptosis levels was observed between the groups by Kruskal-Wallis analysis p=0.57.*

3.5 Phenotypic Heterogeneity – heterogeneity in IC_{50} concentrations of cisplatin in different tumour sites

Half maximal inhibitory concentration experiments (IC_{50}) were conducted alongside the phenotypic assays where possible. IC_{50} assays are commonly used in drug discovery to ascertain the potency of potential drugs against particular targets. They can again give an indication of sensitivity to a compound and the variation between different samples. Depending on the quantity of the cell population extracted from each tumour sample, cells were also seeded in triplicate for IC_{50} assays. Cell samples were treated with two-fold serial dilutions from 100μM to 0μM cisplatin for 72 hours and then IC_{50} values were inferred using an MTT assay.

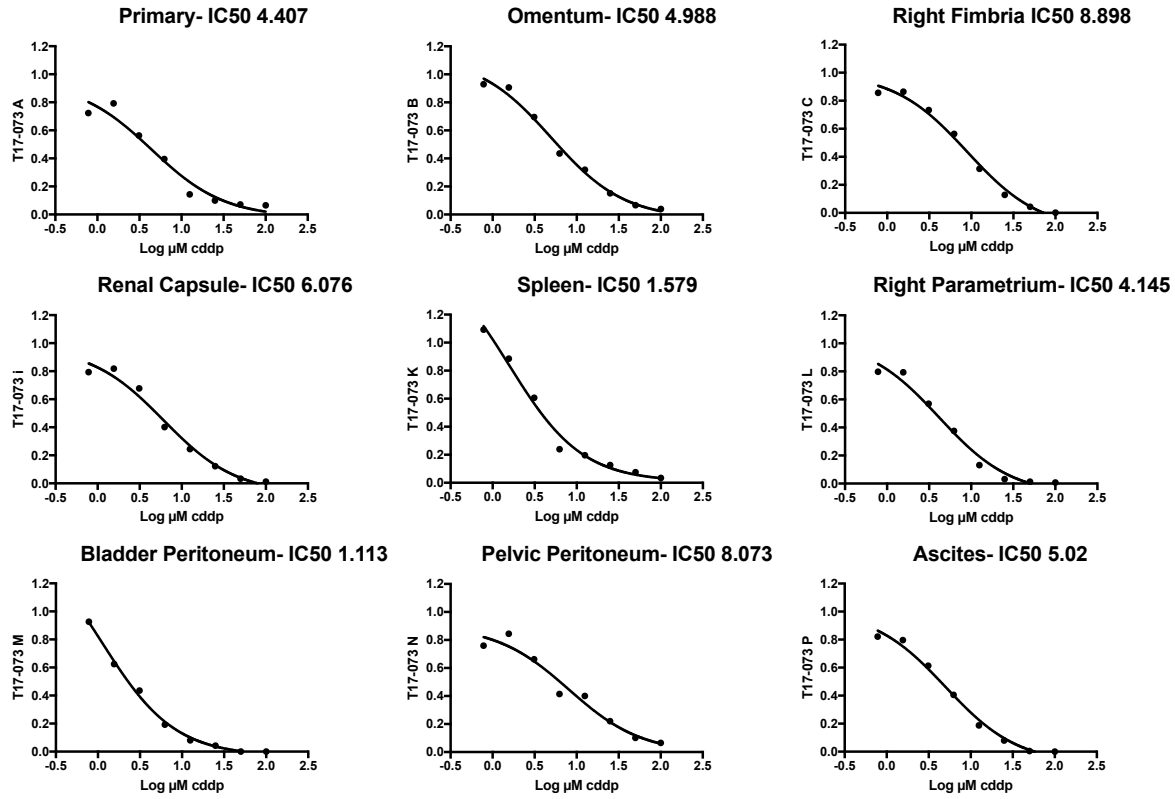


Figure 3.12: Cisplatin IC50 values in example case. *IC_{50} results for individual tumour samples for case T17-073. Samples tested from multiple sites across the abdominal cavity. The resulting μM cisplatin IC_{50} values for each anatomical location are described above each graph.*

Case T17-073 IC_{50} data showed heterogeneity across the tumour samples with a wide range of IC_{50} values (figure 3.12). Tumour samples were tested from across the abdominal cavity, the deposit from the bladder had the lowest IC_{50} value of 1.113 μM whereas the right fimbria had the highest 8.898 μM. The bladder and fimbria are located within the same IMO mapping area and are anatomically very close and yet demonstrate very different sensitivities to platinum. These results highlight, once again, the difficulty in treating HGSOC when even tumours close to each other in the same patient may respond so differently to treatment. Using the same therapy protocols for everyone is suboptimal but to develop effective targeted therapies can be very difficult due to the heterogeneity present.

Samples obtained at secondary debulking surgery following platinum sensitive relapse for case T17-067 were also examined with IC_{50} assays (Table 3.2). These results show some variation but overall high IC_{50} values throughout, demonstrating the reduced sensitivity to platinum that has occurred during the patient's treatment journey, as reflected in the high cisplatin IC_{50} values, given in μM, some close to or much higher than the 25μM which had been used in the apoptosis assays.

Tumour sample location	**IC50 conc (μM)**
A – Right diaphragm	53.03
B - Liver	18.08
C - Mesentery	28.21
E – Large Bowel	12.98
H - Ascites	22.01

Table 3.2: Cisplatin IC50 values in different metastatic sites. *IC50 values for samples in relapse case T17-067. Whilst heterogeneity was seen, the values were consistently high across the samples showing reduced sensitivity at relapse.*

3.6 Ki67 proliferation index

In the search for potential prognostic biomarkers, Ki67 proliferation was examined. Ki67 proliferation index has been applied in cancers such as melanoma and breast carcinoma as a prognostic biomarker[289]. A small number of studies have evaluated its use in ovarian cancer and suggested it has some prognostic potential. However, results were varying and conflicted as the clinical cut off points and protocols utilised were not standardised. Additionally often only one tumour site was tested per patient[290].

To examine the potential for Ki67 as a prognostic biomarker in HGSOC, frozen sections were collected from all tumours used for molecular analysis, both primary and relapse tumours- 270 sections were evaluated in total. H&E and Ki67 staining was undertaken with Ki67 scoring categories defined as <20%, 20-59% and >60%, based on the scoring distribution.

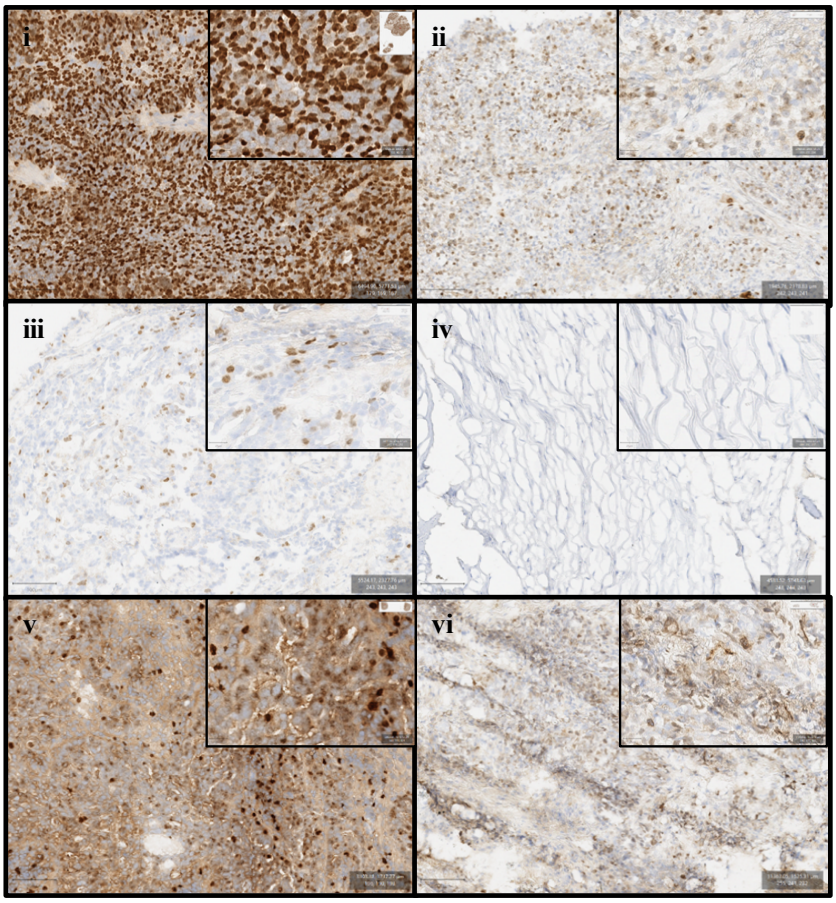


Figure 3.13: Ki67 staining image examples. *Example of staining categories for percentage Ki67 proliferative index. Large images at 4x magnification, inserts at 20x. i = High Ki67, ii = moderate Ki67, iii = low Ki67, iv = No tumour, v&vi = examples of uninterpretable images.*

Heterogeneity in proliferative index scores (Figure 3.14) was observed across the cohort. A third of the patient cohort had tumour samples scoring in all three scoring categories; no significant correlation was observed between the number of scoring categories per case and platinum sensitivity using chi-square analysis (p=0.449).

The MAD was analysed for each case to give an indication of the degree of variation observed in each patient, no significant correlation was seen between Ki67 proliferative index and patient relapse status and outcome (Figure 3.15). No significant associations were observed with Ki67 proliferation (Figure 3.16) with either PFS (p=0.92) or OS (p=0.79). These results, using a broad range of anatomical locations, suggest that evaluating Ki67 scoring would not be a reliable prognostic indicator in HGSOC given the variation observed between sites. This further shows that single site sample analysis is unlikely to give sufficient information for biomarker discovery, reflected in the finding that a third of the patients had tumour samples which scored in all scoring categories.

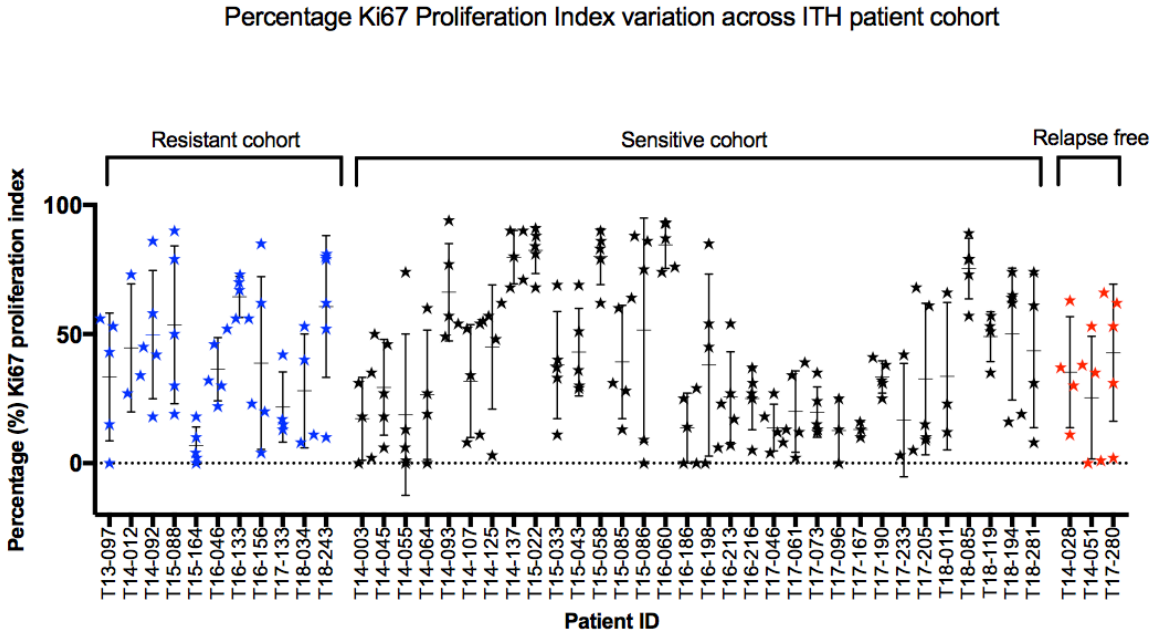


Figure 3.14: Percentage Ki67 proliferative index. *Percentage Ki67 proliferative index scores across the patient cohort (n= 46) by relapse status. Blue = platinum resistant relapse, black= platinum sensitive relapse, red = no relapse at the time of analysis. (n=5 samples per patient)*

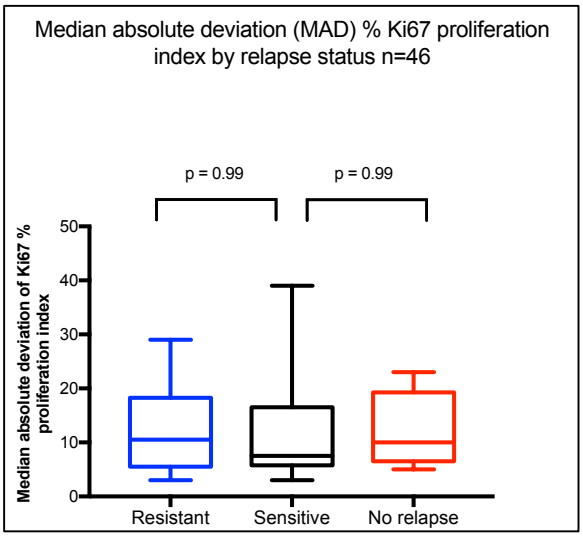


Figure 3.15: Median absolute deviation of Ki67 proliferation index. *Median absolute deviation (MAD) of percentage Ki67 proliferation index shows no correlation with relapse status across the patient cohort. No significant difference was observed between the means of different groups with Kruskal-Wallis testing.*

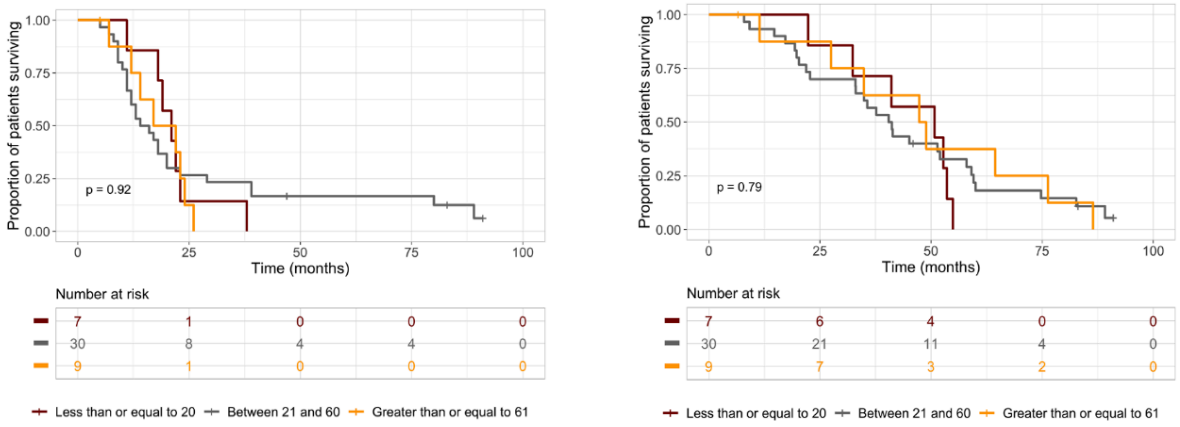


Figure 3.16: Kaplan-Meier curves for Ki67 proliferative index association. *Clinical association of Ki67 proliferative index scoring. Kaplan-Meier curve showing the association between the mean Ki67 proliferative index across different disseminated deposits within a patient and progression free survival (PFS, p = 0.92) and overall survival (OS, p = 0.79). Ki67 proliferative index staining was stratified into 3 categories: low (<20%), moderate (21-60%) and high (>60%) across the cohort (n=46).*

Percentage Ki67 proliferation index was compared with apoptotic response from the matched tumour samples within the ITH cohort. No correlation could be observed between either apoptotic response to cisplatin and percentage Ki67 proliferation index, or between the MAD Ki67 proliferation index and MAD apoptosis (graphs in the appendix figures 9.1 and 9.2). This indicates that proliferation levels in these samples, as analysed via Ki67 proliferation scores, does not relate to tumour platinum sensitivity.

3.7 Discussion

The analysis of ITH patients' response to cisplatin treatment demonstrated heterogeneity in apoptotic response spatially within individual patients and temporally with the study of relapse samples. This extensive level of multisite testing in such a large cohort of patients is unprecedented. Where other studies have examined multiple patient samples, they have often been from single site analysis, most commonly the omentum or ascites, additionally the number of modalities assessed in the ITH project developed a greater picture of the heterogeneity across a variety of tumour behaviour profiles than commonly examined [239, 251].
Here it has been shown that significant variation in response to cisplatin is seen both within individual patient samples and across the cohort. Though relapse sample numbers were small, the analysis seen demonstrated reduced variation in response to cisplatin at relapse between metastatic deposits than in primary cases. IC_{50} values for cisplatin at relapse also displayed reduced sensitivity to the drug.

What is clear from this study, as is widely acknowledged, is that optimal surgical debulking to no macroscopic disease is vital in prolonging PFS and OS. Despite appearing to have different macroscopic appearances, comparing the patients with disseminated miliary nodular carcinosis pattern with those with discrete localised metastatic spread displayed no significant differences in PFS or OS. Heterogeneity in Ki67 percentage proliferation index across the patient cohort tumour samples show the difficulty in finding reliable biomarkers in HGSOC due to the vast sample variation.

A limitation of the cultures used for this study is that they were all 2D monolayer cultures. 2D cultures, though maximising efficiency of throughput, lack the provision of elements of the tumour microenvironment which are crucial in determining the true behaviour of tumour cells as they would exist *in vivo*. The development of 3D culture designs most suitable for analysis of the heterogeneity existing in HGSOC and in patient response to treatment is the focus of the next chapters.

Chapter 4

Results: Development of 3D organotypic HGSOC models

4 Results: Development of 3D Organotypic HGSOC Models

4.1 Introduction

I have shown in the previous chapter that in phenotypic apoptosis assays and cisplatin IC_{50} data there is great variety both across the patient cohort and between different anatomical locations in response to platinum therapy. These experiments were performed using standard 2D cultures which have historically been utilised and relied upon within cancer research and during drug development.

This project aimed to develop a 3D model system based on the layered anatomy of the peritoneal lined omentum. This would be used to culture primary tumour cells from different tumour deposits, in a design representative of the *in vivo* microenvironment, enabling the response to treatment to be studied and compared to the 2D setting. When considering an organotypic model construct the different cell components must be representative of the normal tumour deposit site and, from a practical point of view, must be readily available. The rationale for choosing this system was due to the availability of primary omental stromal cells and HGSOC tumour cells extracted from tissue collected directly from theatre.

Previous groups using omental based 3D organotypic models have optimised protocols using ovarian cancer immortalised cell lines, which are able to retain viability over multiple passages. However, immortalised cell lines are known to exhibit genetic drift making their representation of their cell type of origin less reliable.

Primary cells would be expected to better reflect the *in vivo* behaviour however there are more difficulties encountered with extraction and maintenance of viability.

Optimisation of culture systems reflecting the complex dynamics of the *in vivo* setting is also essential for the progression of development of drug testing platforms, which will hopefully lead to greater understanding of the heterogeneity existing in tumour biology within individual tumours and between patients.

I wished to observe if primary tumour cells could be successfully cultured in this design as immortalised cell lines have been. Additionally, I wanted to examine for patterns and variation in response to cisplatin treatment noting any difference from those in 2D. The provision of a common, equal background of the 3D models would enable study of which tumour sites may thrive in culture compared to others.

4.2 Isolation of stromal cells

Initial stages of the project involved extraction and isolation of stromal cells from non-cancerous omentum. Patients undergoing surgery but with presumed normal omentum based on radiological findings, were counselled and consented prior to surgery and then fresh samples were obtained directly from theatre and processed immediately as per protocols from the Lengyel lab and further optimised. These patients were having omentum resected as part of staging protocols.

Omentum samples were obtained from multiple patients and stromal cells were successfully extracted. Stromal cells were cultured and cell populations determined. Cells were cultured until they reached confluency when they were either used for experiments or split and frozen down for future use. Viability and purity of cell populations could be maintained for up to 3 weeks with passaging 2-4 times. Fibroblasts could be maintained for longer than mesothelial cells and they were also more likely to grow quickly to confluency. However, there were variations in growth of populations between patients. In some cases, the mesothelial cell population would proliferate rapidly and the fibroblasts could be more sluggish and slow to expand and in others the reverse was the case. It was evident when cells were reaching the end of their healthy lifespan due to the distortion in shape and slowing of proliferation observed.

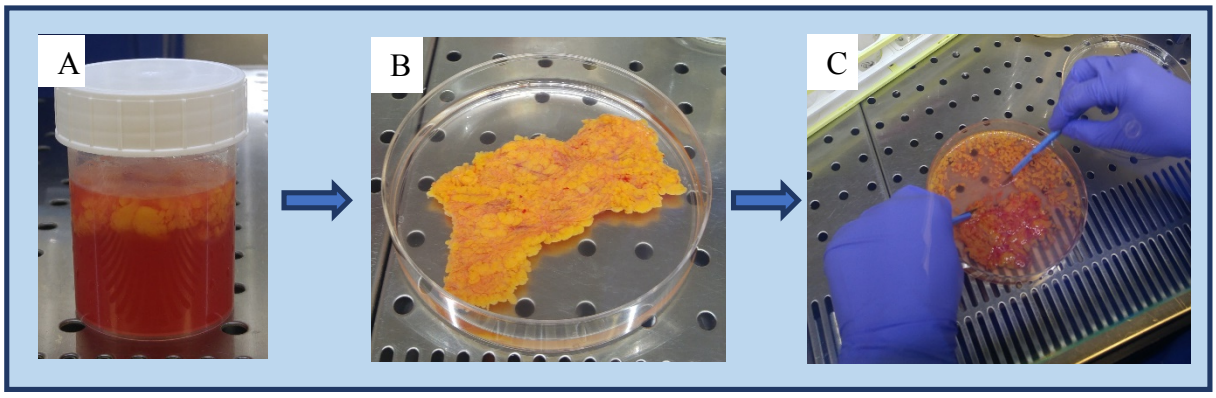


Figure 4.1: Processing of omentum for stromal cell extraction. *Non-cancerous omentum sample is obtained from theatre (A) in PBS, brought to the lab for processing (B), which involved dissecting to 1-3mm pieces with scalpels (C).*

Prior to being included in the 3D organotypic models, images of the cell populations were taken to observe the morphology of isolated stromal cells. Images were captured at day 5 post isolation and at further time points along their lifespan to study the changes and deterioration in the cells. The identity of the individual cell populations was confirmed using immunofluorescence staining and confocal imaging.

4.2.1 Imaging of stromal cell populations

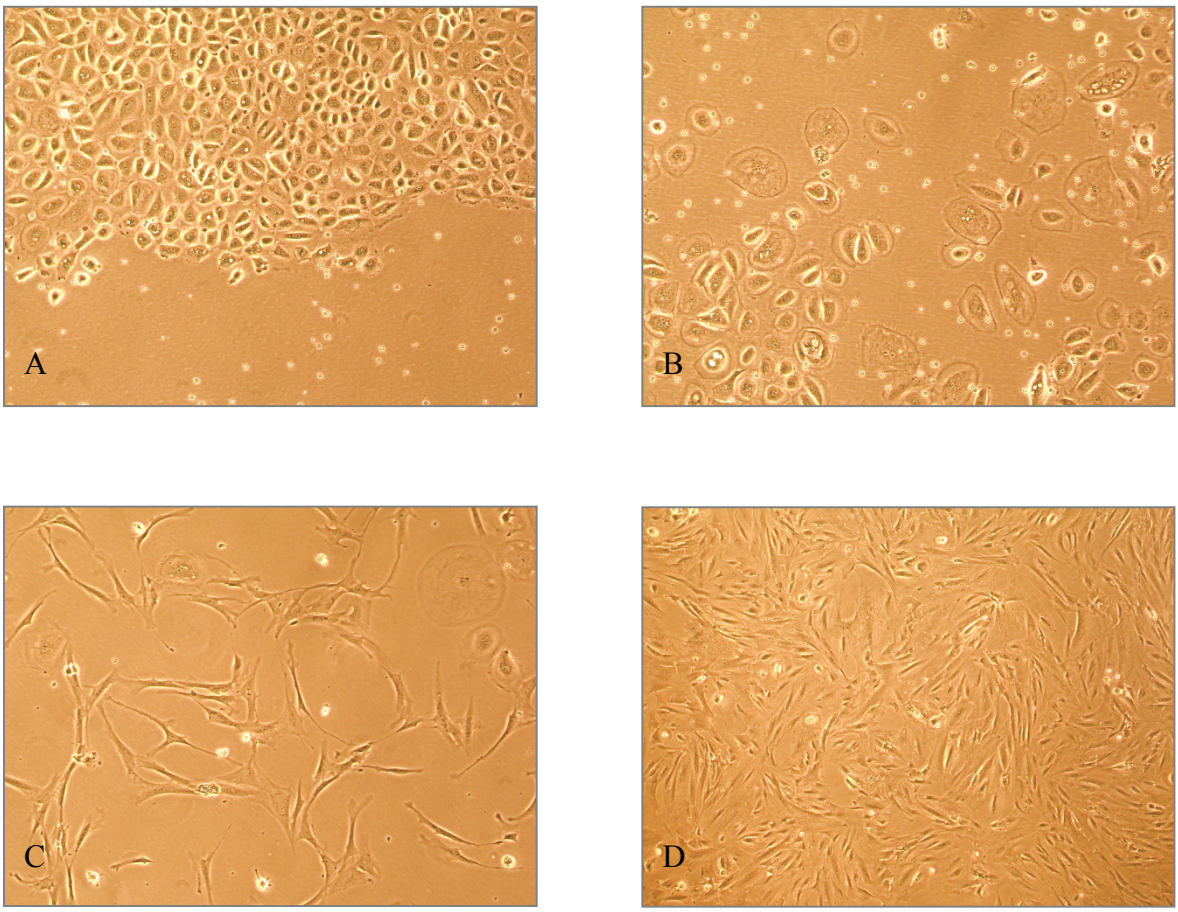


Figure 4.2: Brightfield confocal images of stromal cell populations. *Brightfield confocal images at 10x magnification of stromal cells from case T18-110 at different time points. A- Mesothelial cells isolated and cultured, images taken at 5 days when the cells are achieving confluence and have a characteristic 'cobblestone' appearance. B- Mesothelial cells after 2 weeks' culture have lost their regular morphology and appear senescent. C- Fibroblasts imaged at 5 days demonstrating a slower rate of proliferation compared to the mesothelial cells from the same patient. D- Fibroblasts at 2 weeks, still confluent but showing early signs of loss of structural integrity with bloating of appearance.*

4.2.2 Confirmation of cell populations

Immunofluorescence staining and confocal imaging was used to confirm the individual cell populations. This was undertaken on both the stromal cells extracted from normal-appearing non-cancerous omentum and the primary tumour cells extracted from the tumour deposits obtained from the ITH project patients.

In a few of the normal-appearing omentum samples obtained once the stromal cell cultures were established it became apparent that there were some disseminated cancerous cells present in the culture too. These were then stained for presence of cancer associated fibroblasts. If tumour cells or CAFs were present the mesothelial or fibroblasts cells were deemed to not be appropriate for the models and they were subsequently excluded.

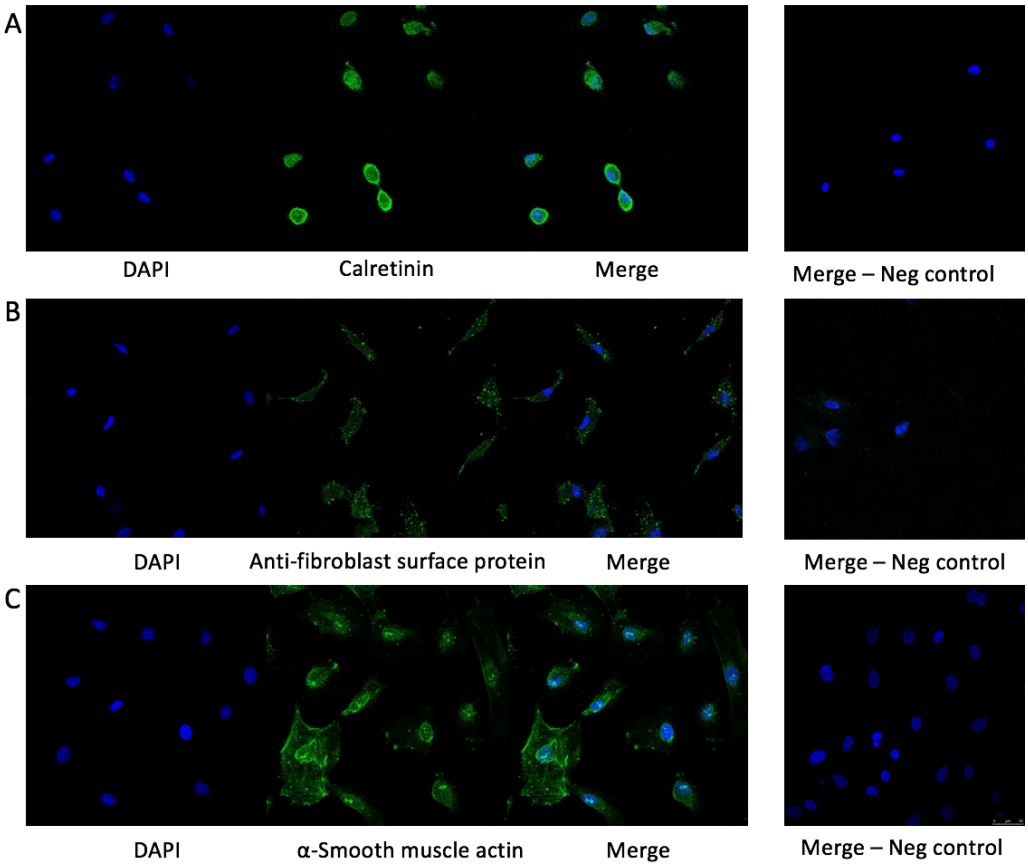


Figure 4.3: Confirmation of stromal cell populations. *Immunofluorescence staining of primary stromal cells. Imaged on Leica Confocal SP5 40x magnification. Case T18-158. Isolated stromal cells were fixed, stained with primary antibody and incubated at 4°C overnight before secondary antibody goat anti-mouse Alexa fluor 488 was applied. A – Mesothelial cells stained with calretinin antibody, DAPI and merged images shown, B- Normal fibroblasts stained with anti-fibroblast surface protein antibody, DAPI and merged images shown. C- There was evidence of cancer cell presence on microscopic examination of the cultures which was confirmed by staining for cancer associated fibroblasts (CAFs) with α-smooth muscle actin, DAPI and merged image shown. Associated negative controls displayed.*

4.3 Optimisation and construction of 3D organotypic models and assay read-out

The aim of this work was to use isolated mesothelial cells and fibroblasts placed within a collagen I extracellular matrix (ECM) model to culture primary tumour cells in an *in vitro* system which was more representative of the *in vivo* environment. The model architecture is based on the anatomy of the omentum which has a peritoneal lining with an outer layer of mesothelial cells on top of a complex ECM containing fibroblasts. Mesothelial cells play an important part in tumour cell surface adhesion and invasion through to the inner tissues. Fibroblasts present within the ECM are recruited by the tumour cells and undergo essential changes to help the tumour cells promote cell-cell interactions and signalling pathways to evolve the microenvironment to a pro-tumour state.

After construction, the models including incorporated tumour cells were treated with cisplatin to observe the difference in response to treatment in a 3D setting compared to 2D and to study the variation in response between different tumour cells derived from anatomical metastatic sites. The construction of models was initially optimised using immortalised ovarian cancer cell lines instead of primary tumour cells due to the limited availability of primary samples and difficulty in maintaining their viability in culture. Tumour cells were seeded on the top of the models and in parallel 2D cultures to undergo the same drug treatment and analysis. The 3D organotypic models were constructed in layers over a series of days and then tumour cells were applied ahead of drug treatment.

Figure 4.4 shows the final design of the 3D organotypic models with the addition of the collagen base layer. Once constructed brightfield images were taken to observe cell population interactions ahead of drug treatment and flow cytometry analysis (figure 4.5).

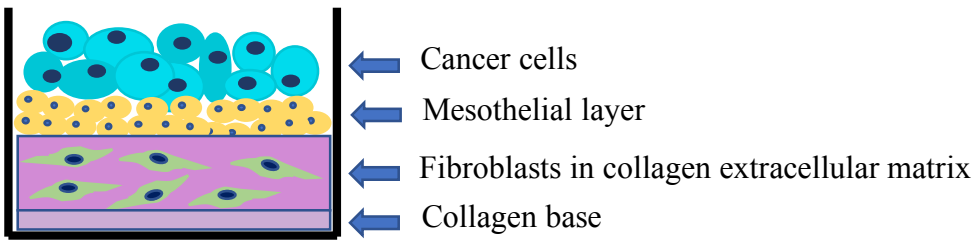


Figure 4.4: Diagram of 3D organotypic model design. *Diagrammatic representation of the constructed 3D organotypic model depicting the different layers of the peritoneal lined omentum.*

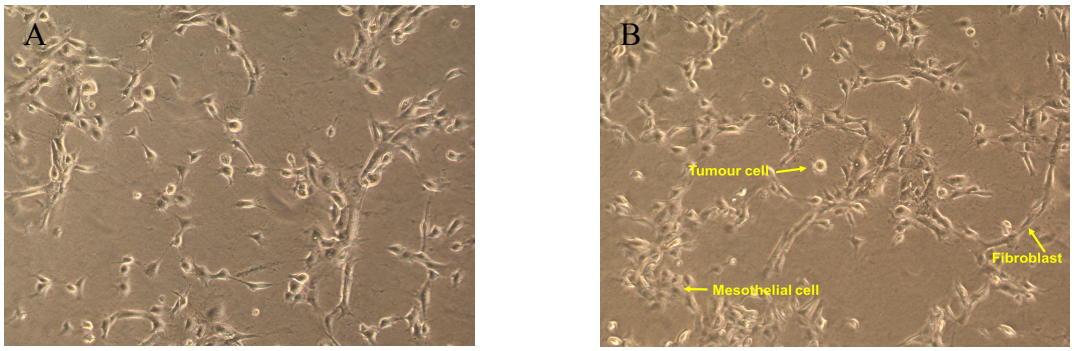


Figure 4.5: Brightfield images of 3D organotypic models. *Brightfield image at 10x magnification of 3D organotypic model taken from above showing A- different cell populations present. B - mesothelial cells' typical 'cobblestone' clustering, fibroblasts and PE01 ovarian cancer cell line tumour cell labelled.*

4.3.1 Processing of 3D organotypic models – Histological read-out optimisation

The original aim was to use immunohistochemistry to analyse the architecture of the models once built and to assess cell death and proliferation, the interactions between layers and the response to platinum treatment. Initially models once constructed and treated, were fixed with formalin then embedded in paraffin and sectioned for staining on a microtome.

Unfortunately, during the optimisation process there was great difficulty in maintaining the integrity of the organotypic model structure during fixation and embedding processes with the end result of no cells present on staining after sections were taken on the microtome.

In the early experiments, the first models had no base layer of collagen I and were built in 96 well plates, this used fewer cell numbers than the eventual models and so multiple models could be constructed.

However, when there was concern over loss of cells during the processing, a further base layer of collagen was introduced to try to protect the model structure. Histogel (Thermofisher) was then also introduced to embed the models into following treatment to help preserve the models further in a 3D structure after fixation. Unfortunately, however these steps were unsuccessful, there were ongoing issues with the loss of the model structure during processing.

Despite further optimisation including adjustments in fixation times and variation in paraffin embedding techniques, results were not able to be achieved with this method and the decision was therefore taken to switch to flow cytometry analysis of tumour cell populations for apoptotic response to treatment. Flow cytometry identifies cell populations in suspension and

uses their fluorescent and light scattering characteristics to analyse different processes. Cells can be selected with different labels depending on the biological process being studied[291].

4.3.2 Processing of 3D organotypic models - Flow cytometry optimisation

Following the decision to use flow cytometry the addition of Carboxyfluorescein succinimidyl ester (CFSE) staining to the tumour cells was required. Within the models there were 3 cell populations however only analysis of the tumour cell response to platinum was measured. Therefore, the tumour cells needed to be easily identifiable in the end analysis. Unlike immortalised cell lines, primary cells can be notoriously difficult to transfect however they can incorporate cell dyes such as CFSE which is commonly used for proliferation assays. This was therefore introduced to the tumour cell cultures prior to their addition to the models.

During optimisation of the assay read-out using flow cytometry analysis it was noted that higher cell numbers were required within the models to provide a sufficient sample for detection and analysis. The 3D organotypic models were therefore adjusted to be constructed in 24 well plates. From the Lengyel lab protocols, to produce a representative anatomical depiction of the omentum, the ratio of fibroblasts to mesothelial cells should be 1:5. The number of fibroblasts was optimised to 4000 with mesothelial cells therefore 20,000. Tumour cell numbers were increased to 50,000 per well. Whilst this enabled analysis to proceed it did unfortunately limit the number of models which could be constructed in each experiment due to the limited numbers of available primary cells. Experiments were performed in duplicate or triplicate where possible, with parallel culturing of 2D samples and processing with flow cytometry to allow for direct comparison of response to platinum.

To measure levels of apoptosis and necrosis in the tumour cells Annexin V and 7AAD were used (BD Biosciences Annexin V apoptosis kit). Annexin V is a phospholipid-binding protein which has a high affinity for the membrane phospholipid phosphatidylserine. During the early stages of apoptosis loss of cell plasma membrane structure leads to high levels of extra-cellular phosphatidylserine to which Annexin V binds. Annexin V can be conjugated to a fluorochrome such as Phycoerythrin (PE) and then used to detect levels of apoptotic cells within samples using flow cytometry. 7-amino-actinomycin (7AAD) dye is used to detect cells which have become necrotic as viable cells or those with intact plasma membranes do not permit entry of

7AAD. Using these two together discerns the spectrum of cells from early apoptosis to necrosis.

Initial FACS analysis showed high levels of apoptosis and necrosis across all 3D model samples, both treated and untreated. For example, in one of the first read outs, 33% of cells in 3D showed apoptotic activity versus 13% in 2D untreated populations. This suggested that the conditions provided in the models were not optimum for sustaining viability. In the original experiments the construction process took longer than the final protocol with fibroblasts being applied in ECM on the first day, mesothelial cells the next and tumour cells the following day ahead of drug treatment on day 4. It was presumed that to improve viability this process required adjusting to reduce the time spent in the wells. The protocol was altered to allow fibroblasts and mesothelial cells to be introduced to the models on the same day and it was observed that this still allowed time for the fibroblasts to establish themselves within the ECM. Foetal calf serum (FCS) was introduced into the ECM composition to better mimic the provisions of primary media given to the other primary cell populations. Additionally, at first the models were being broken down ahead of FACS processing simply by manual methods with gentle pipetting but there were concerns this was further affecting assay read-out. Therefore, a product called Liberase (Sigma-aldrich), which is a blend of Collagenase I, Collagenase II and Thermolysin, was added to the protocol which digested the ECM and released the cells to be collected more efficiently. Finally, Transwell inserts were also added to the 24 well plate to allow for primary media to be added externally to the models allowing for better passage of nutrients. Following these adjustments an improvement in overall viability was observed on FACS analysis.

4.4 Flow cytometry analysis of 3D organotypic models

4.4.1 Apoptotic response of ovarian cancer immortalised cells lines to cisplatin treatment in 3D organotypic models

To minimise usage of primary tumour cells, preliminary optimisation experiments were conducted using immortalised ovarian cancer cell lines. Cell lines PE01, PE04, SKOV3 and Kuramochi were used (ATCC). PE01 ovarian cancer cell lines were selected as they are platinum sensitive therefore were useful for assessing if any response to treatment was observed using the Annexin V detection kit in 2D and whether this was a useful analysis technique. They were also used to compare 2D and 3D responses prior to completing the experiment with 3D models with primary cells. PE04, Kuramochi and SKOV3 cell lines are known platinum resistant ovarian cancer cell lines and could thus also add reliability to the data gathered if these expected responses were observed in the project.

Drug treatment involved treatment with 25μM cisplatin for 24 hours prior to analysis with flow cytometry for apoptosis and necrosis levels.

As discussed above, there were initial concerns regarding the high number of apoptotic and necrotic cells seen in PE01 cells even within the untreated population samples, as seen in Figure 4.6, plot B (apoptosis seen in quadrant 3). Figure 4.6 plot A shows the concurrent 2D monolayer PE01 untreated cells showing less apoptosis. Therefore, adjustments to the construction and deconstruction protocols were made as described and improvements in viable cell numbers were observed, figure 4.6, plot C, apoptosis seen in quadrant 1 here).

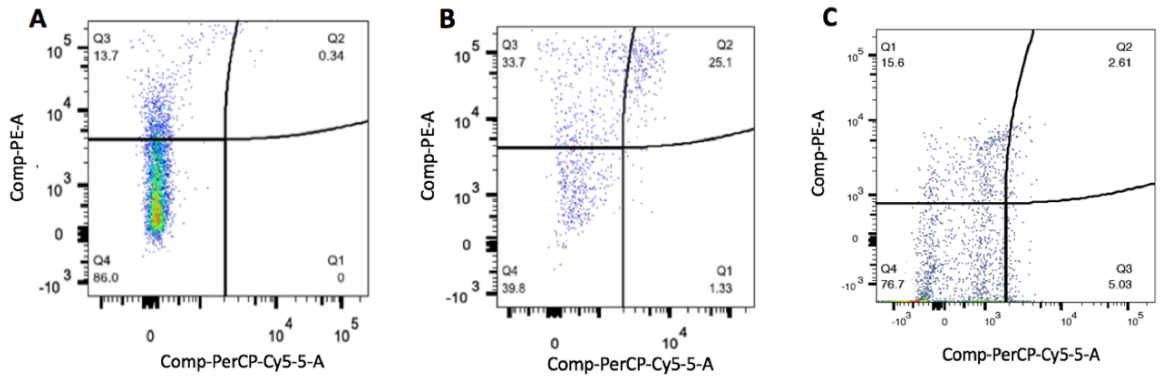


Figure 4.6: Scatter plot FACS analysis of PE01 cell line in 3D model. *3D models containing untreated CFSE stained PE01 cell line cultures were analysed using flow cytometry with concurrent 2D monolayer cultures. Plot A- shows all cells detected in 2D cultures analysed for apoptosis (Annexin shown in the PE-A channel)) and necrosis (7AAD, shown in the PerCP-Cy5-5-A channel). B – 3D PE01 cultures initially showed high levels of apoptosis and necrosis. CFSE labelled cells detected in the FITC channel. C – a reduction in apoptotic activity in 3D model cell cultures was seen following adjustments to culture composition and processing.*

Using the CFSE labelling, tumour cells were identified and separated for further analysis. Doublet cells were removed from the data and then the final apoptosis and necrosis read outs obtained using the PE-A channel for Annexin V and PerCP-Cy5-5-A channel for 7AAD. These results were displayed in scatter plot graphs using quadrant separation to compare outcomes in each sample. The apoptosis levels were normalised to viability and then calculated as a fold change from untreated control.

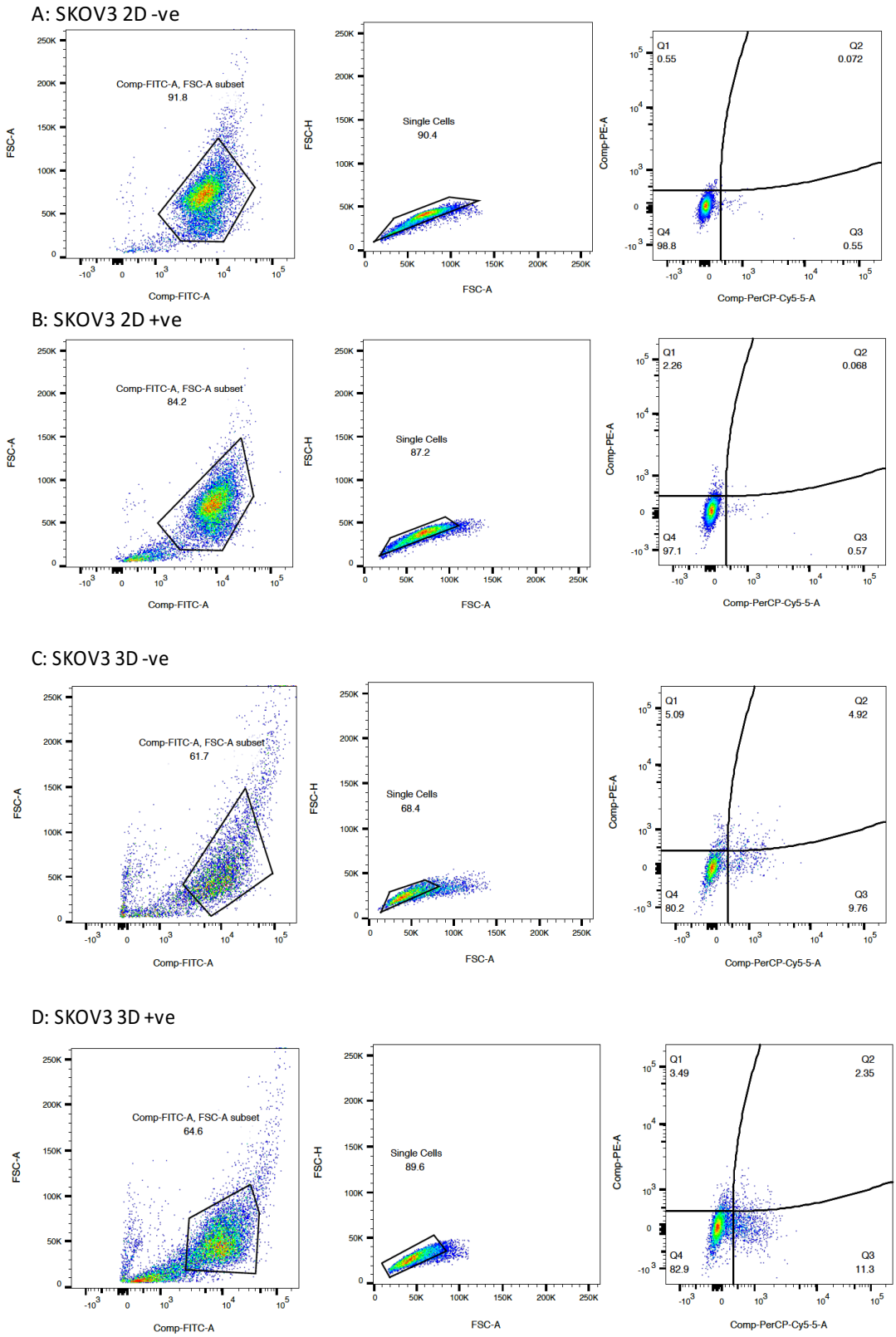


Figure 4.7: Scatter plots of FACS analysis 3D cell line models. *Example scatter plots from experiment with SKOV3 cells. A –untreated SKOV3 cells in 2D culture. B – SKOV3 cells in 2D culture treated for 24hours with 25µM cisplatin. C- untreated SKOV3 cells in 3D organotypic model. D – SKOV3 cells in 3D organotypic culture treated for 24hours with 25µM cisplatin. All samples show initial selection of tumour cells in analysis via CFSE selection in FITC channel, doublet cells were then removed and analysis for apoptosis (Comp-PE-A) and necrosis (Comp-PerCP-Cy5-5-A).*

Once the data for levels of apoptosis and necrosis were obtained and normalised they were plotted to analyse the variation in response to cisplatin treatment both between 2D and 3D samples and between differing cell lines.

Shown here in Figure 4.8 in different cell lines an overall reduced response to cisplatin treatment was seen in 3D model cultures compared to the 2D parallel cultures. There was also variation in the apoptotic response observed between the different cell lines both in 2D and 3D as would be expected based on the known platinum responses of the cell lines used.

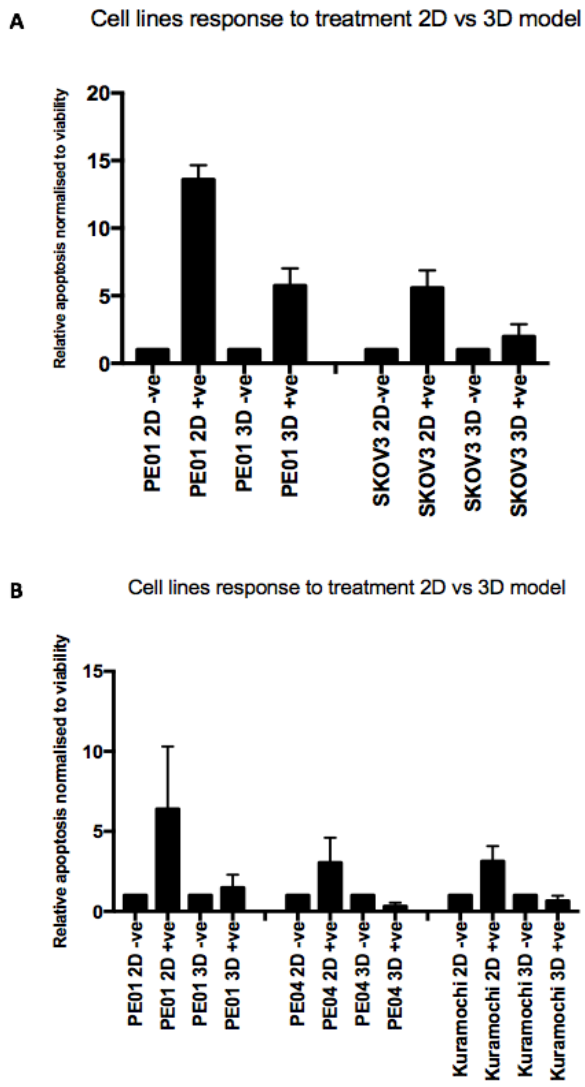


Figure 4.8: Apoptotic response of HGSOC cell lines to cisplatin in 2D and 3D organotypic models. *Cell lines in 2D and 3D organotypic models are treated with 25μM cisplatin. For cell line models, cells were seeded in triplicate prior to 24-hour treatment. The y-axis shows apoptosis levels normalised to viability then expressed as a fold change. Triplicate assays performed. A- Bar chart shows apoptosis normalised to viability for the PE01 and SKOV3 cell lines. Both cell lines show 'expected' sensitivity profile in 2D culture, with the PE0, PE01 line appearing more sensitive than SKOV3. Both cell lines show reduced sensitivity in 3D culture environment. B- Further experiments during optimisation with PE01, PE04 and Kuramochi cell lines again show reduced sensitivity to cisplatin in 3D cultures. Variation in response to treatment between cell lines is observed. Replicate numbers too small to assess statistical significance, trend towards reduced sensitivity in 3D models seen.*

4.4.2 Apoptotic response of primary HGSOC tumour cells to cisplatin treatment in 3D organotypic models

Following optimisation with cell line models, primary tumour cells from multiple deposit sites were applied to the organotypic models. Due to the change to flow cytometry analysis a higher volume of cells were required in culture. A larger 24 well plate was used and 50,000 tumour cells per well were applied and drug treated with 25μM cisplatin the following day. This concentration was chosen to match the ITH phenotypic protocol. Following 24 hours' drug treatment the models were processed for FACS analysis and results obtained. The data was processed as per the cell line models and scatter plots were created to organise the data readouts. Though this change in protocols to flow cytometry analysis was required due to the problems with fixation, it did limit the number of replicates able to be seeded due to the limitations with primary tumour cell numbers and therefore the conclusions able to be drawn from the data.

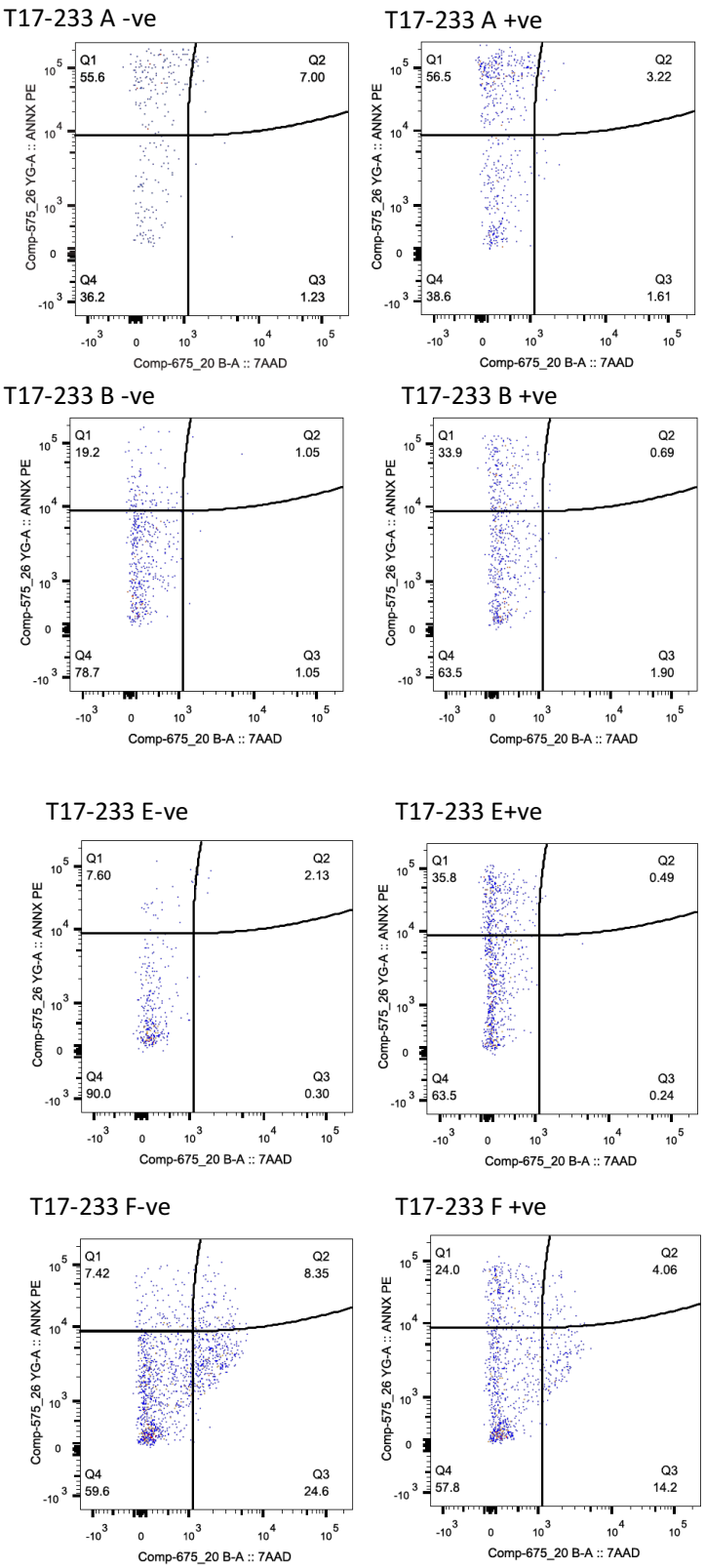


Figure 4.9: Scatter plots from FACS analysis of 3D organotypic models with primary tumour cells. *Case T17-233. Showing apoptosis, (y axis, higher levels shown in quadrant 1 in this example), and necrosis (x axis, higher levels shown in quadrant 3 in this example) readouts from multiple tumour site 3D models. A= Primary, B= Omentum, E= Left Paracolic area, F= Splenic area. Untreated (-ve) and 25μM cisplatin treated (+ve) results shown.*

Using the data from the scatter plot readouts the levels of apoptosis and necrosis were obtained and for each sample these were normalised to viability and expressed as a fold change to untreated control, and data compared between 2D and 3D cultures.

In case T17-233 samples from the primary, omentum, left paracolic area and splenic area were tested. Wide heterogeneity was observed between the different sample sites' response to cisplatin. The left paracolic area had the highest sensitivity compared to others in both 2D and 3D. In all samples, there was a reduced response in 3D compared to 2D. Interestingly the sensitivity relative to other samples was sometimes altered in 2D versus 3D. For example, the primary sample appears to have similar sensitivity compared to the omentum in 2D but is less sensitive in 3D, suggesting certain factors promoted by the 3D environment enabled the primary sample to appear more resistant to cisplatin treatment. The splenic area sample is also greatly changed in sensitivity in 3D, becoming more of a non-responder like the primary sample. Due to limited tumour cell numbers, often only 1-2 cultures per sample site was possible to be seeded. Therefore, analysis can only be observational and statistical analysis between individual samples is not possible.

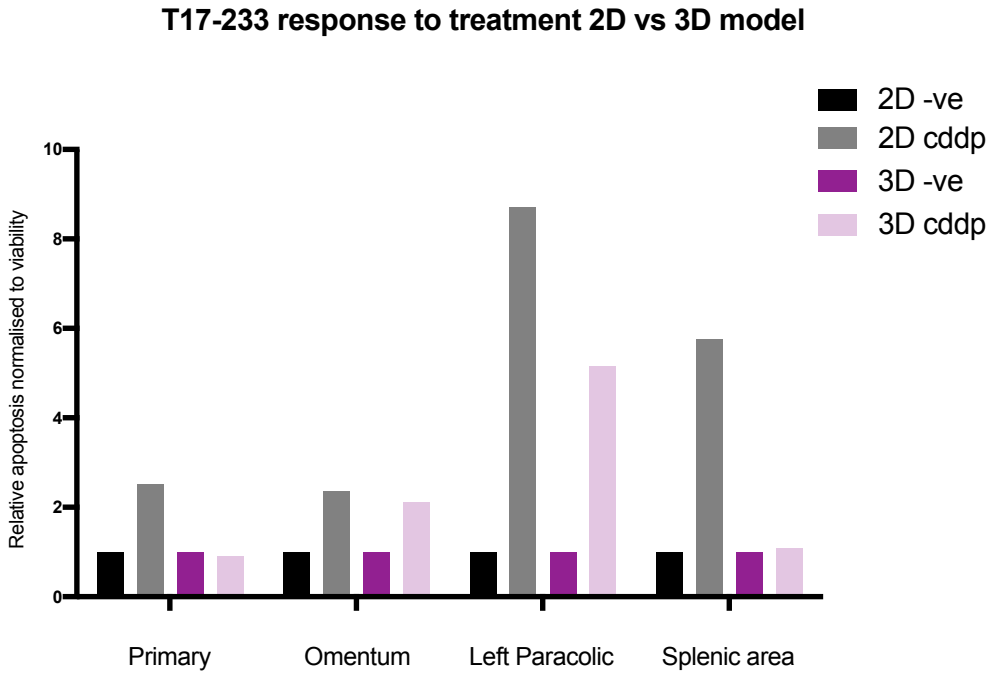


Figure 4.10: Apoptotic response to cisplatin 2D culture vs 3D organotypic models case T17-233. *Bar chart showing Case T17-233 response to cisplatin treatment across multiple tumour sites in both 2D cultures and 3D organotypic models. N=1 per tumour site culture. Assay readouts for apoptosis and necrosis were normalised to viability then expressed as a fold change of untreated.*

In each case the aim was to test as many metastatic sites as possible however this was not feasible for all cases. The quantity of sites for analysis was dependent on the size of samples obtained from theatre, which was entirely variable case by case depending on the volume of metastatic spread. Given the scope of the ITH project with over 400 cultures being established along the time course and multiple factors being examined, the study of primary and omentum samples was prioritised plus any additional anatomical areas where there were sufficient cells extracted and cultured.

For case T18-011 samples were tested from the primary tumour, omentum and pelvic lymph node. The different anatomical locations again show heterogeneity in their response to platinum with an overall trend towards reduced apoptotic response seen in the 3D models compared to the 2D cultures. Here in 3D all the samples appear to have no response to cisplatin treatment (figure 4.11).

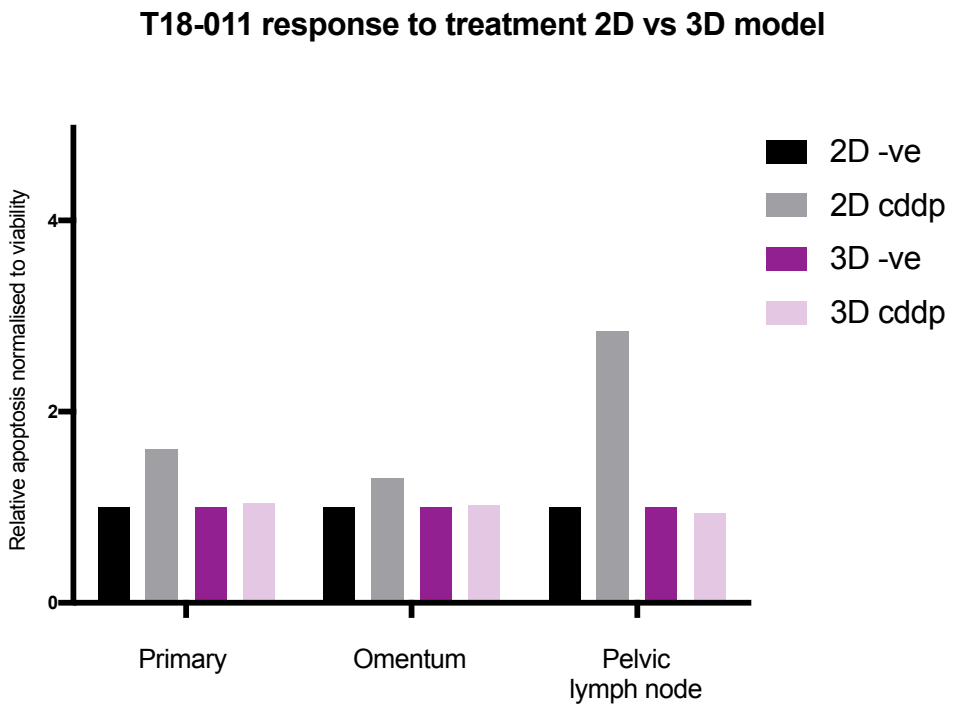


Figure 4.11: Apoptotic response to cisplatin 2D culture vs 3D organotypic models case T18-011. *Bar chart from case T18-011 showing multi tumour site analysis of apoptotic response to cisplatin in both 2D and 3D cultures. N=1 per tumour site cultures. Apoptosis and necrosis assay readouts were normalised to viability then expressed as a fold change of untreated control.*

For case T18-085 I was able to incorporate ascites samples into the 3D models. In this case, again there is heterogeneity in response to treatment between the different sample sites which was seen predominantly in 2D apoptosis levels, with almost two-fold increase in apoptosis in cisplatin treated cells compared to no treatment. The ascites appears to be a non-responder in both 2D and 3D. Studies have found that ovarian cancer ascites derived spheroids can show different adhesion properties between cultures in materials such as plastic, mesothelial cell layers and ECM[261]. This may explain the lack of response of ascites in the 3D model, with the mesothelial layer interacting with the ascites derived tumour cell culture and potentially making them much more susceptible to the platinum treatment.

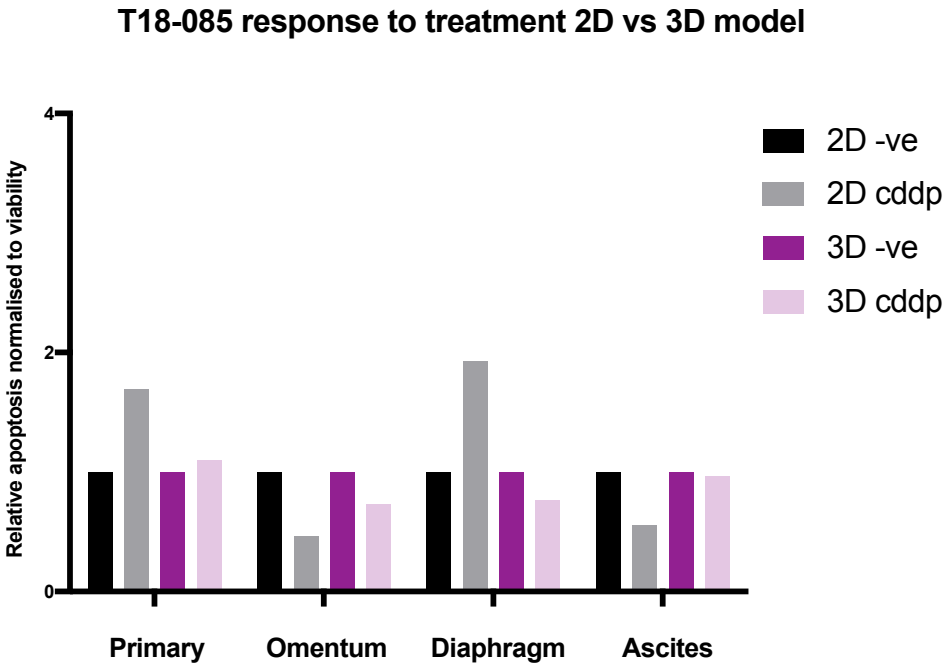


Figure 4.12: Apoptotic response to cisplatin 2D culture vs 3D organotypic models, including ascites sample. *Bar chart from case T18-085 showing multi tumour site analysis of apoptotic response to cisplatin in both 2D and 3D cultures. N=1 per tumour site culture. Ascites cultures were included in the assay and demonstrate the tendency towards reduced response in ascites samples to cisplatin which can be affected by the culture substrate.*

In some cases there were several tumour sample sites available to study and in others only single samples were big enough to provide sufficient cells for the model cultures. Table 4.1 demonstrates the diversity in sample quantities and areas tested. What was observed was a wide heterogeneity in sensitivities between sample sites in cases where more than one area was tested. There was also evidence of an overall trend towards reduced sensitivity to cisplatin in the 3D model cultures compared to the 2D setting. In the ITH project widespread heterogeneity was seen between different cases and this was also apparent in the model cultures.

Case	Sample sites tested	Apoptosis normalised to viability 3D models
T18-055	Omentum	1.1
	Lesser sac	0.7
	Descending colon	0.7
	Ascites	0.9
T18-281	Ovary	1.1
	Omentum	1.6
	Abdominal wall	1.3
T17-195	Duodenal area	2.15

Table 4.1: Example of sample sites examined in different cases and apoptotic responses to cisplatin. *Listing different cases where 3D organotypic models were examined and the variation in sample quantities and locations per case. Apoptosis levels normalised to viability and expressed as a fold change of untreated control in 3D models listed showing variation within sample sites and patients.*

As the sample numbers and replicates were low, analysis was performed grouping all 2D treated samples with all 3D organotypic model samples. This enabled statistical analysis of overall response to cisplatin treatment in 2D culture vs 3D models and allowed for those patients where only 1 sample was obtained to be included. Mann-Whitney testing showed significant reduction in response to cisplatin treatment in the 3D model results compared to 2D cultures analysed via flow cytometry (p=0.0288, figure 4.13).

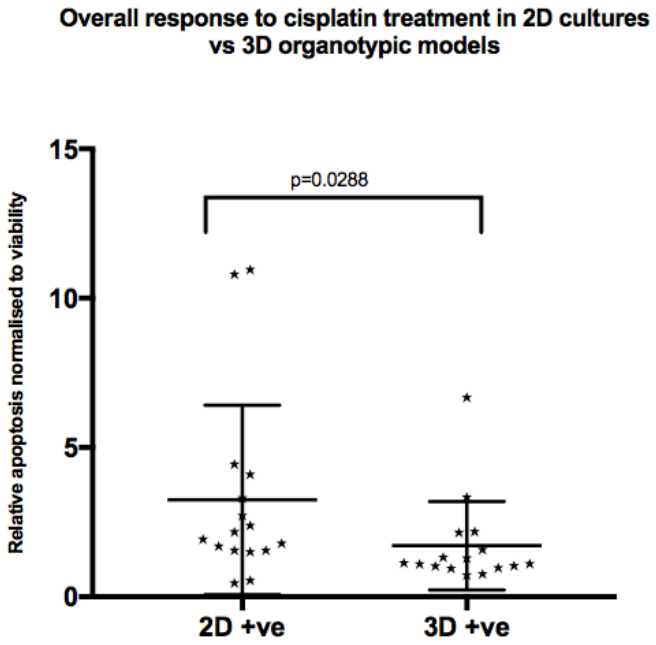


Figure 4.13: Grouped analysis of all 2D and 3D samples; response to cisplatin treatment. *Flow cytometry apoptosis readouts from 2D cultures and 3D organotypic models from different cases were combined to observe for statistical significance. n=16 per group. Overall reduced response to cisplatin was observed in the 3D organotypic models (Mann-Whitney test p=0.0288).*

4.5 Comparison and correlations between 3D model and 2D ITH phenotypic data

Tumour cells extracted from the multiple metastatic sites obtained from theatre varied in quantity dependent on the size of sample. They were processed for multiple assessments including phenotypic apoptosis assays, IC_{50} and RPPA analysis to study the proteomic landscape of the tumour cells. These results form part of the larger ITH project as described previously. To examine the results from the 3D organotypic model data further comparisons were made with the ITH phenotypic apoptosis (caspase 3/7 based) assays.

Using the apoptosis results, analysis was performed for any correlation between the response to cisplatin treatment in 2D versus 3D models. This was compared between both 2D cultures from the ITH phenotypic data and the parallel 2D model cultures. The analysis was limited by the low numbers of sample sites in each model to observe significance in the findings.

Within the ITH cohort there was great variety in response to platinum treatment between metastatic sites and different patients. This paralleled what was observed within the models.

In figure 4.14 case T17-233 demonstrates the heterogeneity in apoptotic response to platinum treatment independent of analysis method (Graphs A&B). Both in 2D and 3D settings the tumour sites behave differently.

In the example in figure 4.14, there was a significant correlation comparing 2D phenotypic data with 2D flow cytometry data ($p=0.001$) with an r value of 0.999 (scatter plot C). This suggests that the sample sites retained their relative sensitivities to cisplatin irrespective of the processing or analysis method used in 2D. Comparing the 3D models with 2D data revealed a positive correlation for both 2D ITH phenotypic data (Graph D, $r= 0.9363$, $p = 0.06$) and 2D flow cytometry parallel cultures (Graph E, $r= 0.9405$, $p = 0.0595$). Achieving significance with such small sample numbers is very difficult however this case appears to suggest a trend towards correlation between 2D and 3D responses.

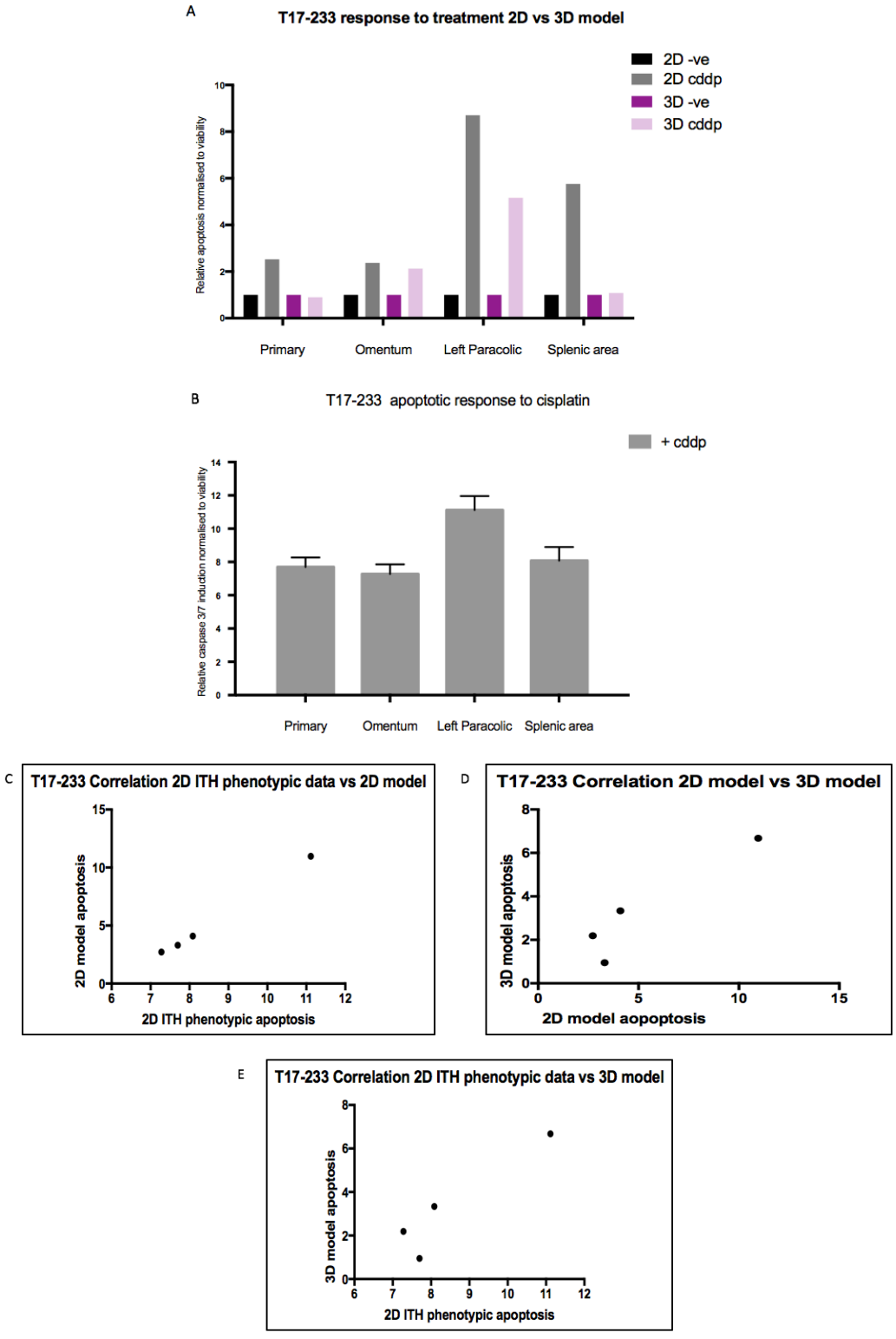


Figure 4.14: Correlation of apoptotic response in 2D cultures and 3D organotypic models analysed using different assays case T17-233. *Graph A shows the bar chart representing response to cisplatin treatment between samples from flow cytometry readouts of 3D models and parallel 2D cultures. Graph B shows bar chart of phenotypic results of apoptotic response to cisplatin using caspase 3/7 assay. Correlation plots representing comparison between the response to cisplatin treatment in 2D ITH phenotypic cultures, 2D cultures processed in parallel with models and in 3D organotypic models. 2D phenotypic data vs 2D model data shows positive correlation with significant r value 0.999 (p=0.001) (C), positive non-significant correlation seen between 2D culture and 3D models (D and E).*

Conversely, in case T18-011 a negative correlation was seen between the different 2D analysis techniques (Figure 4.15, plot C). This may reflect the intratumoural heterogeneity present suggesting that even within individual tumour sites there is a range of sensitivities observed which will give rise to different analysis results depending on culture protocols. The results for this analysis were not significant (r value -0.9951, $p = 0.06$) and it is difficult to draw conclusions based on these limited sample numbers. When the 2D cultures were compared to the 3D model apoptosis data there was no correlation seen in either method (figure 4.15, plot D &E). Again, perhaps demonstrating the unpredictable nature of this heterogeneous tumour biology and different methodologies employed, but caveated by the difficulty to interpret small sample size analysis.

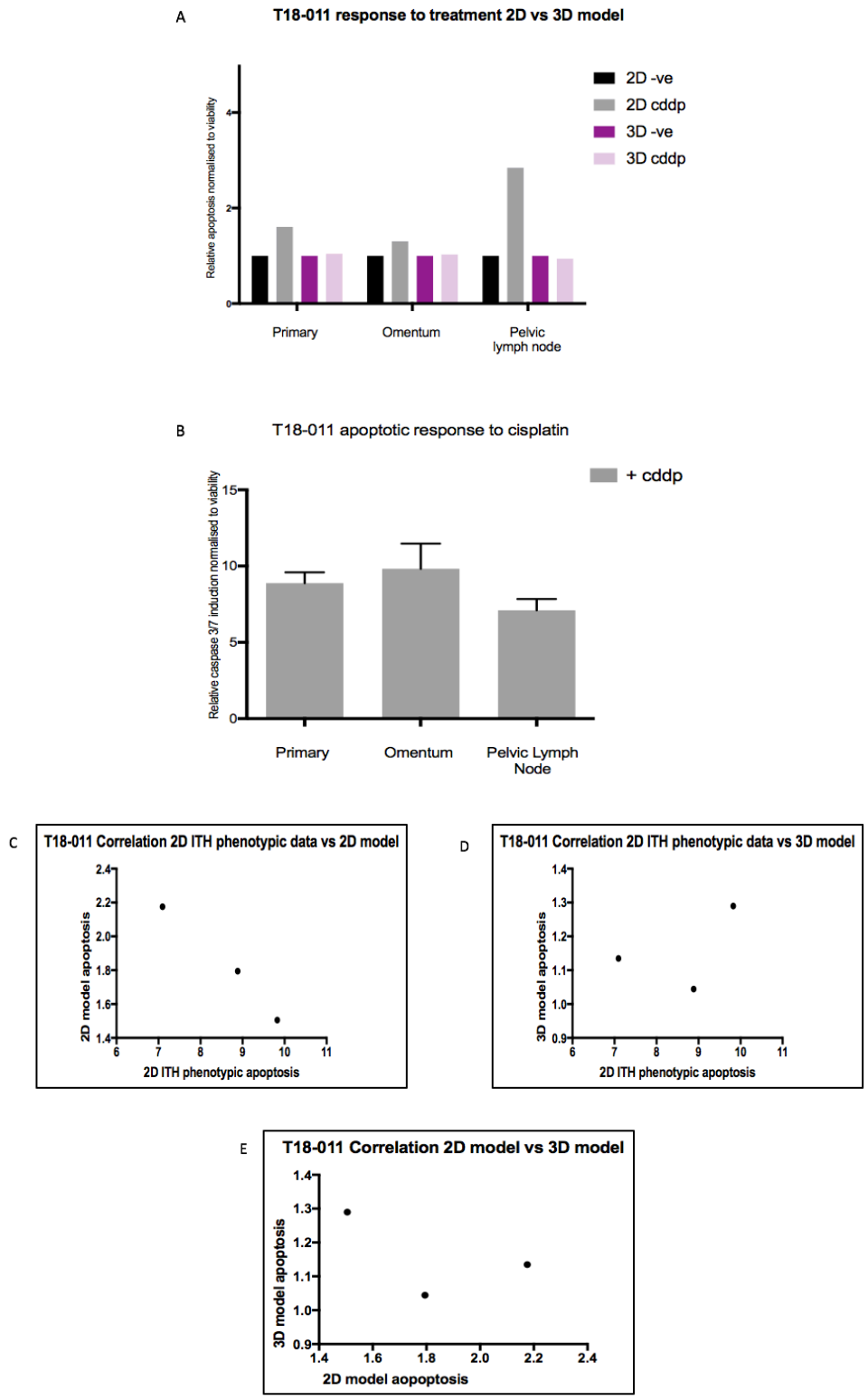


Figure 4.15: Correlation between apoptotic response in 2D cultures and 3D organotypic models analysed using different assays case T18-011. *Graphs A&B show readouts for apoptotic response to cisplatin analysed by different assays, A- flow cytometry analysis of 2D cultures and 3D organotypic models. B – Phenotypic caspase 3/7 assays undertaken for the ITH project. Plots C, D and E show correlation analysis between the different techniques, non-significant trend towards negative correlation between the different 2D culture analyses was observed (C, p = 0.06) No correlation with 3D results was seen (D p=0.68 & E p=0.62).*

4.6 Discussion

The aim of the 3D organotypic model work was to observe the effect placing primary tumour cells within a 3D culture system, mimicking the *in vivo* microenvironment of the omentum, would have on their behaviour, reflected in their sensitivity to cisplatin.

Here, human primary stromal cells were extracted from omental samples and cultured in collagen I ECM to create structural and cellular supporting systems for tumour cells. These 3D organotypic models reflect the anatomical layering of the peritoneal surfaces lining the omentum and intra-abdominal organs. Using apoptotic responses to cisplatin analysed using FACS, it was observed, similarly to 2D cultures, there was wide heterogeneity in platinum sensitivity both between sample populations within individual patients and between different patient samples. With small sample numbers, it is difficult to achieve statistical significance but within the cases there was a general trend observed showing a reduction in sensitivity to platinum in 3D cultures compared to 2D. However, when the 2D and 3D response rates from all patients were grouped together there was observed to be a statistically significant reduction in response to cisplatin in the 3D organotypic model cultures overall.

Limited correlation was seen between the apoptotic response to cisplatin in the 2D cultures examined in the ITH phenotypic work and the 2D and 3D model flow cytometry assays. However, it must be noted that the readouts were based on different apoptosis assay protocols and so comparison is difficult to rely on. However, the differing techniques examined would be assumed to portray similar outcomes as overall apoptosis trends would be expected to be maintained.

There were several limitations with the development of these culture models. The initial plan for analysis had to be altered when difficulties were repeatedly encountered with the FFPE and IHC results. To prevent further loss of valuable primary cultures the decision was made to switch analysis to flow cytometry. Whilst providing a robust method of analysis this had the drawback of requiring a larger number of cells for processing for 24-well sized organotypic models which limited the number of sample sites which could be examined and replicates of these cultures.

Because of these issues and the failure of the models to produce reliable data using different primary tumour cultures, different 3D culture techniques were considered with the goal of producing a more reliable, reproducible system in which to maintain tumour cells from the

multiple metastatic sites in different matrices which would mimic the individual tumour microenvironments as closely as possible.

Chapter 5

Results: Elucidation of tumour extracellular matrix composition in HGSOC

5 Results: Elucidation of tumour extracellular matrix composition in HGSOC

5.1 Introduction

In order to design and construct culture systems better replicating the *in vivo* state, a greater understanding of the tumour microenvironment is required. With the widespread dissemination pattern of HGSOC, metastatic tumour deposits develop within multiple heterogeneous tissue sites and can utilise the properties of the local environments to their advantage[292]. Tumour cells corrupt the signalling pathways existing within tissues, both cell-cell and cell-extracellular matrix (ECM)[293]. Understanding the interactions between a tumour and its local microenvironment can help lead to discoveries of biomarkers for disease and novel targeted therapies[294]. Understanding the biological and structural functions and the interactions of these crucial microenvironment elements is therefore essential in moving forward in establishing *in vitro* culture systems which are more clinically relevant and representative of the tumour *in vivo*.

My ITH study data, described in chapter 3, showed that the different anatomical tumour deposit sites can show variation in response to platinum treatment in 2D culture. This was further shown when the primary tumour cells were applied to 3D organotypic cultures (chapter 4). Studies often analyse tumour deposits from the omentum as it is generally easier to obtain large volume tumour samples from this site. To study the ECM composition, this project examined tumour deposits from all over the abdominal cavity thus giving a unique insight into the variation in composition of ECM from metastatic sites. This is vital to understand differences in response to treatment between patients to aid prediction of outcome, whilst also providing the potential for discovery of biomarkers for use in disease detection or prediction of response to treatment.

Using the multi-site tumour samples gained from the ITH patient cohort, I selected 5 samples from various anatomical locations from 4 different patients for a pilot mass spectrometry based proteomic analysis. Cases were selected to include as much overlap in sample site as possible for comparison and where sufficient tissue was present. I aimed to cover a broad selection of abdominal regions and have matching tumour locations from each case where possible. This would provide 20 different samples to compare the similarities and differences between sites

and patients. The aim following analysis of the breakdown of protein components was to observe any patterns in ECM protein composition which could be applied to future culture systems to tailor more personalised testing platforms for HGSOC.

To collect ECM protein lysates, primary tumour cells were firstly extracted from different tumour deposits as per the ITH protocol to decellularise the matrices and then ECM protein extraction carried out as per the protocol described. An aliquot of each sample was taken for protein quantification and Western blotting. The protein lysates were sent for MS analysis at DC Biosciences, Dundee, UK. The Thermo Scientific™ TMT™ Mass Tag Labeling kits and reagents were used in order to perform multiplex relative quantitation by MS of the processed samples.

5.2 Patient and sample data

5.2.1 Sample information

20 samples were analysed from 4 patients from the ITH project collected between 2016-2018, n=5 samples were taken from each case. All cases had a primary and omentum sample and there was some further duplication of sample sites where possible, for example diaphragm and spleen tumours. These patients had sufficient tumour tissue for analysis from multiple metastatic sites and had similar tumour locations from the IMO mapped samples to be able to make comparisons between patients.

Case	Sample	Anatomical site
T16-060	A	L Ovary (primary)
	B	Omentum
	D	Diaphragm
	G	Spleen
	K	Paracolic
T17-205	A	L Ovary (primary)
	B	Omentum
	H	Spleen
	K	Sigmoid
	L	Appendix
T18-085	A	L Ovary (primary)
	B	Omentum
	C	R Diaphragm
	F	Falciform ligament
	G	R Colic Flexure
T18-119	A	L Ovary (primary)
	B	Omentum
	C	Diaphragm
	E	L Paracolic
	J	Rectum

Table 5.1: Table showing the sample sites studied profiled from 5 anatomical sites from 4 different patients.

5.2.2 Patient demographics

Case	Age	Stage	Grade	Disease state	Platinum status	PFS from surgery
T16-060	46	IVa	3	0	Sensitive	24 months
T17-205	57	IIIC	3	0	Sensitive	12 months
T18-085	75	IVB	3	0	Sensitive	17 months
T18-119	74	IIIC	3	1	Sensitive	20 months

Table 5.2: ECM Patient demographics*. Showing the patient demographics across the 4 cases based on age, stage and grade of disease, disease state where 0 = limited or localised peritoneal carcinosis and 1 = diffuse milliary small nodule carcinosis and progression free survival (PFS calculated from date of surgery).*

Across the 4 patients there was variation in age, ranging from 46-75. All were advanced stage HGSOC at diagnosis (IIIC-IVB). All received adjuvant chemotherapy following successful maximal effort cytoreductive surgery and all experienced relapse in a platinum sensitive timeframe with a PFS from the time of surgery ranging from 12-24 months. Disease state relates to the differing patterns of disease spread seen within patients with HGSOC at time of surgery. Some have more diffusely dispersed small nodules of disease where others still have multiple areas of metastatic spread but in more discrete pockets of disease. In this cohort, case T18-119 had diffuse, milliary pattern of metastatic spread whereas the other 3 cases T16-060, T17-205, and T18-085 had limited/localised carcinosis. Three of the cases were successfully operated to no residual disease, case T17-205 had residual disease <1cm.

The 20 tissue samples underwent protocols to specifically extract ECM protein lysates, modified from [215]. Aliquots were taken from the subsequent protein lysate samples to detect the presence of common ECM proteins prior to sending for MS analysis. Western Blot analysis was performed which confirmed the presence of collagen IV and the glycoprotein fibronectin in all samples from all cases.

5.3 Mass Spectrometry data analysis of ECM composition in HGSOC samples

5.3.1 ECM protein composition shows heterogeneity across the sample cohort

Following confirmation of the presence of common ECM components, the samples were sent for MS analysis. Initial data was normalised and processed by the bioinformatics team internally at DC Biosciences. Data was provided giving relative expressions of ECM proteins within all samples, normalised to a collective pooled expression signature by combining all sample site results. Analysis of the MS data revealed 785 identified proteins within the sample groups.

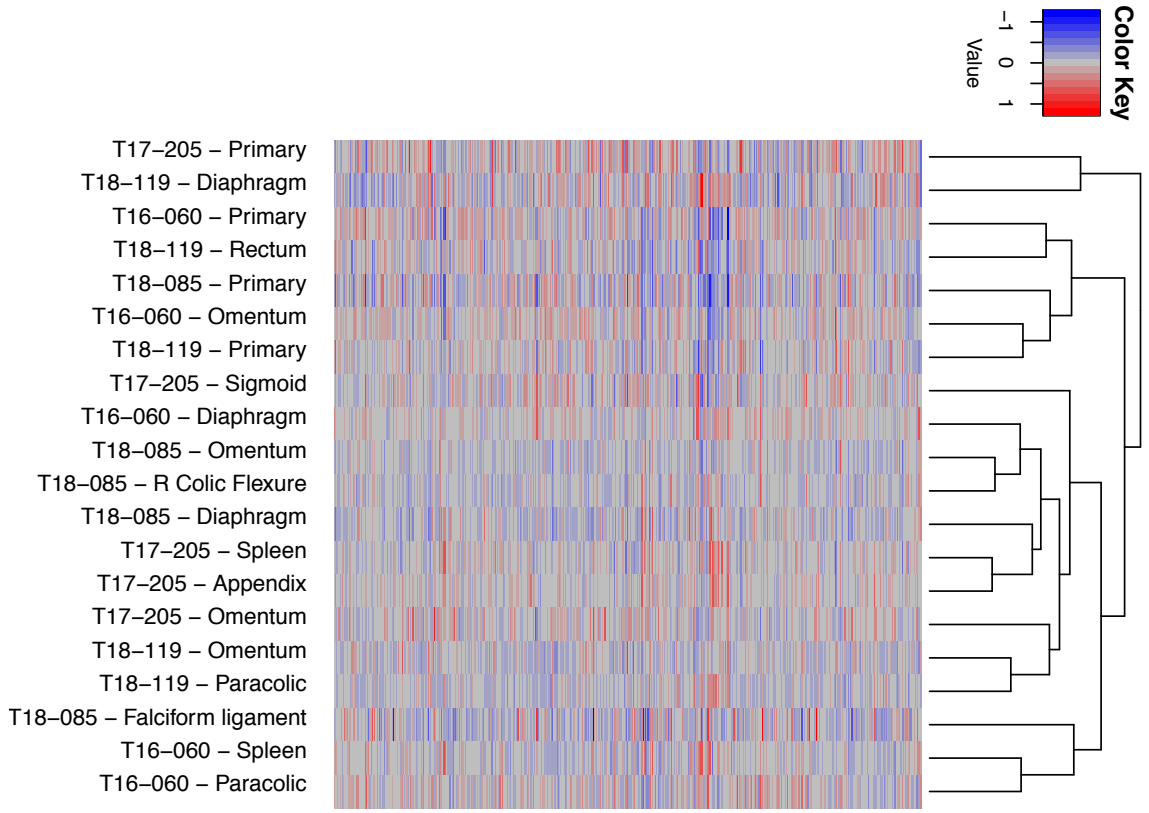


Figure 5.1: Heatmap showing the relative expression of ECM proteins across the patient cohort. *Limited clustering is seen based on sample site or patient*

Heatmaps were created to observe the ECM protein composition differences within the sample group. The heatmap of all samples shows great variation in ECM protein composition across the sample cohort. Whilst a few samples from different cases do appear to cluster together, there is also great inter and intra case heterogeneity demonstrated.

When each case was examined separately, there is again little clustering seen to represent similarities between sample sites in individual cases. Once more showing the heterogeneity often observed when studying different biological properties of HGSOC.

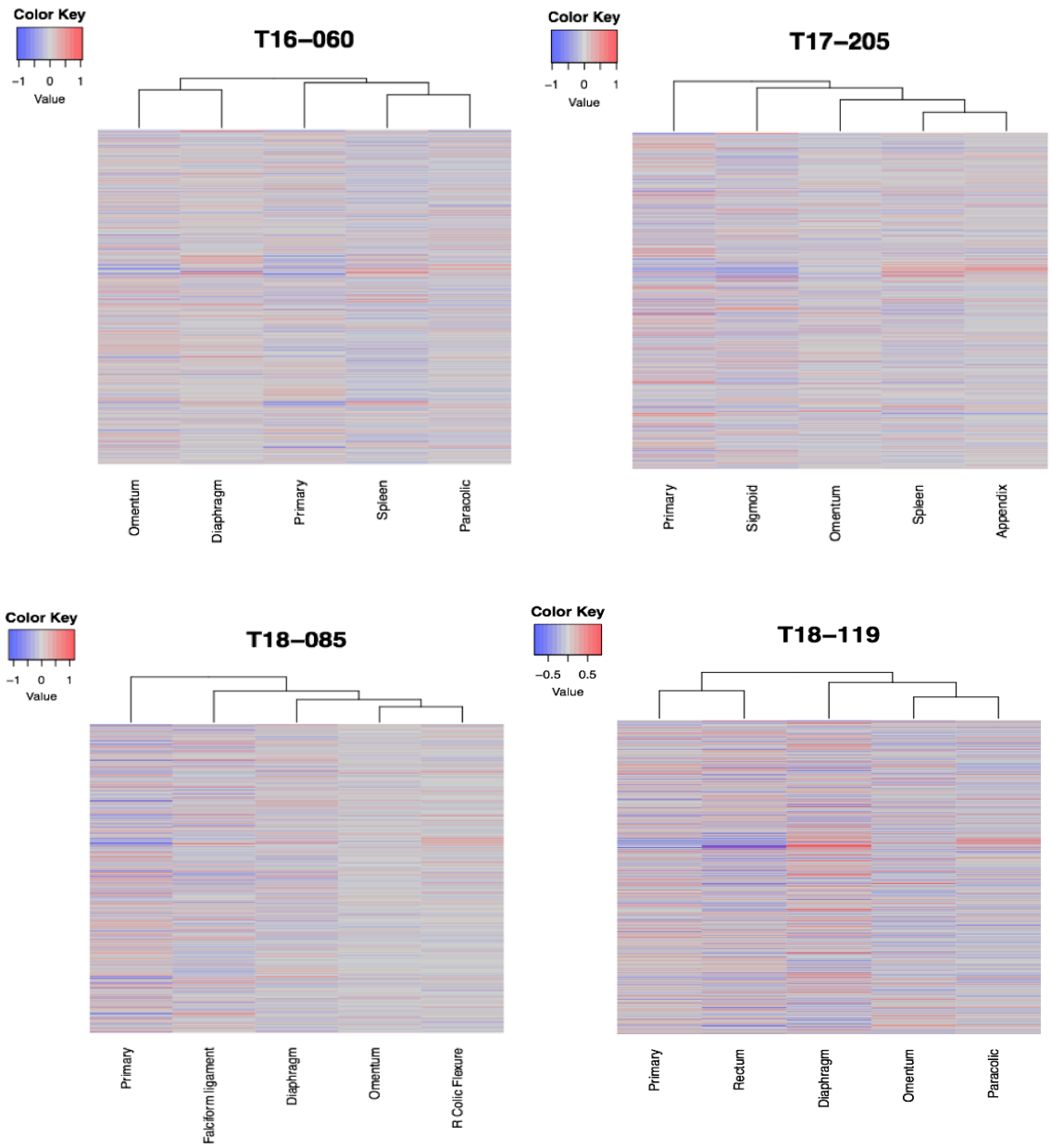


Figure 5.2: Heatmaps by case. *Individual case heatmaps showing minimal correlation of protein composition between the different sample sites in all patients.*

5.3.2 Protein-protein interactions and pathway enrichments analysis

The Search Tool for the Retrieval of Interacting Genes (STRING) database provides insight into the functional links between proteins[194]. In our data set the identified upregulated proteins across the cohort were inputted into the STRING database (n=84) and the readout collated. Figure 5.3 shows the various interactions between the identified proteins. There are some limited connections involving one or two proteins only but a significant clustering of interactions between the collagen family of proteins, highlighting their importance in the microenvironment of tumour tissues. Closely linked to these are TGFβI and MFAP which have been linked to ovarian cancer and will be discussed further below[295, 296].

Pathway analysis discovered numerous significantly enriched pathways. The top 10 significant results are displayed in table 5.3. Of particular interest these include ECM organisation, collagen organisation and cell adhesion pathways.

	Biological Process (Gene Ontology)			
GO-term	*description*	*count in network*	*strength*	*false discovery rate*
GO:0030198	Extracellular matrix organization	18 of 338	1.26	6.19e-14
GO:0030199	Collagen fibril organization	8 of 46	1.78	1.22e-08
GO:0097435	Supramolecular fiber organization	15 of 480	1.03	2.31e-08
GO:0009888	Tissue development	23 of 1760	0.65	6.25e-07
GO:0007155	Cell adhesion	17 of 925	0.8	1.61e-06
GO:0061448	Connective tissue development	10 of 223	1.19	1.95e-06
GO:0051216	Cartilage development	9 of 171	1.26	3.31e-06
GO:0003429	Growth plate cartilage chondrocyte morphogenesis	5 of 17	2.0	5.63e-06
GO:0002063	Chondrocyte development	6 of 42	1.69	5.63e-06
GO:0060351	Cartilage development involved in endochondral bone morp...	6 of 43	1.68	5.63e-06

Table 5.3: Top 10 most significantly enriched pathways in STRING database analysis.

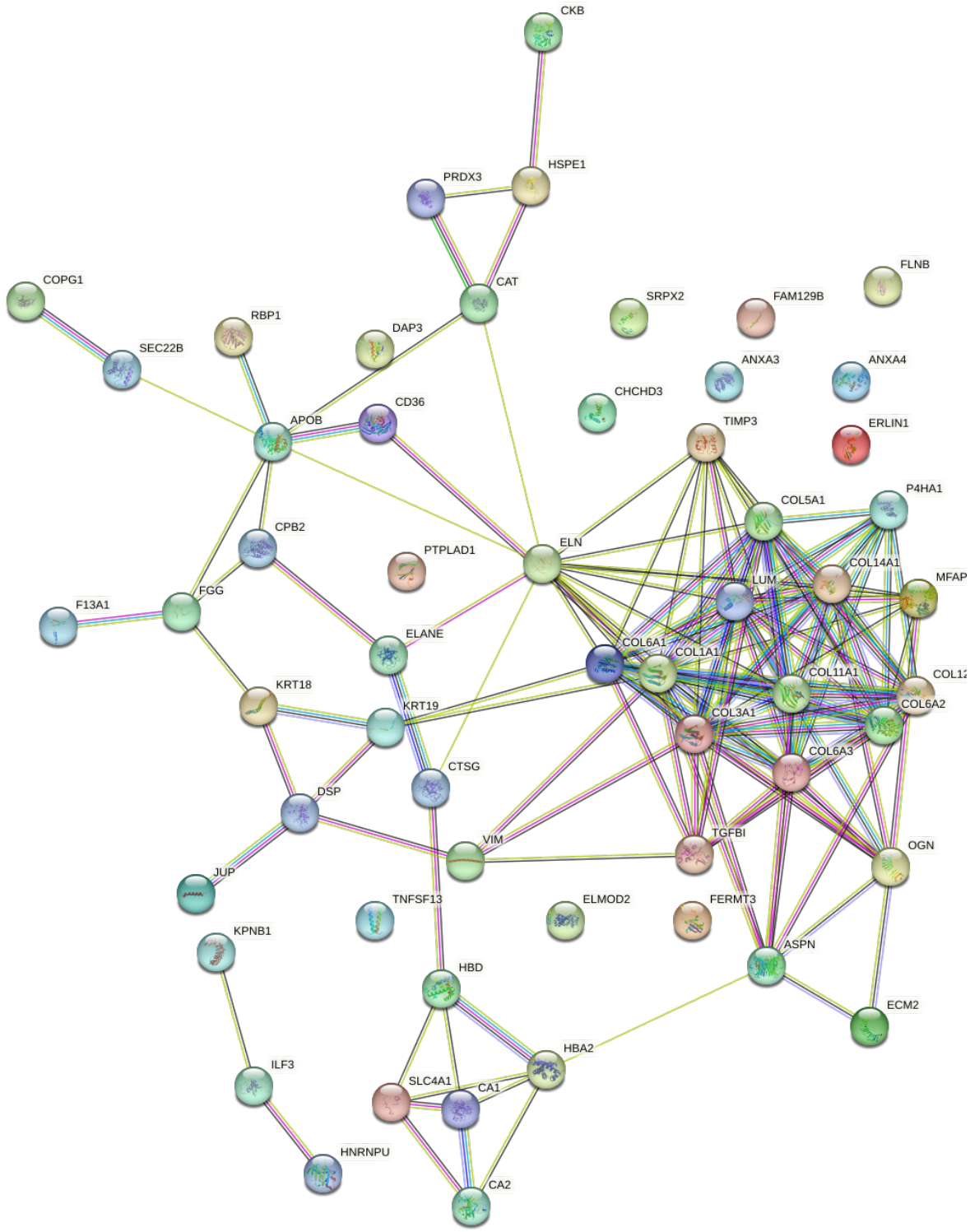
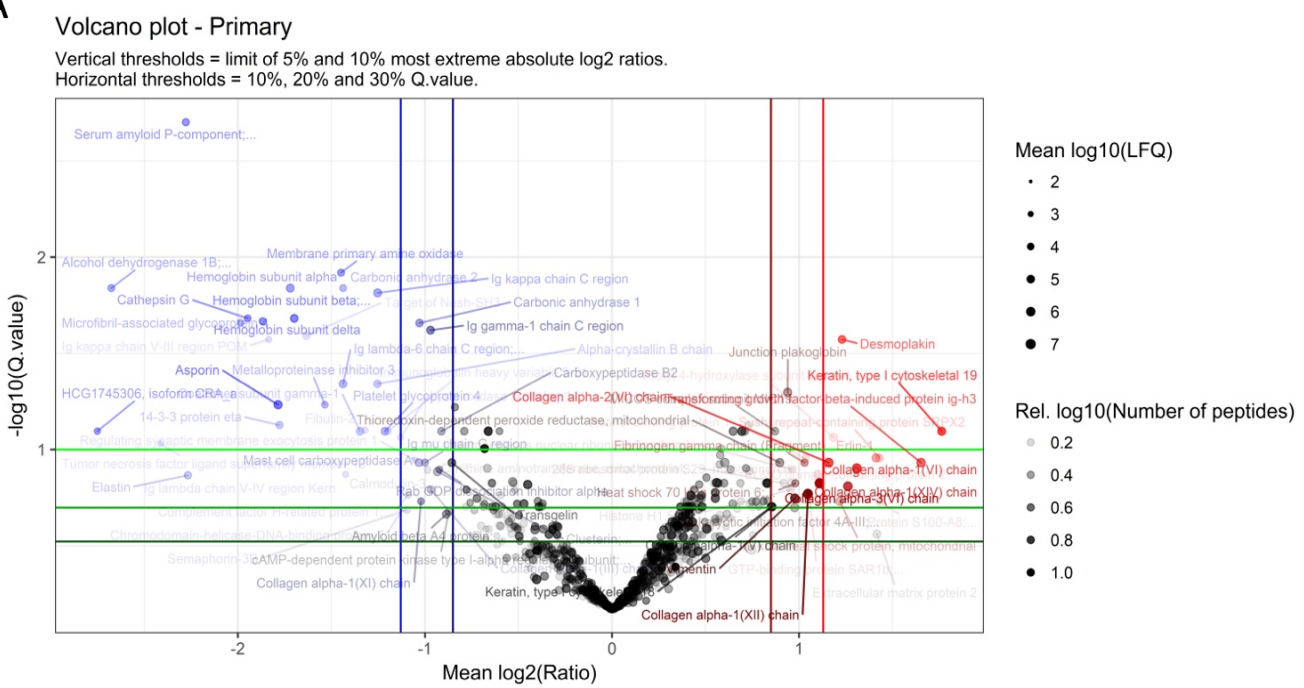


Figure 5.3: Protein-protein interaction map showing the connections between identified upregulated proteins across the sample cohort.

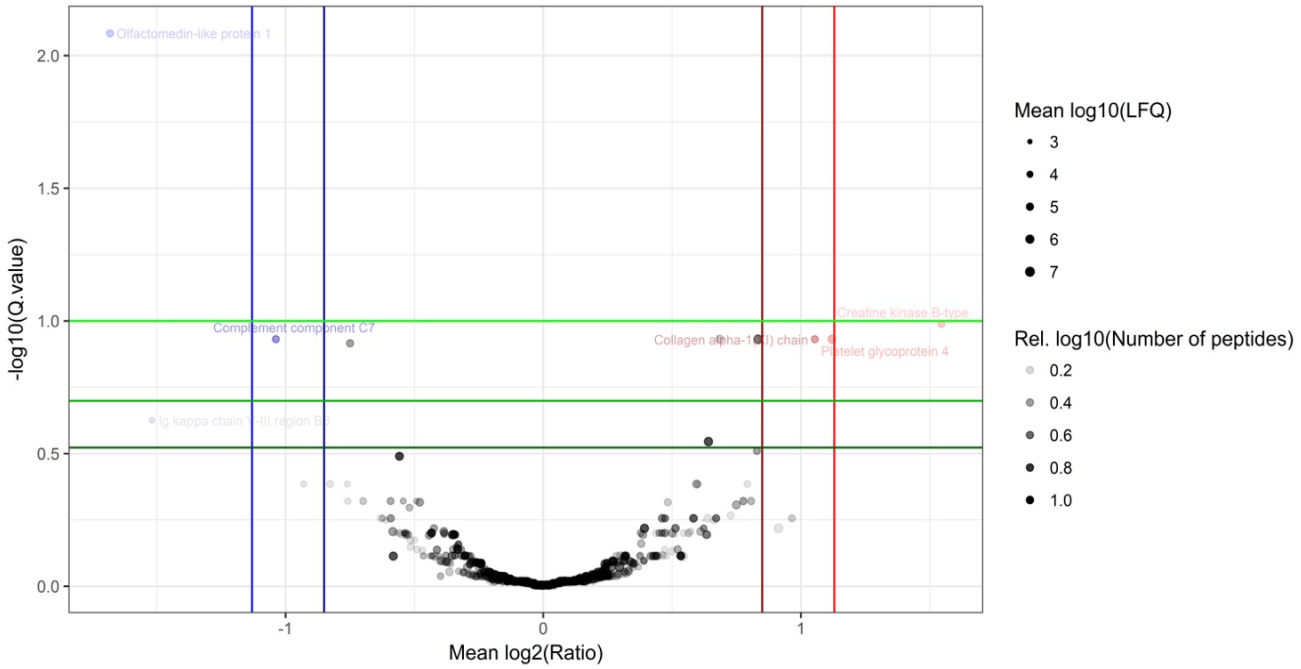
5.3.3 Analysis of variation in ECM composition between different anatomical sites

Volcano plots for represented anatomical sites were created to analyse the relative expressions of ECM proteins in individual tumour locations. There were vast differences in the quantities of proteins identified in different sample sites. The volcano plots below (Figure 5.4) show the mean log2 ratios of proteins at different thresholds, identified in both the primary (A), omentum (B), diaphragm (C), paracolic (D) and spleen (E). There is significant heterogeneity in the numbers of proteins identified across the different sample sites. For example, the primary and splenic samples have much higher numbers of proteins expressed above the log2 ratio threshold than the omentum and paracolic. There is also variation in the specific proteins observed above the thresholds in each location.

A


Volcano plot - Primary
Vertical thresholds = limit of 5% and 10% most extreme absolute log2 ratios.
Horizontal thresholds = 10%, 20% and 30% Q.value.
-log10(Q.value)
Mean log2(Ratio)
Serum amyloid P-component;...
Alcohol dehydrogenase 1B;...
Membrane primary amine oxidase
Hemoglobin subunit alpha
Carbonic anhydrase 2
Ig kappa chain C region
Cathepsin G
Hemoglobin subunit beta;...
Carbonic anhydrase 1
Hemoglobin subunit delta
Ig gamma-1 chain C region
Ig lambda-6 chain C region;...
Alpha-crystallin B chain
Junction plakoglobin
Desmoplakin
Asporin
Metalloproteinase inhibitor 3
Carboxypeptidase B2
Keratin, type I cytoskeletal 19
HCG1745306, isoform CRA_a
Platelet glycoprotein 4
Collagen alpha-2(VI) chain
Transforming growth factor-beta-induced protein ig-h3
14-3-3 protein eta
Thioredoxin-dependent peroxide reductase, mitochondrial
Fibrinogen gamma chain (Fragment)
Erdin-1
Mast cell carboxypeptidase A
Collagen alpha-1(VI) chain
Elastin
Heat shock 70 kDa protein 6
Collagen alpha-1(XIV) chain
Collagen alpha-3(VI) chain
Transgelin
Amyloid-beta A4 protein
cAMP-dependent protein kinase type I-alpha regulatory subunit;...
Tenascin
Collagen alpha-1(XI) chain
Keratin, type I cytoskeletal 18
Collagen alpha-1(XII) chain
Mean log10(LFQ)
2
3
4
5
6
7
Rel. log10(Number of peptides)
0.2
0.4
0.6
0.8
1.0

B


Volcano plot - Omentum
Vertical thresholds = limit of 5% and 10% most extreme absolute log2 ratios.
Horizontal thresholds = 10%, 20% and 30% Q.value.
-log10(Q.value)
Mean log2(Ratio)
Olfactomedin-like protein 1
Creatine kinase B-type
Complement component C7
Collagen alpha-1(XII) chain
Platelet glycoprotein 4
Mean log10(LFQ)
3
4
5
6
7
Rel. log10(Number of peptides)
0.2
0.4
0.6
0.8
1.0

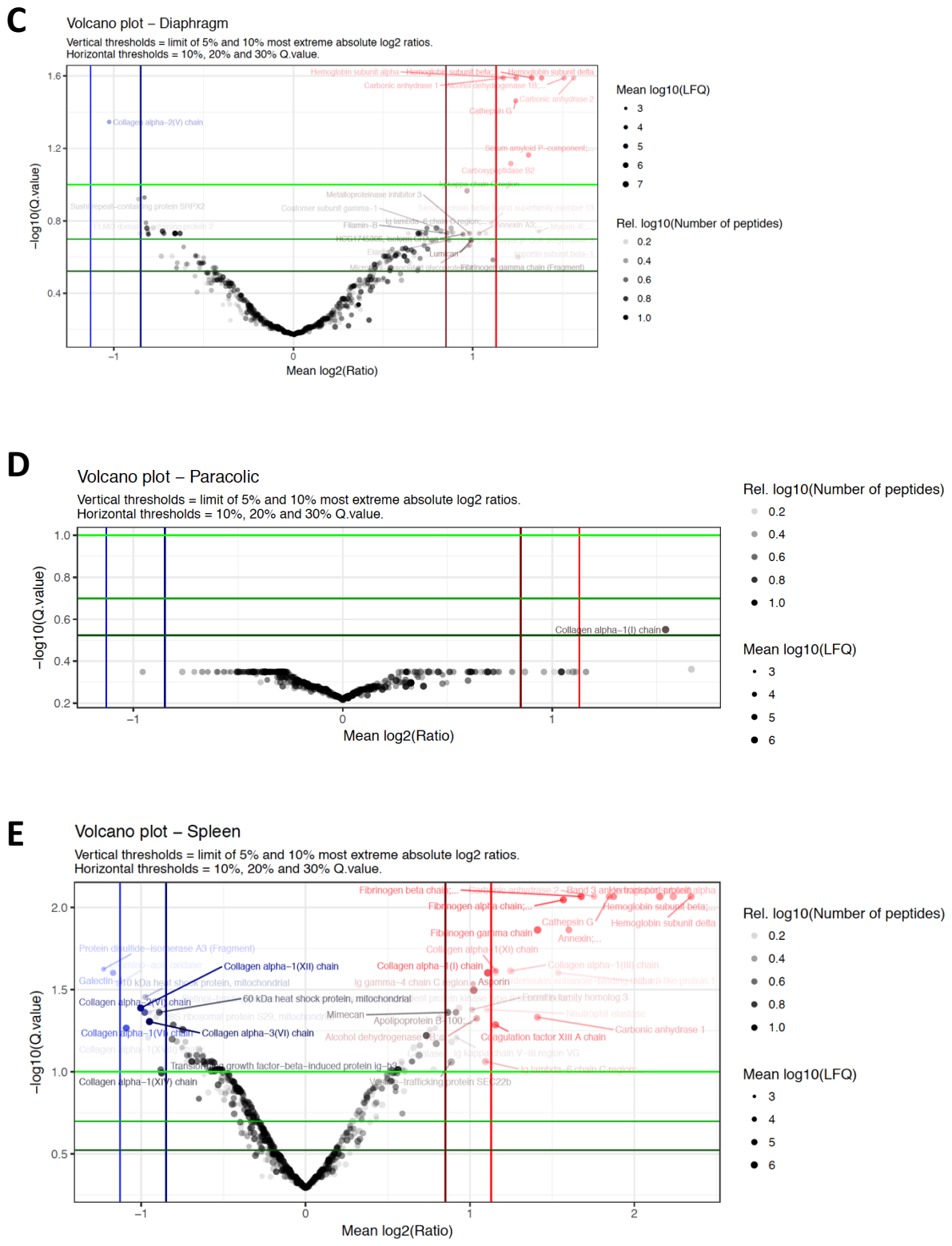
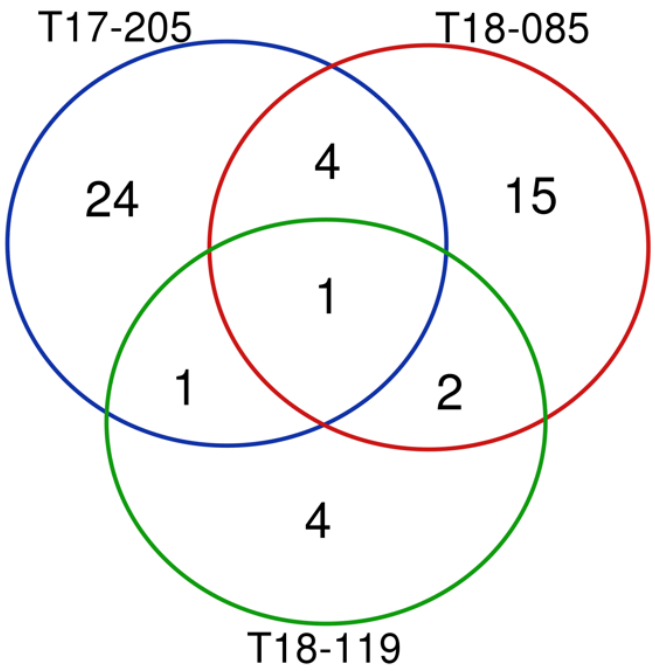


Figure 5.4: Volcano plots. *Volcano plots showing ECM proteins identified by MS analysis, plot A shows proteins found across the primary samples, plot B shows omentum, C shows diaphragm samples, D shows paracolic, E shows splenic samples. Significant variation in the proteins discovered in the different anatomical regions is observed as well as a difference in the quantity of proteins expressed between different tumour sites.*

5.3.4 Primary tumour ECM composition analysis

To observe for any common patterns in ECM protein expression between sample sites, log2 ratio data for each sample was subjected to a cut off limit of 1.3 as applied in other studies[297, 298]. Proteins with higher expression in each sample were identified and comparisons made between the different anatomical locations. In case T16-060 there were no proteins with values above the 1.3 cut-off again showing the variation in protein quantities between samples. Comparing the 3 remaining primary samples there was minimal correlation between the ECM protein composition with only 1 common protein seen across all cases.



Names	total	elements
T17-205 T18-085 T18-119	1	Transforming growth factor-beta-induced protein ig-h3
T17-205 T18-085	4	Vimentin Collagen alpha-1(XIV) chain Collagen alpha-1(V) chain Desmoplakin
T17-205 T18-119	1	Sushi repeat-containing protein SRPX2
T18-085 T18-119	2	10 kDa heat shock protein, mitochondrial Superoxide dismutase [Mn], mitochondrial

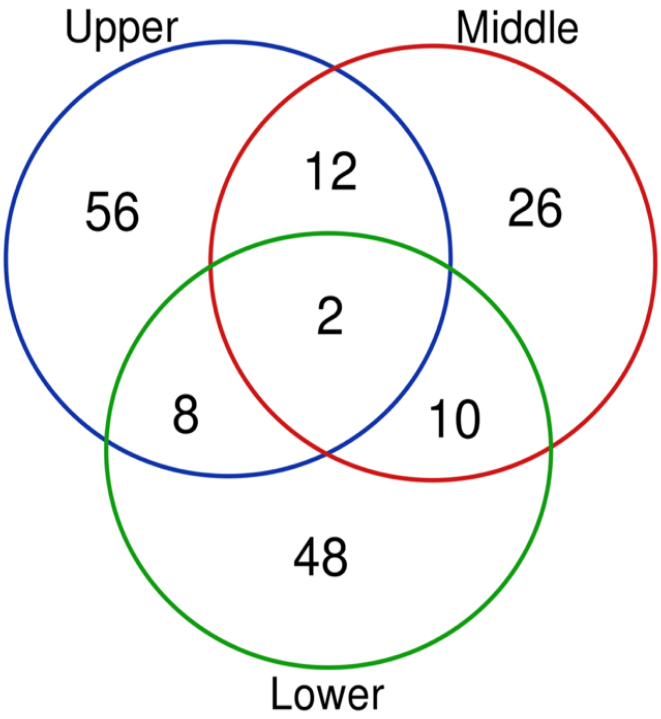
Figure 5.5: Venn Diagram of case crossover. *Venn diagram depicting the crossover observed in ECM composition between different primary samples. Log2 ratios with a cut off of 1.3 were included in the analysis. Case T16-060 did not have any proteins sufficiently expressed above the 1.3 cut off. Only 1 common component was identified across the remaining 3 cases.*

The above Venn diagram (figure 5.5) shows the comparisons between the different primary samples from 3 cases. The one common component observed was transforming growth factor beta induced protein ig-h3 (TGFβI). This cytokine has been reported to be involved in the ECM reaction to tumour cell presence in the early stages of cancer development[202].

Reviewing the expression of TGFβI in our primary samples it was found to be highly expressed in 3 of the cases, negatively in T16-060. The numbers of cases here are too small for correlation with response to treatment or survival outcomes, however with future analysis of ECM composition from a further cohort of patients it may be possible to observe any significance in expression of TGFβI.

5.3.5 Intra-abdominal heterogeneity in ECM composition observed

As we have seen with both the 2D and 3D phenotypic data, HGSOC tumours behave differently depending on their anatomical location within the abdomen. Their microenvironments also vary greatly depending on the metastatic site. The heatmaps show us vast heterogeneity in ECM protein expression across the sample cohort. To assess for any patterns in protein upregulation across the abdominal sites the log2 ratios (with a cut-off of 1.3) for each sample were compared dividing the abdominal cavity into upper, middle and lower regions. With the previous analysis of response to cisplatin in the ITH samples there was variation observed across the abdominal cavity when regions were divided by IMO mapping. Due to the small sample size with the ECM analysis the samples have been further grouped into upper (IMO A3, B3, C3), middle (IMO A2, B2, C2) and lower (IMO A1, B1, C1) regions for comparison to observe for any commonalities which would assist with 3D culture protein 'cocktail' composition.



Names	total	elements
Lower Middle Upper	2	Microfibril-associated glycoprotein 4 Alcohol dehydrogenase 1B;Alcohol dehydrogenase 1A;Alcohol dehydrogenase 1C
Middle Upper	12	Galectin-1 Collagen alpha-1(III) chain Transgelin Vesicle-trafficking protein SEC22b Band 3 anion transport protein Ig kappa chain C region Ig mu chain C region Carbonic anhydrase 1 Mimecan cAMP-dependent protein kinase type I-alpha regulatory subunit;cAMP-dependent protein kinase type I-alpha regulatory subunit, N-terminally processed Collagen alpha-2(IV) chain;Canstatin Collagen alpha-1(I) chain
Lower Upper	8	Serum amyloid P-component;Serum amyloid P-component(1-203) Complement component C9;Complement component C9a;Complement component C9b Lumican Vitronectin;Vitronectin V65 subunit;Vitronectin V10 subunit;Somatomedin-B Sushi repeat-containing protein SRPX Annexin A3;Annexin Metalloproteinase inhibitor 3 Clusterin;Clusterin beta chain;Clusterin alpha chain;Clusterin
Lower Middle	10	Amine oxidase [flavin-containing] B Ig kappa chain V-III region POM Cytochrome c oxidase subunit 5B, mitochondrial Ig kappa chain V-III region B6 Lactadherin;Lactadherin short form;Medin Target of Nesh-SH3 Collagen alpha-2(V) chain Decorin Superoxide dismutase [Mn], mitochondrial L-amino-acid oxidase

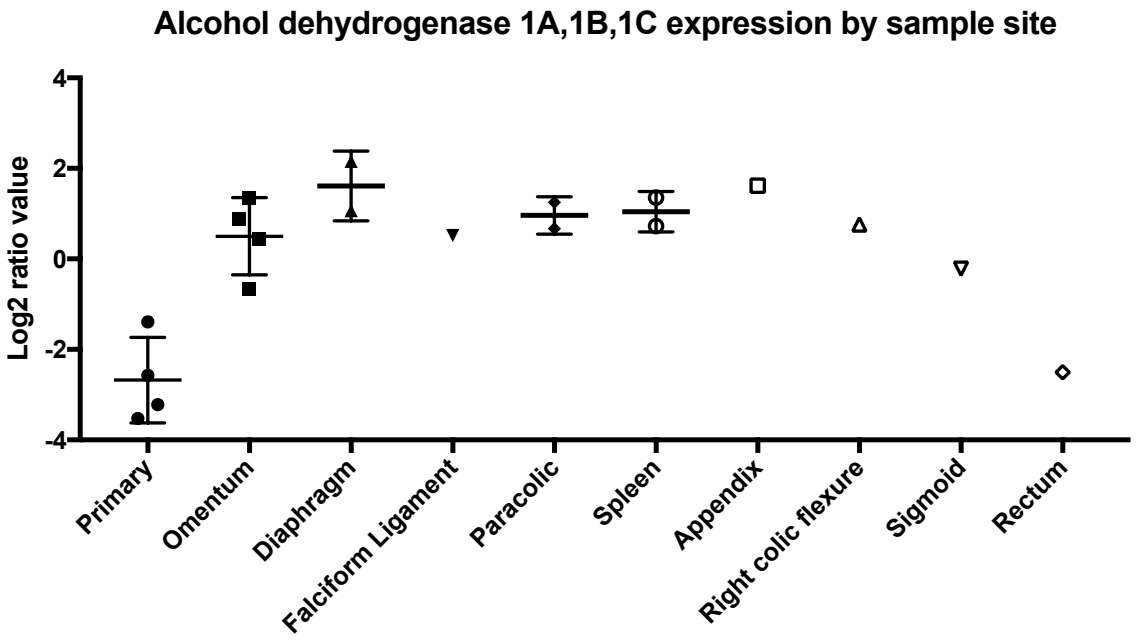
Figure 5.6: Crossover in ECM proteins by abdominal region. *Venn diagram showing the cross over in ECM proteins observed between the upper, middle and lower abdominal regions. Vast variation is seen with only 2 proteins observed to be present in all areas with log2ratio cut-off of 1.3.*

Once again, there are limited ECM components crossing all cases and areas. Only 2 are upregulated in all abdominal regions. Class 1 alcohol dehydrogenases (ADH 1) are a group of enzymes encoded by the gene ADH-1, mainly found intracellularly which are involved in the metabolism of ethanol. Increased expression of ADH-1 genes have been linked to initiation of tumourigenesis in multiple cancers, in part due to the accumulation of acetaldehyde during ethanol metabolism[299].

When expression levels of the class 1 ADH isoenzymes was assessed in our samples separately, across individual anatomical locations, there was significant variation in the mean log2 ratios

between sites (p= 0.02, fig 5.7 A). Particularly, the primary samples had consistently low expression of ADH compared with e.g. the omentum and diaphragm samples. This again demonstrates the difficulties encountered with HGSOC in the heterogeneity observed. If biomarkers are only present in certain tumour microenvironments within the disseminated disease then testing with single site biopsies, ahead of for example surgical planning, may not give an accurate and reliable method of prediction of resectability. The sample biopsied may differ greatly from the primary or other metastatic sites. To examine this further and because some sample sites have only 1 sample in the cohort, the samples were grouped into protein expression levels by abdominal region (figure 5.7 B). This showed significant variation in protein levels with the lower abdominal samples showing significant downregulation compared to both the middle and upper abdominal regions. Examination of ADH 1A, 1B, 1C by case showed variation in expression levels between different sample sites in each case. No significant difference in overall expression was seen between the cases and no relation to surgical outcome was apparent.

A



B

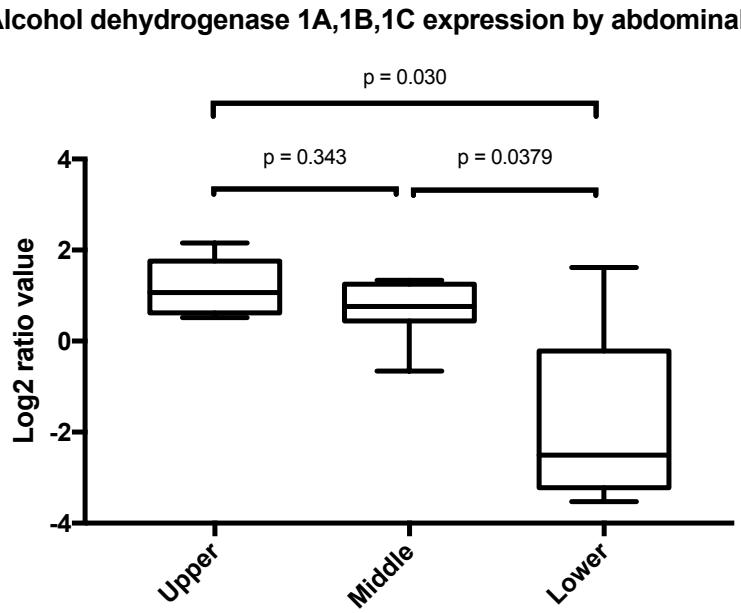


Figure 5.7: Analysis of ADH 1A, 1B, 1C expression. *A - Scatter plot showing log2 ratios of Alcohol dehydrogenase 1A, 1B and 1C across the sample cohort showing variation in expression between different anatomical locations. Significant differences in mean values per sample were observed by Kruskal-Wallis test (p= 0.02). B – Box and whiskers plot of log2 ratios organised by intra-abdominal region showing significant down regulation in the lower abdominal region compared to both the middle (p=0.0379) and upper (p=0.0343) regions using Mann-Whitney test.*

In the Venn diagram comparing the different abdominal areas (figure 5.6) the other common ECM protein observed is microfibril-associated glycoprotein 4 (MFAP4). MFAP4 is an ECM protein produced by vascular smooth muscle cells and belongs to the fibrinogen family. Microfibrils help provide structural integrity in elastic tissues[300].

As can be seen in figure 5.8 graph A below, in our cohort, there was variation in the levels of MFAP 4 seen between different samples however there was no significant difference in the mean log2 ratios by sample site or when grouped into anatomical regions, figure 5.10 graph B.

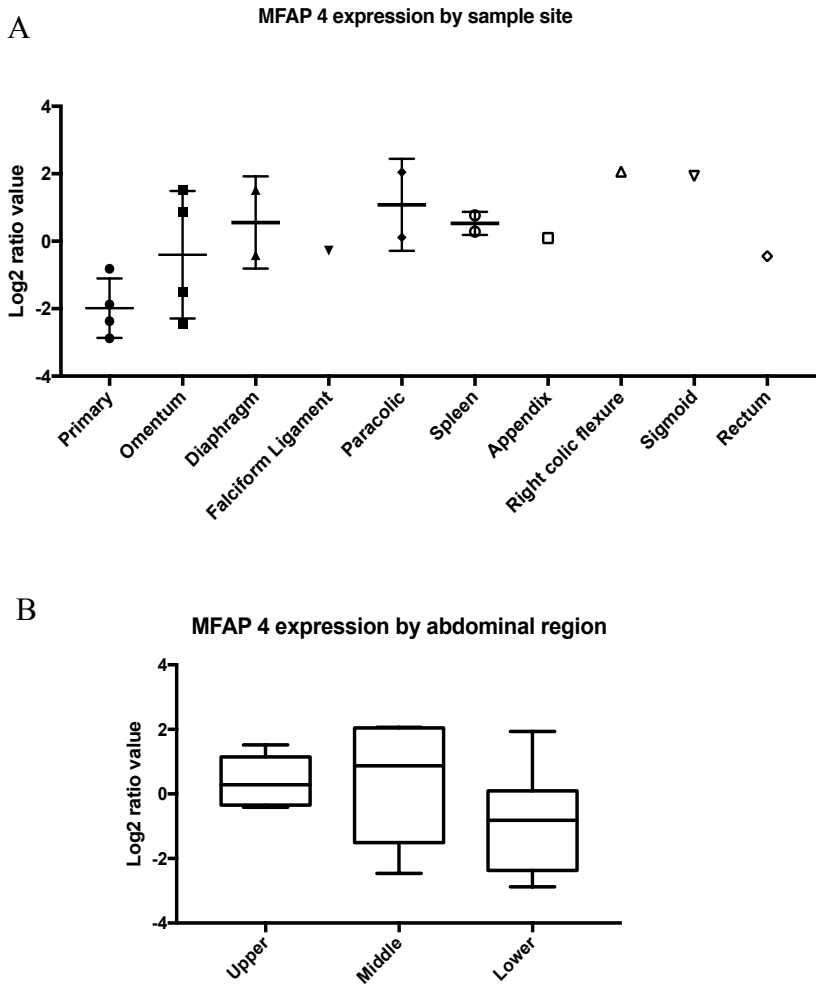


Figure 5.8: Analysis of MFAP4 expression. *A: Scatter plot showing variation in MFAP 4 ECM protein expression by sample site, no significant difference in mean expression values was found between samples. B: Box and whiskers plot showing MFAP4 expression by abdominal region. No significant difference in mean expression values between abdominal areas was found.*

5.4 Examination of ECM proteins of interest

With the increasing recognition of the importance of the involvement of the ECM composition in tumourigenesis, progression and metastasis, different groups have aimed to optimise techniques to examine it further. The Balkwill group have promoted the importance of the ECM components for both their contribution to normal homeostasis and the crucial impact their dysregulation has in the cancer setting and have progressed methods for isolation and examination of the ECM[301]. Collaborations with the MIT based Hynes group and Dr Naba have produced The MatrisomeBD database to provide reference data of common ECM proteins recognised by tissue type for comparison, amongst many other databases[190, 302, 303].

Collagens make up around 30% of the human protein content with 28 different collagens identified so far[304]. Collagens are the most populous ECM component and are responsible for changes in the architecture of the microenvironment and increase in fibrosis[305]. Remodelling of the ECM during tumourigenesis results in dysregulation of the collagen components present. Alterations in collagen composition within the ECM have been suggested to correlate with chemotherapy resistance and patient outcome in HGSOC[306].

Analysis using the MatrisomeBD database of collagens known to be present in human ovarian cancer ECM metastasis show the following relative expressions:

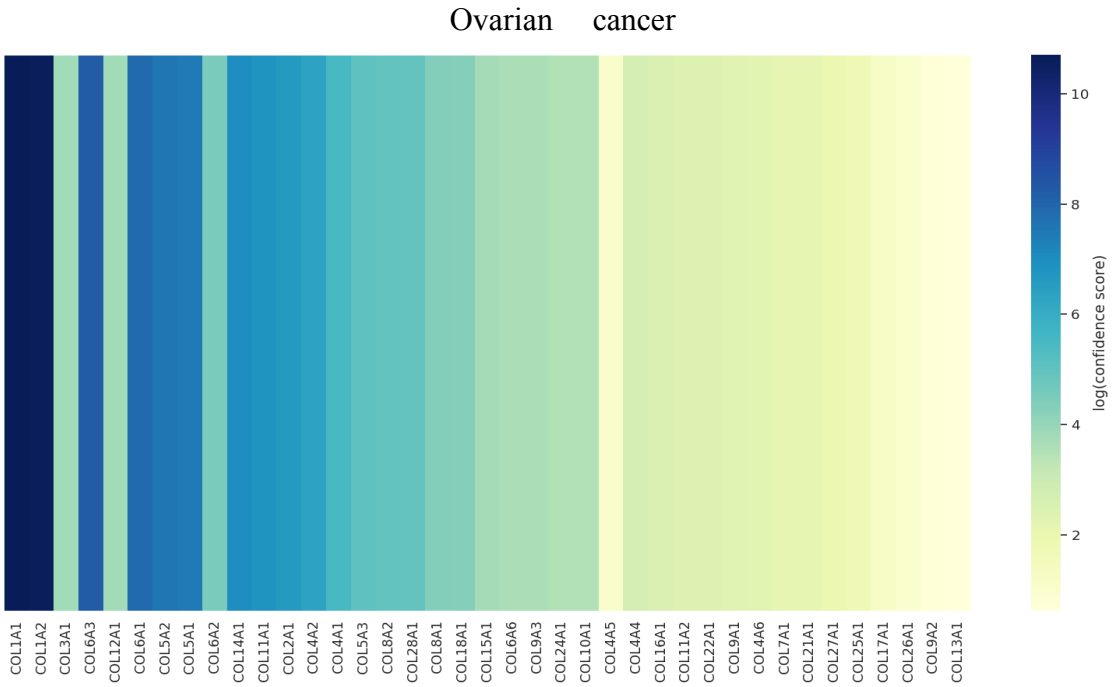


Figure 5.9: MatrisomeBD data identified collagens in ovarian cancer metastatic sites*[303]. Spectrum of collagen proportions identified in HGSOC omental metastatic deposits, compiled for public reference on the MatrisomeBD database.*

As expected, different alpha chains of Collagen I are the most abundant with IV and VI also highly expressed. Using this information and the aims to create a culture system for therapeutic testing involving ECM components representative of the *in vivo* setting, the collagen composition of our sample cohort was further examined.

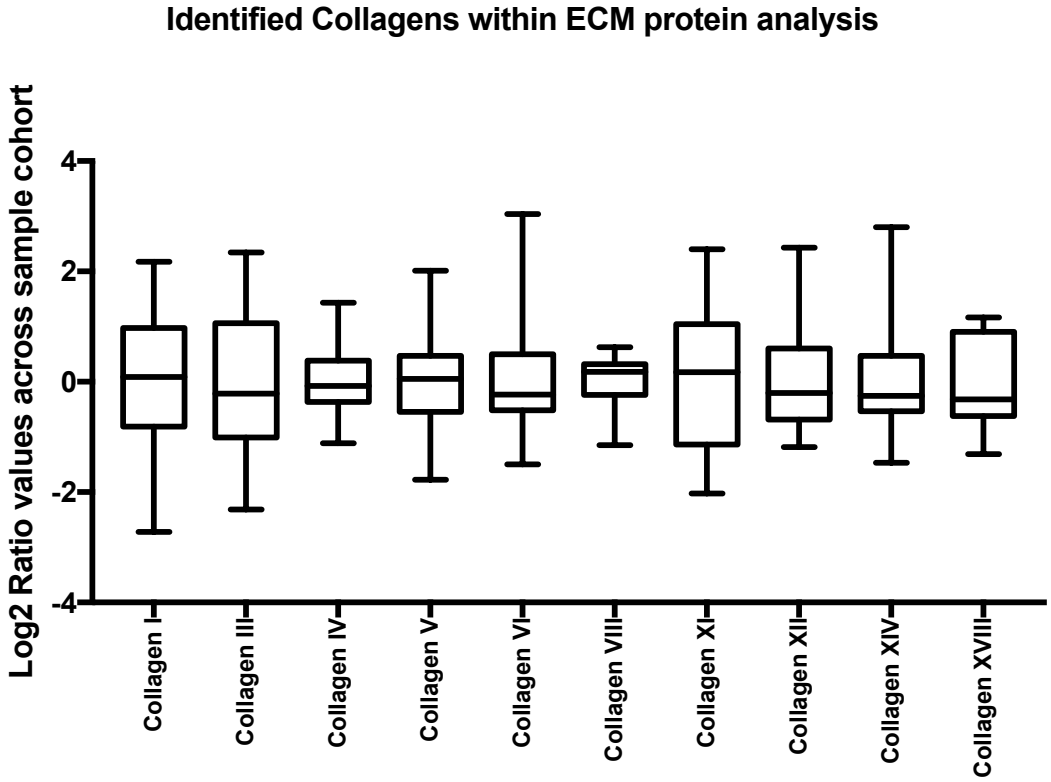


Figure 5.10: ECM Collagen composition analysis. *Box and whiskers plot showing the identified collagens within the ECM MS analysis across the sample cohort.*

The collagens discovered within our 20 samples show variation in their abundance based on log2 ratios (figure 5.10). Collagen I is present as expected, as well as III, IV, V, VI, VIII, XI, XII, XIV and XVIII. There is heterogeneity between values in each patient plus differences in the amount of heterogeneity seen for each collagen type. For example, Collagen VI shows much more variation in the min-max range compared to collagen VIII. Different α chains of each collagen were seen in the ECM protein composition, these α chain values were plotted separately in the analysis, however the expression levels of individual α chains showed minimal variation within each collagen identified.

5.4.1 Collagen I

Individual collagens of interest were studied based on the findings from the MatrisomeDB database. Collagen I showed significant variation in relative values between different anatomical sites (Kruskal-Wallis analysis p= 0.0069). There were more numbers of primary and omentum samples within the cohort which may account for the variation in collagen I levels seen in these sites (figure 5.11 A). When examined by individual case there was again variation observed within the samples in each patient (figure 5.11 graph B) with some samples showing increased expression and decreased expression within individual patients. No case had a significantly different Collagen I composition compared to others. As explained above, different α chains of Collagen I were detected in the MS analysis (α1 and α2), these subunits have been plotted as individual points in the graphs below. Both α chains in each sample site had the same expression profile i.e they always both either showed high or low expression.

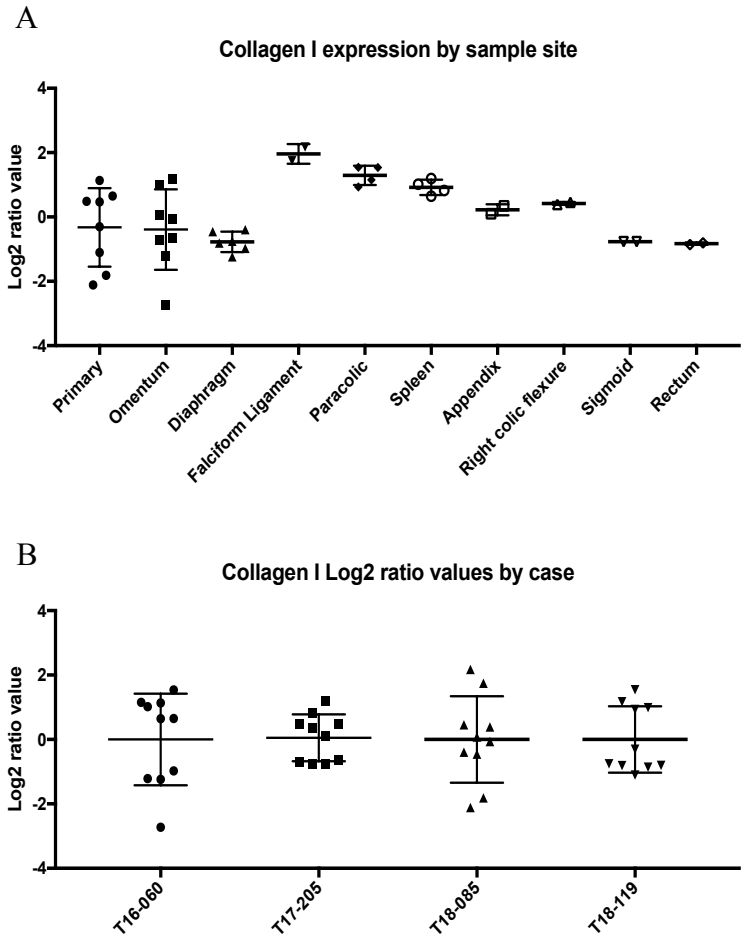


Figure 5.11: Collagen I expression analysis. *Scatter plots showing Collagen I abundance in sample cohort. A - shows variation observed between different anatomical locations, with significant difference observed between sample sites (Kruskal-Wallis test p=0.0069) B - shows variation within individual patient cases with no significant difference in overall expression levels seen.*

5.4.2 Collagen IV

Type IV Collagen is the major component in basement membranes and in combination with laminins has been shown to be involved in cell adhesion, differentiation and migration[307]. The degradation of basement membranes in tumourigenesis via matrix metalloproteinase pathways contributes to increased tumour cell invasion.

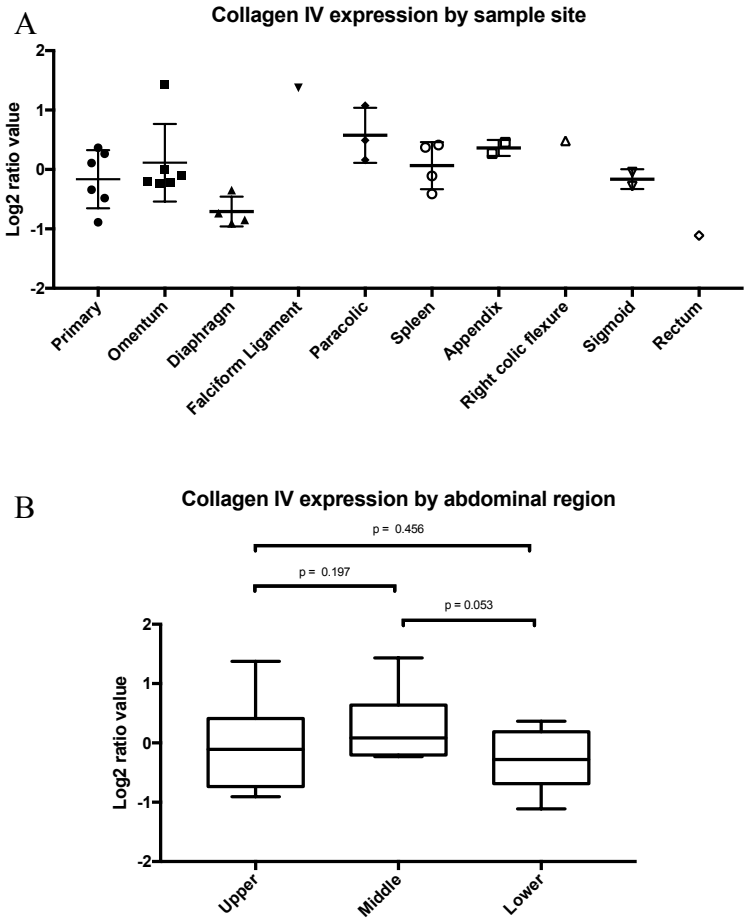


Figure 5.12: Collagen IV expression analysis. *A shows a scatter plot of collagen IV values by sample site. Significant variation in the means across the anatomical areas was observed (Kruskal-Wallis analysis p= 0.001). B shows box and whiskers plot of collagen IV variation by abdominal region, with the difference between the middle and lower abdominal areas approaching significance (Mann-Whitney test p=0.053).*

This is a small sample cohort with only 1 sample in some anatomical areas. Nevertheless, we do see significant differences in the relative expression of collagen IV between anatomical sites (figure 5.12 A). However, the variation between the expression levels between the middle and lower abdominal areas is not statistically significant (figure 5.12 B). All our patients were HGSOC and all advanced stage with widespread dissemination of disease. No significant difference in collagen IV values was observed between the different cases.

5.4.3 Collagen VI

Collagen VI has been proposed as a potential biomarker for different cancers. Within the ECM it has multiple responsibilities, contributing to signalling pathways for apoptotic cell death, proliferation and inflammation[308]. Collagen VI has been found to be overexpressed in multiple cancer types and has been linked to promoting resistance to platinum therapy in ovarian cancer due to its influence on tumour microenvironment remodelling [306].

In our sample cohort, there was less variation seen in distribution compared to Collagen I and IV (figure 5.13 A) with only some heterogeneity within the primary samples. Collagen VI $\alpha 1$, $\alpha 2$ and $\alpha 3$ chains were detected in the protein analysis. The expression levels of each subunit chain were plotted separately with no variation in expression seen between different chains. With this analysis, it does not appear that Collagen VI is overexpressed in the samples though there is more consistency seen than in the other collagens. On closer examination given the apparent outliers in the primary group it appears that these higher expression levels all fall in case T17-205 (figure 5.13 B). By breaking down the analysis in T17-205 down by sample, it can be seen that the primary sample has much higher expression than the other samples (figure 5.13 C) with a significant difference observed between the primary and other sample sites (Kruskal-Wallis test $p= 0.0005$). No correlation could be seen between collagen log2 ratios and phenotypic apoptotic response in the T17-205 samples.

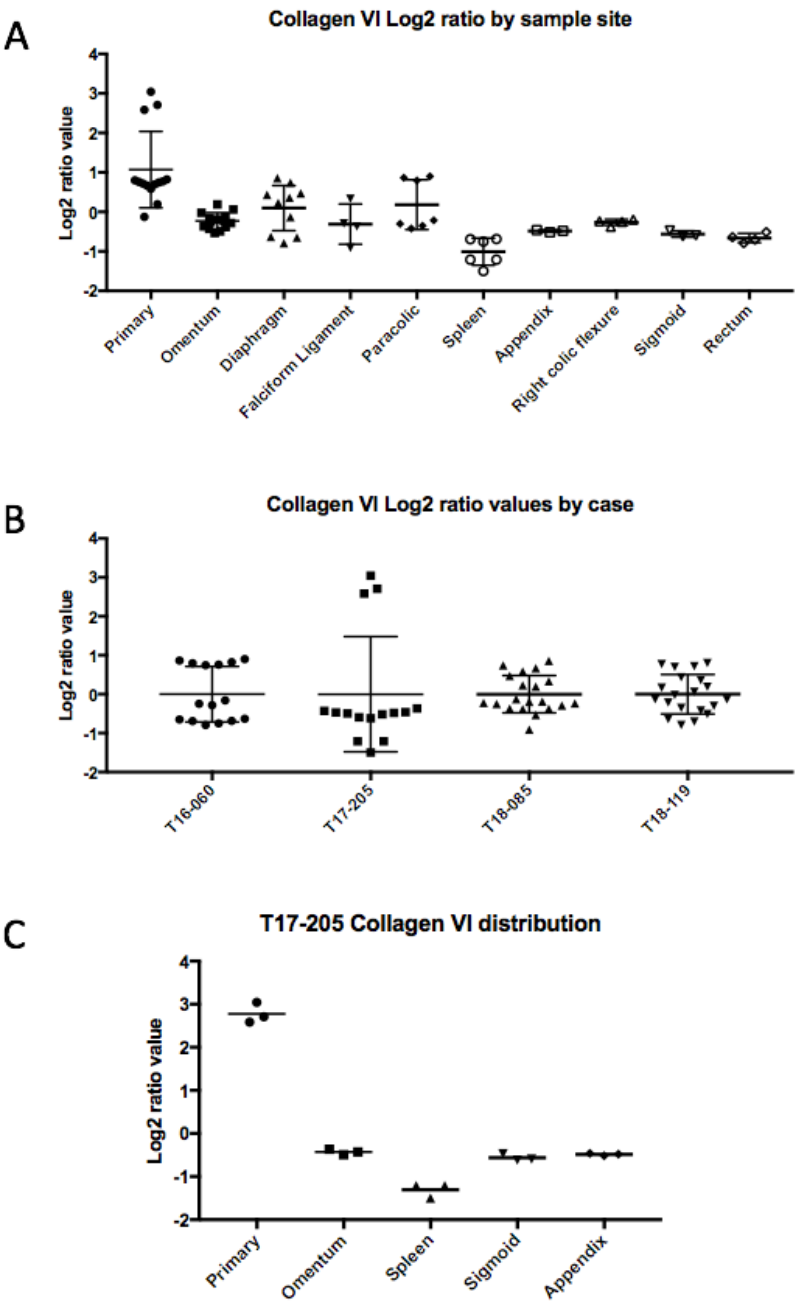


Figure 5.13: Collagen VI expression analysis. *Scatter plots showing Collagen VI distribution displayed by individual sample site (A), by case (B) and further analysis of values within case T17-205 (C) showing the over expression observed in the primary sample which was significantly higher than the other sample sites (Kruskal-Wallis p=0.0005)*

A separate analysis of the relative expression of fibronectin in the MS data was performed for comparison with the observation from Kenny et. al who discovered that fibronectin expression was significantly higher in HGSOC omental metastatic deposits than in matched primary samples. Further examination suggested that mesothelial cell secretion of fibronectin at metastatic sites promoted adhesion, invasion and proliferation of HGSOC cells[309].

In this study fibronectin expression varied across the sample sites examined though all sites showed relatively low expression levels. Analysis of the primary versus omental sample expression did appear to show higher levels in the omentum samples however this was not statistically significant (Mann-Whitney test p=0.114). Grouping the samples by abdominal region however did show significant variation between the regions (Kruskal-Wallis test p=0.0216) with further analysis showing significant variation in expression between the lower region and middle region (Mann-Whitney test p=0.0221. Sample numbers here are low but with a further cohort expected to be examined following this pilot study, it will be interesting to observe for potential trends in fibronectin expression related to response to treatment and patient outcomes.

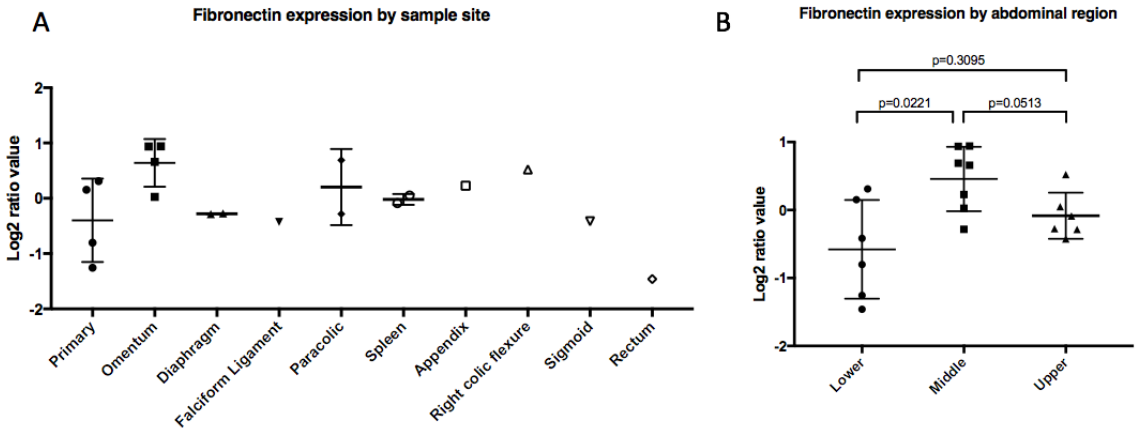


Figure 5.14: Fibronectin expression analysis. *A- scatter plot showing fibronectin expression across different sample sites, no significant difference was observed between expression levels across the locations (one-way Anova test p=0.1710). Omental samples appear to have higher expression than primary samples but this was not statistically significant (Mann-Whitney test p=0.114). B – expression levels grouped by anatomical region. Significant variation in expression of fibronectin was seen comparing all regions (Kruskal-Wallis test p=0.0216) and specifically comparing lower region and middle (Mann-Whitney test p=0.0221)*

5.5 Discussion

The ECM MS protein analysis performed in this project has shown that despite a limited sample size, there is huge variation in ECM protein expression both between cases and between anatomical location. There are also differences in the quantity of ECM proteins found in different metastatic sites. The goal for finding a common combination for use in cultures is therefore more difficult. However, this is a very small pilot sample group with only a maximum of 4 repetitions for sample site. The lead hits that have been identified in this analysis have recognised links to ovarian cancer, disease progression and response to treatment and there is potential for biomarker discovery and validation in larger cohort analysis. The collagens observed are similar to those seen in recognised databases however again a broad range of expression was observed for collagen I and IV.

These findings add to the problem HGSOC confers in the search for reproducible biomarkers and therapeutic targets. The heterogeneity present means that findings specific to certain anatomical locations may not be further observed when metastatic sites are examined. In the case of Collagen VI in T17-205 this was much more highly expressed in the primary sample than in the other sample sites. Further study of collagen VI and fibronectin expression in a higher number of cases will be of interest to observe for trends in relation to response to treatment and patient outcome.

Chapter 6

Results: Development of *ex vivo* tumour slice culture models

6 Results: Development of *ex vivo* tumour slice culture models

6.1 Introduction

2D culture systems, whilst being efficient, have many limitations including the failure to capture the complexities of the tumour microenvironment[310]. Using primary tumour cell cultures over immortalised cell lines has the benefit of better reflecting the individual patient response to treatment, however still lacks the essential elements of the *in vivo* setting.

Many different 3D culture systems have been studied in the search for reliable, reproducible and where possible, high throughput designs[228], that can best represent the *in vivo* background.

To encapsulate more of the tumour microenvironment, *ex vivo* tumour slice cultures have been developed for a range of cancers[263]. These involve taking thin slice segments across tumour tissue extracted most commonly at the time of surgery. The benefit of slice cultures is the ability to mimic the complex tumour tissue which is difficult to achieve with cellular based 3D cultures. They can also be obtained with little injury to the tumour tissue, helping to retain the original tissue functions, unlike with cellular dissociation processes which may alter cell phenotypic behaviour. Originally, brain tissue was used for obtaining tumour slices and the use of this method of culture has now expanded to multiple cancers and for different purposes[311]. The development of the vibrating blade microtome or vibratome has greatly assisted with the ability to achieve accurate slices with minimal damage to tumour tissue and therefore able to deliver multiple slices in a quick timeframe. The use of *ex vivo* tumour tissue slices in HGSOC has not been extensively examined.

6.2 HGSOC *Ex vivo* tissue slice study outline

For the purposes of our study we wished to take the 3D cultures a step further by incorporating more elements of the tumour microenvironment for patients with HGSOC with a view to providing a more clinically relevant model to demonstrate drug treatment responses. The aim was to optimise the slicing techniques for tumour tissues from around the abdominal cavity to assess for heterogeneity in response to treatment. Following culture and drug treatment the slices would be formalin fixed, paraffin embedded and assessed using immunohistochemistry for tissue architecture, confirmation of tumour cellularity, proliferation levels and apoptosis levels. Following examination of these readouts would determine this as a viable drug testing tool for both primary tumours and metastatic sites in HGSOC.

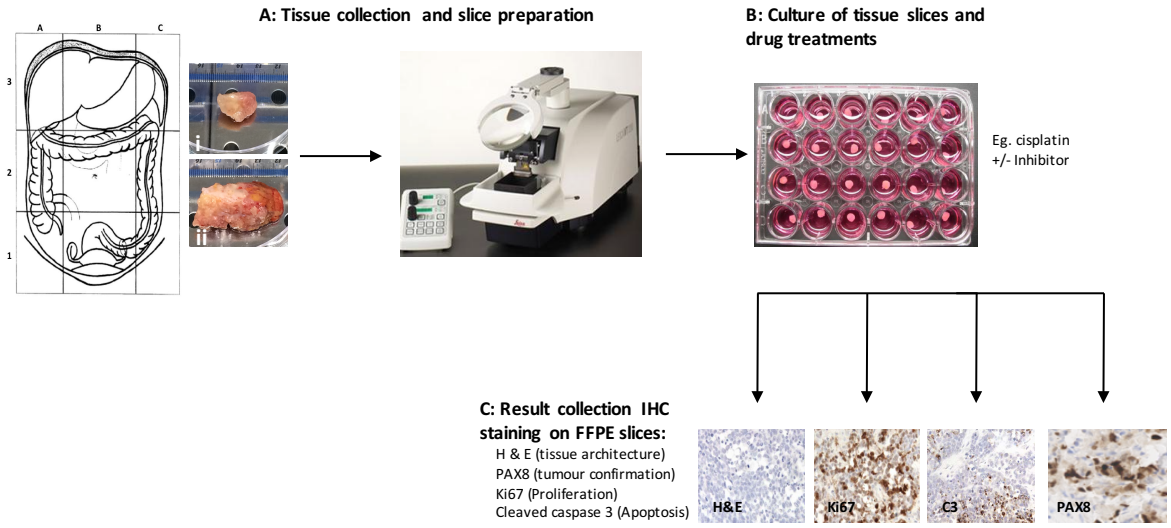


Figure 6.1: Ex vivo slice culture study flowchart. *A shows collection of tumour tissues assessed by IMO mapping tool, followed by slicing by vibratome then B: culture in multi-well plates 6 well plate with membrane inserts for drug treatment ahead of C: Immunohistochemistry staining of FFPE slices.*

6.3 Optimisation of vibratome techniques

Tumour samples were obtained as per the ITH study protocol using the IMO and brought to the lab for processing. Where larger tumours were present, these sites were selected for use for slice cultures. A Leica 1200s vibratome was used with a diamond blade. Tumours were cut with a scalpel to approximately 1cm cube pieces and then adhered to the vibratome cutting base with superglue. Cold RPMI culture media including antibodies (penicillin/streptomycin) was placed around the sample and then the vibratome was used to cut 350μm slices across the tissue. Initial experiments discovered that the ability to achieve optimal slices from the tumours was very variable, depending on the tumour site and consistency. Though most of the time the tumours appeared fibrous and stiff in consistency, when under the pressure of the vibratome blade, they would tend to collapse and the structure could lose its form rather than be cut through cleanly. Some samples were not suitable for direct slicing from the outset, the primary tumours were often softer and not firm enough for dissection. Others were too small and priority was given to the other aspects of the ITH project at that time, for example snap-freezing for genomic characterisation.

The omentum was often the largest sample obtained and the structure of the 'omental cake', which is frequently described in HGSOC dissemination patterns, meant it was a firmer tissue for slicing. A Diamond blade microtome knife was acquired to aide with the precision cutting for less injury to the slices.

As many slices as possible were taken from each sample per patient and placed into culture using 6 well plates with transwell inserts and the same primary culture media as in the ITH and 3D organotypic model experiments. These were then cultured short term initially for 24 hours, and drug treated with cisplatin 25 μM for further 24 hours. Following treatment, the slices were formalin fixed and paraffin embedded.

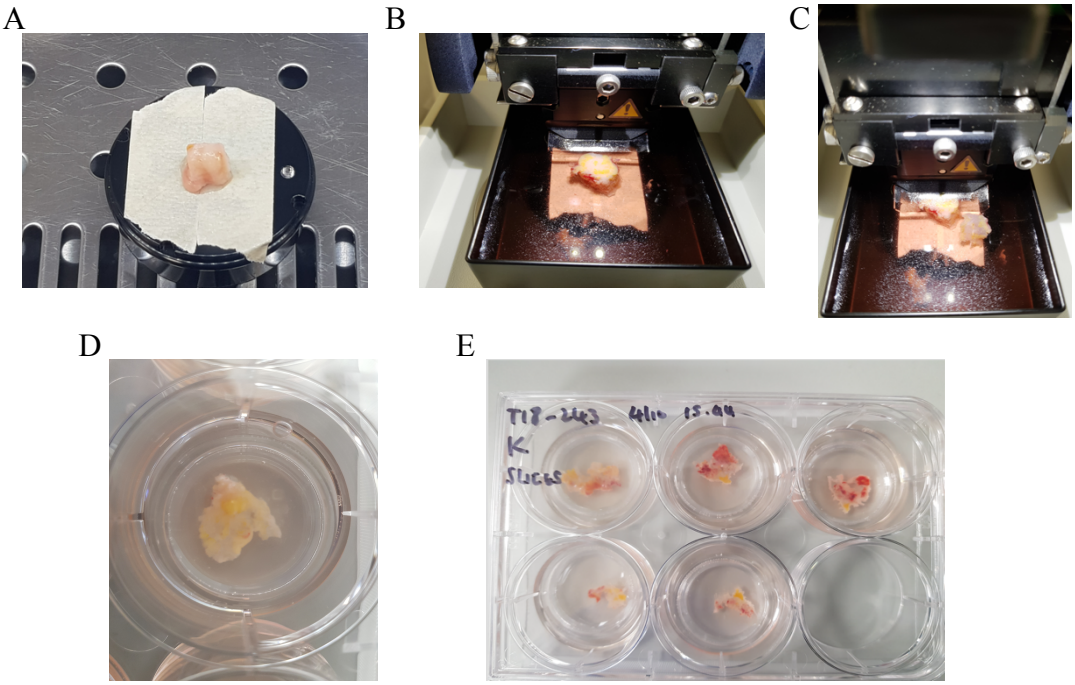


Figure 6.2: Images of tumour slice sample preparation. *Tumour samples were prepared for vibratome sectioning by dividing into approx. 1cm pieces (A) and glued to the cutting platform of the vibratome before being positioned on the vibratome main body (B). Slices were taken (C) at 350 µm and then placed in 6 well plates with transwell inserts (D, E).*

6.4 Confirmation of tissue slice architecture

Following embedding, the tissue slices were sectioned on a microtome at 5μm then mounted on slides. During initial optimisation immunohistochemistry staining was performed for haematoxylin and eosin (H&E) confirmation of tissue architecture. As seen in figure 6.3, H&E staining showed maintained tumour structure and highlighted the differences of tissue type by anatomical location. Figure 6.3, picture A shows a slice of omentum taken at 10x magnification with characteristic adipocytes seen, image B was from a liver metastatic deposit. Liver metastases in HGSOC more commonly occur in the peritoneal liver capsule lining however this was a solid tumour excised from the liver surface. Both examples below were from tissue slices cultured for 24 hours which had not been treated with cisplatin.

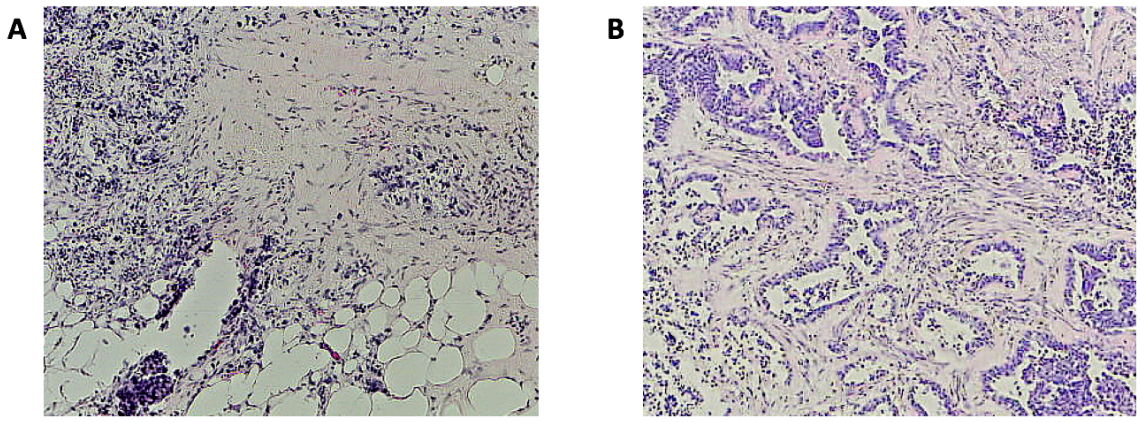


Figure 6.3: Brightfield images of H&E stained ex vivo tumour tissue slices. *Images taken at 10x magnification. Image A shows omentum tissue slice from case T18-243, image B shows liver metastasis slice from case T19-023.*

6.5 Immunohistochemistry read-outs for omental *ex vivo* tumour tissue slices

To characterise the tissue slice culture systems further, immunohistochemistry (IHC) was performed using serial sections from each sample, to determine the optimal read-out for tumour cellularity and drug response. To confirm presence of tumour content in the slices, PAX8 staining was used. PAX8 is a transcription factor known to be frequently expressed in ovarian cancers[312] and is a commonly used staining method to confirm cancer presence and type. Ki67, a nuclear protein which is linked to the cell cycle and known to be associated with tumour growth and, in some cancers prognosis, was used to assess for levels of proliferation within the tumour slices[313]. As these slices were also undergoing drug treatment with cisplatin, as a method of assessing apoptotic response, cleaved caspase 3 was used. Caspase activation is a known indicator of apoptotic activity and has been shown to be a reliable immunohistochemical marker[314]. The embedded slices were processed and stained by the Section of Pathology, Department of Metabolism, Digestion and Reproduction, at Charing Cross Hospital. They were serial sectioned, mounted onto slides and then stained as per protocols in materials and methods. Control samples were used for each antibody. Whole slide scans were taken with a NanoZoomer 2.0-HT (Hamamatsu, Shizuoka, Japan) slide scanner then the images were processed in NDPview.2 software.

6.5.1 Assessment of slice tissue viability over different culture periods

To assess optimum culture protocols, different lengths of culture times were analysed for the tissue slices. IHC was performed as above to observe for maintenance of tumour tissue structure, proliferation levels and signs of apoptosis. Figure 6.4 shows tissue slices from sample G from case T19-023 which was a liver metastases. The images are from day 1 culture (A-D) and from day 4 culture (E-H). Main images are taken at 10x magnification, inserts at 40x. Images A and E show H&E staining confirming tissue structure has been preserved at both time points. B and F show PAX8 positive staining to confirm the site of tumour cell content. C and G show Ki67 staining which interestingly at both time points has limited staining. As seen in the ITH study Ki67 positivity in HGSOC can be very variable and it may be that this

sample was an example of the lower scoring tissues. Images D and H show cleaved caspase 3 staining which is reassuringly minimal at day 1 culture, reflecting lack of apoptotic activity.

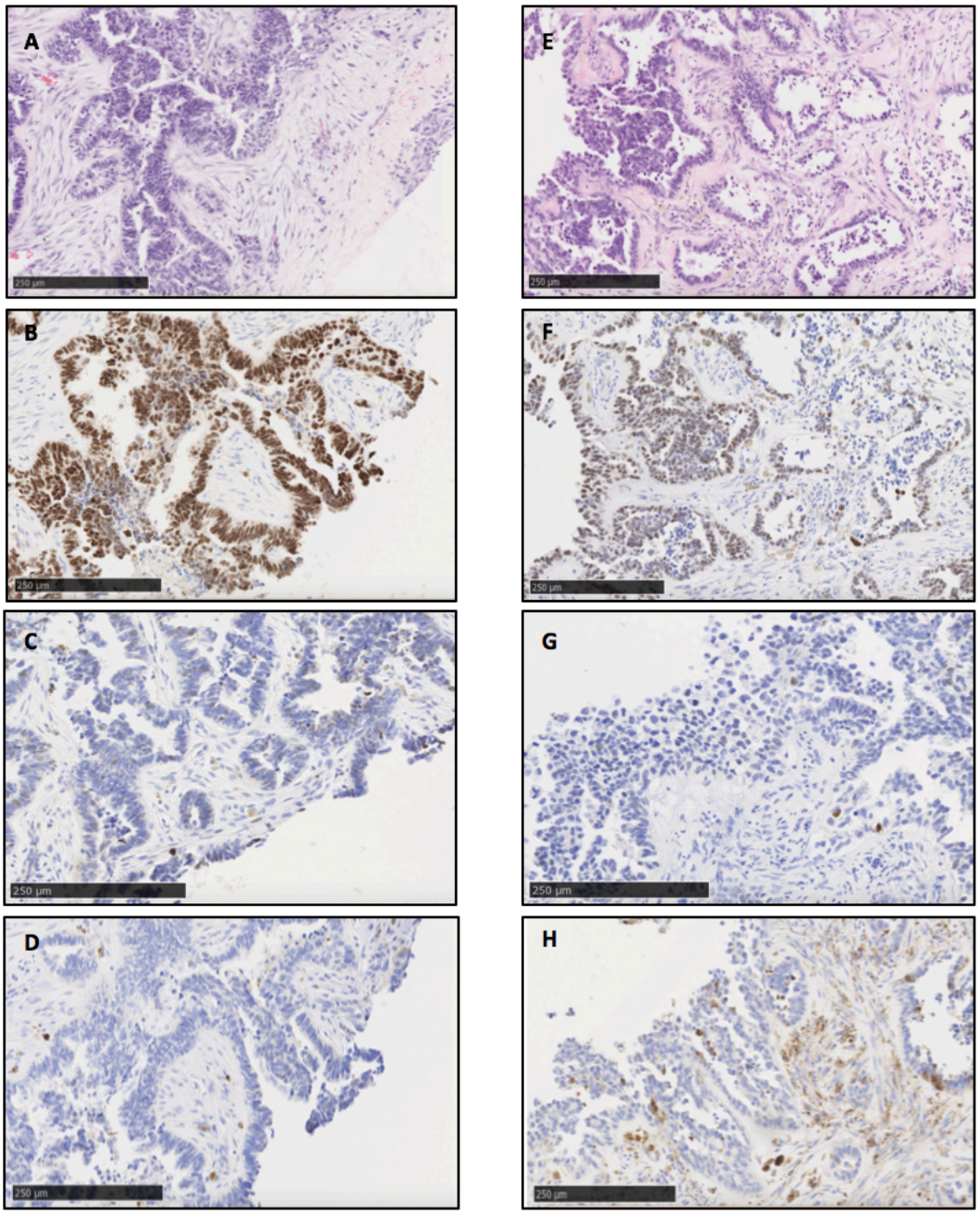


Figure 6.4: IHC staining of tissue slices from liver metastatic deposit from case T19-023. *Images taken via NDP.view 2 software, main image at 10x, insert at 40x.images at 10xmagnification, scale bar 250um. Images A-D show slice culture at day 1, images E-H show day 4. A and E are H&E staining, B and F show PAX8 tumour cell confirmation, C and G show limited Ki67 positivity in both samples. D and H show cleaved caspase 3 staining.*

To investigate long term viability in culture, omental tumour slices from case T18-281 were cultured for 10 days. Figure 6.5 below shows IHC staining profiles for this case, alongside slices from the same sample taken on day 0. Images A-D are the day 0 samples, images E- H are day 10. We can see the difference in tissue structure compared to the liver sample from case T19-023 above. PAX8 staining confirms tumour content (figure 6.5, images B and F), images C and G show Ki67 staining which shows positivity in the tumour cells at both time points, indicating proliferation was still occurring after 10 days in culture. Cleaved caspase 3 staining for apoptotic activity appears similarly low at both time points (images D and H).

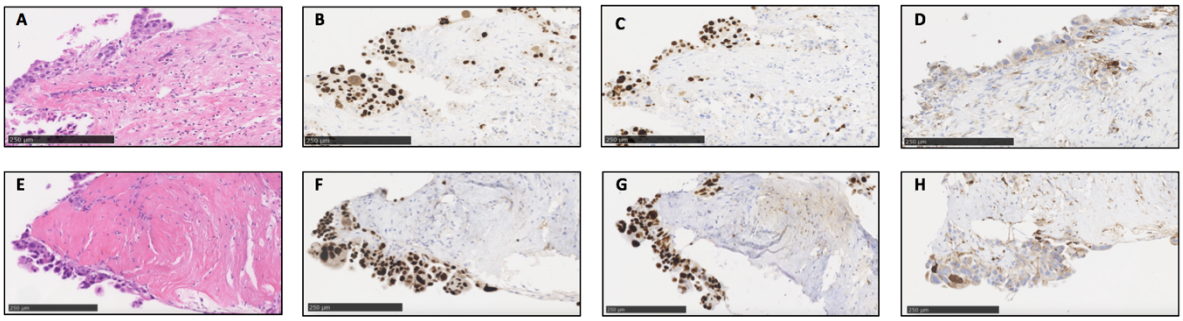


Figure 6.5: IHC staining of tissue slices from omental metastatic deposit from case T18-281 at day both day 0 and after 10 days in culture. *Images taken via NDP.view 2 software. Main images at 10x magnification, scale bar 250um., insert at 40x. A and E show H&E confirmation of tissue structure, B and F show positive PAX8 staining confirming presence of tumour cells. C and G show Ki67 positive staining indicating ongoing proliferation activity at both time points. D and H show apoptotic activity through staining for cleaved caspase 3.*

These results suggest tumour slices can successfully be maintained in culture for up to 4 days, and indeed show proliferative activity beyond this, however with potential for increasing apoptosis levels. More analysis at different time points is required to optimise desired time in culture. Ki67 staining appears to be heterogeneous as found in the ITH study staining of frozen sections.

6.5.2 IHC assessment of response to cisplatin treatment

Following 24 hours in culture, tumour slices underwent treatment with cisplatin with concurrent media change on parallel untreated samples. Figure 6.6 below shows omental tumour slice samples from case T18-243. Images A-D show the untreated omental tumour slice, images E-H show tumour slice treated for 24 hours with 25μM cisplatin. Images A and E show H&E staining confirming tissue structure, B and F show positive PAX8 staining in both treated and untreated samples. C and G show Ki67 staining with a higher number of positively stained cells in the untreated slice than in the treated, suggesting lower proliferation rates in the cisplatin treated slice than in the untreated slice sample. Images D and H show the cleaved caspase 3 stained slices, with higher intensity of staining in the treated slice observed (image H), which would appear to represent the apoptotic response to the cisplatin treatment. However, with limited sample numbers this can only be stated as an observation and requires further replicates within the assay and quantitation of staining.

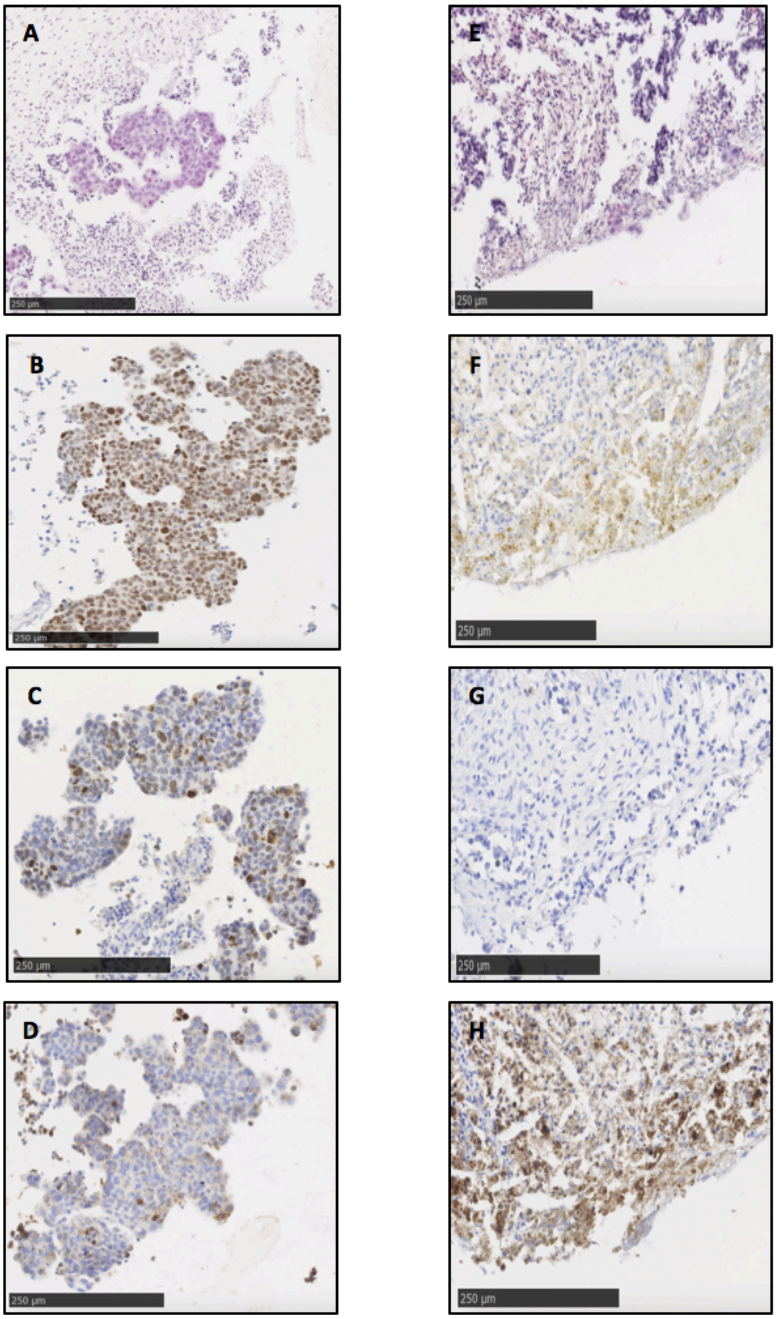


Figure 6.6: Omentum sample from Case T18-243, tumour slices were cultured for 24 hours then drug treated with 25µM Cisplatin for 24 hours with untreated control undergoing media change. *I Main images take at 10x magnification, scale bar 250um, inserts at 40x. Images A-D show sections from the untreated slice sample, images E- H show sections from the treated slice sample. Images A and E show H&E staining, B and F show PAX8 confirming tumour cell presence, C and G show Ki67 staining demonstrating proliferative cells in the untreated sample. D and H show cleaved caspase 3, with higher positivity observed in image H.*

6.6 Discussion

Ex vivo slice cultures present an exciting opportunity to study the evolution of cancers and response to treatments in a culture model which encapsulates more elements of the unique tumour microenvironments than many other systems. The importance of this in HGSOC where the microenvironments are so diverse should not be underestimated. The ability to preserve the architecture and maintain viability has been demonstrated in many studies. Here we have commenced optimisation of tumour slice culture in HGSOC, with optimisation steps in culturing, sectioning and staining for robust histological outputs. We have shown that tumour tissue can be dissected without trauma to the structural integrity and initial IHC analysis suggests differences in proliferation and apoptosis levels between samples. This can be further expanded and potential correlations with patient responses and outcomes made once more samples are obtained. More examination is required into the viability of the tissue slices in longer term culture and what modifications may be needed. Depending on the required output different studies have optimised culture designs for varying time points, Misra et al. demonstrated 4 days as optimum for maintaining key tissue features[315], whereas Kokkinos et al. were able to prolong viability in pancreatic tumour explants to 12 days[316]. In the examples above in this study, some changes in cell apoptotic activity were seen on day 4 and increased by day 10, though proliferation was still occurring. Future work should include time-course experiments to determine the optimal time for tumour slice growth and drug treatment read-outs, and introduce digital pathology software such as QuPath to automate image analysis.

Chapter 7

Discussion and Future perspectives

7 Discussion and Future Perspectives

HGSOC presents challenges on many levels. The genomic instability resulting from ubiquitous *p53* mutations and extensive copy number aberrations results in less potential for mutational or pathway targets than other cancers[44]. The dissemination of metastatic spread occurs rapidly throughout the abdominal cavity and gives only vague symptoms meaning that at the time of diagnosis, most patients have reached an advanced stage III or IV. Most patients will fortunately have platinum sensitive disease at the outset and initially respond well. However, unfortunately the majority will relapse with increasingly resistant disease. Though the overall cure rate for HGSOC remains poor, improvements have been made in PFS and 5-year survival rates can be as high as 65-70% thanks to surgical practice, platinum based and combination chemotherapies and novel targeted treatments such as PARP inhibitors[317]. Despite the nature of dissemination throughout the peritoneum, the advancement of surgical cytoreductive techniques with multivisceral resection has helped to improve outcomes significantly and it has been shown repeatedly that optimal debulking surgery with no residual disease is the most important prognostic indicator for patients[67, 317]. However, the surgery undertaken carries significant morbidity for patients as do the systemic therapeutics. Therefore, the ability to predict those who are likely to respond and benefit from the invasive treatments is crucial for development of personalised patient treatment protocols.

The unstable genomic profile of HGSOC provides vast ITH which makes prediction of response to treatment very difficult[318]. The search for biomarkers enabling the assessment of outcome has prompted multiple studies however so far, the results have been limited and few have been shown to be reproducible[319]. In clinical use currently tumour samples are only assessed for *BRCA* and HRD biomarker status. However amplification of *CCNE1* has been associated with prediction of platinum resistance but has not yet been implemented in clinical practice[320]. Heterogeneity also gives rise to a further problem of development of resistance through the presence of different tumour cell clones, some of which will be resistant from the start and others will become resistant through treatment pressures. Greater understanding of this existing heterogeneity is required to discover potential areas of investigation for markers of response to treatment and outcome to help guide individualised precision medicine delivery.

The requirement for improvement in therapeutic testing strategies is evident in the high failure rate of therapeutics from design to clinical trials. The commonly used 2D cell cultures, while useful tools for drug testing, do not represent the diversity of the *in vivo* state and the need for 3D constructs incorporating more elements of the tumour microenvironment has been recognised. In HGSOC this raises more of a challenge compared to other cancers as there are multiple microenvironments to consider. 80% of HGSOC metastasise to the omentum and there is commonly rapid dispersal all around the peritoneal cavity. Transcriptomic data from different anatomical locations show variation in gene expression between primary and metastatic sites[321, 322]. Previously many studies investigating the heterogeneity in HGSOC have used single site samples for examination, or matched primary and omentum samples. These, though providing important analyses, will not reflect the variation displayed in the rest of the tumour locations[323]. Though recently, studies have expanded to include multisite analysis to investigate genomic alterations and immune phenotypes in HGSOC[277, 324].

The ITH study from our group aimed to determine any associations of spatial and temporal tumour heterogeneity in advanced HGSOC with tumour dissemination patterns, operability, response to platinum chemotherapy, patterns of relapse, PFS and OS. To have no bias due to concerns over surgical capabilities or effect of chemotherapy-induced variations, tumour samples were collected for evaluation from advanced stage HGSOC patients undergoing primary cytoreductive surgery. Systematic mapping of tumour dissemination patterns was carried out during tumour sample collection using a validated intraoperative mapping tool[325, 326], which would eliminate any bias that could arise from random collection of tumours. From the tumours harvested, the project attempted to characterise spatial and temporal heterogeneity on different levels: genomic, proteomic, and phenotypic, all correlated with clinical parameters and outcomes. This was a huge project with over 400 primary cultures established over the time course and multiple modalities examined. The resulting genomic and proteomic analysis of the tumour cohort were outside the scope of this thesis[105]. In the phenotypic assays to detect apoptosis following cisplatin treatment, or IC_{50} levels for cisplatin, we have observed wide heterogeneity in the response of primary tumour cells to cisplatin treatment, both between different patients and between the varied anatomical locations sampled. The variation in apoptotic response to cisplatin was found to be statistically significantly different between samples in individual patients and across the patient cohort. Analysis of the commonly examined omentum in closer detail revealed significant variation in response to cisplatin across the patient cohort, and between the different relapse groups. This indicates that single site

analysis for prediction to response in HGSOC is flawed due to the heterogeneity in responses observed. In the initial stages of the project response to cisplatin was only examined using apoptotic readouts via caspase 3/7 assay. Following optimisation of protocols 25μM cisplatin drug treatment was initiated. However, IC_{50} analysis provides a more nuanced analysis of response to treatment and this was introduced to the project at a later stage providing additional information. The IC_{50} data further corroborated the finding of variation in response to cisplatin treatment in multi-site analysis.

For some patient's tumours, little variation in response to cisplatin treatment was observed, however for many patients we noted large variations in responses to cisplatin. Examination of the MAD of apoptosis in patients' tumour responses to cisplatin revealed no statistical significant difference in heterogeneity levels between different relapse groups.

Testing strategies for therapeutics in HGSOC has proved difficult due to the heterogeneity seen. Recently, Martins et al. have used spheroids derived from patient ascites to investigate the impact of CNAs on responses to different chemotherapies and targeted agents[251]. They observed that ascites derived spheroids could give a reflection of the genomic diversity in HGSOC and were useful in examination of sensitivity to different therapeutics. Use of ascites derived spheroids presents exciting potential medium for examination of HGSOC. However, our data would suggest that further tumours and culture designs should be profiled to be able to adequately represent the spectrum of responses to treatment.

Examination of patient relapse samples demonstrated reduced apoptotic response to cisplatin compared to primary samples and reduced variation in apoptotic response rates between relapse samples. Cisplatin IC_{50} values were also observed to be higher at relapse indicating development of resistance to cisplatin.

Throughout all the genomic, proteomic and phenotypic assessments, the extent of heterogeneity observed has been the paramount discovery. This has highlighted the difficulty in breakthroughs with outcome signatures given one tumour studied in a patient may give a totally different read out to one from another location. In the case of the Ki67 proliferation index, different groups have suggested this to be of benefit as a biomarker in ovarian cancer[290] however our results show extensive variation throughout the patient cohort and different anatomical locations indicating it may not be a representative marker for HGSOC. No correlation could be observed between Ki67 percentage proliferation index and apoptotic response to cisplatin across the cohort. Many existing studies searching for diagnostic or

predictive markers use single site samples. However, from these results it is clear single site samples will not represent the disseminated disease profile. This indicates that to fully profile a patients' disease to guide systemic treatment decisions as many of the tumour sites as possible require examination. This is also true of the pre-surgery setting where decisions of the benefit of debulking surgery are unlikely to be distinguished by single biopsy testing only.

One limitation of the ITH project is that there are few studies of its kind to compare with and validate findings. There is very limited examination of disseminated metastatic HGSOC sites in the literature[287, 322]. To combat this, the group have continued to routinely collect, process and analyse multi-site tumour samples, in order to assemble a large validation cohort, also monitoring any patients for relapse. Secondly, the cultures used to study the phenotypic responses were all based on routinely used 2D cultures. Though the findings are valid and reliable given the consistency in heterogeneity and statistical significance observed, they are limited in terms of prediction of patient response to different therapeutics as testing of tumour cells in isolation, without inclusion of other tumour microenvironment factors and cell types, does not fully recapitulate the *in vivo* microenvironments.

To study the heterogeneity further in cultures better representing the *in vivo* architecture, in an effort to equalise the tumour microenvironment for the primary tumour cells, we developed 3D organotypic models based on the peritoneal lining using rat tail collagen I as an ECM structure with co-cultures of stromal cells to which primary tumour cells were then applied. Through analysis of apoptosis and necrosis readouts following flow cytometry processing of the models it was observed that heterogeneity was present in 3D cultures as it had been in 2D. We also saw that there was a trend towards reduced apoptotic response to cisplatin in the 3D models compared to parallel 2D cultures. To further interrogate the model data, the 2D and 3D readouts were combined. This demonstrated a significant reduction in response to cisplatin in 3D cultures compared to 2D. This correlates with previous findings of 3D cultures having lower response rates likely representing the patient response more closely[327]. Organotypic models in this design have been used by the Lengyel group to assess tumourigenesis in HGSOC and to develop high throughput testing platforms for therapeutics[328]. However, these were performed using immortalised cancer cell lines rather than primary tumour cells as here. Primary cell cultures are much less predictable and are more sensitive to environmental factors affecting viability. This study is novel in its use of primary tumour cells obtained, isolated and cultured directly from surgery. Immortalised cell lines have proved to be extremely useful in

many aspect of disease study however have a trend towards losing their phenotypic identity and therefore not necessarily representing the target cancer[329]. Use of primary cells provides cultures more representative of the tumour phenotype.

However, several difficulties were encountered with the models in their construction and consistency of read-out. Initially I planned to use formalin fixation and paraffin embedding (FFPE) followed by immunohistochemistry (IHC) analysis for multiple testing modalities to observe the architecture characteristics within the models alongside proliferation markers and apoptotic response to treatment. However due to problems arising during the optimisation steps with this processing, we switched to flow cytometry analysis as a potential read-out. As this requires breakdown of the model following construction and drug treatment, it limited the number of readouts possible. It also required more cells at input and therefore reduced the number of cultures able to be established from the samples. This greatly reduced the capacity to validate results with duplicate or triplicate cultures. The volume of cells available for culture is entirely dependent on the size of the tumour resected at surgery and as HGSOC disseminates usually with small widespread carcinosis obtaining large samples is very variable. Despite these limitations however, the results did consistently indicate the differing behaviours and responses of the tumour cells when grown in 3D constructs and highlighted the importance of culture designs involving more complex elements of the tumour microenvironment. The Lengyel group have also used 3D organotypic models for analysis of drug response *in vitro.* Their experiments largely use immortalised ovarian cancer cell lines which are easier to transfect that primary cells. They have used GFP labelled cell lines and fluorescent cytometer analysis for their examination of adhesion, invasion and proliferation assays. Through these methods, they have been able to develop high throughput 3D platforms for analysis of ovarian cancer cell line response to therapeutics. Use of cell lines also facilitates replicate analysis which was a major limitation of the experiments in this project[330]. The Balkwill group have also used 3D organotypic model protocols to develop a 3D tetra-culture model based on the omentum, using human derived adipocytes, mesothelial cells, fibroblasts and ovarian cancer cell lines. They were able to perform FFPE analysis to confirm architecture and histological differentiation with their models[331]. On examination of the protocols used the models were established over a longer time course than was used in this project. This may have allowed the cells to settle into the culture more and provide a more solid construct for fixation and embedding. Primary tumour cultures do not maintain their viability in culture as well as cell lines and so the construction protocol in this project was over a shorter timeframe. This may have affected the success with fixation and subsequent IHC analysis.

To advance the design for 3D culture setup and overcome some of the limitations encountered with the organotypic models, I examined the possibility of developing *ex vivo* tumour slices/explants as a representative tumour model for patients. These culture designs have been used in different cancer types over recent years but minimal investigation into their use in HGSOC has been carried out so far. To complement these cultures and based on evidence in previous studies of common ECM proteomic signatures in specific tumour microenvironments[199, 215] the concept of cultures containing tumours grown in site-specific ECM protein mixes was devised to supplement the culture microenvironment.

The study of the ECM components using MS presents the opportunity to design personalised 3D culture systems in which to test therapeutics with cultures unique to both the patient and the anatomical location. As seen in the Majumder study, introducing patient specific ECM 'protein mixes' into the slice cultures can create a uniquely individualised culture platform in which to test novel therapeutics and gain response rate readouts which can truly reflect patient response and potentially provide prognostic indicators[215].

As a pilot study, MS analysis was performed on decellularised tumour tissue samples from 5 tumour sites across 4 patients to establish the ECM proteome in each site. Vast heterogeneity was observed both in quantity of ECM proteins in the different sites and in the specific protein profiles of each location and patient. Minimal crossovers were seen in enriched proteins by intra-abdominal location. Variation was observed in expression of the most common ECM protein group collagens. In pancreatic cancer, type IV collagen has been shown to be upregulated as part of a loop to increase basement membrane deposition within the tumour microenvironment leading to increased proliferation and avoidance of apoptotic cell death via interactions with integrins[332]. The prognostic possibilities of collagen IV analysis have previously been explored in ovarian cancer with reduced expression correlating with higher grade[333]. In this sample cohort, there was variation in expression of collagen IV by sample location but no significant difference seen when grouped by abdominal region. In our cohort, all patients were high grade and stage therefore correlations with these factors is not possible.

Examination of collagen VI levels was also performed in my samples. Collagen VI has been linked to platinum resistance in ovarian cancer, potentially through its involvement in TME remodelling[306]. Again, variation by sample site was seen in the cohort with one noticeable result of increased expression in the primary sample from case T17-205. No significant correlation with apoptotic response to cisplatin could be observed with collagen VI in these samples, though evaluation is limited by small sample size.

Where previous groups have identified common matrix signatures in omentum sample sites[199], in this sample cohort this was not apparent and variation between the cases was seen. However, it must be noted that this was a small number of samples with limited duplication of sample sites, with higher sample numbers representing each location, common profiles may become more apparent.

Examination of highly expressed proteins between the different abdominal regions (upper, middle and lower) revealed 2 ECM protein hits common between the patient samples, ADH1A,1B,1C and MFAP4. The analysis of ADH 1A,1B and 1C expression also showed significant variation between samples in different abdominal locations. In ovarian cancer, ADH-1B has been observed to be associated with residual disease following cytoreductive surgery and the suggestion of it being a useful biomarker for residual disease has been proposed[334]. Presence of extracellular class 1 ADH isoenzymes has also been recognised in oesophageal cancer with the proposal that during cancer processes it is released from tumour cells into surrounding tissues and circulation[335]. There was significantly reduced expression of ADH-1B found in the lower abdomen in the examined samples. 3 of the patients were successfully operated to no residual disease and the other case had <1cm residual disease so conclusions are not possible to be drawn regarding the prognostic potential in this small sample but with further patient and sample site analysis more significance may be able to be observed. MFAP4 is an ECM protein produced by vascular smooth muscle cells and belongs to the fibrinogen family. MFAP4 has been suggested to contribute to cell adhesion and cell-cell interactions[336]. Expression levels of the gene encoding for MFAP4 protein have been found to correlate with platinum resistance and reduction in progression free survival [337, 338] and its use as a biomarker for resistance to treatment has been considered. Though variation in expression levels was seen between sample sites here, no significant difference was observed. No correlation with apoptotic response was seen though, again, sample numbers are small for comparison and all patients involved had platinum sensitive disease.

To examine for potential common protein signatures, the primary samples from each case were compared. Only one protein was found to be commonly highly expressed in the primary samples, this was TGFβI. TGFβI has been found to be highly expressed in STIC lesions, secreted by TAMs which led to upregulation of $\alpha v\beta_3$ integrin potentially resulting in an

immunosuppressive tumour environment and alteration of the mechanical properties of the TME. TGFβI has been suggested as a potential target in HGSOC[296].
In this pilot study, we have identified TGFβI as a protein of interest which has been linked to HGSOC progression and outcomes and with further analysis of a larger patient cohort more correlations with response to treatment and survival will be possible. Another protein of interest in a larger cohort will be fibronectin, which has previously been shown to have higher expression in omental samples compared to primary and this has been linked to adhesion and invasion properties[171]. Expression did vary between sites in our cohort and further analysis in a larger sample group will be interesting to observe.

As a pilot study the analysis of ECM protein composition demonstrated that extracting out ECM proteins across different sample sites is possible and the results indicate a vast degree of variability between patients and anatomical location. For the advancement of culture designs containing site specific ECM protein mixes, further study with large sample numbers is required. In the case of previous studies observing for common matrices, these have been based on multiple samples of the same location, most commonly the omentum[199], creating the opportunity for a better understanding of individual site signatures. However, as seen in this study, only analysing the components of one site will neglect the heterogeneity demonstrated. When comparing phenotypic response to treatment in the omentum in both 2D and 3D, there was variation between this site and for example, the primary samples, in most cases and also between omental samples from different patients. For the ECM analysis the omentum differed in terms of the quantity of regulated proteins compared to other sample sites observed, there was also minimal cross over in upregulated proteins between the different omental samples. The novelty of this study is the multi-site sampling which has not been explored previously. It is not surprising to see such variation between ECM compositions, given the known heterogeneity of HGSOC and the wide metastatic sites encountered. However, as genomic analysis of different metastatic deposits has highlighted the variation in HR status which can be seen[105], it is possible to surmise there may be important biomarkers or targets within different regions which are not identified through single site analysis.
It has been observed that the ECM and stroma of patients can vary depending on the sensitivity to treatment[143]. All the patients in this pilot study cohort relapsed in a platinum sensitive timeframe. It would be interesting going forward to examine for differences in ECM composition based on observed platinum sensitivity, to then provide tools to assess and predict

response to treatment based on potential matrix signatures. The possibility for biomarkers to be found in the microenvironment components has exciting possibilities, however, to be useful in clinical practice they need to be represented across the patient tumour burden to avoid missing the signature if limited samples are used to guide prognosis and treatment decisions.

Ex vivo tumour slices are becoming increasingly used for 3D culture models to encapsulate more elements of the tumour microenvironment. They have not however been extensively utilised in HGSOC. In the search for the optimum culture in HGSOC in which to study heterogeneity and response to therapeutics, we assessed for the potential to use tissue slices from primary tumour samples, to maintain viability in short term cultures and drug treat with cisplatin. Though this project only covers the initial stages of this study, we were able to obtain tissue slices from different anatomical locations, drug treat and then process with FFPE and immunohistochemistry. Initially, we attempted to optimise and perform all IHC in-house but due to variations in read-outs using manual staining techniques, we switched to using an in-house pathology facility using automated IHC staining for consistency. H&E showed maintenance of tissue structure. PAX8 staining confirmed the presence of HGSOC tumour cells and Ki67 proliferation marker showed variation in staining positivity between samples. Cleaved caspase 3 was used to assess for apoptosis following cisplatin treatment. Further biomarkers such as TUNEL staining for detection of apoptosis were attempted, however could not be optimised in the time remaining. Staining for p53 will also be introduced in a future antibody panel. A difficulty encountered was that by using a direct tumour sectioning method as we employed, not many tumour locations were a good consistency for slicing as they lacked the fibrous composition needed to provide the best result maintaining the tissue architecture. Given the variation in size of the nodular carcinosis seen in HGSOC it may not be possible to reliably predict which cases can provide sufficient tumour sample for establishing slice cultures. Going forward, using embedding techniques to place the tumours and smaller nodules within an inert agarose or agar matrix for sectioning with the vibratome should allow use of all tumours collected, and thus increase the numbers of tumours to be evaluated, and is now being optimised in the laboratory.

The overall aim of this project was to develop 3D culture systems to study HGSOC to accurately encapsulate and depict the heterogeneity existing between patients and tumour locations, in an effort to develop a model to predict responses to chemotherapy. The knowledge gained from the examination of ITH in 2D assays enabled comparisons with 3D models and

showed how important the improvement of 3D model design is to move forward in the search for diagnostic and prognostic signatures in HGSOC. There is significant potential in the use of tumour slices for HGSOC, in particular for estimation of HR status via quantitation of RAD51 foci at sites of DNA damage. The van Gent group introduced a homologous recombination assay called the Repair Capacity (RECAP) test initially in breast cancer tumour slices[267] They have recently applied it to ovarian cancer[268], and ovarian PDOs[257]. Genomic analysis from the larger ITH project has demonstrated variability in HR status scores within patients, with 22% of this current cohort presenting with both HR-Deficient and HR-Proficient tumours amongst their disseminated tumours[105]. As mentioned previously, HR status is one of the few clinically approved biomarkers for HGSOC, stratifying HRD-positive patients for PARP inhibitor treatment. Current clinical practice relies on the genomic assessment of HR status via tumour sections from a single FFPE block that are sent to Myriad Genetics in the USA for assessment, at a significant cost of approximately £3000 per test. Therefore, the potential to employ a quick laboratory-based histological assay, which could be performed on tumour slices from different disseminated tumour sites, staining for markers of DNA damage (γH2AX) and HR deficiency (RAD51) is a very exciting prospect. The potential for this to be performed in a hospital pathology setting or specialised local centres in the UK makes it an even more interesting prospect to help guide treatment options for patients.

Furthermore, based on the discoveries in the novel multi-site ECM protein composition pilot study, a grant was awarded for analysis of ECM signatures in HGSOC with a second cohort of patients. Combining these results, the aim is to gain insight into site specific ECM composition in order to develop ECM protein mixes to use in individual cultures. Following success with the development of HGSOC PDOs, the group aim to develop a more HGSOC-specific matrix for the growth of PDOs, combining hydrogels with tumour-specific ECM proteins. Given the difficulties encountered with the organotypic model processing and requirements of high tumour cell numbers, and potential limitations in tumour slice due to tumour consistency, PDOs provide an exciting future opportunity for study which should be viable for multiple analyses. For this grant, a collaboration with the Dyson School for Design Engineering was established, aiming to manufacture HGSOC specific matrices on-chip using microfluidics and 3D printing based on the proteomic profiles obtained by further ECM MS analysis. Following development, these cultures will undergo treatment with recognised therapeutics to establish a robust drug testing platform.

This study has shown the importance in HGSOC of considering the tumour microenvironment in culture design, attempting to incorporate the heterogeneity of this cancer type into study and so avoid the pitfalls of assuming tumours will respond certain ways in all patients and across all metastatic sites. Expanding culture systems to reflect this complex heterogeneity is essential in the development of personalised treatment plans, reducing the failure rate of therapeutics in trials and, most importantly, to improve patient outcomes.

8 References

1. CRUK. *Ovarian Cancer Statistics*. 2021; Available from: https://www.cancerresearchuk.org/health-professional/cancer-statistics/statistics-by-cancer-type/ovarian-cancer - heading-Zero.
2. Vaughan, S., et al., *Rethinking ovarian cancer: recommendations for improving outcomes.* Nature Reviews Cancer, 2011. **11**(10): p. 719-725.
3. Torre, L.A., et al., *Ovarian cancer statistics, 2018.* CA: a cancer journal for clinicians, 2018. **68**(4): p. 284-296.
4. Rojas, V., et al., *Molecular Characterization of Epithelial Ovarian Cancer: Implications for Diagnosis and Treatment.* International journal of molecular sciences, 2016. **17**(12): p. 2113.
5. Ray-Coquard, I., et al., *Non-epithelial ovarian cancer: ESMO Clinical Practice Guidelines for diagnosis, treatment and follow-up[†].* Annals of Oncology, 2018. **29**: p. iv1-iv18.
6. Banerjee, S. and S.B. Kaye, *New Strategies in the Treatment of Ovarian Cancer: Current Clinical Perspectives and Future Potential.* Clinical Cancer Research, 2013. **19**(5): p. 961-968.
7. Smittenaar, C.R., et al., *Cancer incidence and mortality projections in the UK until 2035.* Br J Cancer, 2016. **115**(9): p. 1147-1155.
8. https://ovarian.org.uk/ovarian-cancer/.
9. Desai, A., et al., *Epithelial ovarian cancer: An overview.* World journal of translational medicine, 2014. **3**(1): p. 1-8.
10. Koshiyama, M., N. Matsumura, and I. Konishi, *Recent concepts of ovarian carcinogenesis: type I and type II.* Biomed Res Int, 2014. **2014**: p. 934261.
11. Shih, I.-M. and R.J. Kurman, *Ovarian Tumorigenesis: A Proposed Model Based on Morphological and Molecular Genetic Analysis.* The American Journal of Pathology, 2004. **164**(5): p. 1511-1518.
12. Bowtell, D.D., *The genesis and evolution of high-grade serous ovarian cancer.* Nat Rev Cancer, 2010. **10**(11): p. 803-8.
13. Anglesio, M.S., et al., *Clear cell carcinoma of the ovary: A report from the first Ovarian Clear Cell Symposium, June 24th, 2010.* Gynecologic Oncology, 2011. **121**(2): p. 407-415.
14. Friedlander, M.L., et al., *Molecular Profiling of Clear Cell Ovarian Cancers: Identifying Potential Treatment Targets for Clinical Trials.* Int J Gynecol Cancer, 2016. **26**(4): p. 648-54.
15. Iida, Y., et al., *Clear cell carcinoma of the ovary: a clinical and molecular perspective.* International Journal of Gynecologic Cancer, 2020: p. ijgc-2020-001656.
16. Scarfone, G., et al., *Characteristics of clear cell ovarian cancer arising from endometriosis: A two center cohort study.* Gynecologic Oncology, 2014. **133**(3): p. 480-484.
17. Kim, S.I., et al., *Genomic landscape of ovarian clear cell carcinoma via whole exome sequencing.* Gynecol Oncol, 2018. **148**(2): p. 375-382.

18. Li, M., et al., *Characterization of ovarian clear cell carcinoma using target drug-based molecular biomarkers: implications for personalized cancer therapy.* Journal of Ovarian Research, 2017. **10**(1): p. 9.
19. Shu, C.A., et al., *Ovarian clear cell carcinoma, outcomes by stage: the MSK experience.* Gynecologic oncology, 2015. **139**(2): p. 236-241.
20. Kim, S.I., et al., *Trends in the Incidence and Survival Rates of Primary Ovarian Clear Cell Carcinoma Compared to Ovarian Serous Carcinoma in Korea.* Frontiers in Oncology, 2022. **12**.
21. Colombo, N., et al., *ESMO–ESGO consensus conference recommendations on ovarian cancer: pathology and molecular biology, early and advanced stages, borderline tumours and recurrent disease.* International Journal of Gynecologic Cancer, 2019. **29**(4): p. 728.
22. Chen, S., et al., *A Review of the Clinical Characteristics and Novel Molecular Subtypes of Endometrioid Ovarian Cancer.* Frontiers in Oncology, 2021. **11**(2116).
23. Lim, D., et al., *Morphological and Immunohistochemical Reevaluation of Tumors Initially Diagnosed as Ovarian Endometrioid Carcinoma With Emphasis on High-grade Tumors.* Am J Surg Pathol, 2016. **40**(3): p. 302-12.
24. Hollis, R.L., et al., *Molecular stratification of endometrioid ovarian carcinoma predicts clinical outcome.* Nature Communications, 2020. **11**(1): p. 4995.
25. Madore, J., et al., *Characterization of the molecular differences between ovarian endometrioid carcinoma and ovarian serous carcinoma.* J Pathol, 2010. **220**(3): p. 392-400.
26. Zhou, J., et al., *The Effect of Histological Subtypes on Outcomes of Stage IV Epithelial Ovarian Cancer.* Frontiers in Oncology, 2018. **8**.
27. Pierson, W.E., et al., *An integrated molecular profile of endometrioid ovarian cancer.* Gynecologic Oncology, 2020. **157**(1): p. 55-61.
28. Babaier, A. and P. Ghatage, *Mucinous Cancer of the Ovary: Overview and Current Status.* Diagnostics, 2020. **10**(1).
29. Simons, M., et al., *A novel algorithm for better distinction of primary mucinous ovarian carcinomas and mucinous carcinomas metastatic to the ovary.* Virchows Archiv, 2019. **474**(3): p. 289-296.
30. Vang, R., et al., *Immunohistochemical expression of CDX2 in primary ovarian mucinous tumors and metastatic mucinous carcinomas involving the ovary: comparison with CK20 and correlation with coordinate expression of CK7.* Mod Pathol, 2006. **19**(11): p. 1421-8.
31. Cheasley, D., et al., *The molecular origin and taxonomy of mucinous ovarian carcinoma.* Nature Communications, 2019. **10**(1): p. 3935.
32. Gorringe, K.L., et al., *Therapeutic options for mucinous ovarian carcinoma.* Gynecologic Oncology, 2020. **156**(3): p. 552-560.
33. Downward, J. and B. Weigelt, *Genomic Determinants of PI3K Pathway Inhibitor Response in Cancer.* Frontiers in Oncology, 2012. **2**.
34. Britten, C.D., *PI3K and MEK inhibitor combinations: examining the evidence in selected tumor types.* Cancer Chemotherapy and Pharmacology, 2013. **71**(6): p. 1395-1409.
35. Kang, J.-H., et al., *Clinical factors associated with prognosis in low-grade serous ovarian carcinoma: experiences at two large academic institutions in Korea and Taiwan.* Scientific Reports, 2020. **10**(1): p. 20012.

36. Gadducci, A. and S. Cosio, *Therapeutic Approach to Low-Grade Serous Ovarian Carcinoma: State of Art and Perspectives of Clinical Research.* Cancers, 2020. **12**(5): p. 1336.
37. Gershenson, D.M., C.C. Sun, and K.-K. Wong, *Impact of mutational status on survival in low-grade serous carcinoma of the ovary or peritoneum.* British Journal of Cancer, 2015. **113**(9): p. 1254-1258.
38. Burotto, M., et al., *The MAPK pathway across different malignancies: A new perspective.* Cancer, 2014. **120**(22): p. 3446-3456.
39. Schink, J.C., et al., *Mutational landscape of low-grade serous carcinoma of the ovary.* Journal of Clinical Oncology, 2022. **40**(16_suppl): p. 5578-5578.
40. Di Lorenzo, P., et al., *Advanced low grade serous ovarian cancer: A retrospective analysis of surgical and chemotherapeutic management in two high volume oncological centers.* Front Oncol, 2022. **12**: p. 970918.
41. Gershenson, D.M., C. Gourley, and J. Paul, *MEK Inhibitors for the Treatment of Low-Grade Serous Ovarian Cancer: Expanding Therapeutic Options for a Rare Ovarian Cancer Subtype.* Journal of Clinical Oncology, 2020. **38**(32): p. 3731-3734.
42. Lima, B., et al., *Impressive and durable clinical responses obtained with dabrafenib and trametinib in low-grade serous ovarian cancer harbouring a BRAF V600E mutation.* Gynecologic Oncology Reports, 2022. **40**: p. 100942.
43. Prat, J. and F.C.o.G. Oncology, *FIGO's staging classification for cancer of the ovary, fallopian tube, and peritoneum: abridged republication.* Journal of gynecologic oncology, 2015. **26**(2): p. 87-89.
44. Bowtell, D.D., et al., *Rethinking ovarian cancer II: reducing mortality from high-grade serous ovarian cancer.* Nature Reviews Cancer, 2015. **15**(11): p. 668-679.
45. Mirza, M.R., S. Pignata, and J.A. Ledermann, *Latest clinical evidence and further development of PARP inhibitors in ovarian cancer.* Annals of Oncology, 2018. **29**(6): p. 1366-1376.
46. Goff, B., *Symptoms associated with ovarian cancer.* Clin Obstet Gynecol, 2012. **55**(1): p. 36-42.
47. Scholler, N. and N. Urban, *CA125 in ovarian cancer.* Biomark Med, 2007. **1**(4): p. 513-23.
48. Kenemans, P., et al., *CA 125 in gynecological pathology—a review.* European journal of obstetrics & gynecology and reproductive biology, 1993. **49**(1-2): p. 115-124.
49. Watson, P., et al., *The Clinical Features of Ovarian Cancer in Hereditary Nonpolyposis Colorectal Cancer.* Gynecologic Oncology, 2001. **82**: p. 223-228.
50. HUNN, J. and G.C. RODRIGUEZ, *Ovarian Cancer: Etiology, Risk Factors, and Epidemiology.* Clinical Obstetrics and Gynecology, 2012. **55**(1): p. 3-23.
51. Labidi-Galy, S.I., et al., *High grade serous ovarian carcinomas originate in the fallopian tube.* Nature Communications, 2017. **8**(1): p. 1093.
52. Bergsten, T.M., J.E. Burdette, and M. Dean, *Fallopian tube initiation of high grade serous ovarian cancer and ovarian metastasis: Mechanisms and therapeutic implications.* Cancer Lett, 2020. **476**: p. 152-160.
53. Finch, A., et al., *Clinical and pathologic findings of prophylactic salpingo-oophorectomies in 159 BRCA1 and BRCA2 carriers.* Gynecol Oncol, 2006. **100**(1): p. 58-64.
54. Shaw, P.A., et al., *Candidate serous cancer precursors in fallopian tube epithelium of BRCA1/2 mutation carriers.* Mod Pathol, 2009. **22**(9): p. 1133-8.

55. Kuhn, E., et al., *TP53 mutations in serous tubal intraepithelial carcinoma and concurrent pelvic high-grade serous carcinoma--evidence supporting the clonal relationship of the two lesions.* J Pathol, 2012. **226**(3): p. 421-6.
56. Howitt, B.E., et al., *Evidence for a dualistic model of high-grade serous carcinoma: BRCA mutation status, histology, and tubal intraepithelial carcinoma.* Am J Surg Pathol, 2015. **39**(3): p. 287-93.
57. Zhang, S., et al., *Both fallopian tube and ovarian surface epithelium are cells-of-origin for high-grade serous ovarian carcinoma.* Nat Commun, 2019. **10**(1): p. 5367.
58. Punzón-Jiménez, P., et al., *Molecular Management of High-Grade Serous Ovarian Carcinoma.* International Journal of Molecular Sciences, 2022. **23**(22): p. 13777.
59. George, S.H.L., R. Garcia, and B.M. Slomovitz, *Ovarian Cancer: The Fallopian Tube as the Site of Origin and Opportunities for Prevention.* Frontiers in oncology, 2016. **6**: p. 108-108.
60. Lisio, M.A., et al., *High-Grade Serous Ovarian Cancer: Basic Sciences, Clinical and Therapeutic Standpoints.* Int J Mol Sci, 2019. **20**(4).
61. Yeung, T.-L., et al., *Cellular and molecular processes in ovarian cancer metastasis. A Review in the Theme: Cell and Molecular Processes in Cancer Metastasis.* American Journal of Physiology-Cell Physiology, 2015. **309**(7): p. C444-C456.
62. Naora, H. and D.J. Montell, *Ovarian Cancer Metastasis: Integrating insights from disparate model organisms.* Nature Reviews Cancer, 2005. **5**(5): p. 355-366.
63. Braicu, E.I., et al., *Role of histological type on surgical outcome and survival following radical primary tumour debulking of epithelial ovarian, fallopian tube and peritoneal cancers.* British Journal of Cancer, 2011. **105**(12): p. 1818-1824.
64. Colombo, N., et al., *Medical therapy of advanced malignant epithelial tumours of the ovary.* Forum (Genova), 2000. **10**(4): p. 323-32.
65. Fotopoulou, C., *How to predict treatment failure in frail patients with advanced epithelial ovarian cancer: strategies to personalize surgical effort.* jgo, 2020. **31**(1): p. 0-0.
66. Chang, S.J. and R.E. Bristow, *Evolution of surgical treatment paradigms for advanced-stage ovarian cancer: redefining 'optimal' residual disease.* Gynecol Oncol, 2012. **125**(2): p. 483-92.
67. Heitz, F., et al., *186 Surgical outcome as prognostic factor in different histologic subtypes of ovarian carcinoma- analysis of 7 phase III trials by AGO Studygroup + ENGOT.* International Journal of Gynecologic Cancer, 2021. **31**(Suppl 3): p. A205-A206.
68. Colombo, N., et al., *ESMO–ESGO consensus conference recommendations on ovarian cancer: pathology and molecular biology, early and advanced stages, borderline tumours and recurrent disease.* International Journal of Gynecologic Cancer, 2019. **29**(4): p. 728-760.
69. Reuss, A., et al., *TRUST: Trial of Radical Upfront Surgical Therapy in advanced ovarian cancer (ENGOT ov33/AGO-OVAR OP7).* Int J Gynecol Cancer, 2019. **29**(8): p. 1327-1331.
70. Herzog, T.J., *Recurrent Ovarian Cancer: How Important Is It to Treat to Disease Progression?* Clinical Cancer Research, 2004. **10**(22): p. 7439-7449.
71. Wagstaff, A.J., et al., *Carboplatin. A preliminary review of its pharmacodynamic and pharmacokinetic properties and therapeutic efficacy in the treatment of cancer.* Drugs, 1989. **37**(2): p. 162-90.

72. Perren, T.J., et al., *A Phase 3 Trial of Bevacizumab in Ovarian Cancer.* New England Journal of Medicine, 2011. **365**(26): p. 2484-2496.
73. Tewari, K.S., et al., *Final Overall Survival of a Randomized Trial of Bevacizumab for Primary Treatment of Ovarian Cancer.* J Clin Oncol, 2019. **37**(26): p. 2317-2328.
74. Banerjee, S., et al., *First-line PARP inhibitors in ovarian cancer: summary of an ESMO Open - Cancer Horizons round-table discussion.* ESMO Open, 2020. **5**(6): p. e001110.
75. Miller, R.E., et al., *ESMO recommendations on predictive biomarker testing for homologous recombination deficiency and PARP inhibitor benefit in ovarian cancer.* Annals of Oncology, 2020. **31**(12): p. 1606-1622.
76. González-Martín, A., et al., *Niraparib in Patients with Newly Diagnosed Advanced Ovarian Cancer.* New England Journal of Medicine, 2019. **381**(25): p. 2391-2402.
77. Dagogo-Jack, I. and A.T. Shaw, *Tumour heterogeneity and resistance to cancer therapies.* Nature Reviews Clinical Oncology, 2018. **15**(2): p. 81-94.
78. Cuello, M., S. Kato, and F. Liberona, *5 The good prognosis of immunoreactive subtype of high-grade serous ovarian cancer (HGSOC) is negatively impacted when obesity and lipid metabolism-related genes are highly expressed.* International Journal of Gynecologic Cancer, 2019. **29**(Suppl 3): p. A3.
79. Ignacio, R.M.C., et al., *Obesity-Induced Peritoneal Dissemination of Ovarian Cancer and Dominant Recruitment of Macrophages in Ascites.* Immune Netw, 2018. **18**(6): p. e47.
80. Vescio, M., et al., *Modulation of gene expression associated with copy number variation identifies key regulatory programs in high-grade serous ovarian carcinoma.* Advances in Cancer Biology - Metastasis, 2023. **7**: p. 100088.
81. Ramón, Y.C.S., et al., *Clinical implications of intratumor heterogeneity: challenges and opportunities.* J Mol Med (Berl), 2020. **98**(2): p. 161-177.
82. Bell, D., et al., *Integrated genomic analyses of ovarian carcinoma.* Nature, 2011. **474**(7353): p. 609-615.
83. Ahmed, A.A., et al., *Driver mutations in TP53 are ubiquitous in high grade serous carcinoma of the ovary.* J Pathol, 2010. **221**(1): p. 49-56.
84. Zhang, Y., et al., *TP53 mutations in epithelial ovarian cancer.* Translational Cancer Research, 2016. **5**(6): p. 650-663.
85. Chen, J., *The Cell-Cycle Arrest and Apoptotic Functions of p53 in Tumor Initiation and Progression.* Cold Spring Harb Perspect Med, 2016. **6**(3): p. a026104.
86. Wallis, B., et al. *The Challenges and Prospects of p53-Based Therapies in Ovarian Cancer*. Biomolecules, 2023. **13**, DOI: 10.3390/biom13010159.
87. Kastan, M.B. and E. Berkovich, *p53: a two-faced cancer gene.* Nature cell biology, 2007. **9**(5): p. 489-491.
88. Dittmer, D., et al., *Gain of function mutations in p53.* Nature Genetics, 1993. **4**(1): p. 42-46.
89. Cole, A.J., et al., *Assessing mutant p53 in primary high-grade serous ovarian cancer using immunohistochemistry and massively parallel sequencing.* Scientific Reports, 2016. **6**(1): p. 26191.
90. Willis, A., et al., *Mutant p53 exerts a dominant negative effect by preventing wild-type p53 from binding to the promoter of its target genes.* Oncogene, 2004. **23**(13): p. 2330-8.
91. *Integrated genomic analyses of ovarian carcinoma.* Nature, 2011. **474**(7353): p. 609-15.

92. van Dijk, E., et al., *Chromosomal copy number heterogeneity predicts survival rates across cancers.* Nature Communications, 2021. **12**(1): p. 3188.
93. Mamlouk, S., et al., *DNA copy number changes define spatial patterns of heterogeneity in colorectal cancer.* Nature Communications, 2017. **8**(1): p. 14093.
94. Macintyre, G., et al., *Copy number signatures and mutational processes in ovarian carcinoma.* Nat Genet, 2018. **50**(9): p. 1262-1270.
95. Kondrashova, O., et al., *Methylation of all BRCA1 copies predicts response to the PARP inhibitor rucaparib in ovarian carcinoma.* Nature Communications, 2018. **9**(1): p. 3970.
96. Bernards, S.S., et al., *Overall survival in BRCA1 or RAD51C methylated vs mutated ovarian carcinoma following primary treatment with platinum chemotherapy.* Gynecologic Oncology, 2017. **145**: p. 24.
97. Kondrashova, O., et al., *Methylation of all BRCA1 copies predicts response to the PARP inhibitor rucaparib in ovarian carcinoma.* Nat Commun, 2018. **9**(1): p. 3970.
98. Pennington, K.P., et al., *Germline and somatic mutations in homologous recombination genes predict platinum response and survival in ovarian, fallopian tube, and peritoneal carcinomas.* Clin Cancer Res, 2014. **20**(3): p. 764-75.
99. Tan, D.S., et al., *"BRCAness" syndrome in ovarian cancer: a case-control study describing the clinical features and outcome of patients with epithelial ovarian cancer associated with BRCA1 and BRCA2 mutations.* J Clin Oncol, 2008. **26**(34): p. 5530-6.
100. Neff, R.T., L. Senter, and R. Salani, *BRCA mutation in ovarian cancer: testing, implications and treatment considerations.* Ther Adv Med Oncol, 2017. **9**(8): p. 519-531.
101. Bashashati, A., et al., *Distinct evolutionary trajectories of primary high-grade serous ovarian cancers revealed through spatial mutational profiling.* J Pathol, 2013. **231**(1): p. 21-34.
102. Vázquez-García, I., et al., *Ovarian cancer mutational processes drive site-specific immune evasion.* Nature, 2022. **612**(7941): p. 778-786.
103. Lahtinen, A., et al., *Evolutionary states and trajectories characterized by distinct pathways stratify patients with ovarian high grade serous carcinoma.* Cancer Cell, 2023. **41**(6): p. 1103-1117.e12.
104. niraparib, N.g.; NICE guidance for Niraparib. Available from: https://www.nice.org.uk/guidance/ta673/chapter/1-Recommendations.
105. Cunnea, P., et al., *Spatial and temporal intra-tumoral heterogeneity in advanced HGSOC: Implications for surgical and clinical outcomes.* Cell Rep Med, 2023. **4**(6): p. 101055.
106. Perez-Villatoro, F., et al., *Optimized detection of homologous recombination deficiency improves the prediction of clinical outcomes in cancer.* NPJ Precis Oncol, 2022. **6**(1): p. 96.
107. Petersen, S., et al., *CCNE1 and BRD4 co-amplification in high-grade serous ovarian cancer is associated with poor clinical outcomes.* Gynecologic Oncology, 2020. **157**(2): p. 405-410.
108. Talbot, T., H. Lu, and E.O. Aboagye, *Amplified therapeutic targets in high-grade serous ovarian carcinoma – a review of the literature with quantitative appraisal.* Cancer Gene Therapy, 2023. **30**(7): p. 955-963.
109. Bardal, S.K., J.E. Waechter, and D.S. Martin, *Chapter 20 - Neoplasia*, in *Applied Pharmacology*, S.K. Bardal, J.E. Waechter, and D.S. Martin, Editors. 2011, W.B. Saunders: Philadelphia. p. 305-324.

110. Lambrechts, S., et al., *Genetic heterogeneity after first-line chemotherapy in high-grade serous ovarian cancer.* European Journal of Cancer, 2016. **53**: p. 51-64.
111. Wang, D. and S.J. Lippard, *Cellular processing of platinum anticancer drugs.* Nature Reviews Drug Discovery, 2005. **4**(4): p. 307-320.
112. Galluzzi, L., et al., *Molecular mechanisms of cisplatin resistance.* Oncogene, 2012. **31**(15): p. 1869-1883.
113. Stewart, D.J., *Mechanisms of resistance to cisplatin and carboplatin.* Critical Reviews in Oncology/Hematology, 2007. **63**(1): p. 12-31.
114. Choi, M.-K. and D.-D. Kim, *Platinum transporters and drug resistance.* Archives of Pharmacal Research, 2006. **29**(12): p. 1067-1073.
115. Holzer, A.K., et al., *The copper influx transporter human copper transport protein 1 regulates the uptake of cisplatin in human ovarian carcinoma cells.* Mol Pharmacol, 2004. **66**(4): p. 817-23.
116. Huang, C.P., et al., *Copper transporter 2 regulates intracellular copper and sensitivity to cisplatin.* Metallomics, 2014. **6**(3): p. 654-61.
117. Stordal, B., et al., *Resistance to Paclitaxel in a Cisplatin-Resistant Ovarian Cancer Cell Line Is Mediated by P-Glycoprotein.* PLOS ONE, 2012. **7**(7): p. e40717.
118. Patch, A.-M., et al., *Whole–genome characterization of chemoresistant ovarian cancer.* Nature, 2015. **521**(7553): p. 489-494.
119. Christie, E.L., et al., *Multiple ABCB1 transcriptional fusions in drug resistant high-grade serous ovarian and breast cancer.* Nat Commun, 2019. **10**(1): p. 1295.
120. Yoshida, G.J., *Metabolic reprogramming: the emerging concept and associated therapeutic strategies.* Journal of Experimental & Clinical Cancer Research, 2015. **34**(1): p. 111.
121. Zhang, X.-Y., et al., *Hexokinase 2 confers resistance to cisplatin in ovarian cancer cells by enhancing cisplatin-induced autophagy.* The International Journal of Biochemistry & Cell Biology, 2018. **95**: p. 9-16.
122. Baguley, B.C., *Multidrug Resistance in Cancer*, in *Multi-Drug Resistance in Cancer*, J. Zhou, Editor. 2010, Humana Press: Totowa, NJ. p. 1-14.
123. Zhou, J., et al., *The Drug-Resistance Mechanisms of Five Platinum-Based Antitumor Agents.* Front Pharmacol, 2020. **11**: p. 343.
124. Kong, L.R., et al., *MEK Inhibition Overcomes Cisplatin Resistance Conferred by SOS/MAPK Pathway Activation in Squamous Cell Carcinoma.* Molecular Cancer Therapeutics, 2015. **14**(7): p. 1750-1760.
125. Miow, Q.H., et al., *Epithelial-mesenchymal status renders differential responses to cisplatin in ovarian cancer.* Oncogene, 2015. **34**(15): p. 1899-907.
126. Wiedemeyer, W.R., J.A. Beach, and B.Y. Karlan, *Reversing Platinum Resistance in High-Grade Serous Ovarian Carcinoma: Targeting BRCA and the Homologous Recombination System.* Front Oncol, 2014. **4**: p. 34.
127. Damia, G. and M. D'Incalci, *Targeting DNA repair as a promising approach in cancer therapy.* European Journal of Cancer, 2007. **43**(12): p. 1791-1801.
128. Swisher, E.M., et al., *Secondary BRCA1 Mutations in BRCA1-Mutated Ovarian Carcinomas with Platinum Resistance.* Cancer Research, 2008. **68**(8): p. 2581-2586.
129. Dagogo-Jack, I. and A.T. Shaw, *Tumour heterogeneity and resistance to cancer therapies.* Nat Rev Clin Oncol, 2018. **15**(2): p. 81-94.
130. Gerlinger, M., et al., *Intratumor heterogeneity and branched evolution revealed by multiregion sequencing.* N Engl J Med, 2012. **366**(10): p. 883-892.

131. Lee, A.J., et al., *Chromosomal instability confers intrinsic multidrug resistance.* Cancer Res, 2011. **71**(5): p. 1858-70.
132. Birkbak, N.J., et al., *Paradoxical relationship between chromosomal instability and survival outcome in cancer.* Cancer Res, 2011. **71**(10): p. 3447-52.
133. Masoodi, T., et al., *Genetic heterogeneity and evolutionary history of high-grade ovarian carcinoma and matched distant metastases.* British Journal of Cancer, 2020. **122**(8): p. 1219-1230.
134. Kotnik, E.N., et al., *Genetic characterization of primary and metastatic high-grade serous ovarian cancer tumors reveals distinct features associated with survival.* Communications Biology, 2023. **6**(1): p. 688.
135. Davis, A., A.V. Tinker, and M. Friedlander, *"Platinum resistant" ovarian cancer: What is it, who to treat and how to measure benefit?* Gynecologic Oncology, 2014. **133**(3): p. 624-631.
136. Aguirre-Ghiso, J.A., *Models, mechanisms and clinical evidence for cancer dormancy.* Nat Rev Cancer, 2007. **7**(11): p. 834-46.
137. Aguirre-Ghiso, J.A., et al., *ERK(MAPK) activity as a determinant of tumor growth and dormancy; regulation by p38(SAPK).* Cancer Res, 2003. **63**(7): p. 1684-95.
138. Peart, T., et al., *Intact LKB1 activity is required for survival of dormant ovarian cancer spheroids.* Oncotarget, 2015. **6**(26): p. 22424-38.
139. Cooke, S.L. and J.D. Brenton, *Evolution of platinum resistance in high-grade serous ovarian cancer.* The Lancet. Oncology, 2011. **12 12**: p. 1169-74.
140. Schwarz, R.F., et al., *Spatial and Temporal Heterogeneity in High-Grade Serous Ovarian Cancer: A Phylogenetic Analysis.* PLOS Medicine, 2015. **12**(2): p. e1001789.
141. Colombo, N., et al., *ESMO-ESGO consensus conference recommendations on ovarian cancer: pathology and molecular biology, early and advanced stages, borderline tumours and recurrent disease†.* Ann Oncol, 2019. **30**(5): p. 672-705.
142. Li, Y., et al., *Establish of an Initial Platinum-Resistance Predictor in High-Grade Serous Ovarian Cancer Patients Regardless of Homologous Recombination Deficiency Status.* Front Oncol, 2022. **12**: p. 847085.
143. Uno, K., et al., *Significance of platinum distribution to predict platinum resistance in ovarian cancer after platinum treatment in neoadjuvant chemotherapy.* Scientific Reports, 2022. **12**(1): p. 4513.
144. Khalique, L., et al., *Genetic intra-tumour heterogeneity in epithelial ovarian cancer and its implications for molecular diagnosis of tumours.* The Journal of Pathology, 2007. **211**(3): p. 286-295.
145. Kessenbrock, K., V. Plaks, and Z. Werb, *Matrix Metalloproteinases: Regulators of the Tumor Microenvironment.* Cell, 2010. **141**(1): p. 52-67.
146. Watters, K.M., P. Bajwa, and H.A. Kenny, *Organotypic 3D Models of the Ovarian Cancer Tumor Microenvironment.* Cancers (Basel), 2018. **10**(8).
147. Mendoza-Martinez, A., et al., *Modeling the Tumor Microenvironment of Ovarian Cancer: The Application of Self-Assembling Biomaterials.* Cancers, 2021. **13**: p. 5745.
148. Quail, D.F. and J.A. Joyce, *Microenvironmental regulation of tumor progression and metastasis.* Nature Medicine, 2013. **19**(11): p. 1423-1437.
149. Bremnes, R.M., et al., *The Role of Tumor Stroma in Cancer Progression and Prognosis: Emphasis on Carcinoma-Associated Fibroblasts and Non-small Cell Lung Cancer.* Journal of Thoracic Oncology, 2011. **6**(1): p. 209-217.

150. Kipps, E., D.S.P. Tan, and S.B. Kaye, *Meeting the challenge of ascites in ovarian cancer: new avenues for therapy and research.* Nature Reviews Cancer, 2013. **13**(4): p. 273-282.
151. Naba, A., et al., *The matrisome: in silico definition and in vivo characterization by proteomics of normal and tumor extracellular matrices.* Mol Cell Proteomics, 2012. **11**(4): p. M111.014647.
152. Frantz, C., K.M. Stewart, and V.M. Weaver, *The extracellular matrix at a glance.* J Cell Sci, 2010. **123**(Pt 24): p. 4195-200.
153. Harburger, D.S. and D.A. Calderwood, *Integrin signalling at a glance.* Journal of Cell Science, 2009. **122**(2): p. 159-163.
154. Desgrosellier, J.S. and D.A. Cheresh, *Integrins in cancer: biological implications and therapeutic opportunities.* Nat Rev Cancer, 2010. **10**(1): p. 9-22.
155. Weidle, U.H., et al., *Mechanisms and Targets Involved in Dissemination of Ovarian Cancer.* Cancer Genomics Proteomics, 2016. **13**(6): p. 407-423.
156. Lengyel, E., *Ovarian cancer development and metastasis.* Am J Pathol, 2010. **177**(3): p. 1053-64.
157. Efthymiou, G., et al., *Shaping Up the Tumor Microenvironment With Cellular Fibronectin.* Frontiers in Oncology, 2020. **10**.
158. Moreno-Layseca, P. and C.H. Streuli, *Signalling pathways linking integrins with cell cycle progression.* Matrix Biology, 2014. **34**: p. 144-153.
159. Zaidel-Bar, R., et al., *Functional atlas of the integrin adhesome.* Nature Cell Biology, 2007. **9**(8): p. 858-867.
160. Walker, J.L. and R.K. Assoian, *Integrin-dependent signal transduction regulating cyclin D1 expression and G1 phase cell cycle progression.* Cancer and Metastasis Reviews, 2005. **24**(3): p. 383-393.
161. Horbinski, C., C. Mojesky, and N. Kyprianou, *Live Free or Die: Tales of Homeless (Cells) in Cancer.* The American Journal of Pathology, 2010. **177**(3): p. 1044-1052.
162. Giancotti, F.G. and E. Ruoslahti, *Integrin Signaling.* Science, 1999. **285**(5430): p. 1028-1033.
163. Weaver, V.M., et al., *Reversion of the Malignant Phenotype of Human Breast Cells in Three-Dimensional Culture and In Vivo by Integrin Blocking Antibodies.* Journal of Cell Biology, 1997. **137**(1): p. 231-245.
164. Breuss, J.M., et al., *Expression of the β6 integrin subunit in development, neoplasia and tissue repair suggests a role in epithelial remodeling.* Journal of Cell Science, 1995. **108**(6): p. 2241-2251.
165. Guo, W. and F.G. Giancotti, *Integrin signalling during tumour progression.* Nature Reviews Molecular Cell Biology, 2004. **5**(10): p. 816-826.
166. Liappas, G., et al., *T Helper 17/Regulatory T Cell Balance and Experimental Models of Peritoneal Dialysis-Induced Damage.* BioMed Research International, 2015. **2015**: p. 1-9.
167. Lengyel, E., *Ovarian cancer development and metastasis.* The American journal of pathology, 2010. **177**(3): p. 1053-1064.
168. Iwanicki, M.P., et al., *Ovarian cancer spheroids use myosin-generated force to clear the mesothelium.* Cancer Discov, 2011. **1**(2): p. 144-57.
169. Heath, R.M., et al., *Tumour-induced apoptosis in human mesothelial cells: a mechanism of peritoneal invasion by Fas Ligand/Fas interaction.* Br J Cancer, 2004. **90**(7): p. 1437-42.

170. Mikuła-Pietrasik, J., et al., *Peritoneal mesothelium promotes the progression of ovarian cancer cells in vitro and in a mice xenograft model in vivo.* Cancer Lett, 2014. **355**(2): p. 310-5.
171. Kenny, H.A., et al., *Mesothelial cells promote early ovarian cancer metastasis through fibronectin secretion.* J Clin Invest, 2014. **124**(10): p. 4614-28.
172. Rozario, T. and D.W. DeSimone, *The extracellular matrix in development and morphogenesis: a dynamic view.* Dev Biol, 2010. **341**(1): p. 126-40.
173. Ricard-Blum, S., *The Collagen Family.* Cold Spring Harbor Perspectives in Biology, 2011. **3**(1).
174. Hotary, K.B., et al., *Membrane Type I Matrix Metalloproteinase Usurps Tumor Growth Control Imposed by the Three-Dimensional Extracellular Matrix.* Cell, 2003. **114**(1): p. 33-45.
175. Klymenko, Y., et al., *Cadherin composition and multicellular aggregate invasion in organotypic models of epithelial ovarian cancer intraperitoneal metastasis.* Oncogene, 2017. **36**(42): p. 5840-5851.
176. Rankin, E.B. and A.J. Giaccia, *Hypoxic control of metastasis.* Science, 2016. **352**(6282): p. 175-80.
177. Osada, R., et al., *Expression of hypoxia-inducible factor 1α, hypoxia-inducible factor 2α, and von Hippel–Lindau protein in epithelial ovarian neoplasms and allelic loss of von Hippel-Lindau gene: nuclear expression of hypoxia-inducible factor 1α is an independent prognostic factor in ovarian carcinoma.* Human Pathology, 2007. **38**(9): p. 1310-1320.
178. Natarajan, S., et al., *Collagen Remodeling in the Hypoxic Tumor-Mesothelial Niche Promotes Ovarian Cancer Metastasis.* Cancer Res, 2019. **79**(9): p. 2271-2284.
179. Agarwal, A., et al., *Identification of a Metalloprotease-Chemokine Signaling System in the Ovarian Cancer Microenvironment: Implications for Antiangiogenic Therapy.* Cancer Research, 2010. **70**(14): p. 5880-5890.
180. Périgny, M., et al., *Role of Immunohistochemical Overexpression of Matrix Metalloproteinases MMP-2 and MMP-11 in the Prognosis of Death by Ovarian Cancer.* American Journal of Clinical Pathology, 2008. **129**(2): p. 226-231.
181. Huang, H., *Matrix Metalloproteinase-9 (MMP-9) as a Cancer Biomarker and MMP-9 Biosensors: Recent Advances.* Sensors (Basel), 2018. **18**(10).
182. Lengyel, E., et al., *Expression of latent matrix metalloproteinase 9 (MMP-9) predicts survival in advanced ovarian cancer.* Gynecol Oncol, 2001. **82**(2): p. 291-8.
183. Huang, H., *Matrix Metalloproteinase-9 (MMP-9) as a Cancer Biomarker and MMP-9 Biosensors: Recent Advances.* Sensors, 2018. **18**(10): p. 3249.
184. Zhang, Y. and Q. Chen, *Relationship between matrix metalloproteinases and the occurrence and development of ovarian cancer.* Braz J Med Biol Res, 2017. **50**(6): p. e6104.
185. Stamenkovic, I., *Extracellular matrix remodelling: the role of matrix metalloproteinases.* J Pathol, 2003. **200**(4): p. 448-64.
186. Lyu, Y., et al., *Potent delivery of an MMP inhibitor to the tumor microenvironment with thermosensitive liposomes for the suppression of metastasis and angiogenesis.* Signal Transduction and Targeted Therapy, 2019. **4**(1): p. 26.
187. Winer, A., S. Adams, and P. Mignatti, *Matrix Metalloproteinase Inhibitors in Cancer Therapy: Turning Past Failures Into Future Successes.* Molecular Cancer Therapeutics, 2018. **17**(6): p. 1147-1155.

188. *Marimastat: BB 2516, TA 2516.* Drugs R D, 2003. **4**(3): p. 198-203.
189. Naba, A., et al., *The Matrisome: In Silico Definition and In Vivo Characterization by Proteomics of Normal and Tumor Extracellular Matrices *.* Molecular & Cellular Proteomics, 2012. **11**(4).
190. Naba, A., et al., *Characterization of the Extracellular Matrix of Normal and Diseased Tissues Using Proteomics.* Journal of Proteome Research, 2017. **16**(8): p. 3083-3091.
191. Byron, A., J.D. Humphries, and M.J. Humphries, *Defining the extracellular matrix using proteomics.* Int J Exp Pathol, 2013. **94**(2): p. 75-92.
192. Zhang, Y., et al., *Protein Analysis by Shotgun/Bottom-up Proteomics.* Chemical Reviews, 2013. **113**(4): p. 2343-2394.
193. Jones, M.B., et al., *Proteomic analysis and identification of new biomarkers and therapeutic targets for invasive ovarian cancer.* PROTEOMICS, 2002. **2**(1): p. 76-84.
194. Szklarczyk, D., et al., *The STRING database in 2011: functional interaction networks of proteins, globally integrated and scored.* Nucleic Acids Research, 2010. **39**(suppl_1): p. D561-D568.
195. White, N.M., et al., *Quantitative proteomic analysis reveals potential diagnostic markers and pathways involved in pathogenesis of renal cell carcinoma.* Oncotarget, 2014. **5**(2): p. 506-18.
196. Mieulet, V., et al., *Stiffness increases with myofibroblast content and collagen density in mesenchymal high grade serous ovarian cancer.* Sci Rep, 2021. **11**(1): p. 4219.
197. Tothill, R.W., et al., *Novel Molecular Subtypes of Serous and Endometrioid Ovarian Cancer Linked to Clinical Outcome.* Clinical Cancer Research, 2008. **14**(16): p. 5198-5208.
198. Cho, A., V.M. Howell, and E.K. Colvin, *The Extracellular Matrix in Epithelial Ovarian Cancer – A Piece of a Puzzle.* Frontiers in Oncology, 2015. **5**.
199. Pearce, O.M.T., et al., *Deconstruction of a Metastatic Tumor Microenvironment Reveals a Common Matrix Response in Human Cancers.* Cancer Discovery, 2018. **8**(3): p. 304-319.
200. Liu, S., J. Ren, and P. ten Dijke, *Targeting TGFβ signal transduction for cancer therapy.* Signal Transduction and Targeted Therapy, 2021. **6**(1): p. 8.
201. Lecker, L.S.M., et al., *TGFBI Production by Macrophages Contributes to an Immunosuppressive Microenvironment in Ovarian Cancer.* Cancer Research, 2021. **81**(22): p. 5706-5719.
202. Steitz, A.M., et al., *Tumor-associated macrophages promote ovarian cancer cell migration by secreting transforming growth factor beta induced (TGFBI) and tenascin C.* Cell Death Dis, 2020. **11**(4): p. 249.
203. Tarin, D. and C.B. Croft, *Ultrastructural features of wound healing in mouse skin.* J Anat, 1969. **105**(Pt 1): p. 189-90.
204. Gabbiani, G., *The myofibroblast in wound healing and fibrocontractive diseases.* The Journal of Pathology: A Journal of the Pathological Society of Great Britain and Ireland, 2003. **200**(4): p. 500-503.
205. Fukumura, D., et al., *Tumor induction of VEGF promoter activity in stromal cells.* Cell, 1998. **94**(6): p. 715-725.
206. Tomasek, J.J., et al., *Myofibroblasts and mechano-regulation of connective tissue remodelling.* Nature reviews Molecular cell biology, 2002. **3**(5): p. 349-363.

207. Chang, H.Y., et al., *Diversity, topographic differentiation, and positional memory in human fibroblasts.* Proceedings of the National Academy of Sciences, 2002. **99**(20): p. 12877-12882.
208. Yoshida, G.J., *Regulation of heterogeneous cancer-associated fibroblasts: the molecular pathology of activated signaling pathways.* Journal of Experimental & Clinical Cancer Research, 2020. **39**(1): p. 112.
209. Givel, A.-M., et al., *miR200-regulated CXCL12β promotes fibroblast heterogeneity and immunosuppression in ovarian cancers.* Nature Communications, 2018. **9**(1): p. 1056.
210. Nwani, N.G., et al., *Targeting the Microenvironment in High Grade Serous Ovarian Cancer.* Cancers, 2018. **10**(8): p. 266.
211. Gilad, A.A., et al., *Functional and molecular mapping of uncoupling between vascular permeability and loss of vascular maturation in ovarian carcinoma xenografts: The role of stroma cells in tumor angiogenesis.* International Journal of Cancer, 2005. **117**(2): p. 202-211.
212. Balkwill, F.R., M. Capasso, and T. Hagemann, *The tumor microenvironment at a glance.* Journal of Cell Science, 2012. **125**(23): p. 5591-5596.
213. Wang, W., et al., *Effector T Cells Abrogate Stroma-Mediated Chemoresistance in Ovarian Cancer.* Cell, 2016. **165**(5): p. 1092-1105.
214. Zhang, Y., et al., *Ovarian cancer-associated fibroblasts contribute to epithelial ovarian carcinoma metastasis by promoting angiogenesis, lymphangiogenesis and tumor cell invasion.* Cancer Letters, 2011. **303**(1): p. 47-55.
215. Majumder, B., et al., *Predicting clinical response to anticancer drugs using an ex vivo platform that captures tumour heterogeneity.* Nature Communications, 2015. **6**(1): p. 6169.
216. https://www.nature.com/articles/d43747-020-00450-4. *Canscript Company Mitra Biotech*.
217. Pampaloni, F., E.G. Reynaud, and E.H.K. Stelzer, *The third dimension bridges the gap between cell culture and live tissue.* Nature Reviews Molecular Cell Biology, 2007. **8**(10): p. 839-845.
218. Cunnea, P. and E.A. Stronach, *Modeling Platinum Sensitive and Resistant High-Grade Serous Ovarian Cancer: Development and Applications of Experimental Systems.* Frontiers in Oncology, 2014. **4**.
219. Haycock, J.W., *3D Cell Culture: A Review of Current Approaches and Techniques*, in *3D cell culture*. 2011, Springer.
220. Langhans, S.A., *Three-Dimensional in Vitro Cell Culture Models in Drug Discovery and Drug Repositioning.* Frontiers in Pharmacology, 2018. **9**(6).
221. Breslin, S. and L. O'Driscoll, *Three-dimensional cell culture: the missing link in drug discovery.* Drug Discov Today, 2013. **18**(5-6): p. 240-9.
222. Lee, G.Y., et al., *Three-dimensional culture models of normal and malignant breast epithelial cells.* Nature methods, 2007. **4**(4): p. 359-365.
223. Cavo, M., et al., *Microenvironment complexity and matrix stiffness regulate breast cancer cell activity in a 3D in vitro model.* Scientific Reports, 2016. **6**(1): p. 35367.
224. Melissaridou, S., et al., *The effect of 2D and 3D cell cultures on treatment response, EMT profile and stem cell features in head and neck cancer.* Cancer Cell International, 2019. **19**(1): p. 16.

225. Kenny, P.A., et al., *The morphologies of breast cancer cell lines in three-dimensional assays correlate with their profiles of gene expression.* Molecular Oncology, 2007. **1**(1): p. 84-96.
226. Myungjin Lee, J., et al., *A three-dimensional microenvironment alters protein expression and chemosensitivity of epithelial ovarian cancer cells in vitro.* Laboratory Investigation, 2013. **93**(5): p. 528-542.
227. Hoarau-Véchot, J., et al., *Halfway between 2D and Animal Models: Are 3D Cultures the Ideal Tool to Study Cancer-Microenvironment Interactions?* International Journal of Molecular Sciences, 2018. **19**: p. 181.
228. Meijer, T.G., et al., *Ex vivo tumor culture systems for functional drug testing and therapy response prediction.* Future Science OA, 2017. **3**(2): p. FSO190.
229. Reid, J.A., et al., *Consistent and reproducible cultures of large-scale 3D mammary epithelial structures using an accessible bioprinting platform.* Breast Cancer Research, 2018. **20**(1): p. 122.
230. Chen, C., et al., *A matrigel-free method to generate matured human cerebral organoids using 3D-Printed microwell arrays.* Bioactive Materials, 2021. **6**(4): p. 1130-1139.
231. Heredia-Soto, V., et al., *High-throughput 3-dimensional culture of epithelial ovarian cancer cells as preclinical model of disease.* Oncotarget, 2018. **9**(31): p. 21893-21903.
232. Liu, S., et al., *A Novel Controlled PTEN-Knockout Mouse Model for Prostate Cancer Study.* Frontiers in Molecular Biosciences, 2021. **8**.
233. Kenny, H.A., et al., *Use of a novel 3D culture model to elucidate the role of mesothelial cells, fibroblasts and extra-cellular matrices on adhesion and invasion of ovarian cancer cells to the omentum.* Int J Cancer, 2007. **121**(7): p. 1463-72.
234. Zanoni, M., et al., *Modeling neoplastic disease with spheroids and organoids.* Journal of Hematology & Oncology, 2020. **13**(1): p. 97.
235. Lee, G.Y., et al., *Three-dimensional culture models of normal and malignant breast epithelial cells.* Nat Methods, 2007. **4**(4): p. 359-65.
236. Elias, K.M., et al., *Beyond genomics: Critical evaluation of cell line utility for ovarian cancer research.* Gynecologic Oncology, 2015. **139**(1): p. 97-103.
237. Domcke, S., et al., *Evaluating cell lines as tumour models by comparison of genomic profiles.* Nature Communications, 2013. **4**(1): p. 2126.
238. Miserocchi, G., et al., *Management and potentialities of primary cancer cultures in preclinical and translational studies.* Journal of Translational Medicine, 2017. **15**(1): p. 229.
239. Nelson, L., et al., *A living biobank of ovarian cancer ex vivo models reveals profound mitotic heterogeneity.* Nature Communications, 2020. **11**(1): p. 822.
240. Ravi, M., et al., *3D Cell Culture Systems: Advantages and Applications.* Journal of Cellular Physiology, 2015. **230**(1): p. 16-26.
241. Cen, L., et al., *Collagen Tissue Engineering: Development of Novel Biomaterials and Applications.* Pediatric Research, 2008. **63**(5): p. 492-496.
242. Chaudhuri, O., *Viscoelastic hydrogels for 3D cell culture.* Biomaterials Science, 2017. **5**(8): p. 1480-1490.
243. Hofer, M. and M.P. Lutolf, *Engineering organoids.* Nat Rev Mater, 2021. **6**(5): p. 402-420.
244. Correia, I., *Spheroids Formation on Non-Adhesive Surfaces by Liquid Overlay Technique: Considerations and Practical Approaches.* Biotechnology Journal, 2017.

245. Wan, X., et al., *Three-dimensional perfused tumour spheroid model for anti-cancer drug screening.* Biotechnology Letters, 2016. **38**(8): p. 1389-1395.
246. Weber, G.F., M.A. Bjerke, and D.W. DeSimone, *Integrins and cadherins join forces to form adhesive networks.* J Cell Sci, 2011. **124**(Pt 8): p. 1183-93.
247. Cui, X., Y. Hartanto, and H. Zhang, *Advances in multicellular spheroids formation.* Journal of The Royal Society Interface, 2017. **14**(127): p. 20160877.
248. Ding, Y., et al., *Molecular characteristics and tumorigenicity of ascites-derived tumor cells: mitochondrial oxidative phosphorylation as a novel therapy target in ovarian cancer.* Mol Oncol, 2021. **15**(12): p. 3578-3595.
249. Boylan, K.L.M., et al., *Inhibition of Ovarian Cancer Cell Spheroid Formation by Synthetic Peptides Derived from Nectin-4.* International journal of molecular sciences, 2020. **21**(13): p. 4637.
250. Velletri, T., et al., *Single cell-derived spheroids capture the self-renewing subpopulations of metastatic ovarian cancer.* Cell Death & Differentiation, 2022. **29**(3): p. 614-626.
251. Martins, F.C., et al., *Clonal somatic copy number altered driver events inform drug sensitivity in high-grade serous ovarian cancer.* Nature Communications, 2022. **13**(1): p. 6360.
252. Tofani, L.B., et al., *Generation of a Three-Dimensional in Vitro Ovarian Cancer Co-Culture Model for Drug Screening Assays.* J Pharm Sci, 2021. **110**(7): p. 2629-2636.
253. Clevers, H., *Modeling Development and Disease with Organoids.* Cell, 2016. **165**(7): p. 1586-1597.
254. Drost, J. and H. Clevers, *Organoids in cancer research.* Nature Reviews Cancer, 2018. **18**(7): p. 407-418.
255. Kim, J., B.-K. Koo, and J.A. Knoblich, *Human organoids: model systems for human biology and medicine.* Nature Reviews Molecular Cell Biology, 2020. **21**(10): p. 571-584.
256. Simian, M. and M.J. Bissell, *Organoids: A historical perspective of thinking in three dimensions.* The Journal of cell biology, 2017. **216**(1): p. 31-40.
257. Kopper, O., et al., *An organoid platform for ovarian cancer captures intra- and interpatient heterogeneity.* Nature Medicine, 2019. **25**(5): p. 838-849.
258. de Witte, C.J., et al., *Patient-Derived Ovarian Cancer Organoids Mimic Clinical Response and Exhibit Heterogeneous Inter- and Intrapatient Drug Responses.* Cell Rep, 2020. **31**(11): p. 107762.
259. Nanki, Y., et al., *Patient-derived ovarian cancer organoids capture the genomic profiles of primary tumours applicable for drug sensitivity and resistance testing.* Scientific Reports, 2020. **10**(1): p. 12581.
260. Hayden, P.J. and J.W. Harbell, *Special review series on 3D organotypic culture models: Introduction and historical perspective.* In Vitro Cellular & Developmental Biology - Animal, 2021. **57**(2): p. 95-103.
261. Kenny, H.A., et al., *Organotypic models of metastasis: A three-dimensional culture mimicking the human peritoneum and omentum for the study of the early steps of ovarian cancer metastasis.* Cancer Treat Res, 2009. **149**: p. 335-51.
262. Krumdieck, C.L., J. dos Santos, and K.-J. Ho, *A new instrument for the rapid preparation of tissue slices.* Analytical Biochemistry, 1980. **104**(1): p. 118-123.

263. Hickman, J.A., et al., *Three-dimensional models of cancer for pharmacology and cancer cell biology: Capturing tumor complexity in vitro/ex vivo.* Biotechnology Journal, 2014. **9**(9): p. 1115-1128.
264. van der Kuip, H., et al., *Short term culture of breast cancer tissues to study the activity of the anticancer drug taxol in an intact tumor environment.* BMC Cancer, 2006. **6**(1): p. 86.
265. Holliday, D.L., et al., *The practicalities of using tissue slices as preclinical organotypic breast cancer models.* Journal of Clinical Pathology, 2013. **66**(3): p. 253-255.
266. Gavert, N., et al., *Ex vivo organotypic cultures for synergistic therapy prioritization identify patient-specific responses to combined MEK and Src inhibition in colorectal cancer.* Nat Cancer, 2022. **3**(2): p. 219-231.
267. Meijer, T.G., et al., *Functional Ex Vivo Assay Reveals Homologous Recombination Deficiency in Breast Cancer Beyond BRCA Gene Defects.* Clin Cancer Res, 2018. **24**(24): p. 6277-6287.
268. van Wijk, L.M., et al., *The RECAP Test Rapidly and Reliably Identifies Homologous Recombination-Deficient Ovarian Carcinomas.* Cancers (Basel), 2020. **12**(10).
269. Weitz, J., et al., *An Ex Vivo Organotypic Culture Platform for Functional Interrogation of Human Appendiceal Cancer Reveals a Prominent and Heterogenous Immunological Landscape.* Clinical Cancer Research, 2022. **28**(21): p. 4793-4806.
270. Garcia-Garcia, F.C., et al., *Microfluidic technologies for ex vivo tissue biopsies: A review.* Organs-on-a-Chip, 2022. **4**: p. 100020.
271. Yoshida, G.J., *Applications of patient-derived tumor xenograft models and tumor organoids.* Journal of Hematology & Oncology, 2020. **13**(1): p. 4.
272. Tentler, J.J., et al., *Patient-derived tumour xenografts as models for oncology drug development.* Nature Reviews Clinical Oncology, 2012. **9**(6): p. 338-350.
273. Evans, K.W., et al., *A Population of Heterogeneous Breast Cancer Patient-Derived Xenografts Demonstrate Broad Activity of PARP Inhibitor in BRCA1/2 Wild-Type Tumors.* Clinical Cancer Research, 2017. **23**(21): p. 6468-6477.
274. Neufeld, L., et al., *3D bioprinted cancer models: from basic biology to drug development.* Nature Reviews Cancer, 2022.
275. Shi, J., et al., *The fidelity of cancer cells in PDX models: Characteristics, mechanism and clinical significance.* International Journal of Cancer, 2020. **146**(8): p. 2078-2088.
276. Cybula, M., et al., *Patient-Derived Xenografts of High-Grade Serous Ovarian Cancer Subtype as a Powerful Tool in Pre-Clinical Research.* Cancers (Basel), 2021. **13**(24).
277. Vázquez-García, I., et al., *Ovarian cancer mutational processes drive site-specific immune evasion.* Nature, 2022.
278. Sehouli, J., et al., *["IMO"--intraoperative mapping of ovarian cancer].* Zentralbl Gynakol, 2003. **125**(3-4): p. 129-35.
279. Thompson, A., et al., *Tandem Mass Tags: A Novel Quantification Strategy for Comparative Analysis of Complex Protein Mixtures by MS/MS.* Analytical Chemistry, 2003. **75**(8): p. 1895-1904.
280. Dao, F., et al., *Characteristics of 10-year survivors of high-grade serous ovarian carcinoma.* Gynecol Oncol, 2016. **141**(2): p. 260-263.
281. Fotopoulou, C., et al., *Quality indicators for advanced ovarian cancer surgery from the European Society of Gynaecological Oncology (ESGO): 2020 update.* Int J Gynecol Cancer, 2020. **30**(4): p. 436-440.

282. Miller, R.E., et al., *ESMO recommendations on predictive biomarker testing for homologous recombination deficiency and PARP inhibitor benefit in ovarian cancer.* Ann Oncol, 2020. **31**(12): p. 1606-1622.
283. Ledermann, J., et al., *Olaparib Maintenance Therapy in Platinum-Sensitive Relapsed Ovarian Cancer.* New England Journal of Medicine, 2012. **366**(15): p. 1382-1392.
284. Ledermann, J., et al., *Olaparib maintenance therapy in patients with platinum-sensitive relapsed serous ovarian cancer: a preplanned retrospective analysis of outcomes by BRCA status in a randomised phase 2 trial.* The Lancet Oncology, 2014. **15**(8): p. 852-861.
285. Coleman, R.L., et al., *Rucaparib maintenance treatment for recurrent ovarian carcinoma after response to platinum therapy (ARIEL3): a randomised, double-blind, placebo-controlled, phase 3 trial.* The Lancet, 2017. **390**(10106): p. 1949-1961.
286. Jiménez-Sánchez, A., et al., *Unraveling tumor-immune heterogeneity in advanced ovarian cancer uncovers immunogenic effect of chemotherapy.* Nat Genet, 2020. **52**(6): p. 582-593.
287. McPherson, A., et al., *Divergent modes of clonal spread and intraperitoneal mixing in high-grade serous ovarian cancer.* Nat Genet, 2016. **48**(7): p. 758-67.
288. Schwarz, R.F., et al., *Spatial and temporal heterogeneity in high-grade serous ovarian cancer: a phylogenetic analysis.* PLoS Med, 2015. **12**(2): p. e1001789.
289. Soliman, N.A. and S.M. Yussif, *Ki-67 as a prognostic marker according to breast cancer molecular subtype.* Cancer Biol Med, 2016. **13**(4): p. 496-504.
290. Chen, M., et al., *The prognostic value of Ki67 in ovarian high-grade serous carcinoma: an 11-year cohort study of Chinese patients.* Oncotarget, 2017. **8**(64): p. 107877-107885.
291. McKinnon, K.M., *Flow Cytometry: An Overview.* Curr Protoc Immunol, 2018. **120**: p. 5.1.1-5.1.11.
292. Yang, Y., et al., *Tumor Microenvironment in Ovarian Cancer: Function and Therapeutic Strategy.* Frontiers in Cell and Developmental Biology, 2020. **8**.
293. Lukashev, M.E. and Z. Werb, *ECM signalling: orchestrating cell behaviour and misbehaviour.* Trends in Cell Biology, 1998. **8**(11): p. 437-441.
294. Huang, J., et al., *Extracellular matrix and its therapeutic potential for cancer treatment.* Signal Transduction and Targeted Therapy, 2021. **6**(1): p. 153.
295. Spivey, K.A. and J. Banyard, *A prognostic gene signature in advanced ovarian cancer reveals a microfibril-associated protein (MAGP2) as a promoter of tumor cell survival and angiogenesis.* Cell Adh Migr, 2010. **4**(2): p. 169-71.
296. Lecker, L.S.M., et al., *TGFBI Production by Macrophages Contributes to an Immunosuppressive Microenvironment in Ovarian Cancer.* Cancer Res, 2021. **81**(22): p. 5706-5719.
297. Chaves, D.F.S., et al., *Comparative Proteomic Analysis of the Aging Soleus and Extensor Digitorum Longus Rat Muscles Using TMT Labeling and Mass Spectrometry.* Journal of Proteome Research, 2013. **12**(10): p. 4532-4546.
298. Wang, H., S. Alvarez, and L.M. Hicks, *Comprehensive Comparison of iTRAQ and Label-free LC-Based Quantitative Proteomics Approaches Using Two Chlamydomonas reinhardtii Strains of Interest for Biofuels Engineering.* Journal of Proteome Research, 2012. **11**(1): p. 487-501.

299. Seitz, H.K. and F. Stickel, *Acetaldehyde as an underestimated risk factor for cancer development: role of genetics in ethanol metabolism.* Genes Nutr, 2010. **5**(2): p. 121-8.
300. Yang, J., et al., *Integrated analysis of microfibrillar-associated proteins reveals MFAP4 as a novel biomarker in human cancers.* Epigenomics, 2019. **11**(1): p. 5-21.
301. Naba, A., et al., *Characterization of the Extracellular Matrix of Normal and Diseased Tissues Using Proteomics.* J Proteome Res, 2017. **16**(8): p. 3083-3091.
302. Naba, A., et al., *The extracellular matrix: Tools and insights for the "omics" era.* Matrix Biology, 2016. **49**: p. 10-24.
303. Shao, X., et al., *MatrisomeDB: the ECM-protein knowledge database.* Nucleic Acids Research, 2020. **48**(D1): p. D1136-D1144.
304. van Huizen, N.A., et al., *Collagen analysis with mass spectrometry.* Mass Spectrometry Reviews, 2020. **39**(4): p. 309-335.
305. Xu, S., et al., *The role of collagen in cancer: from bench to bedside.* Journal of Translational Medicine, 2019. **17**(1): p. 309.
306. Sherman-Baust, C.A., et al., *Remodeling of the extracellular matrix through overexpression of collagen VI contributes to cisplatin resistance in ovarian cancer cells.* Cancer Cell, 2003. **3**(4): p. 377-386.
307. Tanjore, H. and R. Kalluri, *The role of type IV collagen and basement membranes in cancer progression and metastasis.* Am J Pathol, 2006. **168**(3): p. 715-7.
308. Chen, P., M. Cescon, and P. Bonaldo, *Collagen VI in cancer and its biological mechanisms.* Trends in Molecular Medicine, 2013. **19**(7): p. 410-417.
309. Kenny, H.A., et al., *Mesothelial cells promote early ovarian cancer metastasis through fibronectin secretion.* The Journal of Clinical Investigation, 2014. **124**(10): p. 4614-4628.
310. *Three-Dimensional Cell Culture Systems and Their Applications in Drug Discovery and Cell-Based Biosensors.* ASSAY and Drug Development Technologies, 2014. **12**(4): p. 207-218.
311. Bousquet, J. and J.M. Meunier, *[Organotypic culture, on natural and artificial media, of fragments of the adult rat hypophysis].* Comptes rendus des seances de la Societe de biologie et de ses filiales, 1962. **156**: p. 65-67.
312. Tacha, D., D. Zhou, and L. Cheng, *Expression of PAX8 in normal and neoplastic tissues: a comprehensive immunohistochemical study.* Appl Immunohistochem Mol Morphol, 2011. **19**(4): p. 293-9.
313. Li, L.T., et al., *Ki67 is a promising molecular target in the diagnosis of cancer (Review).* Mol Med Rep, 2015. **11**(3): p. 1566-1572.
314. Gown, A.M. and M.C. Willingham, *Improved Detection of Apoptotic Cells in Archival Paraffin Sections: Immunohistochemistry Using Antibodies to Cleaved Caspase 3.* Journal of Histochemistry & Cytochemistry, 2002. **50**(4): p. 449-454.
315. Misra, S., et al., *Ex vivo organotypic culture system of precision-cut slices of human pancreatic ductal adenocarcinoma.* Sci Rep, 2019. **9**(1): p. 2133.
316. Kokkinos, J., et al., *Ex vivo culture of intact human patient derived pancreatic tumour tissue.* Scientific Reports, 2021. **11**(1): p. 1944.
317. du Bois, A., et al., *Role of surgical outcome as prognostic factor in advanced epithelial ovarian cancer: a combined exploratory analysis of 3 prospectively randomized phase 3 multicenter trials: by the Arbeitsgemeinschaft Gynaekologische Onkologie Studiengruppe Ovarialkarzinom (AGO-OVAR) and the Groupe d'Investigateurs*

Nationaux Pour les Etudes des Cancers de l'Ovaire (GINECO). Cancer, 2009. **115**(6): p. 1234-44.
318. Cooke, S.L., et al., *Genomic analysis of genetic heterogeneity and evolution in high-grade serous ovarian carcinoma.* Oncogene, 2010. **29**(35): p. 4905-4913.
319. Dorayappan, K.D.P., et al., *A Microfluidic Chip Enables Isolation of Exosomes and Establishment of Their Protein Profiles and Associated Signaling Pathways in Ovarian Cancer.* Cancer Research, 2019. **79**(13): p. 3503-3513.
320. Gorski, J.W., F.R. Ueland, and J.M. Kolesar, *CCNE1 Amplification as a Predictive Biomarker of Chemotherapy Resistance in Epithelial Ovarian Cancer.* Diagnostics (Basel), 2020. **10**(5).
321. Sallinen, H., et al., *Comparative transcriptome analysis of matched primary and distant metastatic ovarian carcinoma.* BMC Cancer, 2019. **19**(1): p. 1121.
322. Masoodi, T., et al., *Genetic heterogeneity and evolutionary history of high-grade ovarian carcinoma and matched distant metastases.* Br J Cancer, 2020. **122**(8): p. 1219-1230.
323. Gerlinger, M., et al., *Intratumor Heterogeneity and Branched Evolution Revealed by Multiregion Sequencing.* New England Journal of Medicine, 2012. **366**(10): p. 883-892.
324. Vázquez-García, I., et al., *Immune and malignant cell phenotypes of ovarian cancer are determined by distinct mutational processes.* bioRxiv, 2021: p. 2021.08.24.454519.
325. Sehouli, J., et al., *["IMO"--intraoperative mapping of ovarian cancer].* Zentralbl Gynakol, 2003. **125**(3-4): p. 129-35.
326. Sehouli, J., et al., *Intra-abdominal tumor dissemination pattern and surgical outcome in 214 patients with primary ovarian cancer.* J Surg Oncol., 2009. **99**.
327. Nowacka, M., et al., *Drug resistance evaluation in novel 3D in vitro model.* Biomedicine & Pharmacotherapy, 2021. **138**: p. 111536.
328. Lal-Nag, M., et al., *A High-Throughput Screening Model of the Tumor Microenvironment for Ovarian Cancer Cell Growth.* SLAS DISCOVERY: Advancing the Science of Drug Discovery, 2017. **22**(5): p. 494-506.
329. Nims, R.W. and Y. Reid, *Best practices for authenticating cell lines.* In Vitro Cellular & Developmental Biology - Animal, 2017. **53**(10): p. 880-887.
330. Kenny, H.A., et al., *Quantitative High-Throughput Screening Using an Organotypic Model Identifies Compounds that Inhibit Ovarian Cancer Metastasis.* Mol Cancer Ther, 2020. **19**(1): p. 52-62.
331. Malacrida, B., et al., *A human multi-cellular model shows how platelets drive production of diseased extracellular matrix and tissue invasion.* iScience, 2021. **24**(6): p. 102676.
332. Öhlund, D., et al., *Type IV collagen stimulates pancreatic cancer cell proliferation, migration, and inhibits apoptosis through an autocrine loop.* BMC Cancer, 2013. **13**(1): p. 154.
333. Anttila, M., et al., *Clinical significance of alpha-catenin, collagen IV, and Ki-67 expression in epithelial ovarian cancer.* J Clin Oncol, 1998. **16**(8): p. 2591-600.
334. Tucker, S.L., et al., *Molecular biomarkers of residual disease after surgical debulking of high-grade serous ovarian cancer.* Clin Cancer Res, 2014. **20**(12): p. 3280-8.
335. Jelski, W., et al., *Alcohol dehydrogenase isoenzymes and aldehyde dehydrogenase activity in the sera of patients with esophageal cancer.* Clinical and Experimental Medicine, 2009. **9**(2): p. 131-137.

336. Ong, S.L.M., et al., *Microfibril-associated glycoprotein 4 (Mfap4) regulates haematopoiesis in zebrafish.* Scientific Reports, 2020. **10**(1): p. 11801.
337. Zhao, H., et al., *High Expression Levels of AGGF1 and MFAP4 Predict Primary Platinum-Based Chemoresistance and are Associated with Adverse Prognosis in Patients with Serous Ovarian Cancer.* J Cancer, 2019. **10**(2): p. 397-407.
338. Chang, P.Y., et al., *An epigenetic signature of adhesion molecules predicts poor prognosis of ovarian cancer patients.* Oncotarget, 2017. **8**(32): p. 53432-53449.

9 Appendix

Table 9.1 Summary table of all patient sample and clinical data: *including tumour sample sites, IMO locations and corresponding abdominal region, status after first line treatment, stage and residual disease after primary debulking.*

patient ID	tissue site	IMO	Abdominal Region	status	stage	residual disease
T13-097	bladder	B1	lower abdomen	Resistant	IV	no
T13-097	omentum	B2	middle abdomen	Resistant		
T13-097	spleen	C3	upper abdomen	Resistant		
T13-097	rectum	B1	lower abdomen	Resistant		
T13-097	ovary	B1	lower abdomen	Resistant		
T13-097	paraaortic LN	B2	middle abdomen	Resistant		
T13-097	bladder	B1	lower abdomen	Resistant		
T13-097	small bowel	B2	middle abdomen	Resistant		
T14-003	ovary	B1	lower abdomen	Sensitive	IIIC	no
T14-003	omentum	B2	middle abdomen	Sensitive		
T14-003	mesentery	B2	middle abdomen	Sensitive		
T14-003	right paracolic	A2	middle abdomen	Sensitive		
T14-003	peritoneum	B1	lower abdomen	Sensitive		
T14-003	left paracolic	C2	middle abdomen	Sensitive		
T14-003	omentum bursa	B2	middle abdomen	Sensitive		
T14-003	left colic	C3	upper abdomen	Sensitive		
T14-003	ascites	N/A	N/A	Sensitive		
T14-012	ovary	B1	lower abdomen	Resistant	IIIC	no
T14-012	right diaphragm	A3	upper abdomen	Resistant		
T14-012	liver capsule	A3	upper abdomen	Resistant		
T14-012	peritoneum	B1	lower abdomen	Resistant		
T14-012	falciform ligament	A3	upper abdomen	Resistant		
T14-028	right pelvic wall	A1	lower abdomen	No relapse	IIIC	no
T14-028	right diaphragm	A3	upper abdomen	No relapse		
T14-028	large bowel	B2	middle abdomen	No relapse		
T14-028	omentum	B2	middle abdomen	No relapse		
T14-028	diaphragm	A3	upper abdomen	No relapse		
T14-028	left pelvic wall	C1	lower abdomen	No relapse		
T14-028	mesentery	B2	middle abdomen	No relapse		
T14-028	rectum	B1	lower abdomen	No relapse		

T14-045	falciform ligament	B3	upper abdomen	Sensitive	IIIC	no
T14-045	right diaphragm	A3	upper abdomen	Sensitive		
T14-045	right ovary	B1	lower abdomen	Sensitive		
T14-045	omentum	B2	middle abdomen	Sensitive		
T14-045	spleen	C3	upper abdomen	Sensitive		
T14-045	paracolic	B2	middle abdomen	Sensitive		
T14-051	rectum	B1	lower abdomen	No relapse	IIIC	no
T14-051	vagina	B1	lower abdomen	No relapse		
T14-051	ovary	B1	lower abdomen	No relapse		
T14-051	left pelvic wall	C1	lower abdomen	No relapse		
T14-051	right ovary	B1	lower abdomen	No relapse		
T14-051	pouch of douglas	B1	lower abdomen	No relapse		
T14-055	para aortic ln	B2	middle abdomen	Sensitive	IIIC	no
T14-055	omentum	B2	middle abdomen	Sensitive		
T14-055	ovary	B1	lower abdomen	Sensitive		
T14-055	left ovary	B1	lower abdomen	Sensitive		
T14-055	stomach	B1	lower abdomen	Sensitive		
T14-055	mesenteric root	B2	middle abdomen	Sensitive		
T14-055	left paracolic	C2	middle abdomen	Sensitive		
T14-055	rectum	B1	lower abdomen	Sensitive		
T14-055	bladder peritoneum	B1	lower abdomen	Sensitive		
T14-055	abdominal wall	B2	middle abdomen	Sensitive		
T14-055	left abdominal wall	C2	middle abdomen	Sensitive		
T14-064	mesentery	B2	middle abdomen	Sensitive	IIIA	no
T14-064	left infra renal	B2	middle abdomen	Sensitive		
T14-064	ovary	B1	lower abdomen	Sensitive		
T14-064	omentum	B2	middle abdomen	Sensitive		
T14-064	renal capsule	B2	middle abdomen	Sensitive		
T14-092	diaphragm	A3	upper abdomen	Resistant	IIIC	no
T14-092	mesentery	B2	middle abdomen	Resistant		
T14-092	omentum	B2	middle abdomen	Resistant		
T14-092	sigmoid	B1	lower abdomen	Resistant		
T14-092	spleen	C3	upper abdomen	Resistant		
T14-092	ascites	N/A	N/A	Resistant		
T14-093	caecum	A1	lower abdomen	Sensitive	IIIC	no
T14-093	diaphragm	A3	upper abdomen	Sensitive		
T14-093	omentum	B2	middle abdomen	Sensitive		

T14-093	ovary	B1	lower abdomen	Sensitive		
T14-093	paracolic	A2	middle abdomen	Sensitive		
T14-093	omentum	B2	middle abdomen	Sensitive		
T14-093	right paracolic	A2	middle abdomen	Sensitive		
T14-093	mesenteric root	B2	middle abdomen	Sensitive		
T14-093	duodenum	B2	middle abdomen	Sensitive		
T14-093	sigmoid	C1	lower abdomen	Sensitive		
T14-107	spleen	C3	upper abdomen	Sensitive	IV	no
T14-107	ovary	B1	lower abdomen	Sensitive		
T14-107	right pelvic ln	A1	lower abdomen	Sensitive		
T14-107	omentum	B2	middle abdomen	Sensitive		
T14-107	caecum	A1	lower abdomen	Sensitive		
T14-125	omentum	B2	middle abdomen	Sensitive	IIIB	no
T14-125	right ovary	B1	lower abdomen	Sensitive		
T14-125	left ovary	B1	lower abdomen	Sensitive		
T14-125	diaphragm	A3	upper abdomen	Sensitive		
T14-125	paracolic	A2	middle abdomen	Sensitive		
T14-125	right abdominal wall	A2	middle abdomen	Sensitive		
T14-137	ovary	B1	lower abdomen	Sensitive	IIIC	no
T14-137	omentum	B2	middle abdomen	Sensitive		
T14-137	diaphragm	A3	upper abdomen	Sensitive		
T14-137	right pelvic side wall	B1	lower abdomen	Sensitive		
T14-137	rectum	B1	lower abdomen	Sensitive		
T14-137	liver capsule	A3	upper abdomen	Sensitive		
T15-022	left diaphragm	A1	upper abdomen	Sensitive	IIIC	no
T15-022	bladder	B1	lower abdomen	Sensitive		
T15-022	ovary	B1	lower abdomen	Sensitive		
T15-022	omentum	B2	middle abdomen	Sensitive		
T15-022	rectum	B1	lower abdomen	Sensitive		
T15-022	renal capsule	B2	middle abdomen	Sensitive		
T15-022	spleen	C3	upper abdomen	Sensitive		
T15-022	liver capsule	A3	upper abdomen	Sensitive		
T15-033	omentum	B2	middle abdomen	Sensitive	IV	no
T15-033	right diaphragm	A3	upper abdomen	Sensitive		
T15-033	liver capsule	A3	upper abdomen	Sensitive		
T15-033	sigmoid	B1	lower abdomen	Sensitive		
T15-033	ovary	B1	lower abdomen	Sensitive		
T15-033	left diaphragm	A1	upper abdomen	Sensitive		
T15-033	bladder peritoneum	B1	lower abdomen	Sensitive		
T15-033	abdominal wall	B2	middle abdomen	Sensitive		

T15-033	spleen	C3	upper abdomen	Sensitive		
T15-033	mesenteric root	B2	middle abdomen	Sensitive		
T15-043	right diaphragm	A3	upper abdomen	Sensitive	IIIC	no
T15-043	left paracolic	A2	middle abdomen	Sensitive		
T15-043	sigmoid	B1	lower abdomen	Sensitive		
T15-043	ovary	B1	lower abdomen	Sensitive		
T15-043	omentum	B2	middle abdomen	Sensitive		
T15-043	bladder peritoneum	B1	lower abdomen	Sensitive		
T15-043	posterior gastric wall	B3	upper abdomen	Sensitive		
T15-043	rectum	B1	lower abdomen	Sensitive		
T15-043	mesentery	B2	middle abdomen	Sensitive		
T15-058	mesentery	B2	middle abdomen	Sensitive	IIIC	no
T15-058	omental bursa	B2	middle abdomen	Sensitive		
T15-058	ovary	B1	lower abdomen	Sensitive		
T15-058	rectum	B1	lower abdomen	Sensitive		
T15-058	spleen	C3	upper abdomen	Sensitive		
T15-058	diaphragm	A3	upper abdomen	Sensitive		
T15-058	omentum	B2	middle abdomen	Sensitive		
T15-058	bladder	B1	lower abdomen	Sensitive		
T15-058	diaphragm	A3	upper abdomen	Sensitive		
T15-085	ovary	B1	lower abdomen	Sensitive	IIIC	no
T15-085	omentum	B2	middle abdomen	Sensitive		
T15-085	diaphragm	A3	upper abdomen	Sensitive		
T15-085	bladder	B1	lower abdomen	Sensitive		
T15-085	uterus	B1	lower abdomen	Sensitive		
T15-086	ovary	B1	lower abdomen	Sensitive	IIIC	yes
T15-086	omentum	B2	middle abdomen	Sensitive		
T15-086	diaphragm	A3	upper abdomen	Sensitive		
T15-086	mesentery	B2	middle abdomen	Sensitive		
T15-086	sigmoid	B1	lower abdomen	Sensitive		
T15-086	renal capsule	B2	middle abdomen	Sensitive		
T15-086	bladder peritoneum	B1	lower abdomen	Sensitive		
T15-086	ileocaecal area	A2	middle abdomen	Sensitive		
T15-088	omentum	B2	middle abdomen	Resistant	IVB	no
T15-088	diaphragm	A3	upper abdomen	Resistant		
T15-088	porta hepatis	A3	upper abdomen	Resistant		
T15-088	mesentery	B2	middle abdomen	Resistant		
T15-088	ovary	B1	lower abdomen	Resistant		
T15-088	uterus	B1	lower abdomen	Resistant		
T15-088	left paracolic	C2	middle abdomen	Resistant		

T15-088	right paracolic	A2	middle abdomen	Resistant		
T15-088	small bowel	B2	middle abdomen	Resistant		
T15-088	bladder peritoneum	B1	lower abdomen	Resistant		
T15-088	rectum	B1	lower abdomen	Resistant		
T15-088	rectum (second sample)	B1	lower abdomen	Resistant		
T15-088	lesser sac	B3	upper abdomen	Resistant		
T15-164	ovary	B1	lower abdomen	Resistant	IIIC	no
T15-164	central diaphragm	B3	upper abdomen	Resistant		
T15-164	left colic flexure	C2	middle abdomen	Resistant		
T15-164	spleen	C3	upper abdomen	Resistant		
T15-164	pelvic peritoneum	B1	lower abdomen	Resistant		
T15-164	bladder peritoneum	B1	lower abdomen	Resistant		
T15-164	right paracolic	A2	middle abdomen	Resistant		
T15-164	left paracolic	C2	middle abdomen	Resistant		
T15-164	rectosigmoid	B1	lower abdomen	Resistant		
T15-164	ascites	N/A	N/A	Resistant		
T15-164	large bowel mesentery	B2	middle abdomen	Resistant		
T16-046	mesenteric root	B2	middle abdomen	Resistant	IV	no
T16-046	small bowel mesentery	B2	middle abdomen	Resistant		
T16-046	ovary	B1	lower abdomen	Resistant		
T16-046	omentum	B2	middle abdomen	Resistant		
T16-046	pancreas	B2	middle abdomen	Resistant		
T16-046	liver capsule	A3	upper abdomen	Resistant		
T16-046	caecum	A1	lower abdomen	Resistant		
T16-046	pelvic peritoneum	B1	lower abdomen	Resistant		
T16-046	Rectosigmoid	B1	lower abdomen	Resistant		
T16-046	ascites	N/A	N/A	Resistant		
T16-060	omentum	B2	middle abdomen	Sensitive	IVA	no
T16-060	omentum	B2	middle abdomen	Sensitive		
T16-060	right ovary	B1	lower abdomen	Sensitive		
T16-060	left diaphragm	A3	upper abdomen	Sensitive		
T16-060	right diaphragm	A3	upper abdomen	Sensitive		
T16-060	liver capsule	A3	upper abdomen	Sensitive		
T16-060	right paracolic	A2	middle abdomen	Sensitive		
T16-060	left paracolic	B2	middle abdomen	Sensitive		
T16-060	pelvic peritoneum	B1	lower abdomen	Sensitive		
T16-060	ascites	N/A	N/A	Sensitive		

T16-133	ovary	B1	lower abdomen	Resistant	IV	yes <1cm
T16-133	mesentery	B2	middle abdomen	Resistant		
T16-133	right diaphragm	A3	upper abdomen	Resistant		
T16-133	lesser sac	B2	middle abdomen	Resistant		
T16-133	omentum	B2	middle abdomen	Resistant		
T16-133	bladder peritoneum	B1	lower abdomen	Resistant		
T16-133	falciform ligament	A3	upper abdomen	Resistant		
T16-133	subhepatic	A3	upper abdomen	Resistant		
T16-133	right pelvic wall	A1	lower abdomen	Resistant		
T16-133	sigmoid	C1	lower abdomen	Resistant		
T16-133	ascites	N/A	N/A	Resistant		
T16-156	ovary	B1	lower abdomen	Resistant	IV	no
T16-156	paracolic	A2	middle abdomen	Resistant		
T16-156	small bowel mesentery	B2	middle abdomen	Resistant		
T16-156	omentum	B2	middle abdomen	Resistant		
T16-156	diaphragm	A3	upper abdomen	Resistant		
T16-186	ovary	B1	lower abdomen	Sensitive	IV	no
T16-186	omentum	B2	middle abdomen	Sensitive		
T16-186	diaphragm	A3	upper abdomen	Sensitive		
T16-198	ovary	B1	lower abdomen	Sensitive	IV	no
T16-198	paracolic	A2	middle abdomen	Sensitive		
T16-198	omentum	B2	middle abdomen	Sensitive		
T16-198	diaphragm	A3	upper abdomen	Sensitive		
T16-198	falciform ligament	B3	upper abdomen	Sensitive		
T16-213	ovary	B1	lower abdomen	Sensitive	IVB	no
T16-213	omentum	B2	middle abdomen	Sensitive		
T16-213	diaphragm	A3	upper abdomen	Sensitive		
T16-213	omentum	B2	middle abdomen	Sensitive		
T16-213	right pelvic wall	A1	lower abdomen	Sensitive		
T16-213	bladder peritoneum	B1	lower abdomen	Sensitive		
T16-213	mesenteric root	B2	middle abdomen	Sensitive		
T16-213	Rectosigmoid	B1	lower abdomen	Sensitive		
T16-213	ascites	N/A	N/A	Sensitive		
T16-216	omentum	B2	middle abdomen	Sensitive	IV	no
T16-216	ovary	B1	lower abdomen	Sensitive		
T16-216	diaphragm	A3	upper abdomen	Sensitive		
T16-216	falciform ligament	B3	upper abdomen	Sensitive		
T16-216	left paracolic	A2	middle abdomen	Sensitive		
T16-216	right paracolic	A2	middle abdomen	Sensitive		

T16-216	liver capsule	A3	upper abdomen	Sensitive		
T16-216	mesentery	B2	middle abdomen	Sensitive		
T16-216	lesser sac	B3	upper abdomen	Sensitive		
T16-216	rectum	B1	lower abdomen	Sensitive		
T16-216	ascites	N/A	N/A	Sensitive		
T16-216	pyloric area	B3	upper abdomen	Sensitive		
T17-046	mesentery	B2	middle abdomen	Sensitive	IIIC	yes <0.5cm
T17-046	ovary	B1	lower abdomen	Sensitive		
T17-046	sub hepatic	A3	upper abdomen	Sensitive		
T17-046	left pelvic side wall	C1	lower abdomen	Sensitive		
T17-046	omentum	B2	middle abdomen	Sensitive		
T17-046	pancreas	B2	middle abdomen	Sensitive		
T17-046	sigmoid	B1	lower abdomen	Sensitive		
T17-046	transverse colon	B2	middle abdomen	Sensitive		
T17-046	lesser sac	B3	upper abdomen	Sensitive		
T17-046	right paracolic	A2	middle abdomen	Sensitive		
T17-061	omentum	B2	middle abdomen	Sensitive	IV	no
T17-061	ovary	B1	lower abdomen	Sensitive		
T17-061	omentum	B2	middle abdomen	Sensitive		
T17-061	right diaphragm	A3	upper abdomen	Sensitive		
T17-061	bladder	B1	lower abdomen	Sensitive		
T17-061	falciform ligament	B3	upper abdomen	Sensitive		
T17-061	ascites	N/A	N/A	Sensitive		
T17-061	left paracolic	C2	middle abdomen	Sensitive		
T17-061	paracardiac LN	B2	middle abdomen	Sensitive		
T17-061	omentum minor	B2	middle abdomen	Sensitive		
T17-073	right fimbria	B1	lower abdomen	Sensitive	IV	no
T17-073	ovary	B1	lower abdomen	Sensitive		
T17-073	falciform ligament	B3	upper abdomen	Sensitive		
T17-073	spleen	C3	upper abdomen	Sensitive		
T17-073	omentum	B2	middle abdomen	Sensitive		
T17-073	diaphragm	A3	upper abdomen	Sensitive		
T17-073	renal capsule	B2	middle abdomen	Sensitive		
T17-073	right parametrium	B1	lower abdomen	Sensitive		
T17-073	bladder peritoneum	B1	lower abdomen	Sensitive		
T17-073	pelvic peritoneum	B1	lower abdomen	Sensitive		
T17-073	ascites	N/A	N/A	Sensitive		
T17-096	ovary	B1	lower abdomen	Sensitive	IIIC	no

T17-096	omentum	B2	middle abdomen	Sensitive		
T17-096	right diaphragm	A3	upper abdomen	Sensitive		
T17-096	gastric wall	B3	upper abdomen	Sensitive		
T17-096	mesenteric nodules	B2	middle abdomen	Sensitive		
T17-096	pelvic peritoneum	B1	lower abdomen	Sensitive		
T17-096	falciform ligament	A3	upper abdomen	Sensitive		
T17-112	ovary	B1	lower abdomen	n/a		yes <1cm
T17-112	omentum	B2	middle abdomen	n/a		
T17-112	diaphragm	A3	upper abdomen	n/a		
T17-112	para aortic	B2	middle abdomen	n/a		
T17-112	falciform ligament	A3	upper abdomen	n/a		
T17-112	pelvic peritoneum	B1	lower abdomen	n/a		
T17-112	bladder peritoneum	B1	lower abdomen	n/a		
T17-112	caecum	A2	middle abdomen	n/a		
T17-112	right paracolic	A2	middle abdomen	n/a		
T17-112	pelvic LN	B1	lower abdomen	n/a		
T17-112	duodenum	B2	middle abdomen	n/a		
T17-112	rectum	B1	lower abdomen	n/a		
T17-112	sigmoid	C1	lower abdomen	n/a		
T17-133	omentum	B2	middle abdomen	Resistant	IIIC	yes <0.5cm
T17-133	large bowel	B2	middle abdomen	Resistant		
T17-133	ovary	B1	lower abdomen	Resistant		
T17-133	omentum	B2	middle abdomen	Resistant		
T17-133	left diaphragm	C3	upper abdomen	Resistant		
T17-133	left paracolic	C2	middle abdomen	Resistant		
T17-133	splenic area	C3	upper abdomen	Resistant		
T17-133	renal capsule	B2	middle abdomen	Resistant		
T17-133	sigmoid	C1	lower abdomen	Resistant		
T17-133	ileocaecal area	A2	middle abdomen	Resistant		
T17-167	ovary	B1	lower abdomen	Sensitive	IV	no
T17-167	omentum	B2	middle abdomen	Sensitive		
T17-167	falciform ligament	B3	upper abdomen	Sensitive		
T17-167	small bowel	B2	middle abdomen	Sensitive		
T17-167	right diaphragm	A3	upper abdomen			
T17-167	duodenum	B2	middle abdomen			
T17-190	ovary	B1	lower abdomen	Sensitive	IIIC	no
T17-190	spleen	C3	upper abdomen	Sensitive		

T17-190	falciform ligament	B3	upper abdomen	Sensitive		
T17-190	omentum	B2	middle abdomen	Sensitive		
T17-190	diaphragm	A3	upper abdomen	Sensitive		
T17-190	coeliac trunk	B2	middle abdomen	Sensitive		
T17-190	abdominal wall	B2	middle abdomen	Sensitive		
T17-190	rectum	B1	lower abdomen	Sensitive		
T17-205	pelvic peritoneum	B1	lower abdomen	Sensitive	IIIC	no
T17-205	pelvic side wall	B1	lower abdomen	Sensitive		
T17-205	ovary	B1	lower abdomen	Sensitive		
T17-205	right pelvic wall	A1	lower abdomen	Sensitive		
T17-205	spleen	C3	upper abdomen	Sensitive		
T17-205	omentum	B2	middle abdomen	Sensitive		
T17-205	right diaphragm	A3	upper abdomen	Sensitive		
T17-205	bladder	B1	lower abdomen	Sensitive		
T17-205	ascending colon	A2	middle abdomen	Sensitive		
T17-205	appendix	A1	lower abdomen	Sensitive		
T17-205	ascites	N/A	N/A	Sensitive		
T17-233	left paracolic	C2	middle abdomen	Sensitive	IIIC	yes <1cm
T17-233	ovary	B1	lower abdomen	Sensitive		
T17-233	renal capsule	B2	middle abdomen	Sensitive		
T17-233	omentum	B2	middle abdomen	Sensitive		
T17-233	left diaphragm	C3	upper abdomen	Sensitive		
T17-233	spleen	C3	upper abdomen	Sensitive		
T17-233	sigmoid	C1	lower abdomen	Sensitive		
T17-280	omentum	B2	middle abdomen	No relapse	IVB	no
T17-280	ovary	B1	lower abdomen	No relapse		
T17-280	falciform ligament	B3	upper abdomen	No relapse		
T17-280	omentum	B2	middle abdomen	No relapse		
T17-280	diaphragm	A3	upper abdomen	No relapse		
T17-280	spleen	C3	upper abdomen	No relapse		
T17-280	Rectosigmoid	B1	lower abdomen	No relapse		
T17-280	ascites	N/A	N/A	No relapse		
T18-011	mesenteric ln	B2	middle abdomen	Sensitive	IV	no
T18-011	ovary	B1	lower abdomen	Sensitive		
T18-011	omentum	B2	middle abdomen	Sensitive		
T18-011	diaphragm	A3	upper abdomen	Sensitive		
T18-011	right colic flexure	A2	middle abdomen	Sensitive		

T18-011	pelvic peritoneum	B1	lower abdomen	Sensitive		
T18-011	pelvic LN	B2	middle abdomen	Sensitive		
T18-011	falciform ligament	A3	upper abdomen	Sensitive		
T18-011	sigmoid	C1	lower abdomen	Sensitive		
T18-011	duodenal area	B2	middle abdomen	Sensitive		
T18-011	bladder peritoneum	B1	lower abdomen	Sensitive		
T18-011	mesenteric ln	B2	middle abdomen	Sensitive		
T18-034	ovary	B1	lower abdomen	Resistant	IIIC	no
T18-034	small bowel mesentery	B2	middle abdomen	Resistant		
T18-034	omentum	B2	middle abdomen	Resistant		
T18-034	para aortic ln	B2	middle abdomen	Resistant		
T18-034	right pelvic wall	A1	lower abdomen	Resistant		
T18-034	duodenal area	B2	middle abdomen	Resistant		
T18-034	spleen	C3	upper abdomen	Resistant		
T18-034	liver capsule	A3	upper abdomen	Resistant		
T18-034	bladder	B1	lower abdomen	Resistant		
T18-034	transverse colon	B2	middle abdomen	Resistant		
T18-034	caecum	A2	middle abdomen	Resistant		
T18-034	rectum	B1	lower abdomen	Resistant		
T18-085	ovary	B1	lower abdomen	Sensitive	IVB	no
T18-085	omentum	B2	middle abdomen	Sensitive		
T18-085	right diaphragm	A3	upper abdomen	Sensitive		
T18-085	lesser sac	B2	middle abdomen	Sensitive		
T18-085	right colic flexure	A2	middle abdomen	Sensitive		
T18-085	small bowel	B2	middle abdomen	Sensitive		
T18-085	ascites	N/A	N/A	Sensitive		
T18-085	falciform ligament	A3	upper abdomen	Sensitive		
T18-085	duodenal area	B2	middle abdomen	Sensitive		
T18-085	small bowel mesentery	B2	middle abdomen	Sensitive		
T18-119	uterus	B1	lower abdomen	Sensitive	IIIC	no
T18-119	left ovary	B1	lower abdomen	Sensitive		
T18-119	rectum	B1	lower abdomen	Sensitive		
T18-119	omentum	B2	middle abdomen	Sensitive		
T18-119	diaphragm	A3	upper abdomen	Sensitive		
T18-119	spleen	C3	upper abdomen	Sensitive		
T18-119	bladder	B1	lower abdomen	Sensitive		
T18-119	left paracolic	C2	middle abdomen	Sensitive		
T18-119	uterus	B1	lower abdomen	Sensitive		
T18-119	sigmoid	C1	lower abdomen	Sensitive		

T18-119	Rectosigmoid	B1	lower abdomen	Sensitive		
T18-119	rectum	B1	lower abdomen	Sensitive		
T18-194	ovary	B1	lower abdomen	Sensitive	IV	yes <1cm
T18-194	omentum	B2	middle abdomen	Sensitive		
T18-194	diaphragm	A3	upper abdomen	Sensitive		
T18-194	right paracolic	A2	middle abdomen	Sensitive		
T18-194	paracolic	A2	middle abdomen	Sensitive		
T18-194	falciform ligament	A3	upper abdomen	Sensitive		
T18-194	liver capsule	A3	upper abdomen	Sensitive		
T18-194	stomach	B1	lower abdomen	Sensitive		
T18-194	lesser sac	B2	middle abdomen	Sensitive		
T18-194	spleen	C3	upper abdomen	Sensitive		
T18-243	omentum	B2	middle abdomen	Resistant	IIIC	no
T18-243	right diaphragm	A3	upper abdomen	Resistant		
T18-243	minor omentum	B2	middle abdomen	Resistant		
T18-243	bladder	B1	lower abdomen	Resistant		
T18-243	mesenteric root	B2	middle abdomen	Resistant		
T18-243	descending colon	C2	middle abdomen	Resistant		
T18-243	sigmoid	B1	lower abdomen	Resistant		
T18-243	ovary	B1	lower abdomen	Resistant		
T18-243	small bowel	B2	middle abdomen	Resistant		
T18-243	Rectosigmoid	B1	lower abdomen	Resistant		
T18-243	Rectosigmoid (second sample)	B1	lower abdomen	Resistant		
T18-243	gall bladder	A3	upper abdomen	Resistant		
T18-281	left ovary	B1	lower abdomen	Sensitive	IIIC	no
T18-281	omentum	B2	middle abdomen	Sensitive		
T18-281	right diaphragm	A3	upper abdomen	Sensitive		
T18-281	liver capsule	A3	upper abdomen	Sensitive		
T18-281	lesser sac	B2	middle abdomen	Sensitive		
T18-281	abdominal wall	B2	middle abdomen	Sensitive		
T18-281	left paracolic	C2	middle abdomen	Sensitive		
T18-281	stomach	B3	upper abdomen	Sensitive		
T18-281	small bowel serosa	B2	middle abdomen	Sensitive		
T18-281	pelvic side wall	B1	lower abdomen	Sensitive		
T18-281	left ovary (second sample)	B1	lower abdomen	Sensitive		

Table 9.2 Additional apoptotic data from the ITH project (table 1/4) *Additional apoptotic data from the ITH cases, apoptosis measured by induction of cleaved caspase 3/7. Apoptosis normalised to viability and expressed as a fold change of untreated control. Broad heterogeneity observed in response to cisplatin between metastatic sites and individual patients.*

Case	Sample Site	Apoptotic response
T13-097	Ovary	2.762550463
	Omentum 1	9.928379758
	Omentum 2	6.566021844
	Para aortic lymph node	7.85473594
	Bladder	3.616636624
	Small bowel	9.407601144
	Splenic area	3.698269581
	Rectum	2.680167783
T14-003	Primary	5.063446726
	Omentum	6.222720423
	Mesentery	4.504222791
	Peritoneum	3.853881508
	Paracolic 1	5.175115159
	Paracolic 2	4.682602709
	Omental bursa	3.084367602
	Left colic flexure	5.945856728
	Ascites	2.403271183
T14-012	Primary	3.198251057
	Diaphragm	1.852752462
	Liver capsule	2.240975845
	Peritoneum	3.123262519
	Falciform ligament	2.296076987
T14-051	Primary	4.604024302
	Ovary	6.674965305
	Rectum	2.922290514
	Vaginal wall	1.766911018
	Pouch of douglas	2.552811433
	Pelvic side wall	2.961636041
T14-107	Primary	7.402262217
	Omentum	23.75917921
	Splenic area	8.789728238
	Caecum	7.319729339
	Pelvic lymph node	7.062565786

Additional apoptotic data from the ITH project (table 2/4)

T14-125	Primary	5.381119638
	Ovary	9.992836367
	Omentum	17.06594911
	Diaphragm	2.017906777
	Paracolic	5.102800273
	Pelvic side wall	4.019089273
T15-058	Primary	7.935590608
	Omentum	5.620808844
	Diaphragm	6.828711174
	Para aortic lymph node	2.013373604
	Spleen	6.260100257
	Mesentery	7.071843108
	Bladder	6.908930906
	Rectum	9.997278178
	Omental bursa	6.970976526
T15-085	Primary	4.328747042
	Omentum	4.292951093
	Diaphragm	4.623908905
	Para aortic lymph node	5.169652086
	Mesentery	3.1103461
	Bladder	2.614236169
	Small Bowel	3.472548596
	Rectum	2.94476493
	Paracolic	3.77711806
	Omental Bursa	3.493660901
T16-060	Primary	4.603416446
	Omentum	7.022024371
	Diaphragm	10.25191752
	Liver capsule	5.874906712
	Peritoneum	8.059465266
	Paracolic	5.53171396
	Ascites	7.518919754
T16-156	Primary	7.25429
	Omentum	5.9204
	Diaphragm	3.28512
	Mesentery	3.9594
	Paracolic	4.52361

Additional apoptotic data from the ITH project (table 3/4)

T16-213	Primary	12.15234756
	Omentum	14.85309247
	Diaphragm	12.37591581
	Mesentery	17.69377467
	Bladder	12.57805194
	Rectum	18.26268299
	Omental bursa	28.32131775
	Falciform ligament	12.30192191
	Pelvic side wall	16.86081991
	Ascites	28.71055726
	Pancreatic area	11.415889
T16-216	Primary	3.624661373
	Omentum	1.836198361
	Diaphragm	3.964089845
	Mesentery	2.272297889
	Liver capsule	6.923255148
	Rectum	3.715301626
	Paracolic	3.720416514
	Omental bursa	7.364392883
	Falciform ligament	4.240730295
	Stomach	9.050614493
	Posterior gastric wall	7.471633002
	Ascites	6.980316577
T17-046	Primary	7.057382307
	Omentum	6.997682491
	Mesentery	6.469431602
	Liver capsule	6.769696545
	Bladder	3.547004382
	Paracolic	14.34425188
	Omental bursa	2.246398807
	Left colic flexure	7.807842399
	Sigmoid	9.434849102
	Pelvic side wall	4.986663258
	Pancreatic area	5.822811413

Additional apoptotic data from the ITH project (table 4/4)

T17-061	Primary	3.865
	Omentum 1	5.07135
	Omentum 2	14.3946
	Diaphragm	3.04
	Bladder	5.23864
	Paracolic	2.57721
	Falciform ligament	6.35635
	Ascites	3.21336
	Paracardiac lymph node	1.61172
T17-073	Primary	7.684192795
	Ovary	12.29558175
	Omentum	11.61921346
	Diaphragm	13.84451939
	Mesentery	13.17266736
	Bladder	16.47177832
	Splenic area	8.07775582
	Falciform ligament	8.544649739
	Pouch of douglas	8.458631875
	Renal capsule	13.61834177
	Pelvic side wall	20.92954022
	Ascites	21.82125971

Table 9.3 Additional IC_{50} data from ITH project (table 1/3)*: Additional data from the ITH project, cisplatin IC_{50} values for individual sample sites in different cases. Variation in IC_{50} values is seen across the sample cohort.*

	CDDP IC50	μM cddp
	T15-058	
A	Primary	0.5368
B	Omentum	3.21
C	Mesenteric	3.177
D	Omental Bursa	6.603
E	Spleen LN	1.982
G	Bladder Peritoneum	3.166
H	Rectal wall	8.987
I	R Diaphragm	3.97
	R Diaphragm second sample	3.135
	T16-046	
A	Primary	8.569
B	Omentum	3.488
D	Mesenteric Root	3.694
E	Pancreatic area	2.48
F	Small Bowel Mesentery	3.219
G	Liver Capsule	3.252
H	Pelvic Peritoneum	5.985
J	Rectosigmoid	4.829
K	Ileocaecal area	2.413
L	Ascites	5.378
	T16-097	
A	Primary	6.308
B	Omentum	17.72
D	Falciform ligament	76.66
E	Appendix	34.63
ASC	Ascites	8.366
	T16-111	
	Supra-renal lymph node 1	2.584
	Supra-renal lymph node 2	2.954
	T16-156	
A	Primary	5.26
B	Omentum	4.45
C	Diaphragm	7.196
F	Right Paracolic	5.32
H	Small Bowel Mesentery	4.813

Additional IC_{50} data from ITH project (table 2/3)

	T16-213	
A	Primary	1.42
B	Omentum	1.19
C	R Diaphragm	1.724
D	Lesser sac	0.9866
G	R Pelvic side wall	2.017
H	Bladder peritoneum	1.121
I	Mesenteric root	1.573
J	Rectosigmoid	2.868
K	Ascites	2.962
	T17-007	
C	small bowel mesentery	2.271
D	large bowel	2.327
E	ascites	5.124
	T17-046	
A	Primary	7.979
B	Sub hepatic	8.581
E	L Pelvic side wall	8.292
F	Mesentery	9.279
G	Sigmoid	9.983
H	Omentum	16.55
K	Transverse colon	24.72
	T17-061	
A	Primary	0.9094
B	Omentum	1.139
C	Omentum minor	1.571
E	Bladder	0.2859
I	Ascites	17.59

Additional IC_{50} data from ITH project (table 3/3)

	T17-067	
A	R Diaphragm	53.03
B	Liver	18.08
C	Mesentery	28.21
E	Large bowel	12.98
H	Ascites	22.01
	T17-073	
A	Primary	4.407
B	Omentum	4.988
C	Right Fimbria	8.898
I	Renal capsule	6.076
K	Spleen	1.579
L	Right parametrium	4.145
M	Bladder peritoneum	1.113
N	Pelvic peritoneum	8.073
P	Ascites	5.02

Figure 9.1: Correlation of ITH cohort samples apoptotic response to cisplatin with percentage Ki67 proliferation index. *No correlation was observed between apoptotic response and percentage Ki67 proliferation index p=0.9772.*

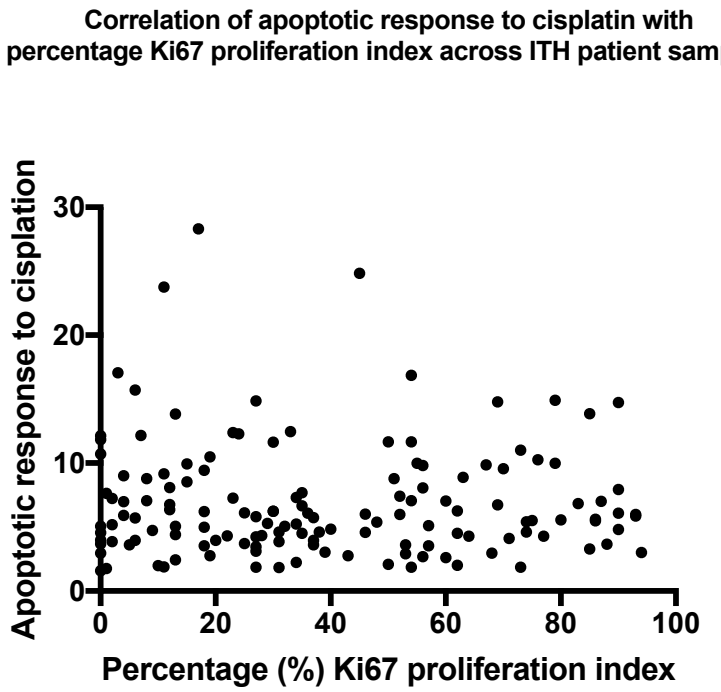


Figure 9.2: Correlation of MAD apoptosis with MAD percentage Ki67 proliferation index. No correlation is seen p=0.6928

